

# The Universe During Epochs of Accelerating Expansion

Charlotte Owen



Department of Physics

Lancaster University

June 2019

A thesis submitted to Lancaster University for the degree of  
Doctor of Philosophy in the Faculty of Science and Technology

*Supervised by Dr. Konstantinos Dimopoulos*

# Abstract

Cosmic inflation, the accelerated expansion of the early Universe, is an accepted pillar in the foundations of modern cosmology. This is due mainly to its success at explaining several anomalies between observations and the existing Hot Big Bang model of the Universe, but a specific model is not agreed upon in the literature. The Universe has also recently been observed to enter another phase of accelerating expansion, driven by an unexplained mechanism called ‘dark energy’.

The research presented in this thesis grows organically; starting with an investigation into novel inflationary models and developing into quintessential inflation models. The latter explain both the primordial inflation and dark energy observations using one minimal framework.

A new family of inflation models is presented, which excellently match observations for natural parameter values, and a derivation from supergravity is demonstrated. A period of thermal inflation allows the supergravity realisation of hybrid inflation to be realigned with observations. A new approach to inflection-point inflation is developed, which is considerably less fine-tuned and exotic than previous models.

Two novel quintessential inflation models are introduced, the first embedded in  $\alpha$ -attractors - a compelling framework of inflationary model building and the second in Gauss-Bonnet gravity - an extension to General Relativity.

Detailed investigations of reheating after inflation are undertaken, focusing on gravitational reheating and instant preheating, analysing the necessary constraints including those from supergravity. Along the way, there is a brief diversion into primordial black holes, investigating how a slow reheating period affects their formation rates.

## Acknowledgements

There are many people I owe thanks to for their support and encouragement during my PhD, but the following deserve a special mention.

My first and foremost thanks go to my supervisor, Kostas, whose belief in my ability and unwavering championing has been a steadfast pillar of my PhD studies. His influence has made me a better physicist as well as a better person and his impact cannot be over-emphasised.

To my Mum, whom I love dearly, a huge thanks for too many things to list. I cannot find the words to do you justice, except to say thank you for being ever-present, constantly and unreservedly *there*. Also to my brother, Alex, who keeps me on my toes but always has my back.

To my flatmates, Jim and Miguel, who have made my time in Lancaster very special, and have made more of an impact on my life than I think they realise. To Adam and Ben, with whom I started this journey, Lancaster wouldn't have been the same without you, even when we were separated by continents.

To Grace, a big thanks for distracting me from my PhD with numerous adventures, I hope we never stop travelling the world together. To the girls in London, patiently awaiting my return, and my friends elsewhere who remind me that life is bigger than the research bubble in Lancaster, thank you.

To the cosmology group at Lancaster for engaging discussions and continued support. In particular James, who brought the group to life and Leonora, whose passion for physics continues to inspire me.

Finally, I wish to thank all of my collaborators that have patiently shared their enthusiasm and expertise with me: Mindaugas Karciuskas, Bernard Carr, Tommi Tenkanen, Antonio Racioppi and Chris Longden, who have all been a pleasure to work with, but especially Carsten van de Bruck, who made my first collaborative project such a positive experience.

## **Declaration**

This thesis is my own work and no portion of the work referred to in this thesis has been submitted in support of an application for another degree or qualification at this or any other institute of learning.

# Contents

<b>List of Figures</b>	<b>viii</b>
<b>List of Tables</b>	<b>xv</b>
<b>1 Introduction</b>	<b>1</b>
1.1 Conventions . . . . .	3
<b>2 Background Theory</b>	<b>5</b>
2.1 Brief History of the Universe . . . . .	5
2.1.1 The Very Beginning . . . . .	7
2.1.2 The Electro-weak Scale Onwards . . . . .	9
2.1.3 The CMB as an Observational Probe . . . . .	12
2.2 Describing the Dynamics of the Universe . . . . .	14
2.2.1 Einstein Field Equations . . . . .	15
2.2.2 F(L)RW Metric Solutions to the EFE . . . . .	17
2.2.3 The Evolution of the Universe . . . . .	19
2.3 Problems with the HBB . . . . .	22
2.3.1 Flatness Problem . . . . .	22
2.3.2 Horizon Problem . . . . .	24
2.3.3 The Origin of Structure . . . . .	26
2.3.4 Additional Considerations for the HBB . . . . .	28
2.4 Introducing Inflation . . . . .	28
2.4.1 Solving the Problems of the HBB . . . . .	29
2.4.2 Accelerated Expansion with a Scalar Field . . . . .	31

2.4.3	Slow-roll Inflation . . . . .	33
2.4.4	How Much Slow-roll Inflation? . . . . .	36
2.4.5	Inflationary Observables . . . . .	40
2.5	Inflationary Model Building . . . . .	50
2.5.1	Global and Local Supersymmetry . . . . .	51
2.5.2	The $\eta$ Problem of Supergravity . . . . .	52
2.6	Models of Inflation . . . . .	53
2.6.1	Large Field vs Small Field Inflation . . . . .	54
2.6.2	The Lyth Bound . . . . .	56
2.6.3	Super-Planckian Field Variations . . . . .	57
2.6.4	Hybrid Inflation . . . . .	58
2.6.5	Thermal Inflation . . . . .	60
2.6.6	Eternal Inflation . . . . .	63
2.6.7	$f(R)$ Theories . . . . .	64
2.7	Reheating the Universe after Inflation . . . . .	64
2.7.1	Perturbative Reheating . . . . .	66
2.7.2	Preheating . . . . .	70
2.7.3	Instant Preheating . . . . .	73
2.7.4	Gravitational Reheating . . . . .	76
2.7.5	Constraints on Reheating . . . . .	78
2.8	Dark Energy and Quintessential Inflation . . . . .	79
2.8.1	$\Lambda$ CDM . . . . .	80
2.8.1.1	The Cosmological Constant Problem . . . . .	81
2.8.1.2	Future Horizons Problem of $\Lambda$ CDM . . . . .	82
2.8.2	Quintessence . . . . .	82
2.8.3	Quintessential Inflation . . . . .	84
2.8.4	Early-time Kinematics of Quintessential Inflation . . . . .	85
2.8.4.1	Gravitational Waves During Kination . . . . .	87
2.8.5	Late-time Kinematics of Quintessential Inflation . . . . .	89

<b>3</b>	<b>Power-law Plateau Inflation:</b>	
	<b>A New Family of Inflationary Models</b>	<b>94</b>
3.1	Introduction . . . . .	94
3.2	Power-law Plateau Inflation . . . . .	96
3.3	A Low e-folding Number . . . . .	99
	3.3.1 The Reheating Temperature . . . . .	99
	3.3.2 Thermal Inflation . . . . .	101
3.4	A Single Mass Scale . . . . .	103
3.5	Large-field Power-law Plateau Inflation . . . . .	104
3.6	Supersymmetric Power-law Plateau Inflation . . . . .	105
	3.6.1 Global Supersymmetry . . . . .	106
	3.6.2 Local Supersymmetry . . . . .	107
3.7	Discussion . . . . .	112
<b>4</b>	<b>How Thermal Inflation Can Save</b>	
	<b>Minimal Hybrid Inflation in Supergravity</b>	<b>114</b>
4.1	Introduction . . . . .	114
4.2	Minimal Hybrid Inflation in Supergravity . . . . .	116
4.3	Thermal Inflation to Reduce $N_*$ . . . . .	119
4.4	Results . . . . .	120
4.5	Discussion . . . . .	123
<b>5</b>	<b>Loop Inflection-Point Inflation</b>	<b>125</b>
5.1	Introduction . . . . .	125
5.2	Loop Inflection-point Inflation . . . . .	126
5.3	Computing $N_*$ and $\xi$ . . . . .	130
5.4	Inflationary Observables . . . . .	133
5.5	Higher-order Non-renormalisable Terms . . . . .	133
5.6	The Inflationary Energy Scale and Reheating Temperature . . . . .	136
5.7	Additional Considerations . . . . .	140
	5.7.1 Negative $\delta$ Values . . . . .	140
	5.7.2 A Diffusion Zone Around $\phi_f$ . . . . .	141

5.7.3	Ultra Slow-roll Inflation . . . . .	143
5.8	Discussion . . . . .	145
<b>6</b>	<b>Primordial Black Hole Formation</b>	
	<b>During Slow Reheating After Inflation</b>	<b>147</b>
6.1	Introduction . . . . .	147
6.2	PBH Production . . . . .	149
6.3	The Effect of a Slow Reheating Period . . . . .	152
6.4	Primordial Black Hole Mass Function . . . . .	156
6.5	Discussion . . . . .	163
<b>7</b>	<b>Quintessential Inflation with <math>\alpha</math>-attractors</b>	<b>164</b>
7.1	Introduction . . . . .	164
7.2	The Potential and its Embedding in $\alpha$ -Attractors . . . . .	165
	7.2.1 Initial Conditions . . . . .	169
7.3	Inflation . . . . .	169
	7.3.1 Inflationary Energy Scale and e-folding Number . . . . .	171
	7.3.2 Parameter Space from Observational Constraints . . . . .	174
7.4	Freezing of the Scalar Field . . . . .	176
7.5	Quintessence . . . . .	179
	7.5.1 Observational Constraints on Quintessence . . . . .	181
	7.5.1.1 Transient Accelerated Expansion . . . . .	181
	7.5.1.2 Eternal Accelerated Expansion . . . . .	183
7.6	Gravitational Reheating . . . . .	185
7.7	Considerations for Gravitational Reheating . . . . .	189
	7.7.1 Overproduction of Gravitinos . . . . .	189
	7.7.2 Overproduction of Gravitational Waves . . . . .	190
7.8	Instant Preheating . . . . .	191
7.9	Considerations for Instant Preheating . . . . .	195
	7.9.1 Radiation Domination . . . . .	197
	7.9.2 Backreaction . . . . .	197
	7.9.3 Overproduction of Gravitinos . . . . .	199

---

7.9.4	Overproduction of Gravitational Waves . . . . .	200
7.10	Additional Considerations . . . . .	201
7.10.1	Suppressed Interactions . . . . .	201
7.11	Results . . . . .	204
7.12	Discussion . . . . .	208
<b>8</b>	<b>Gauss-Bonnet Quintessential Inflation</b>	<b>213</b>
8.1	Introduction . . . . .	213
8.2	Gauss-Bonnet Gravity and the Model . . . . .	214
8.3	Inflation . . . . .	217
8.4	After Inflation . . . . .	219
8.4.1	Kinetic Regime . . . . .	221
8.4.2	Gauss-Bonnet Regime . . . . .	222
8.4.3	Stitching and Boundary Condition . . . . .	222
8.5	Reheating . . . . .	226
8.6	Dark Energy Today . . . . .	227
8.7	Constraints and Results . . . . .	230
8.7.1	Gravitational Waves in Gauss-Bonnet Gravity . . . . .	231
8.8	Discussion . . . . .	233
<b>9</b>	<b>Conclusion</b>	<b>235</b>
	<b>References</b>	<b>242</b>

# List of Figures

2.1	Depicts how two different physical wavelength scales grow with the scale factor, and the corresponding behaviour of the horizon in the radiation dominated and matter dominated eras. . . . .	27
2.2	Constraints in the $r$ vs $n_s$ plane using <i>Planck</i> 2018 data, reproduced from [1]. $2\sigma$ ( $1\sigma$ ) constraints are indicated by dashed (solid) lines respectively. . . . .	49
2.3	A sketch of the potential in hybrid inflation using arbitrary units, shown from two different perspectives. . . . .	59
2.4	A sketch of the thermal inflation flaton potential using arbitrary units. As the temperature drops the potential opens up, allowing the flaton to move towards its VEV. The black (solid) line indicates the highest temperature, with the red (dashed), blue (dot-dashed) and green (dotted) lines at respectively lower temperatures. . . . .	61
2.5	Mathieu instability bands (blue regions) which are interpreted as exponential particle production. . . . .	74
2.6	A spike in gravitational waves appears at high frequencies when there is a period of kination, the reheating temperature determines the length of kination and therefore the magnitude of the spike. N.B. This is an example sketch to show the behaviour and should not be used as a representative reference for particular values etc... . . . . .	88

2.7	Log-log plot depicting the evolution of the energy density of the scalar field, $\rho_\phi$ (solid line), compared the energy density of the background, $\rho_b$ (dashed line), which initially evolves as radiation ( $\rho \propto a^{-4}$ ) and then matter ( $\rho \propto a^{-3}$ ). The scalar field is kinetically dominated ( $\rho \propto a^{-6}$ ) until it freezes, when its energy density becomes constant. The red dotted line indicates the present time, when the scalar field has recently become the dominant energy density of the Universe again. This plot shows the scalar field following the dominant attractor solution. . . . .	90
3.1	$n_s$ and $r$ for maximum $a$ values for each $n$ and $q$ combination. . .	98
3.2	$n_s$ and $r$ for $q = 1$ and the maximum allowed $a$ value from Eq. (3.18) for $1 \leq n \leq 4$ and $33 \leq N_* \leq 50$ . $N_*$ is shown on the colour map. . . . .	102
3.3	Values for $n_s$ and $r$ in the case of a single mass scale. Using the $a$ value from Eq. (3.28) for $1 \leq n \leq 4$ , $q = 1$ and $33 \leq N_* \leq 50$ . $N_*$ is shown on the colour map. . . . .	104
3.4	Values for $n_s$ and $r$ with $q = 1$ , $1 \leq n \leq 4$ when super-Planckian field displacements are allowed. E-folding number varies between $33 \leq N_* \leq 60$ , as shown on the colour map. . . . .	105
3.5	A comparison of the scalar field potentials for the power-law plateau inflation model with $n = 2$ , $q = 1$ , and the SUGRA potential Eq. (3.42) . . . . .	110
3.6	A comparison of the $r$ predictions for the typical power-law plateau inflation potential (Eq. (3.4), dotted line) and the potential derived in SUGRA (Eq. (3.42), solid line), for varying $a$ values. . . . .	111
4.1	$n_s$ and $r_{\max}$ in hybrid inflation as a function of $\langle\theta\rangle$ and therefore $N_*$ . The solid, black line depicts the values of $n_s$ . The dashed, red line depicts the maximum allowed value for $r$ , which corresponds to $\kappa = 1$ . The Planck 2018 $1\sigma$ and $2\sigma$ bounds are indicated by the horizontal shaded regions. . . . .	122

5.1	The scalar field potential with $n = 1$ . $V_{\text{CW}}$ and $V_{\text{higher}}$ refer to the first and second terms in Eq. (5.8) respectively. This example is plotted for $\delta = 10^{-5.95}$ , defined in Eq. (5.13), with $\xi$ calculated via the iteration process detailed in Section 5.3. . . . . .	129
5.2	$\epsilon - 1$ and $N$ for varying $\phi$ . In the iteration process we first find $\epsilon = 1$ , denoted by the dotted vertical lines, the smaller of which allows us to find $\phi_e$ . Using $\phi_e$ as the lower integration limit and $\phi$ for the higher, $N$ is then plotted from Eq. (2.85). The point at which $N = N_*$ then allows $\phi_*$ to be determined. The dashed vertical line indicates the inflection point. . . . . .	132
5.3	Values of $\delta$ for which $n_s$ (solid black line) and $r$ (dashed red line) fall within the Planck bounds for $n_s$ depicted with the shaded horizontal bands (light: $2\sigma$ and dark: $1\sigma$ ). . . . . .	134
5.4	A comparison of the $n_s$ predictions for varying orders of the non-renormalisable term, $n$ , focusing on the $\delta$ values for which $n_s$ falls within the Planck bounds depicted by the shaded horizontal bands (light: $2\sigma$ and dark: $1\sigma$ ). . . . . .	136
5.5	Predictions of $n_s$ for $\delta = 10^{-5.9}$ with varying $n$ in the potential in Eq. (5.6). . . . . .	137
5.6	The scalar field potential when $\delta$ takes negative values, showing the appearance of a local maximum and minimum. In this example $\delta = -10^{-7}$ . Due to the scales involved we define $V(\phi) = V_0 + \varepsilon$ where $V_0 = 2.507017 \times 10^{57} \text{GeV}^4$ . . . . . .	139
5.7	The Lambert W function . . . . . .	142

6.1 The fraction of the total energy density collapsing into PBHs,  $\beta$ , as a function of  $\sigma(M)$ . During radiation domination and matter domination different considerations control  $\beta$ . The green dotted line shows  $\beta$  in a radiation dominated Universe, given by Eq. (6.2) with  $\delta_c = w_r$ . The red line shows  $\beta$  in a matter dominated Universe when the limiting factor controlling  $\beta$  is the fraction of overdensities which are sufficiently spherically symmetric, Eq. (6.3), valid for  $0.005 < \sigma < 0.2$ . The black line shows  $\beta$  in a matter dominated Universe when the limiting factor controlling  $\beta$  is the angular momentum of the region and Eq. (6.4) is appropriate, when  $\sigma < 0.005$ . When the red (black) line is solid rather than dashed, this indicates the red (black) line is the limiting factor controlling  $\beta$  in the matter dominated regime. . . . . 151

6.2 Solutions to Eq. (6.9); the solid red line uses  $\beta(M)$  defined in Eq. (6.3) for the complete range of  $\sigma$  values, the dashed red line uses  $\beta(M)$  defined in Eq. (6.4) in the region  $\sigma < 0.005$ . The dotted horizontal line denotes  $\Gamma/H = 1$ . . . . . 153

6.3 The fraction of overdensities able to collapse from Eq. (6.2) in red and Eq. (6.3) in blue. For  $\Gamma/H \ll 1$ , when  $w_{\text{eff}} \simeq 0$ , the fraction of overdensities with  $\delta > \delta_c$  is almost unity but the fraction which are sufficiently spherical is much lower, hindering the PBH formation rate. As  $\Gamma/H$  increases the fraction with  $\delta > \delta_c$  drops drastically as  $w_{\text{eff}} \rightarrow 1/3$  and limits the PBH formation rate. The solid line indicates the limiting factor affecting formation rate at any time. Two example values of  $\sigma$  are shown via the dashed and dotted lines. 154

6.4 The duration of effective MD when  $\Gamma \simeq H$  signifies an immediate transition to RD (dotted, black line) and calculated  $\Gamma/H$  from Eq. (6.9), taking into account the growing thermal bath (dashed, black line). The red line shows the difference between the two calculations. . . . . 156

6.5	The PBH mass function for three example $\sigma$ values (all below $\sigma_c$ ). The solid lines represent the new cut-off taking into account the sub-dominant radiation bath, the dashed lines show the standard result in the literature where the mass cut-off occurs at $H_{\text{reh}}$ . The minimum mass used here is $M_{\text{evap}} \simeq 2 \times 10^{-19}$ GeV, the mass of PBHs evaporating today [2]. . . . .	161
6.6	The mass function for $\sigma = 10^{-3.5}$ with (solid, red line) and without (dashed, blue line) taking spin effects into consideration. . . . .	162
7.1	The potential in Eq. (7.7). It features two flat regions for $ \phi  \gg \sqrt{6\alpha} m_{\text{Pl}}$ ; the inflationary plateau and the quintessential tail, with a steep dip between them. An example freezing value for the field is indicated by $\phi_F$ , defined in Eq. (7.33). . . . .	168
7.2	The tensor-to-scalar ratio, $r$ , versus the spectral index, $n_s$ for our model is displayed overlaying the Planck 2018 results. $\alpha$ varies from 0 to 28 according to the colour map on the right, stars represent $N = 55$ and circles represent $N = 65$ . The slope of the line for large values of $\alpha$ is understood as $n_s \rightarrow 0$ when $\alpha \gg 1$ (cf. Eq. (7.17)). Note that the line corresponding to the values of $n_s$ and $r$ curves back on itself for small $\alpha$ (values of $\alpha \lesssim 0.1$ or so) so that the spectral index becomes insensitive to $\alpha$ when it is small. This region is shown in more detail in Fig. 7.7. . . . .	175
7.3	Transient accelerated expansion for $\lambda = \sqrt{2}$ . We find $w < -1/3$ , but the minimum value of $w$ is well outside of the Planck bounds. . . . .	182
7.4	Eternal accelerated expansion for $\lambda = \sqrt{0.4}$ . The scalar field has unfrozen, but is yet to settle on the attractor solution. . . . .	183
7.5	Time dependence of $w_\phi$ as modelled by the Taylor expansion in Eq. (7.40). The allowed parameter space depicted lies well within the $1\sigma$ Planck contour for $\lambda^2 < 0.46 \Leftrightarrow \alpha > 1.45$ . . . . .	184

7.6	Possible range of values for $\alpha$ and $\lambda^2$ , from the Planck constraints on $w$ . It is shown that the $2\sigma$ upper bound on $w_{\text{DE}}$ is satisfied only for $\lambda^2 < 0.46$ or equivalently $\alpha = 2/3\lambda^2 > 1.45$ . The allowed ranges of $w$ and $w_\phi$ reflect the observed range in $\Omega_{\text{DE}}/\Omega_m$ . Values in the text are quoted to 2 s.f. . . . .	185
7.7	The tensor-to-scalar ratio, $r$ , versus the spectral index, $n_s$ for $\alpha$ varying from 1.5 to 4.2 according to the colour map on the right. All of these results are well within the Planck $1\sigma$ range. Values of $r$ are potentially observable in the near future. . . . .	189
7.8	$\dot{\varphi}$ is maximised very close to $\varphi \simeq 0 \simeq \phi$ . . . . .	194
7.9	The interaction strength, $\mathcal{G}$ , for the range of allowed $g$ values and allowed $\alpha$ values between 1.5 and 4.2. The bounds arising from backreaction and gravitino constraints are indicated. . . . .	203
7.10	Final parameter spaces for $n$ , for the range of allowed $g$ values and allowed $\alpha$ values between 1.5 and 4.2. The bounds arising from backreaction and gravitino constraints are indicated. . . . .	204
7.11	Final parameter spaces for $\kappa$ , for the range of allowed $g$ values and allowed $\alpha$ values between 1.5 and 4.2. The bounds arising from backreaction and gravitino constraints are indicated. . . . .	205
7.12	Final parameter spaces for $N_*$ , for the range of allowed $g$ values and allowed $\alpha$ values between 1.5 and 4.2. The bounds arising from backreaction and gravitino constraints are indicated. . . . .	206
7.13	Final parameter spaces for $T_{\text{reh}}$ , for the range of allowed $g$ values and allowed $\alpha$ values between 1.5 and 4.2. The bounds arising from backreaction and gravitino constraints are indicated. . . . .	207
7.14	Final parameter spaces for the spectral index, $n_s$ and the tensor-to-scalar ratio, $r$ , for the range of allowed $g$ values and allowed $\alpha$ values between 1.5 and 4.2. The bounds arising from backreaction and gravitino constraints are indicated. . . . .	208
7.15	Final parameter spaces for the inflationary energy scale, $M$ , for the range of allowed $g$ values and allowed $\alpha$ values between 1.5 and 4.2. The bounds arising from backreaction and gravitino constraints are indicated. . . . .	209

- 
- 7.16 Final parameter spaces for  $V_0^{1/4}$  for the range of allowed  $g$  values and allowed  $\alpha$  values between 1.5 and 4.2. The bounds arising from backreaction and gravitino constraints are indicated. . . . . 210
- 7.17 Final parameter spaces for  $\Lambda^{1/4}$  for the range of allowed  $g$  values and allowed  $\alpha$  values between 1.5 and 4.2. The bounds arising from backreaction and gravitino constraints are indicated. . . . . 211
- 8.1 Constraints for a model with  $q = 4p$ ,  $G_0 m_{\text{Pl}}^2 = 1$  and  $g = 0.8$ . The left window shows the value of  $\phi_{\text{DE}}$  for a range of  $p$  values and the red shaded region represents the parameter space where  $\phi_{\text{DE}}$  is super-Planckian. The right window shows the energy densities involved in the instant preheating conditions of Eq. (8.47). The black solid line represents  $\rho_\chi$ , while the blue dashed line and green dot-dashed line respectively represent the lower and upper bounds that  $\rho_\chi$  must lie between. The shaded region on the right encloses the  $p$  values for which these inequalities are violated. . . . . 231

# List of Tables

1.1	Reference values for cosmological parameters as quoted in Ref. [3].	4
3.1	Maximum $a$ values with $q = 1$ , $N_* = 50$ , whilst $\phi$ remains sub-Planckian and the corresponding values of $n_s$ , $r$ and $\frac{dn_s}{d \ln k}$ .	99
3.2	The maximum values of $r$ , for which $n_s$ is within the Planck $1\sigma$ bounds, and the corresponding maximum $a$ (obtained using Eq. (3.18)) and minimum $N_*$ values for the $n$ values shown in Fig. 3.2.	103
4.1	$\langle \theta \rangle$ , $N_*$ , $n_s$ and $r_{\max}$ (using $\kappa = 1$ ) values.	121
5.1	$\delta$ values producing $n_s$ within the Planck $2\sigma$ bounds.	133
5.2	Values of $(\phi_f/m_{\text{Pl}})^{2n}$ for $n \geq 1$ .	135
5.3	Results for $\phi^8$ .	135
5.4	Results for $\phi^{10}$ .	135
5.5	Results for $\phi^{12}$ .	135
7.1	Values of $M$ calculated from Eq. (7.24) for various $\alpha$ values.	173
7.2	Allowed $n$ and $\kappa$ values for specific choices of $g$ , within the allowed $\alpha$ range, before consideration of backreaction and gravitino constraints.	196
7.3	Parameter values for the allowed range of $n$ , prior to consideration of backreaction and gravitino constraints.	198
7.4	Final values for the parameters when considering the tightest constraints on $g$ , from the backreaction bound.	199

8.1	Table showing limits on $p$ in the theory for various cases of the size of $G_0$ , $q$ and $g$ , due to constraints coming from sub-Planckian field displacements and instant preheating's efficacy. In each case, the lower bound on $p$ occurs as, below this threshold, $\phi_{\text{DE}}$ would have to undergo a super-Planckian displacement to serve as dark energy today. Similarly, the upper limits on $p$ arise as, above these limits, the inequality in Eq. (8.47) is violated. . . . .	232
-----	--	-----

## Relevant Publications by the Author

- **“Modelling Inflation with a Power-law Approach to the Inflationary Plateau”**  
K. Dimopoulos & C. Owen, *Physical Review D*, 94 (2016) no.6, 063518, arXiv:1607.02469
- **“How Thermal Inflation Can Save Minimal Hybrid Inflation in Supergravity”**  
K. Dimopoulos & C. Owen, *JCAP*, 1610 (2016) no.10, 020, arXiv:1606.06677
- **“Loop Inflection-point Inflation”**  
K. Dimopoulos, C. Owen & A. Racioppi, *Astropartical Physics*, 103 (2018) 16-20, arXiv:1706.09735
- **“Primordial Black Hole Formation During Slow Reheating After Inflation”**  
B. Carr, K. Dimopoulos, C. Owen & T. Tenkanen, *Physical Review D*, 97 (2018) no.12, 123535, arXiv:1804.08639
- **“Quintessential Inflation with  $\alpha$ -attractors”**  
K. Dimopoulos & C. Owen, *JCAP*, 1706 (2017) no.06, 027, arXiv:1703.00305
- **“Instant Preheating in Quintessential Inflation with  $\alpha$ -attractors”**  
K. Dimopoulos, L. Donaldson Wood & C. Owen, *Physical Review D*, 97 (2018) no.6, 063525, arXiv:1712.01760
- **“Gauss-Bonnet-coupled Quintessential Inflation”**  
C. van de Bruck, K. Dimopoulos, C. Longden & C. Owen, arXiv:1707.06839  
Withdrawn from submission to *Physical Review D* (2017)

# Chapter 1

## Introduction

*“Through our eyes, the Universe is perceiving itself. Through our ears, the Universe is listening to its harmonies. We are the witnesses through which the Universe becomes conscious of its glory, of its magnificence.”*

---

Alan Wilson Watts

Cosmology, as a field of study in its current form, emerged relatively recently in human history. The heavens have fascinated mankind for centuries; delighting and confounding in equal measures, but for most of human history the Universe, as we now understand it, was unknown and unexplored. Set in this context, the amount we are now able to explain becomes astounding, rivalling the greatest epic ever written: a description of 13.7 billion years of cosmological history which culminates in all the beautiful structure of the Universe, including the presence of a nondescript star, orbited by a nondescript rock, inhabited by a nondescript life-form. A life-form which harbours an innate desire to understand the inner workings of the Universe around them.

This thesis examines the very beginning of this history, a time period almost unfathomable without mathematics. We then travel approximately 9 billion years towards the present day, to the beginning of the current epoch of Universe history,

---

where the mysterious dark energy begins to control the dynamics of the Universe.

Chapter 2 provides an introduction to the cosmology used throughout this thesis, starting with an overview of the history of the Universe, detailing the shortcomings of the Hot Big Bang model and introducing inflation as a means to overcome them. Moving chronologically through the reheating epoch to the modern day with dark energy domination of the Universe, the topics covered in the following research chapters are introduced.

Chapters 3 to 8 present the original research of the author, in collaboration with Konstantinos Dimopoulos and in some cases additional collaborators. Full details and links to the research articles are given in the list of publications preceding this introduction.

The first three chapters of this thesis focus on the very beginning of the Universe, and detailed models of inflation. Chapter 3 introduces a family of inflation models, motivated by the recent Planck [1, 4] results, that excellently reproduce the observables without fine-tuning of mass scales. A toy model derived in the context of global and local supersymmetry is examined and the chapter introduces the idea of a low reheating temperature and a subsequent period of thermal inflation. Chapter 4 develops these ideas and utilises them to resurrect the model of minimal hybrid inflation in supergravity. The mechanisms are general but have a profound effect in this model, which had previously been ruled out by the 2015 Planck results but is once again viable with the modifications presented here. Continuing the theme of inflationary models, Chapter 5 introduces loop inflection-point inflation. Again motivated by Planck's preference for a 'plateau' model of inflation, this research generates a plateau in the model via loop-corrections to the potential. This research improves previous work on inflection-point inflation because it negates the need for an elaborate set-up in a theoretical extension to the Standard Model of particle physics.

Chapter 6 is a brief interlude between the investigations into periods of accelerated expansion studied in the rest of the chapters of this thesis, instead investigating primordial black holes. We study the effect on primordial black hole formation of a period of slow reheating after inflation. We present constraints on the maximum cut-off for primordial black hole mass which is particularly pertinent after the recent LIGO observations of black hole mergers.

---

Chapters 7 and 8 return the focus to accelerated expansion of the Universe, incorporating not only primordial inflation which is the focus of the earlier chapters of this thesis but also late-time accelerated expansion of the Universe, the epoch in which we currently exist. Chapter 7 introduces quintessential inflation for the first time and the exciting embedding of such a model in the  $\alpha$ -attractor theories of inflation. An in-depth analysis of reheating and detailed discussion of the constraints arising in different extensions to the Standard Model of particle physics are presented. Chapter 8 investigates a model of quintessential inflation embedded in a modified gravity theory, which utilises additional couplings between the inflaton and gravity to sidestep some of the issues normally associated with quintessential inflation models.

We conclude, in Chapter 9, with a discussion of the body of work as a whole, the current state of the research field, including open questions and look to further work.

## 1.1 Conventions

Throughout this thesis we set  $\hbar = k_b = c = 1$  so that the reduced Planck mass is

$$m_{\text{Pl}}^2 = \frac{1}{8\pi G}, \quad (1.1)$$

where  $G$  is the gravitational constant. When using tensor notation, for 4-dimensional indices we use Greek letters:  $\mu, \nu, \rho, \sigma$ , for purely spatial indices we use Roman letters:  $i, j, k$ . The Einstein summation convention is assumed. Throughout this thesis, a subscript ‘0’ means a quantity is defined at the present time. Unless otherwise stated, over-dots denote derivatives with respect to cosmic time and primes denote derivatives with respect to the scalar field.

As is typical in cosmology we work in electron-volts rather than Joules, where the conversion is  $1\text{J} = 6.242 \times 10^{18}\text{eV}$  and due to the large energy scales required in most of the discussions throughout, we mainly work in units of giga-electron-volts (GeV) which are equivalent to  $10^9\text{eV}$ . We use the mainly positive convention

---

Parameter	Value in standard units	Value in energy units
$t_0$	13.7 Gyr	$6.52 \times 10^{41} \text{ GeV}^{-1}$
$H_0$	$70 \text{ km s}^{-1} \text{ Mpc}^{-1}$	$1.51 \times 10^{-42} \text{ GeV}$
$T_{eq}$	6200 K	$5.34 \times 10^{-10} \text{ GeV}$
$t_{eq}$	61,000 yr	$3.11 \times 10^{35} \text{ GeV}^{-1}$
$M_\odot$	$1.99 \times 10^{33} g$	$1.12 \times 10^{57} \text{ GeV}$

**Table 1.1:** Reference values for cosmological parameters as quoted in Ref. [3].

for the metric signature:  $(-, +, +, +)$  and reference values for commonly used cosmological parameters are shown in Table 1.1.

In Chapters 3 to 8, care is taken to avoid repeating notation unnecessarily but in some instances it is unavoidable. Please note that unless explicitly stated, repeated parameters in separate chapters are unrelated and should be treated as distinct.

# Chapter 2

## Background Theory

### 2.1 Brief History of the Universe

It is generally accepted that the Universe evolved from an initially hot and dense state into the cooler, less dense Universe full of interesting objects we see around us today. This model of the Universe is called the ‘Hot Big Bang’ (HBB) model and includes the fascinating discovery that the Universe is expanding, and has been for its entire history that we are aware of.

The Hot Big Bang model of the Universe has grown from observations of galactic redshift. In 1929, Edwin Hubble [5] constructed his famous velocity-distance relation for nearby galaxies

$$v = H_0 r, \tag{2.1}$$

where  $v$  is the (recessional) velocity of the galaxy,  $r$  is its distance from the observer and  $H_0$  is a constant of proportionality. Hubble’s law, as it came to be called, describes the motion of distant galaxies away from one another. The linearity of Hubble’s law means it is valid for any observer in any galaxy, who will see all other galaxies receding. This means all galaxies are moving away from all other galaxies, as long as they are separated by some minimum distance. We can define the scale factor of the Universe,  $a(t)$ , to parametrise the expansion,

and the Hubble parameter,  $H$ , to quantify the rate of expansion, both of which depend only on cosmic time,  $t$ :

$$H(t) = \frac{\dot{a}(t)}{a(t)}. \quad (2.2)$$

The proportionality constant in Eq. (2.1) is the Hubble parameter at the present time, the Hubble *constant*,  $H_0 \equiv H(t_0)$ . From Hubble's law we can infer that at a distant time in the past everything was much closer together and extrapolating even further, we reach a 'time zero', where everything was infinitely dense, the singularity called the *Big Bang*. A singularity in this sense refers to a point in spacetime where the Einstein equations (introduced in Section 2.2.1) break down and are no longer predictive differential equations [6].

Hubble's law only holds above a certain length scale, taken to be approximately 100 Mpc. On such large scales, the Universe is isotropic and homogeneous, meaning it looks the same in every direction we look in, and this is true from whichever point we choose to observe. This is the 'Cosmological Principle', which will be used as a simplifying assumption throughout sections of this thesis. We also have the 'Copernican Principle', which states that we as observers hold no special place in the Universe. Below these length scales however, the Universe appears to be the exact opposite of isotropic and homogeneous. Descriptions of the Universe are therefore generally separated into two regimes, the 'non-perturbed' at large length scales where the cosmological principle holds and the 'perturbed' at small length scales where it breaks down.

In the non-perturbed regime everything is homogeneous, isotropic and it is relatively simple to describe the entire Universe as a whole using a few equations, as long as quantities are averaged and statistical methods are used. However, in the perturbed regime the Universe is not homogeneous and cannot be treated as a whole. It is necessary to treat different scales individually and assess the behaviour of Universe components on a local, rather than a global, scale. The perturbed regime concerns objects on the scale of galaxy clusters and below. We discuss the primordial origins of these structures in Section 2.4.5 but the majority of this thesis is concerned with the non-perturbed description of the

Universe, following its evolution from the very beginning through to the present day. We start with an overview of what we think we understand about the early Universe.

### 2.1.1 The Very Beginning

Looking back in time towards the beginning of the Universe, we reach a limit of our understanding. As far back as we can sensibly think about we conjecture that the four fundamental forces; electromagnetism, the weak nuclear force, the strong nuclear force and gravity, will be unified in a ‘Theory of Everything’ (ToE).

Going backwards in time from the present day, the electromagnetic and weak forces are successfully unified at the electroweak (EW) scale, at energies of approximately 1 TeV, for which Glashow [7], Salam [8] and Weinberg [9] won the 1979 Nobel Prize. Current particle accelerators are able to probe physics around the EW scale and have confirmed several predictions of the Standard Model of particle physics (SM), cementing its position as the currently accepted theoretical model of physics up to the EW scale.

At earlier times, corresponding to higher energies<sup>1</sup>, we expect the EW and strong nuclear force to unite as well. Theories to describe this are called Grand Unified Theories (GUTs) and the GUT energy scale is around  $10^{16}$  GeV, thirteen orders of magnitude higher than the EW scale which is approximately the limit of our experimental capacity. The main two competing GUT models are the SO(10) [10] and the Pati-Salam [11] models. The Georgi-Glashow SU(5) [12] model is also very popular for its simplicity but the most minimal version of the theory has been ruled out by observations of proton decay, meaning the model now needs to be realised in supersymmetry<sup>2</sup> (SUSY), which itself is an unverified extension of the SM. GUT models predict new particles with masses of the order of the GUT scale. Experiments have not yet detected any of these new particles to verify any predictions, so there is currently no generally accepted GUT model.

Going back in time further, we expect to reach an energy scale where gravity can be combined with the other forces as well and a ToE would be able to de-

---

<sup>1</sup>The Universe becomes hotter as we go back in time,  $T \propto 1/a$  .

<sup>2</sup>An extension to the standard model, introduced in Section 2.5.1.

scribe the four forces united. Gravity is described by general relativity (GR) and the various GUT models use quantum field theory (QFT) descriptions for the electromagnetic, weak and strong nuclear forces. Describing gravity using QFT is referred to as a quantum gravity model. Quantum gravity becomes important at the Planck scale, where the Planck mass, equivalent to the Planck energy in the units of this thesis, is

$$M_{\text{P}} = 1.22 \times 10^{19} \text{ GeV}, \quad (2.3)$$

and defines the scale where general relativity breaks down. Though as noted in Section 1.1, throughout this thesis we use the reduced Planck mass for convenience, defined as

$$m_{\text{Pl}} = \frac{M_{\text{P}}}{\sqrt{8\pi}}. \quad (2.4)$$

String theory [13–15], supergravity [16] and loop quantum gravity [17–19] are all models of quantum gravity, but there is no accepted model of quantum gravity and they are not complete theories. Loop quantum gravity is not considered in this thesis but the applications and limitations of string theory are touched upon in Section 2.8.1.2 and supergravity is introduced in Section 2.5.1 and utilised in Chapters 3, 4 and 7. When our classical description breaks down at such high energies we cannot accurately describe spacetime any more and it is often referred to as spacetime foam [20]. What happens before this point becomes a nonsensical question because time itself is non-linear; the arrow of time is not well defined.

As such, the notion of the Universe starting with the Big Bang singularity becomes less sensible and instead we should view the emergence of the Universe from the spacetime foam into our classical understanding, at approximately the Planck time,  $t_{\text{Pl}}$ , as ‘time zero’, at  $t_{\text{Pl}} \approx 10^{-43} \text{ s}$ .

Hence, we reach an important distinction in terminology. The original use of ‘Big Bang’ for the origin of the Universe refers to the singularity which cannot be described sensibly in our theories. We define the *Hot* Big Bang (HBB) starting at a later time when the Universe contains particles of the SM and starts to resemble a form of the Universe we might recognise. This occurs after a period of cosmological inflation, the overarching topic of this thesis which is introduced

fully in Section 2.4. For now, let us move on with the knowledge that the HBB is distinct from the singularity whose name it closely resembles.

Going forwards in time now from the era of spacetime foam, when the four fundamental forces decouple from each other there are phase transitions due to the breaking of symmetries. As mentioned, the first two phase transitions (expected to be at the Planck scale and the GUT scale respectively) are not well understood because of the uncertainty of beyond SM physics.

When the electromagnetic and the weak nuclear forces decouple, SM particles with mass proportional to the Higgs field expectation value become massive via the Higgs mechanism. The Higgs boson has been observed at particle accelerators [21, 22] and we enter the realm of SM physics which we are able to describe using accepted physics. However, how the earlier phase transitions proceed might have implications for cosmology in the form of dangerous relics and baryogenesis which are addressed in Section 2.3.1. There is also another phase transition in the early Universe called the quantum chromodynamic (QCD) phase transition, below which quarks become bound together into baryons and mesons, which occurs at energy scales of around 150 MeV.

### 2.1.2 The Electro-weak Scale Onwards

From the EW symmetry breaking scale onwards, the Universe is reasonably well understood and described by known physics. These epochs are most often examined from a thermodynamical point of view. The Universe is in a state of high temperature and pressure, with relativistic electrons and high energy photons in thermal equilibrium; the number density of electrons,  $n_e$ , is very high<sup>1</sup> and the interaction rates of different particle species are much higher than the expansion rate of the Universe:

$$\Gamma \gg H, \tag{2.5}$$

where  $\Gamma$  is the interaction rate of a particle species with the thermal bath of the HBB. This means different particle species interact very frequently and local thermal equilibrium is reached before any effects from the expansion of the Universe

---

<sup>1</sup>After the QCD phase transition.

are felt. The interaction rates for different species depend on the temperature, which as mentioned, is cooling as the Universe expands:

$$T \propto t^{-\frac{1}{2}}. \tag{2.6}$$

At different times, different particle species leave thermal equilibrium, as their interaction rates slow and they ‘decouple’ from the thermal bath of particles.

The first known species to decouple are the neutrinos at around 1 MeV, approximately 1 second after the Universe emerges from spacetime foam, which then travel freely through the Universe. Shortly after, when the temperature is lower than the mass of electrons, electron-positron annihilation takes place, which halts some time later due to the baryon asymmetry<sup>1</sup>.

Big bang nucleosynthesis (BBN) describes the initial production of light chemical elements and is generally accepted to begin at around 100 keV, which corresponds to the binding energy of light nuclei. The Universe reaches this temperature about 3 minutes after it emerges from spacetime foam. Before this time, photons in the thermal bath had enough energy for photon-nucleon collisions to photo-disintegrate any nuclei that formed but now, with the subsequent expansion of the Universe, they no longer do. BBN is an inherently interesting but complicated aspect of the early Universe; controlled by many coupled Boltzmann equations. Predicting the final ratios of light elements is a study in numerical cosmology which depends on the relative masses of those elements, the strength of the fundamental forces, the number of relativistic degrees of freedom and most importantly the baryonic density. We will not go into it here except to point out that it is a strong test of fundamental physics in the early Universe. The most relevant aspect for this thesis is the timescale; the photons, electrons, protons and neutrons (and previously positrons and neutrinos) have to exist in thermal equilibrium before  $T \approx 100$  keV, ready for BBN to commence.

Throughout this first part of the Universe history, relativistic particles dominate the energy budget of the Universe and the Universe is in a state of radiation domination. Gradually, non-relativistic matter particles become more and more

---

<sup>1</sup>A mechanism for generating the observed baryon asymmetry, baryogenesis, is an open research question discussed briefly in Section 2.3.1.

numerous, primarily because radiation dilutes more quickly with the expansion of the Universe than matter does, meaning matter eventually comes to dominate. Matter-radiation equality is reached approximately 60,000 years after BBN.

Around 320,000 years after matter-radiation equality, electrons and photons remain coupled together via Thomson scattering. The Universe is almost completely ionised because the photons are very energetic: the ionisation energy of Hydrogen is 13.6eV, and the average photon energy at this time is approximately 60eV, meaning any neutral Hydrogen that does form is quickly ionised again. As the energy of the photons drops with the expansion of the Universe, the Hydrogen nuclei and free electrons begin to combine into neutral Hydrogen without the threat of being re-ionised by the photons.

The physics of this recombination is rather involved (see [23, 24] for the details), but at a certain point the Universe is equally full of ionised and neutral Hydrogen. The time at which this occurs is determined to be recombination,  $t_{\text{rec}}$ . The number density of free electrons has now dropped dramatically, meaning the interaction rate of photons and electrons is greatly reduced (in addition to the dilution from the expansion of the Universe) and so, soon after recombination, we reach ‘decoupling’,  $t_{\text{dec}}$ , when  $\Gamma < H$  for the photons and electrons.

The photons are now able to escape the electrons and travel freely through space, and so  $t_{\text{dec}}$  is also described as the time when the Universe becomes transparent. Even though the photons are no longer coupled to the electrons, they still scatter off free electrons if they encounter them, therefore we have another time defined as the ‘time of last scattering’. Photon diffusion means not all the photons underwent their last scattering at the same time, so their point of last contact occurs at slightly different times resulting in a temporal ‘surface’ of last scattering. The photons travel on geodesics towards the observer and this stream of photons is the Cosmic Microwave Background (CMB), often described as an ‘afterglow’ of the HBB; we will never be able to observe beyond this limit using electromagnetic radiation.

### 2.1.3 The CMB as an Observational Probe

Since the discovery of the CMB in 1964 [25] (predicted by Alpher & Herman in 1948 [26], extending the work of Gamow [27] and recognised by Dicke [28]), different observational experiments have mapped and analysed it. Observations show the CMB spectrum is an almost perfect blackbody with a temperature of 2.73K. The wavelengths of the CMB photons have been redshifted since they were emitted, shifting the peak of the blackbody, and the CMB was released in the early Universe, when temperatures were much hotter than they are today, meaning the photon temperature has been cooling ever since.

The CMB is found to be almost perfectly isotropic, but on angular scales smaller than approximately one degree, anisotropies are present. These anisotropies are an encoding of the density perturbations in the early Universe that go on to form all of the structure in the Universe today and their discovery won John Mather and George Smoot the Nobel Prize in 2006.

Spatial variations in the baryonic density mean photons originating from different regions have slightly different temperatures. The motion of the photons through space is affected by growing inhomogeneities in the gravitational field which also affects their energies. As such, it is possible to correlate temperature fluctuations in the CMB to cosmological perturbations. The intricacies of the CMB are many and varied. We direct the reader to Ref. [29] for the subtleties and only give a brief overview of the relevant aspects here.

Cold dark matter particles do not interact with photons and so in the early Universe they are free to gravitationally cluster and grow. Baryons and photons then fall into these density wells. However, before decoupling, baryons and photons are tightly coupled via the Thomson scattering of electrons. When the baryons fall into a density well and encounter a large number of photons, there is a restorative pressure due to the Thomson scattering of the photons which pushes the baryonic matter back out of the density well. There is a tug of war between the gravitational attraction of the CDM and the photon pressure which means the baryons oscillate in and out of the density well. These oscillations (known as baryonic acoustic oscillations (BAO)) manifest themselves in the CMB and

there is a finite distance the soundwave could have travelled before recombination, which is known as the sound horizon,  $r_s$ .

The soundwave can be decomposed into its Fourier components and different wavelengths will have had time to oscillate a different number of times. The frequency of an oscillation is  $\omega_s = kc_s$  where  $k$  is a wavenumber in the Fourier expansion and  $c_s$  is the sound speed which quantifies the relationship between pressure fluctuations and density fluctuations. Larger scales complete fewer oscillations than smaller scales. Scales which are at the extremum of a compression or rarefaction when the CMB is released appear in the power spectrum of temperature fluctuations as peaks, often referred to as acoustic peaks.

Modelling the evolution of the density perturbations of the early Universe forwards in time allows the power spectrum of temperature fluctuations in the CMB to be recreated. The subtleties of the locations, widths and heights of the peaks depend on the specifics of the Universe model being used. As such, the CMB, as an imprint of the evolution of Large Scale Structure (LSS) in the Universe, is a powerful test of both structure formation and the component densities of the Universe including its curvature. To reproduce the CMB primordial anisotropy, even though a detailed knowledge of the evolution of perturbations is needed, only five cosmological parameters are required. However, the parameters in question are degenerate, meaning the CMB cannot be used to constrain individual cosmological parameters, only combinations of them.

Observations of the CMB provide valuable evidence to support a recent development in the history of the Universe, that of a late-time accelerated expansion. Two separate groups in the 1990s discovered that the Universe expansion is currently accelerating. They were studying distant supernovae and comparing their redshifts at different distances. Their results unequivocally point to a current period of accelerating expansion of the Universe, for which Adam Riess, Brian Schmidt and Saul Perlmutter won the Nobel prize in 2011 [30, 31].

Subsequent detailed analysis of the CMB has allowed the energy content of the Universe to be tightly constrained, and remarkably these observations leave approximately 70% of the energy content of the Universe unaccounted for. It is now generally accepted that the ‘missing’ energy component is responsible for the late-time accelerated expansion of the Universe. Primarily because it must be a

non-luminous substance (to account for the fact we have not observed it) and as a nod to its elusive nature it has been named ‘Dark Energy’, and has recently (relatively speaking) come to dominate the energy content of the Universe and drive the accelerated expansion. Just what this dark energy might be is a hotly debated topic and motivates a large portion of the original research in this thesis in Chapters 7 and 8, it is discussed further in Section 2.8.

First and foremost, analysis of the CMB allows a ‘concordance model of cosmology’ to be formulated;  $\Lambda$ CDM. The acronym combines the cosmological constant,  $\Lambda$ , with Cold Dark Matter, CDM, both of which attempt to shed light on the ‘dark’ aspects of our Universe; dark energy and dark matter respectively. Neither constituent interacts with electromagnetic radiation but it is fair to say their nomenclature arises equally from the fact that little is understood about them. That being said, the  $\Lambda$ CDM concordance model provides a very good description of the Universe we observe around us.

The CMB provides a host of information about the perturbed Universe but also encodes important information on the non-perturbed Universe and its primordial origins. The observational constraints are detailed in Section 2.4.5 and we make use of them continually in the original research presented in this thesis, to analyse and constrain models of the Universe. This thesis is predominantly focused on the non-perturbed regime and the Universe as a whole. It is concerned with the parts of the evolution history which are less well understood than the epoch after the EW symmetry breaking; the time before the HBB, the transition between inflation and radiation domination, and the modern day when the expansion of the Universe again begins to accelerate. To be able to discuss these epochs of the Universe we need a formalism to describe the dynamics of the Universe.

## 2.2 Describing the Dynamics of the Universe

Einstein’s theories of special [32] and general [33] relativity transformed cosmology and the way we think about the Universe. Linking the geometry of spacetime with the motion of mass in the spacetime opened up a world of possibilities with

regards to tracing the evolution of the Universe from its inception to the modern day.

To describe spacetime we use a Lorentzian manifold, which is a topological spacetime that locally resembles Minkowski spacetime. In Minkowski spacetime the reference frame of an inertial observer does not affect the observation and the spacetime interval between events is preserved. A metric,  $g_{\mu\nu}$ , describes the path of geodesics on the manifold, and an object called the energy momentum tensor,  $T_{\mu\nu}$ , describes the dynamics of a test mass on the manifold; the two are related via the Einstein Field Equations (EFE).

### 2.2.1 Einstein Field Equations

The derivation of the EFE follows the least-action principle of classical mechanics, in which an action describing the dynamics of the system is minimised to find the equations of motion (EoM). The Einstein-Hilbert (EH) action yields the Einstein equations:

$$S_{EH} = \frac{m_{\text{Pl}}^2}{2} \int d^4x \sqrt{-g} R, \quad (2.7)$$

where  $g$  is the determinant of the metric,  $g_{\mu\nu}$ ,  $m_{\text{Pl}}$  is the reduced Planck mass and  $R$  is the Ricci curvature scalar. At this point, it would produce the Einstein equation in a vacuum, but to model the real Universe we must include the action for matter:

$$S_{\text{mat}} = \int d^4x \sqrt{-g} \mathcal{L}_{\text{mat}}, \quad (2.8)$$

where  $\mathcal{L}_{\text{mat}}$  is the Lagrangian density for matter. Varying Eqs. (2.7) and (2.8) with respect to the metric tensor, according to the least-action principle,  $\delta S / \delta g_{\mu\nu} = 0$ , yields the EFE:

$$G_{\mu\nu} = m_{\text{Pl}}^{-2} T_{\mu\nu}, \quad (2.9)$$

where we have defined the Einstein tensor

$$G_{\mu\nu} = R_{\mu\nu} - \frac{1}{2} R g_{\mu\nu}, \quad (2.10)$$

and  $T_{\mu\nu}$  is the energy momentum tensor. The Einstein tensor includes the Ricci tensor and scalar,  $R_{\mu\nu}$  and  $R$  respectively, which are related via a tensor contraction

$$R = g^{\mu\nu} R_{\mu\nu}. \quad (2.11)$$

The Einstein, energy momentum and Ricci tensors are all symmetric, meaning they have ten independent components rather than sixteen. The Ricci tensor is equal to the Riemann curvature tensor with contracted first and third indices;  $R_{\mu\nu} = R^{\alpha}{}_{\mu\alpha\nu}$ , which can be expressed in terms of the connection  $\Gamma^{\mu}{}_{\nu\rho}$ , which in turn can be represented in terms of the metric and its derivatives:

$$R^{\mu}{}_{\nu\rho\sigma} = \Gamma^{\mu}{}_{\nu\sigma,\rho} - \Gamma^{\mu}{}_{\nu\rho,\sigma} + \Gamma^{\mu}{}_{\rho\alpha}\Gamma^{\alpha}{}_{\sigma\nu} - \Gamma^{\mu}{}_{\sigma\alpha}\Gamma^{\alpha}{}_{\nu\rho}, \quad (2.12)$$

$$\Gamma^{\mu}{}_{\nu\rho} = \frac{g^{\mu\sigma}}{2} (g_{\nu\sigma,\rho} + g_{\rho\sigma,\nu} - g_{\nu\rho,\sigma}), \quad (2.13)$$

where commas denote partial derivatives, i.e.  $X_{,\mu} = \frac{\partial X}{\partial x^{\mu}}$  with respect to the co-ordinates  $x^{\mu}$ . Hence, to find solutions to the Einstein equations one must specify not only an energy momentum tensor but also a metric. For derivations of Eqs. (2.9), (2.12) and (2.13), we refer the reader to Ref. [34].

The energy-momentum tensor is given by [3]

$$T_{\mu\nu} = g_{\mu\nu}\mathcal{L}_{\text{mat}} - 2\frac{\partial\mathcal{L}_{\text{mat}}}{\partial g^{\mu\nu}}, \quad (2.14)$$

and acts as the source of space-time curvature. It is generally valid to treat the source as a collection of perfect fluids, allowing us to treat the vast collection of particles in the Universe in terms of their bulk quantities. Perfect fluids by definition have no viscosity or heat conduction and the energy momentum tensor is written as [34]

$$T^{\mu\nu} = (\rho + p)U^{\mu}U^{\nu} + pg^{\mu\nu}, \quad (2.15)$$

where  $U^{\mu}$  is the fluid 4-velocity and  $\rho$  and  $p$  are the energy density and pressure defined in the rest frame. In the local rest frame of the fluid (if we are in co-moving co-ordinates where the expansion of the Universe is factored out, defined formally in Eq. (2.42)) the 4-velocity is  $U^{\mu} = (1, 0, 0, 0)^{\text{T}}$  and we can represent

the components of the stress-energy tensor in matrix notation as

$$(T^{\mu\nu})_{\mu,\nu=0,1,2,3} = \begin{pmatrix} \rho & 0 & 0 & 0 \\ 0 & p & 0 & 0 \\ 0 & 0 & p & 0 \\ 0 & 0 & 0 & p \end{pmatrix}. \quad (2.16)$$

The cosmological constant,  $\Lambda$ , can also appear in the EFE as

$$G_{\mu\nu} - \Lambda g_{\mu\nu} = m_{\text{Pl}}^{-2} T_{\mu\nu}. \quad (2.17)$$

As mentioned in the previous section, the cosmological constant is a possible explanation of the observations that the expansion of the Universe is currently accelerating. This is addressed in detail in Section 2.8, as this observation forms a motivation for a large part of this thesis. It appears in the Lagrangian from an extra term in the action

$$S_\Lambda = -m_{\text{Pl}}^2 \int d^4x \sqrt{-g} \Lambda. \quad (2.18)$$

### 2.2.2 F(L)RW Metric Solutions to the EFE

As noted above different solutions to the EFE exist for different metrics and energy momentum tensors, for example solutions describing a vacuum or different types of black holes. For our purposes we need a solution to describe the entire Universe on the largest scales. At face value, solutions to the EFE for particular localised portions of the Universe, such as a black hole, may seem easier to achieve. Describing the entire Universe with one (set of 10) equation sounds very unlikely, but observations of the Universe on the largest scales provide some simplifying assumptions to help.

As introduced in Section 2.1, on the largest scales the Universe is isotropic and homogeneous, and the most general spacetime metric consistent with this is the Friedmann-Lemâitre-Robertson-Walker (FLRW) metric which produces the

line element

$$ds^2 = -dt^2 + a^2(t) \left[ \frac{dr^2}{1 - kr^2} + r^2 d\theta^2 + r^2 \sin^2 \theta d\phi^2 \right], \quad (2.19)$$

where we use co-moving spherical co-ordinates which remain unchanged with any expansion or contraction of space,  $a$  is the scale factor of the Universe and  $k$  is the spatial curvature parameter. The line element shows how the spacetime separation varies with changes in 4-dimensional spacetime.

Specific solutions to the Einstein equations exist for the FLRW metric and the perfect fluid energy momentum tensor (Eq. (2.16)). The temporal-temporal component gives us the first Friedmann equation

$$\left( \frac{\dot{a}}{a} \right)^2 = \frac{\rho}{3m_{\text{Pl}}^2} - \frac{k}{a^2} + \frac{\Lambda}{3}, \quad (2.20)$$

where  $a$  is the scale factor of the Universe,  $\rho$  is the total energy density in the Universe,  $k$  is the spatial curvature parameter and  $\Lambda$  is the cosmological constant. The left hand side of this equation is often rewritten as  $H^2$ , the Hubble parameter introduced in Eq. (2.2).

Any one of the three temporal-spatial components of the Einstein equations produce the same equation

$$\frac{\ddot{a}}{a} + \frac{1}{2} \left( \frac{\dot{a}}{a} \right)^2 = -\frac{p}{2m_{\text{Pl}}^2} + \frac{\Lambda}{2} - \frac{k}{2a^2}, \quad (2.21)$$

which when combined with Eq. (2.20) produces the second Friedmann equation, often called the acceleration equation:

$$\frac{\ddot{a}}{a} = -\frac{1}{6m_{\text{Pl}}^2}(\rho + 3p) + \frac{\Lambda}{3}. \quad (2.22)$$

The two Friedmann equations describe the evolution of a homogeneous, isotropic Universe, with components which can be described as perfect fluids, meaning they can be represented by the energy-momentum tensor in Eq. (2.16).

Local conservation of energy implies the covariant divergences of the energy momentum tensor must be zero, i.e.  $\nabla_\mu T^{\mu\nu} = 0$  which enables us to derive an evolution equation for the energy density of the perfect fluid, defined as the continuity equation

$$\dot{\rho} + 3H(\rho + p) = 0. \quad (2.23)$$

The three equations, Eqs. (2.20), (2.22) and (2.23) are not independent, in fact Eq. (2.23) can be obtained by taking the time derivative of Eq. (2.20) and substituting in Eqs. (2.20) and (2.22). As such we have two independent equations (generally taken to be Eq. (2.20) and Eq. (2.23)) comprised of three unknowns: the scale factor, the energy density and the pressure. To be able to solve them for the evolution of the Universe it is necessary to eliminate an unknown. Fortunately, perfect fluids have a simple equation of state which describes the relationship between the energy density and pressure

$$p = w\rho, \quad (2.24)$$

where  $w$  is a dimensionless number restricted to the values<sup>1</sup>  $-1 \leq w \leq 1$ , called the barotropic equation of state parameter.

### 2.2.3 The Evolution of the Universe

Introducing a relationship between the energy density and the pressure allows us to replace  $p$  in Eq. (2.23) to see how the energy density of the Universe scales with the cosmic scale factor:

$$\rho(a) \propto a^{-3(1+w)}, \quad (2.25)$$

---

<sup>1</sup>The upper limit arises from the sound speed, which for adiabatic perturbations in a gas is given by  $c_s^2 = c^2 \left(\frac{dp}{d\rho}\right)$ . For a substance with  $w > 0$  this becomes  $c_s = \sqrt{w}c$  and hence  $w \leq 1$  to ensure causality is not violated. The lower limit arises because a substance with negative pressure is ill-defined as a perfect fluid which obeys the null energy condition, if the null energy condition is violated  $w < -1$  is not a problem, as in phantom dark energy [35]; in fact, observations may support  $w < -1$ .

for constant  $w$ . Non-relativistic (matter) and relativistic (radiation) particles in the Universe can both be approximated as a perfect fluid, with  $w = 0$  and  $w = 1/3$  respectively. Hence, their energy densities scale as

$$\rho_m \propto a^{-3}, \quad (2.26)$$

$$\rho_r \propto a^{-4}. \quad (2.27)$$

The cosmological constant can also be modelled as a perfect fluid which is time invariant as

$$\rho_\Lambda = m_{\text{Pl}}^2 \Lambda, \quad (2.28)$$

because (as the name implies),  $\Lambda$  is a constant.

It is often convenient to write the Friedmann equation in a dimensionless form. We define the critical density of the Universe, defined as the density a flat Universe would have for a particular value of the Hubble parameter, as  $\rho_{\text{crit}} = 3m_{\text{Pl}}^2 H^2$ . If we divide the Friedmann equation, Eq. (2.20), by  $H^2$ , we can express it in terms of dimensionless density parameters,  $\Omega_i$ :

$$1 = \Omega_m + \Omega_r + \Omega_K + \Omega_\Lambda, \quad (2.29)$$

where

$$\Omega_m = \frac{\rho_m}{\rho_{\text{crit}}}, \quad \Omega_r = \frac{\rho_r}{\rho_{\text{crit}}}, \quad \Omega_K = -\frac{k}{a^2 H^2} \quad \text{and} \quad \Omega_\Lambda = \frac{\Lambda}{3H^2}. \quad (2.30)$$

If we define the dimensionless quantities at the present time, with the subscript ‘0’, we can use the scaling relationships defined in Eq. (2.25) to express the Friedmann equation as a time-dependent function:

$$\frac{H^2}{H_0^2} = \Omega_{m,0} \left(\frac{a}{a_0}\right)^{-3} + \Omega_{r,0} \left(\frac{a}{a_0}\right)^{-4} + \Omega_{K,0} \left(\frac{a}{a_0}\right)^{-2} + \frac{\Lambda}{3H_0^2}, \quad (2.31)$$

where the third term in Eq. (2.30) demonstrates the scaling behaviour of  $\Omega_k$ .

The eventual fate of the Universe depends on the behaviour of the cosmic scale factor. Presuming for a moment that  $\Lambda = 0$  and the final term in Eq. (2.31)

is omitted, we see that the terms proportional to the energy density of matter and radiation decrease proportionally faster than the curvature term which scales as  $a^{-2}$ . As such, throughout the evolution of the Universe the curvature term becomes increasingly important until it dominates the Friedmann equation and controls the fate of the Universe. Rewriting Eq. (2.29) as

$$1 - \Omega = -\frac{k}{(aH)^2}, \quad (2.32)$$

where  $\Omega$  contains all contributions to the energy density except curvature, we can see that the curvature of the Universe controls the final value of  $\Omega$ . The critical density,  $\rho_{\text{crit}} = 3m_{\text{Pl}}^2 H^2$ , introduced above is defined to be the energy density of the Universe if it is perfectly flat; energy density above or below this value will result in a ‘closed’ or ‘open’ Universe:

- $k > 0$ :       $\Omega > 1$ ,      Closed Universe ,
- $k = 0$ :       $\Omega = 1$ ,      Flat Universe ,
- $k < 0$ :       $\Omega < 1$ ,      Open Universe .

A closed Universe is one which contains more energy density than that required for a perfectly flat Universe. The excess energy density acts to positively curve the geometry of the Universe. An open Universe is one containing less energy density than a perfectly flat Universe, acting to negatively curve the geometry of the Universe and allowing it to expand forever as  $H > 0$  always. A flat Universe is the intermediary case, where  $H_{t \rightarrow \infty} \rightarrow 0$ , but as the ultimate  $t$  is assumed to be infinite this also results in an ever expanding Universe.

In a flat Universe with no cosmological constant, Eq. (2.20) simplifies to  $3m_{\text{Pl}}^2 H^2 = \sum_i \rho_i$  where  $i$  represents the individual components of the Universe and we can find how the scale factor evolves with time if we substitute in Eq. (2.25) and integrate the result:

$$a \propto t^{\frac{2}{3(1+w)}}, \quad (2.33)$$

where  $w$  is the barotropic equation of state parameter of the dominant fluid the Universe and so depends on the relative energy densities of the different

components of the Universe and which is dominant. This equation is only valid for  $w > -1$ . From this we can also see the Hubble parameter evolves as

$$H = \frac{2}{3(1+w)t}. \quad (2.34)$$

We are now equipped with the tools to describe the dynamics of our Universe and we return to the HBB to critically assess a few shortcomings of the model which motivate the introduction of ‘inflation’, the main topic of this thesis which has so far only been alluded to.

## 2.3 Problems with the HBB

The HBB model explains many of the observations about our Universe, from the expansion itself to the presence of the CMB and the intricacies of BBN. However, there are aspects which it does not explain. The three main issues left unanswered by the HBB are the flatness problem, the horizon problem and the origin of structure in the Universe.

### 2.3.1 Flatness Problem

The crux of the flatness problem is that we live in a Universe which is very, very close to being exactly flat. However, throughout the history of our Universe, as the HBB model accounts for it, the curvature of the Universe evolves *away* from being exactly flat. Hence, for the initial curvature of the Universe to have been even *closer* to being exactly flat to start with, it appears to have been incredibly fine-tuned. The 2018 Planck satellite data release found  $\Omega_K = -0.056_{-0.050}^{+0.044}$  and, upon combining CMB measurements with BAO data, is consistent with  $\Omega_K = 0.0007_{-0.0037}^{+0.0037}$ , both at the 95% confidence level [4].

Using

$$\Omega_K \equiv -\frac{k}{a^2 H^2}, \quad (2.35)$$

we can see how  $\Omega_K$  changes over time. From Eqs. (2.33) and (2.34) we know  $a \propto t^{1/2}(t^{2/3})$  during radiation (matter) domination and  $H \propto 1/t$  in both. As

such we find  $\Omega_K \propto t(t^{2/3})$  during radiation (matter) domination; growing in both. If  $\Omega_K$  has been growing through radiation and matter domination, but is observed to be less than 0.001 today, it must have been extremely small at early times.

We can calculate an approximate value for how small by equating the spatial curvature of the Universe at previous times with today, and writing the evolution of the normalised density parameter as

$$1 - \Omega(t) = \left( \frac{a_0 H_0}{a H} \right)^2 (1 - \Omega_0). \quad (2.36)$$

In periods of the Universe history where radiation and/or matter dominate we know from Eq. (2.31):

$$\frac{H^2}{H_0^2} = \Omega_{r,0} \left( \frac{a_0}{a} \right)^4 + \Omega_{m,0} \left( \frac{a_0}{a} \right)^3, \quad (2.37)$$

meaning we can rewrite Eq. (2.36) as

$$1 - \Omega(t) = \frac{a^2}{a_0^2} (1 - \Omega_0) \left( \Omega_{r,0} + \frac{a}{a_0} \Omega_{m,0} \right)^{-1}. \quad (2.38)$$

At the Planck time, as far back as we can sensibly go without accounting for quantum gravity, we have  $\frac{a_{Pl}}{a_0} \simeq \frac{T_0}{T_{Pl}} \simeq \frac{10^{-13} \text{ GeV}}{M_P} \simeq 10^{-32}$ . Substituting this into Eq. (2.38) gives

$$|\Omega_K(t_{Pl})| = |1 - \Omega(t_{Pl})| \simeq 10^{-62}. \quad (2.39)$$

Hence, because the density parameter grows as a power law during the radiation and matter dominated eras since the HBB, using  $\Omega_{K,0} \simeq 10^{-4}$ , the Universe was originally at least  $10^{58}$  times flatter than we observe today. The standard HBB model offers no explanation for this level of fine-tuning, which is called the Flatness Problem.

### 2.3.2 Horizon Problem

The horizon problem stems from the fact that light travels at a finite speed and so particles travelling at light speed can only travel a finite distance in a particular length of time. Observations of the CMB cannot be explained by extrapolating the distances travelled by photons backwards using the standard HBB.

Light rays follow null geodesics, meaning the line element  $ds^2 = 0$ . The flat FLRW metric in Cartesian co-ordinates thus rearranges to

$$dt^2 = a^2(dx^2 + dy^2 + dz^2). \quad (2.40)$$

If the light ray is only travelling spatially in the  $x$ -direction, then between time  $t_1$  and  $t_2$  it will travel a distance of

$$x = \int_{t_1}^{t_2} \frac{dt}{a(t)}, \quad (2.41)$$

where  $x$  is the co-moving distance, related to the physical distance<sup>1</sup>,  $r$ , by

$$r = a(t)x. \quad (2.42)$$

At a particular time, this distance defines the observable Universe and it is called the (co-moving) cosmological horizon,  $D_H(t)$ . Depending on the limits taken for the integration this can be either a particle horizon or an event horizon. A particle horizon defines the distance light could have travelled until today and an event horizon defines the distance light may ultimately travel in the future. To be able to find  $D_H(t)$  we need to know the dependence of  $a$  on  $t$ , which is different for different epochs of the Universe evolution, as per Eq. (2.33). We can define the limits in two ways:

$$\text{Particle Horizon : } D_H(t_0) = a(t_0) \int_{t_i}^{t_0} \frac{dt}{a(t)} \quad t_i \ll t_0, \quad (2.43)$$

---

<sup>1</sup>Note this is *not* the co-moving distance ‘ $r$ ’ in spherical co-ordinates from Eq. (2.19).

$$\text{Event Horizon : } \quad D_H(t_0) = a(t_0) \int_{t_0}^{t_f} \frac{dt}{a(t)} \quad t_0 \ll t_f. \quad (2.44)$$

The cosmological horizon can only ever be a particle horizon or an event horizon, never both. As an example, consider the Universe in the matter-dominated era with  $w = 0$ . Using Eq. (2.33), the particle horizon is then

$$D_H(t_0) = Ct_0^{2/3} \int_0^{t_0} C^{-1}t^{-2/3}dt = 3t_0, \quad (2.45)$$

where  $C$  is a constant of proportionality arising from the  $a = Ct^{\frac{2}{3(1+w)}}$  substitution which cancels out in the following calculations. In contrast, the event horizon is undefined as

$$D_H(t_0) = t_0^{2/3} \int_{t_0}^{t_f} t^{-2/3}dt \quad \xrightarrow[t_f \rightarrow \infty]{} \quad \infty. \quad (2.46)$$

Conversely, for an era of the Universe with  $w < -1/3$ , we see the opposite is true. If we use  $w = -1/2$  the particle horizon is

$$D_H(t_0) = t_0^{4/3} \int_{t_i}^{t_0} t^{-4/3}dt \quad \xrightarrow[t_i \rightarrow 0]{} \quad \infty, \quad (2.47)$$

but the event horizon is now defined as

$$D_H(t_0) = t_0^{4/3} \int_{t_0}^{\infty} t^{-4/3}dt = 3t_0. \quad (2.48)$$

For a region of the CMB to be in thermal equilibrium, the photons must have been in causal contact at some point in their history. Observations of the CMB show an almost perfectly uniform temperature across the entire sky, an homogeneity we use to great advantage when we use the FLRW metric to describe the Universe. The observations are obtained via experiments such as COBE [36], WMAP [37] and Planck [38] and are independent of the cosmological theory, meaning a cosmological explanation is required.

In the standard HBB cosmology the Universe is dominated by radiation in the era preceding CMB emission. When the CMB is produced the particle horizon has a finite value of  $2t_{\text{LSS}}$ , where  $t_{\text{LSS}}$  is the time of last scattering for the photons

of the CMB. This means the CMB photons have only been able to travel this finite distance in the history of the Universe. Regions of the CMB separated by more than this distance at the time of last scattering could never have interacted with each other. The standard HBB cosmology cannot explain why the CMB is almost perfectly homogeneous over distances much greater than this, which is the Horizon Problem.

### 2.3.3 The Origin of Structure

The Universe today contains complex structure and detailed inhomogeneities on sub-galactic scales. Inhomogeneities grow from density perturbations in the early Universe and we can define a density contrast by

$$\delta(\mathbf{x}) = \frac{\rho(\mathbf{x}) - \bar{\rho}}{\bar{\rho}}. \quad (2.49)$$

Taking a Fourier decomposition of the density perturbation field gives

$$\delta(\mathbf{x}) = \int \delta(\mathbf{k}) e^{-i\mathbf{k}\cdot\mathbf{x}} d^3\mathbf{k}, \quad (2.50)$$

where  $k = |\mathbf{k}|$  is the co-moving wavenumber<sup>1</sup>, which is related to the physical wavelength of a perturbation via

$$\lambda_{\text{phys}} = \frac{2\pi a}{k}, \quad (2.51)$$

so we see the physical wavelength grows proportional to the scale factor of the Universe. The horizon is always proportional to  $t$ , which grows as  $a^{3/2}$  during matter domination and  $a^2$  during radiation domination. As shown in Fig. 2.1, scales we observe within the horizon today originated from outside of the horizon. This presents us with a second horizon problem because, as discussed in the last section, super-horizon means outside of causal contact but the COBE satellite

---

<sup>1</sup>Note this is *not* the spatial curvature parameter used in the previous section.

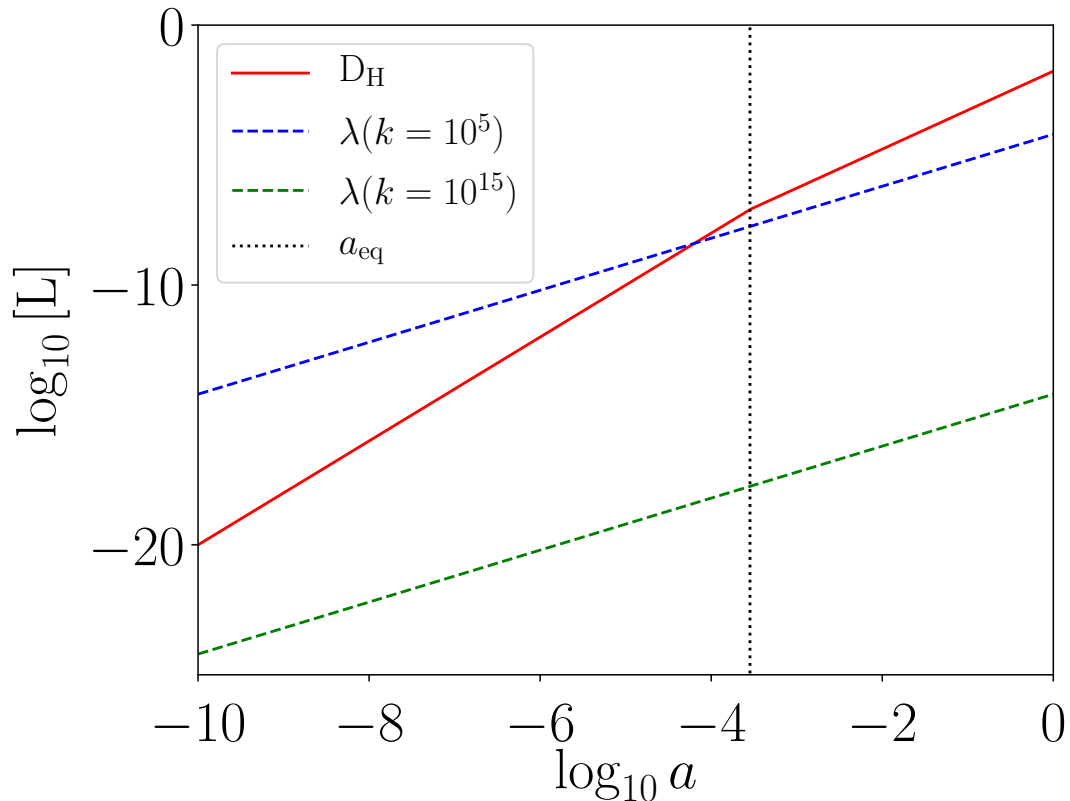


**Figure 2.1:** Depicts how two different physical wavelength scales grow with the scale factor, and the corresponding behaviour of the horizon in the radiation dominated and matter dominated eras.

[36] observed a spectrum of density perturbations which is scale invariant, with Fourier amplitudes of  $\mathcal{O}(10^{-5})$  across all scales.

For scales which have not been in causal contact, we would expect  $\delta(k)$  to have a random distribution of values, with no correlation over different scales. The HBB model therefore provides no explanation for this scale invariance. Secondly, the HBB model has no explanation for the origin of the perturbations, so not only are they being generated with a scale invariant spectrum, but there is no explanation for why they exist at all, which amounts to a severe fine-tuning problem within the HBB.

### 2.3.4 Additional Considerations for the HBB

The problem of the origin of structure in the Universe is closely followed by the problem of the observed baryon asymmetry in the Universe. We expect matter and antimatter to be produced equally in the early Universe but the Universe we observe contains an imbalance of matter. Mechanisms to explain this are theories of baryogenesis which is an open research area in its own right. We do not investigate it in detail in this thesis but the main point to note is that baryogenesis requires a period of Universe evolution which is outside of thermal equilibrium. In the HBB model, the only candidate is the EW phase transition, but baryogenesis at the EW phase transition is very constrained and generally points to extensions to the SM being required [3].

Historically, another concern was the monopole problem. A magnetic monopole is a theoretical particle that consists of only one pole of a magnet. It is a form of topological defect that can be formed during symmetry breaking in the early Universe. Topological defects are boundaries, in a sense, which occur when a symmetry is broken and a field has different values in neighbouring regions of space. This can occur suddenly and violently if it is a first-order phase transition or relatively smoothly if it is a second-order phase transition. If monopoles exist they pose a problem because their energy density would act to overclose the Universe. However, the creation of monopoles is dependent on the symmetry group of the GUT, which is unknown so we do not know that monopoles (and other dangerous relics) are necessarily a problem. They are generally not viewed as a major shortcoming of the HBB model any more.

## 2.4 Introducing Inflation

The problems with the HBB detailed in the last section are neatly remedied by a disarmingly simple idea, a period of accelerating expansion in the very early Universe. We have been alluding to this phenomenon since the beginning of the thesis; it is called ‘cosmic inflation’ and we now introduce it fully. When referring to a period of cosmic inflation occurring before the traditional HBB, as opposed to a period of late-time accelerated expansion which we explore in Section 2.8, or

a second period of accelerated expansion after reheating, explored in Section 2.7, it is called *primordial* cosmic inflation.

When talking about the acceleration of the expansion, it is useful to think about the behaviour of the scale factor of the Universe. When  $\ddot{a} > 0$  (introduced in far greater detail momentarily in Section 2.4.2) the expansion is accelerating. Accelerating expansion may take many forms, a simple example is power-law inflation [39] where  $a \propto t^p$  for  $p > 1$ , but this is now ruled out by observations of the scale invariance of perturbations generated during inflation (see Section 2.4.5).

The type of inflation most supported by observations is quasi de-Sitter inflation, where  $a \propto e^{Ht}$ . Perfectly exponential accelerated expansion is called a ‘de-Sitter’ spacetime, a vacuum solution of the Einstein equations with a negative pressure substance as its dominant component. A real de-Sitter Universe would be exponentially accelerating forever, without any matter or radiation present. The inflation posited to have occurred in our Universe is hence ‘quasi’ de-Sitter because it comes to an end and the Universe is not empty.

### 2.4.1 Solving the Problems of the HBB

We address the problems of the HBB model from Section 2.3 in order; first, the flatness problem. During quasi de-Sitter expansion the scale factor of the Universe grows as

$$a \propto e^{Ht}, \quad (2.52)$$

and  $H \approx \text{constant}$ . Therefore from Eq. (2.35):

$$\Omega_K \equiv -\frac{k}{a^2 H^2} \propto e^{-2Ht}. \quad (2.53)$$

Throughout inflation  $\Omega_K$  is exponentially suppressed. This explains very naturally why  $\Omega_K$  is so small today and also means the Universe can start with arbitrary curvature before inflation.

Secondly, the horizon problem is solved because the history of the Universe before the LSS now contains a period of quasi de-Sitter expansion with  $a \propto e^{Ht}$ .

The horizon is expressed as

$$\begin{aligned}
 D_H(t_0) &= a(t_0)x = a(t_0) \int_{t_i}^{t_f} C e^{-Ht} dt = e^{Ht_0} \left[ \frac{-e^{-Ht}}{H} \right]_{t_i}^{t_f} \\
 &= \frac{-e^{Ht_0}}{H} (e^{-Ht_f} - e^{-Ht_i}). \quad (2.54)
 \end{aligned}$$

The particle horizon ( $t_i = -\infty$ ,  $t_f = t_0$ )<sup>1</sup> is therefore undefined because

$$D_H(t_0) = \frac{-e^{Ht_0}}{H} (e^{-Ht_0} - e^{-Ht_i}) \xrightarrow{t_i \rightarrow -\infty} \infty, \quad (2.55)$$

but the event horizon ( $t_1 = t_0$ ,  $t_2 = \infty$ ) is now well defined:

$$D_H(t_0) = \frac{-e^{Ht_0}}{H} (e^{-H\infty} - e^{-Ht_0}) = \frac{1}{H} \approx \text{const}. \quad (2.56)$$

When inflation occurs, it takes causally connected regions and increases their separation exponentially, meaning the entire CMB we observe originated from a region of space that was once in causal contact, thereby explaining the temperature isotropy.

In a similar way, the physical wavelengths proportional to  $a$  stretch to large length scales and perturbations which are initially inside the horizon become super-horizon during inflation. Furthermore, the mechanism for the accelerated expansion, as we will see in the next section, is thought to be a quantum scalar field. Quantum fluctuations of the field during inflation, a product of the Heisenberg uncertainty principle, very naturally explain the presence of fluctuations in the quantum field driving inflation. Within the horizon, quantum fluctuations of the field oscillate but if they pass outside of the causal horizon they are ‘frozen in’ to the field, at which point we treat it as a classical perturbation whose amplitude is preserved until it re-enters the horizon.

As we saw in Section 2.3.2, during radiation domination (RD) and matter domination (MD) the horizon grows again meaning perturbations will re-enter the horizon and begin to evolve again, going on to form the structure we see

<sup>1</sup>At the Big Bang  $a \rightarrow 0$  which requires  $t \rightarrow -\infty$  in  $a \propto e^{Ht}$ .

in the Universe. As mentioned in Section 2.1.3, the temperature fluctuations of the CMB are a tracer of density perturbations in the early Universe, allowing us to constrain aspects of the Universe evolution and primordial inflation, they are addressed in more detail in Section 2.4.5.

Before inflation was postulated, the origin of density perturbations in the Universe was essentially put in by hand, a necessary initial condition as it were. One of the most remarkable things about inflation is that it not only explains the origin of the perturbations, but it predicts the spectrum. This allows us to distinguish between different inflationary models by contrasting predictions about the spectrum with observations.

Finally, inflation solves the monopole problem in a reasonably simplistic way, if inflation occurs at an energy scale lower than that of GUT symmetry breaking. Monopoles formed during the phase transition are inflated away. Monopoles are expected to be separated by approximately the distance of  $H^{-1}$  at the time of their creation, which is much more than the observable Universe. As such, one monopole within the particle horizon *then* is now, at most, one monopole within the observable Universe, which does not threaten to overclose the Universe. As such, monopoles should perhaps more accurately be viewed as a constraint on the symmetry group of the GUT if the symmetry breaking scale is lower than the inflationary energy scale, or unimportant for cosmology if not.

## 2.4.2 Accelerated Expansion with a Scalar Field

Examining the equations controlling the dynamics of the Universe we see that for increasing acceleration we need  $\ddot{a}$  to be positive. From Eq. (2.22) (setting  $\Lambda = 0$ ), because  $a$  is always positive we see the sum of the energy densities and pressure in the Universe must be negative. If we do not want to have negative energy density<sup>1</sup>, we require the dominant contribution to the pressure in the Universe to be negative enough. Extending this, we can rewrite Eq. (2.22) in terms of the equation of state parameter and see  $1 + 3w < 0$  and hence for accelerated

---

<sup>1</sup>Though it is possible for the vacuum energy density to be negative if  $\Lambda < 0$ , see e.g. [40, 41].

expansion:

$$w < -1/3. \quad (2.57)$$

A component which is able to satisfy this condition is a scalar field, which has a Lagrangian of the form

$$\mathcal{L} = \frac{1}{2} \left( \frac{\partial\phi}{\partial t} \right)^2 - \frac{1}{2} (\nabla\phi)^2 - V(\phi), \quad (2.58)$$

where the first term represents the kinetic energy density, the second the gradient energy density, with  $\nabla$  representing the physical spatial derivatives, and the third term is the potential energy density.

We presume<sup>1</sup> that the Universe is *almost* homogeneous and so we set the spatial dependencies of Eq. (2.58) to zero. The pressure and energy density of a homogeneous scalar field are defined as

$$p = \frac{1}{2} \dot{\phi}^2 - V(\phi), \quad (2.59)$$

$$\rho = \frac{1}{2} \dot{\phi}^2 + V(\phi). \quad (2.60)$$

Requiring the pressure of the scalar field to be negative means requiring  $V(\phi) > \frac{1}{2} \dot{\phi}^2$ . For accelerated expansion we therefore require the energy density of a scalar field to dominate the energy budget of the Universe, whilst its potential energy density is greater than its kinetic energy density. The scalar field in an inflationary model is referred to as the ‘inflaton’ and controls the dynamics of inflation.

---

<sup>1</sup>The initial conditions before inflation are not known, indeed presuming homogeneous initial conditions may be a fine-tuning problem in itself, undermining the fine-tuning of initial conditions (of the HBB) that inflation purports to solve. The initial conditions of inflation are an active area of research, a recent computational investigation is conducted in Ref. [42].

### 2.4.3 Slow-roll Inflation

For a scalar field, the action is

$$S_\phi = -\frac{1}{2} \int d^4x \sqrt{-g} [\partial_\mu \phi \partial^\mu \phi + 2V(\phi)], \quad (2.61)$$

which we can minimise to find the equation of motion (EoM)

$$\ddot{\phi} + 3H\dot{\phi} + V'(\phi) = 0, \quad (2.62)$$

which is the Klein-Gordon (KG) equation. This can also be derived from the conservation of the energy momentum tensor in Eq. (2.23). The Klein-Gordon equation resembles the EoM for a ball rolling down a slope in classical mechanics, so the motion of the scalar field along its potential in field space is often likened to a ball slowly rolling along a gradual slope. It is then called ‘slow-roll inflation’. Options other than a slowly-rolling scalar field driving a period of accelerating expansion exist (the ekpyrotic universe [43], string gas cosmology [44] and bouncing cosmologies [45] to name a few) but the slowly-rolling scalar field is the simplest and most compelling which is able to explain observations.

The time variation of the scalar field depends on the slope of the potential and the rate of expansion of the Universe, which oppose each other in the EoM. Similarly to the radiation and matter components of the Universe, a homogeneous scalar field can also be described as a perfect fluid. This means we can model a scalar field in the Friedmann equations using the definition of its energy density given in Eq. (2.60). The Friedmann equation for the Universe at this time is dominated by the energy density of the inflaton, and as such is simply

$$3m_{\text{Pl}}^2 H^2 = \frac{\dot{\phi}^2}{2} + V(\phi). \quad (2.63)$$

We can quantify the length of time inflation lasts for in a few different ways. Firstly, we can define

$$\epsilon_H = -\frac{\dot{H}}{H^2} = \frac{d \ln H}{dN}, \quad (2.64)$$

which is a direct test of inflation arising from the requirement  $\ddot{a} > 0$ . In the second equality<sup>1</sup> we have introduced the quantity ‘ $N$ ’ which is the number of e-folds of inflation, defined as

$$\frac{a(t)}{a(t_{\text{end}})} \simeq e^{-N(t)}, \quad (2.65)$$

where the subscript ‘end’ refers to the end of inflation; it is conventional to count e-folding numbers backwards so that at the end of inflation  $N = 0$  and ‘ $N$ ’ encodes the number of e-folds left until the end of inflation. Secondly, we can define a parameter

$$\eta_H = -\frac{d \ln \epsilon_H}{dN} = \frac{\dot{\epsilon}_H}{H \epsilon_H}, \quad (2.66)$$

which is a check that inflation lasts for a sufficiently long time. Finally, we can define the acceleration per Hubble time

$$\delta_H = -\frac{\ddot{\phi}}{H \dot{\phi}}. \quad (2.67)$$

Assuming nothing about slow-roll so far, we can express  $\eta_H$  in terms of the other two parameters as

$$\eta_H = 2(\epsilon_H - \delta_H), \quad (2.68)$$

where we have used

$$\dot{H} = -\frac{\dot{\phi}^2}{2m_{\text{Pl}}^2}, \quad (2.69)$$

obtained by differentiating Eq. (2.63) with respect to time and using

$$\dot{\epsilon}_H = \frac{\dot{\phi} \ddot{\phi}}{m_{\text{Pl}}^2 H^2} - \frac{\dot{\phi}^2 \dot{H}}{m_{\text{Pl}}^2 H^3}, \quad (2.70)$$

obtained by differentiating Eq. (2.64) with respect to time.

---

<sup>1</sup>The Hubble parameter,  $H$  is not dimensionless so there is an implicit normalisation omitted from this equation, which formally should be written as the logarithm of  $H/H_0$  where  $H_0$  is some constant value (not the Hubble constant).

From Eq. (2.69) we can write Eq. (2.64) in the form

$$\epsilon_H = \frac{\dot{\phi}^2}{2m_{\text{Pl}}^2 H^2}, \quad (2.71)$$

which makes it clear that  $\epsilon_H < 1$  corresponds to  $\dot{\phi}^2 < V$ . In this way  $\{\epsilon, |\delta|\} \ll 1$  characterises a period of slow-roll inflation, during which we can make two simplifying assumptions

$$\ddot{\phi} \ll 3H\dot{\phi}, \quad (2.72)$$

$$\frac{1}{2}\dot{\phi}^2 \ll V(\phi), \quad (2.73)$$

which are known as the slow-roll assumptions. These then simplify the Friedmann equation to

$$3m_{\text{Pl}}^2 H^2 \simeq V(\phi), \quad (2.74)$$

and the KG equation (Eq. (2.62)) for the evolution of the scalar field to

$$\dot{\phi} \simeq -\frac{V'(\phi)}{3H}. \quad (2.75)$$

The slow-roll simplifications to the Friedmann and KG equations allow us to re-express the Hubble parameters for successful inflation in terms of the scalar field potential and its derivatives as

$$\epsilon_H \simeq \frac{m_{\text{Pl}}^2}{2} \left( \frac{V'}{V} \right)^2 \equiv \epsilon_V, \quad (2.76)$$

$$\delta_H + \epsilon_H \simeq m_{\text{Pl}}^2 \frac{V''}{V} \equiv \eta_V, \quad (2.77)$$

where we write approximately equal to because the equalities only hold in the regime of slow-roll. In this way, if the Hubble (subscript ‘ $H$ ’) and potential (subscript ‘ $V$ ’) definitions are equivalent, the slow-roll inflation assumptions are valid. For slow-roll inflation we hence also require:

$$\epsilon_V \ll 1 \quad |\eta_V| \ll 1. \quad (2.78)$$

Using Eqs. (2.59) and (2.60) we express the equation of state parameter for a scalar field as

$$w + 1 = \frac{p}{\rho} + 1 = \frac{\dot{\phi}^2}{\frac{1}{2}\dot{\phi}^2 + V}, \quad (2.79)$$

which allows us to recast  $\epsilon_H$  from Eq. (2.71) as

$$\epsilon_H = \frac{3}{2}(w + 1). \quad (2.80)$$

Additionally, the second derivative of a scalar field potential describes the mass squared of the scalar field. Rewriting Eq. (2.77) with  $V \simeq 3m_{\text{pl}}^2 H^2$  shows us that slow-roll inflation requires a light scalar field compared to the Hubble scale:

$$V'' \equiv m_\phi^2 \ll 3H^2. \quad (2.81)$$

#### 2.4.4 How Much Slow-roll Inflation?

From the definitions of the slow-roll parameters in the previous section, it is clear the slope of the potential has great bearing on the dynamics of slow-roll inflation. In general, the flatter the potential the longer inflation lasts. To solve the flatness and horizon problems introduced in Section 2.3 requires inflation to last a minimum of 50-60 e-foldings. Inflation could have lasted for any length of time greater than this but we have no way of observing it yet because the observable scales re-entering the horizon today only left about 60 e-folds ago.

To investigate the duration of inflation we rewrite the e-folding number in Eq. (2.65) as

$$N_{\text{tot}} = \int_{t_{\text{end}}}^{t_{\text{beg}}} H dt. \quad (2.82)$$

The times in this integration are unknown and so we change the variable ‘ $t$ ’ to one we can more easily describe, the field value of the inflaton, for which we have an evolution equation (the KG equation):

$$N_{\text{tot}} = \int_{\phi_{\text{end}}}^{\phi_{\text{beg}}} \frac{H}{\dot{\phi}} d\phi, \quad (2.83)$$

and from the relationship between  $\dot{H}$  and  $\dot{\phi}$  in Eq. (2.69) we can write this as

$$N_{\text{tot}} = \frac{1}{\sqrt{2}m_{\text{Pl}}} \int_{\phi_{\text{end}}}^{\phi_{\text{beg}}} \frac{1}{\sqrt{\epsilon_H}} d\phi, \quad (2.84)$$

which defines the total number of inflationary e-folds.

If the Universe is in a period of slow-roll inflation, we can use the relationship between the Hubble slow-roll parameters and the potential slow-roll parameters to see:

$$N_{\text{tot}} = \frac{1}{m_{\text{Pl}}^2} \int_{\phi_{\text{end}}}^{\phi_{\text{beg}}} \frac{V(\phi)}{V'(\phi)} d\phi, \quad (2.85)$$

where ‘beg’ and ‘end’ now refer to the beginning and end of the slow-roll period of inflation.

The end of inflation is identified with the end of the slow-roll regime; when the constraints in Eq. (2.78) no longer hold. Unsurprisingly, from the definitions in the previous section, inflation ends when the potential is no longer flat enough for the potential energy density to dominate over the kinetic energy.

At this point the Universe is very flat, with all entropy and pre-existing fields diluted away, and very cold<sup>1</sup>. The Universe needs to ‘reheat’ itself - transfer its energy from the scalar field driving inflation to the particles of the standard model to produce the HBB scenario and allow the Universe evolution to continue to the present day. Reheating is addressed in detail in Section 2.7.

When the evolution of the Universe after inflation is specified, there exists a way to extrapolate the number of e-folds of inflation, via the relationship

$$\frac{k}{a_0 H_0} = \frac{a_* H_*}{a_0 H_0} = \left( \frac{a_*}{a_{\text{end}}} \right) \left( \frac{a_{\text{end}}}{a_{\text{reh}}} \right) \left( \frac{a_{\text{reh}}}{a_{\text{eq}}} \right) \left( \frac{a_{\text{eq}}}{a_0} \right) \frac{H_*}{H_0}, \quad (2.86)$$

where ‘end’ refers to the end of inflation, ‘reh’ the moment reheating completes which is the onset of radiation domination, ‘eq’ the epoch of radiation-matter equality and ‘0’ today. We denote a particular co-moving scale, as introduced in Eq. (2.51) by ‘ $k$ ’. As mentioned there, during inflation scales leave the horizon

<sup>1</sup>Temperature is defined in terms of the thermal bath, which here does not exist.

when  $k = aH$  and re-enter later in the Universe evolution. For scales re-entering at the pivot scale<sup>1</sup>, we define the moment they first left by the subscript ‘\*’.

The first term on the right hand side of Eq. (2.86) can be expressed in terms of the e-folding number. Using the definition of the Hubble parameter, Eq. (2.82) can be expressed as

$$N_{\text{tot}} = \int_{t_{\text{end}}}^{t_{\text{beg}}} a^{-1} da, \quad (2.87)$$

which becomes

$$e^{N_{\text{tot}}} = \frac{a_{\text{end}}}{a_{\text{beg}}}, \quad (2.88)$$

and so the first term on the right hand side of Eq. (2.86) is  $e^{-N_*}$ . We hence find

$$e^{N_*} = \frac{a_0 H_0}{k} \left( \frac{a_{\text{end}}}{a_{\text{reh}}} \right) \left( \frac{a_{\text{reh}}}{a_{\text{eq}}} \right) \left( \frac{a_{\text{eq}}}{a_0} \right) \frac{H_*}{H_0}. \quad (2.89)$$

The terms within the brackets each correspond to an epoch of the Universe; the time in between the end of inflation and the beginning of radiation domination, radiation domination and matter domination respectively. For these epochs we know how the scale factor grows with either the energy density of the Universe, cosmic time or the temperature, and so we rewrite as

$$e^{N_*} = \frac{a_0 H_0}{k} \left( \frac{\rho_{\text{reh}}}{\rho_{\text{end}}} \right)^{\frac{1}{3(1+w)}} \left( \frac{T_{\text{eq}}}{T_{\text{reh}}} \right) \left( \frac{t_{\text{eq}}}{t_0} \right)^{\frac{2}{3}} \frac{H_*}{H_0}, \quad (2.90)$$

where  $w$  is the equation of state parameter of the Universe between the end of inflation and the beginning of radiation domination. If we focus on scales which re-enter our horizon today, we know these scales left the horizon during slow-roll and we can equate

$$H_* \simeq \sqrt{\frac{V_*}{3m_{\text{Pl}}^2}}, \quad (2.91)$$

---

<sup>1</sup>Discussed after Eq. (2.129).

where  $V_* = V(\phi(t_*))$ . We see

$$e^{N_*} = \frac{a_0 H_0}{k} \left( \frac{\rho_{\text{reh}}}{\rho_{\text{end}}} \right)^{\frac{1}{3(1+w)}} \left( \frac{T_{\text{eq}}}{T_{\text{reh}}} \right) \left( \frac{t_{\text{eq}}}{t_0} \right)^{\frac{2}{3}} \frac{\sqrt{V_*}}{\sqrt{3} m_{\text{Pl}}} \frac{3t_0}{2}, \quad (2.92)$$

where we have used  $H = 2/3t$  (Eq. (2.34)) during matter domination and neglect the small contribution of dark energy at the present day. The second term on the right hand side describes the epoch between the end of inflation and the onset of radiation domination, controlled by the reheating mechanism and its efficiency. At the end of inflation, the potential energy of the scalar field no longer dominates and by definition, we have

$$\frac{1}{2} \dot{\phi}_{\text{end}}^2 \simeq V(\phi_{\text{end}}) \quad \rightarrow \quad \rho_{\text{end}} = 2V(\phi_{\text{end}}), \quad (2.93)$$

where we have used Eq. (2.60), and the energy density of a thermalised fluid can be related to its temperature via

$$\rho_{\text{reh}} = \frac{g_* \pi^2 T_{\text{reh}}^4}{30}, \quad (2.94)$$

where  $g_*$  are the number of relativistic degrees of freedom, so that the second term in Eq. (2.92) transforms as

$$e^{N_*} = \frac{a_0 H_0}{k_*} \left( \frac{g_* \pi^2 T_{\text{reh}}^4}{45 V_{\text{end}}} \right)^{\frac{1}{3(1+w)}} \left( \frac{T_{\text{eq}}}{T_{\text{reh}}} \right) \left( \frac{t_{\text{eq}}}{t_0} \right)^{\frac{2}{3}} \frac{\sqrt{V_*}}{\sqrt{3} m_{\text{Pl}}} \frac{3t_0}{2}. \quad (2.95)$$

Reorganising terms and taking the logarithm allows us to find  $N_*$ :

$$\begin{aligned} N_* = & \ln \left( \frac{a_0 H_0}{k_*} \right) + \ln \left( \frac{\sqrt{3}}{2} \right) + \ln(t_0 T_{\text{eq}}) + \frac{2}{3} \ln \left( \frac{t_{\text{eq}}}{t_0} \right) \\ & + \frac{1}{3(1+w)} \ln \left( \frac{g_* \pi^2}{60} \right) + \ln \left( \frac{V_*^{1/4}}{m_{\text{Pl}}} \right) + \ln \left( \frac{V_*^{1/4}}{T_{\text{reh}}} \right) + \frac{4}{3(1+w)} \ln \left( \frac{T_{\text{reh}}}{V_{\text{end}}^{1/4}} \right), \end{aligned} \quad (2.96)$$

where only the terms on the second line depend on the inflationary model. Terms

on the first line can all be evaluated using the values given in Table 1.1 and we find

$$N_* = 59.7 + \frac{1}{3(1+w)} \ln \left( \frac{g_* \pi^2}{60} \right) + \ln \left( \frac{V_*^{1/4}}{m_{\text{Pl}}} \right) + \ln \left( \frac{V_*^{1/4}}{T_{\text{reh}}} \right) + \frac{4}{3(1+w)} \ln \left( \frac{T_{\text{reh}}}{V_{\text{end}}^{1/4}} \right), \quad (2.97)$$

where we have used a pivot scale<sup>1</sup> of  $k_* = 0.05 \text{ Mpc}^{-1}$ .

Depending on the reheating mechanism,  $w$  can vary from  $w = 0$  for perturbative reheating, to  $w = 1$  if the Universe is dominated by the kinetic energy of the inflaton for a period of time, these are addressed in detail in Section 2.7. The value of  $w$  introduces a correction of approximately 0.4 ( $w = 0$ ) to 0.2 ( $w = 1$ ) from the second term in Eq. (2.97), where we have used  $g_* = 106.75$ . The final three terms have more of an influence on the value of  $N_*$  and depend on the energy scale of inflation and the duration of reheating. Typically the energy scale of inflation is expected to be of the order of  $10^{15} \text{ GeV}$  and  $T_{\text{reh}}$  can vary from the energy scale of inflation, if reheating is prompt, down to the energy scale of BBN, at approximately  $1 \text{ MeV}$ ; constraints on  $T_{\text{reh}}$  are detailed in Section 2.7.5.

Now that we have considered the dynamics of slow-roll inflation and how to quantify its duration we can introduce the observational constraints on models of inflation.

### 2.4.5 Inflationary Observables

As touched upon in Section 2.3.3, the density perturbations which will go on to form the large scale structure in the Universe are generated naturally from quantum fluctuations in the inflaton field [46–52]. Our observations of the early Universe are based upon these density perturbations which manifest as temperature changes in the CMB, thereby providing a window into when they were seeded during inflation. At a given moment in time we can characterise the small

---

<sup>1</sup>Discussed after Eq. (2.129).

inhomogeneities in the inflaton field by their spatial distribution, which is a random distribution and therefore well approximated by the statistics of a Gaussian random field.

For a Universe assumed to be isotropic and homogeneous the spatial two-point correlation function is only a function of the magnitude of the separation between two points, not the absolute position or orientation, which simplifies the calculations. Working in Fourier space, as in Eq. (2.50), the power spectrum,  $\mathcal{P}_{\mathcal{R}}$ , is the Fourier transform of the two-point correlation function, which provides a measure of the amplitude of the perturbations in Fourier space. It is defined as

$$P_{\delta_k}(k) = |\delta_k|^2, \quad \mathcal{P}_{\delta_k}(k) = \frac{k^3}{2\pi^2} |\delta_k|^2, \quad (2.98)$$

where  $\mathcal{P}_{\delta_k}(k)$  simplifies subsequent equations involving the power spectrum, which we will use from now on.

To calculate the perturbations it is convenient to work in conformal time,  $\eta$ , where

$$dt = a d\eta, \quad (2.99)$$

and the KG equation for a generic, massless quantum field is expressed as

$$\phi'' + 2\frac{a'}{a}\phi' - \nabla^2\phi = 0, \quad (2.100)$$

where a prime in this instance denotes a derivative with respect to  $\eta$ . To solve for  $\phi$  it is useful to define  $\nu = a\phi$  which leaves

$$\nu'' - \frac{a''}{a}\nu - \nabla^2\nu = 0. \quad (2.101)$$

If we perturb this background equation as  $\nu \rightarrow \nu + \delta\nu$  then the perturbed quantities obey the same KG equation. Decomposing into Fourier modes we see

$$\delta_k'' + \left(k^2 - \frac{a''}{a}\right)\delta_k = 0, \quad (2.102)$$

where the term dependent on the co-moving wavenumber arises from the gradient

term and we have suppressed the field notation so that  $\delta\nu_k = \delta_k$ . When  $H$  is approximately constant we can use the substitution  $a = -1/H\eta$  to simplify and we arrive at

$$\eta^2 \delta_k'' + (\eta^2 k^2 - 2) \delta_k = 0, \quad (2.103)$$

which has a general solution in terms of the Hankel functions of

$$\delta_k = \frac{\sqrt{\eta}}{2} \left[ (A - iB) H_{3/2}^+(k\eta) + (A + iB) H_{3/2}^-(k\eta) \right], \quad (2.104)$$

where  $H_{3/2}^\pm = J_{3/2} \pm iY_{3/2}$  where  $J_n$  and  $Y_n$  are Bessel functions of the first and second kind respectively and the  $3/2$  arises because we have a massless field. To solve this equation for  $\delta_k$  it is necessary to determine the constants  $A$  and  $B$ . To do this we impose the boundary condition that when  $k\eta \rightarrow -\infty$ , deep inside the horizon, curvature is negligible and the solution should correspond to the Bunch-Davies vacuum

$$\delta_k = \frac{1}{\sqrt{2k}} e^{-ik\eta}. \quad (2.105)$$

In this limit the Hankel functions asymptote to

$$H_{3/2}^\pm \simeq \sqrt{\frac{2}{\pi k\eta}} \exp \pm i(k\eta - \pi), \quad (2.106)$$

which allows us to determine the solution

$$\delta_k = \frac{\sqrt{\pi\eta}}{2} e^{-i\pi} H_{3/2}^-(k\eta), \quad (2.107)$$

which using the general form of  $H_{3/2}^-$  becomes

$$\delta_k = \frac{e^{-ik\eta}}{\sqrt{2k^3\eta}} (k\eta - i). \quad (2.108)$$

On super-horizon scales, when  $k\eta \ll 1$  this simplifies to

$$\delta_k \simeq \frac{aH}{\sqrt{2k^3}}, \quad (2.109)$$

where we have used  $-1/\eta \simeq aH$ . Remembering the initial field redefinition of  $\nu = a\phi$  this becomes

$$\delta\phi_k \simeq \frac{H}{\sqrt{2k^3}}, \quad (2.110)$$

leading to the power spectrum

$$\mathcal{P}_{\phi_k}(k) = \left(\frac{H}{2\pi}\right)^2, \quad (2.111)$$

which is constant for constant  $H$ .

During inflation, any light field (see Eq. (2.81)) develops super Horizon fluctuations with a mean amplitude of  $H/2\pi$  and an almost scale invariant power spectrum [3], varying only for small changes in  $H(t)$  arising from the fact inflation is not a perfect de-Sitter spacetime as we have assumed in Eq. (2.111).

This analysis is for a generic quantum field during inflation, which could be the inflaton. However, to model the real Universe we need to think about what fluctuations are present. From the quantum uncertainty principle we know there are small spatial variations in the inflaton field which can be modelled via linear perturbation theory as

$$\phi = \bar{\phi}(t) + \delta\phi(\mathbf{x}, t), \quad (2.112)$$

where  $\bar{\phi}$  is the homogeneous background value of the inflaton field and  $\delta\phi$  is a small perturbation to it, taken to be  $|\delta\phi| \ll \bar{\phi}$ . However, because of the presence of  $\phi$  in the energy-momentum tensor and subsequently the Einstein tensor (Eqs. (2.9) and (2.10)), any perturbations to  $\phi$  will be reflected in the space-time metric as well. We model this perturbation in a similar fashion to the inflaton perturbation as

$$g_{\mu\nu}(t, \mathbf{x}) = \bar{g}_{\mu\nu}(t) + \delta g_{\mu\nu}(t, \mathbf{x}), \quad (2.113)$$

where again  $\bar{g}_{\mu\nu}$  is the homogeneous background value of the metric and  $\delta g_{\mu\nu}$  is a small perturbation to it, presumed to be  $|\delta g_{\mu\nu}| \ll \bar{g}_{\mu\nu}$ .

$\delta g_{\mu\nu}(t, \mathbf{x})$  is a symmetric  $4 \times 4$  tensor with ten degrees of freedom, grouped into scalars, vectors and tensors. Performing a scalar-vector-tensor (SVT) decomposi-

tion results in four scalar degrees of freedom, describing Newtonian gravity, four vector degrees of freedom, describing gravito-magnetism, and two tensor degrees of freedom, describing gravitational waves. At first order perturbation theory none of these are coupled together; they all have separate equations governing their evolution. However, the scalar metric perturbations couple with the scalar field perturbation  $\delta\phi$  from the previous section. The vector perturbations of the metric have decaying solutions and will not be mentioned further but the tensor perturbations have non-decaying solutions (to their equation of motion) and will be examined at the end of this section.

When we move from a background spacetime to a perturbed spacetime we associate points in the background spacetime with points in the perturbed spacetime via a particular coordinate system. Any coordinate system could be chosen, but we choose one which ensures the perturbations are small. There are still multiple coordinate system choices though and a gauge transformation describes a coordinate transformation between such coordinate systems in the perturbed spacetime. It turns out that a gauge transformation sometimes causes perturbations to vanish, meaning the perturbed spacetime differed from the background spacetime only by having a perturbed coordinate system and the perturbation in question was a gauge artefact.

To avoid the pitfalls of fictitious perturbations, we need to define perturbations in a coordinate-invariant way. We define new variables which are special combinations of the scalar metric perturbations and do not transform under a change of coordinates, the Bardeen variables,  $\Psi$  and  $\Phi$  [53]. The tensor perturbation remains unchanged as tensors are unaffected by gauge transformations. These gauge-invariant variables can be considered as the ‘real’ spacetime perturbations.

We are motivated to consider the metric perturbations because they are coupled to the scalar field perturbations via the Einstein equation. We can define the co-moving curvature perturbation,  $\mathcal{R}$ , which in single-field inflation encodes both

$$\mathcal{R} = \Phi + H \frac{\delta\phi}{\dot{\phi}} = \Phi + \mathcal{H} \frac{\delta\phi}{\phi'}, \quad (2.114)$$

where  $\mathcal{H} = \frac{a'}{a}$  and a prime indicates differentiation with respect to the conformal time,  $\eta$ .

The quadratic action for the perturbation  $\mathcal{R}$  is

$$S^{(2)} = \int dt d^3\mathbf{x} \frac{a^3 \dot{\phi}^2}{2H^2} \left[ \dot{\mathcal{R}}^2 - \frac{1}{a^2} (\nabla \mathcal{R})^2 \right] + \dots \quad (2.115)$$

To canonically normalise this equation we switch variables to

$$u = z\mathcal{R}, \quad (2.116)$$

where

$$z = \frac{a\dot{\phi}}{H}. \quad (2.117)$$

Moving to conformal time the action becomes

$$S^{(2)} = \frac{1}{2} \int d\eta d^3\mathbf{x} \left[ (u')^2 - (\nabla u)^2 + \frac{z''}{z} u^2 \right], \quad (2.118)$$

which conveniently produces the same KG evolution equation as the generic quantum field from the previous section, with  $a \rightarrow z$ :

$$u_{\mathbf{k}}'' + \left( k^2 - \frac{z''}{z} \right) u_{\mathbf{k}} = 0. \quad (2.119)$$

During slow-roll  $\dot{\phi}$  and  $H$  evolve much more slowly than  $a$  and so we assume  $\frac{z''}{z} \approx \frac{a''}{a}$  and obtain the same solution as before;  $\mathcal{R}$  is frozen on super-horizon scales and the power spectrum is

$$\mathcal{P}_{\mathcal{R}}(k) = \frac{k^3}{2\pi^2} \frac{|u_k|^2}{z^2} = \left( \frac{H^2}{\dot{\phi}^2} \right) \left( \frac{H}{2\pi} \right)^2 \Big|_{k=aH}. \quad (2.120)$$

As mentioned after Eq. (2.111),  $H$  is a function of time in a quasi de-Sitter spacetime, so we expect the power spectrum may now deviate from scale-invariance. However,  $H$  changes only slightly during slow-roll inflation and so we approximate

the power spectrum as a power law

$$\mathcal{P}_{\mathcal{R}}(k) \propto k^{(n_s-1)}, \quad (2.121)$$

where  $n_s$  is the scalar spectral tilt, referencing the fact that the co-moving curvature perturbation traces the primordial scalar perturbations. The tilt represents the variation with scale; a red-tilt ( $n_s < 1$ ) represents a power excess at large scales and a blue-tilt ( $n_s > 1$ ) represents a power excess at small scales. We can rearrange Eq. (2.121) to find the scalar spectral tilt as

$$n_s - 1 \equiv \frac{d \ln \mathcal{P}_{\mathcal{R}}(k)}{d \ln k}, \quad (2.122)$$

where it is necessary to take the derivative to remove the constant of proportionality. Rewriting this slightly as

$$n_s - 1 \equiv \frac{d \ln \mathcal{P}_{\mathcal{R}}}{d \ln k} = \frac{d \ln \mathcal{P}_{\mathcal{R}}}{d\phi} \frac{d\phi}{dt} \frac{dt}{d \ln k}, \quad (2.123)$$

allows us to express  $n_s$  in terms of the slow-roll parameters. As noted,  $\mathcal{R}$  is frozen as soon as it leaves the horizon and so we evaluate at the point of horizon exit,  $k = aH$ , which allows us to write

$$\frac{d \ln k}{dt} = \frac{d \ln a}{dt} + \frac{d \ln H}{dt} = H(1 - \epsilon_H), \quad (2.124)$$

which in turn reduces Eq. (2.123) to

$$n_s - 1 = \frac{\dot{\phi}}{H(1 - \epsilon_H)} \frac{d \ln \mathcal{P}_{\mathcal{R}}}{d\phi}. \quad (2.125)$$

Utilising the slow-roll assumptions (Eqs. (2.72) and (2.73)) allows us to express the spectral index in terms of the potential slow-roll parameters

$$n_s = 1 + 2\eta_V - 6\epsilon_V, \quad (2.126)$$

and we compute the running of this quantity via

$$n'_s = \frac{dn_s}{d \ln k}. \quad (2.127)$$

A similar calculation can be followed for the tensor perturbations of the metric, which produces

$$\mathcal{P}_T(k) = \frac{2H^2}{\pi^2 m_{\text{Pl}}^2} \Big|_{k=aH}. \quad (2.128)$$

Rather than looking at the scale dependence of the tensor spectrum directly, it is more common to look at the ratio of the tensor-to-scalar perturbations:

$$r = \frac{\mathcal{P}_T(k)}{\mathcal{P}_\mathcal{R}(k)} = \frac{8\dot{\phi}^2}{m_{\text{Pl}}^2 H^2} = 16\epsilon_H, \quad (2.129)$$

where we see  $r \ll 1$ ; the amplitude of the scalar perturbations is much greater than the amplitude of the tensor perturbations.

As is evident from the descriptions of the power spectrum, the spectral index and tensor-to-scalar ratio are functions of  $k$ . To best evaluate the predictions from different models of inflation we compare their values for a given  $k$ , termed the ‘pivot scale’. If we parametrise the scalar power spectrum as

$$\mathcal{P}_\mathcal{R}(k) = A_s \left( \frac{k}{k_*} \right)^{n_s-1}, \quad (2.130)$$

where  $A_s$  is the amplitude, then  $k_*$  corresponds to the pivot scale. As mentioned in Section 2.1.3, when scales re-enter the horizon they oscillate, buoyed by the radiation pressure, with decreasing amplitude. The pivot scale is chosen to correspond to a scale which has recently re-entered the horizon, so it is not too damped, and a scale for which the uncertainties in the amplitude of the spectrum are not too large, the pivot scale most commonly used at the time of writing is  $k = 0.05 \text{ Mpc}^{-1}$ . A mode becomes super-Horizon when its physical wavelength is larger than the horizon size, at a time,  $t_*$ , when

$$k = a(t_*)H(t_*), \quad (2.131)$$

and so observables involving  $k$  are evaluated at this time to ensure they are frozen in.

For the pivot scale  $k = 0.05 \text{ Mpc}^{-1}$ , the Planck 2018 (68% confidence level) paper gives

$$n_s = 0.965 \pm 0.004, \quad (2.132)$$

which assumes a constant value for  $n_s$  and a standard  $\Lambda$ CDM cosmology. For the tensor-to-scalar ratio Planck 2018 uses  $k = 0.002 \text{ Mpc}^{-1}$  and gives (95% confidence level)

$$r_{0.002} < 0.1, \quad (2.133)$$

for its analysis alone with the base model. This constraint is tightened when combined with other data sources but becomes slightly more model dependent, for example combining the Planck 2018 data with the BICEP-Keck Array data gives a 95% CL constraint of

$$r_{0.002} < 0.064. \quad (2.134)$$

The Planck 2018 results for the  $r - n_s$  contour are shown in Fig. 2.2 and we henceforth use the bound  $r < 0.07$ .

A final parameter which our observations of the CMB constrain is the energy scale of inflation, via the COBE constraint on the amplitude of the scalar perturbation [1], namely

$$A_s = (2.101_{-0.034}^{+0.031}) \times 10^{-9}. \quad (2.135)$$

Rewriting Eq. (2.120) in light of the slow-roll assumptions in Eqs. (2.72) and (2.73) it becomes

$$\sqrt{A_s} = \frac{V^{3/2}}{2\sqrt{3}\pi m_{\text{Pl}}^3 V'}, \quad (2.136)$$

meaning for a particular scalar field potential, we are able to constrain the inflationary energy scale. This is sometimes presented in terms of the tensor-to-scalar ratio as

$$V = \frac{3A_s\pi^2 m_{\text{Pl}}^4 r}{2}, \quad (2.137)$$

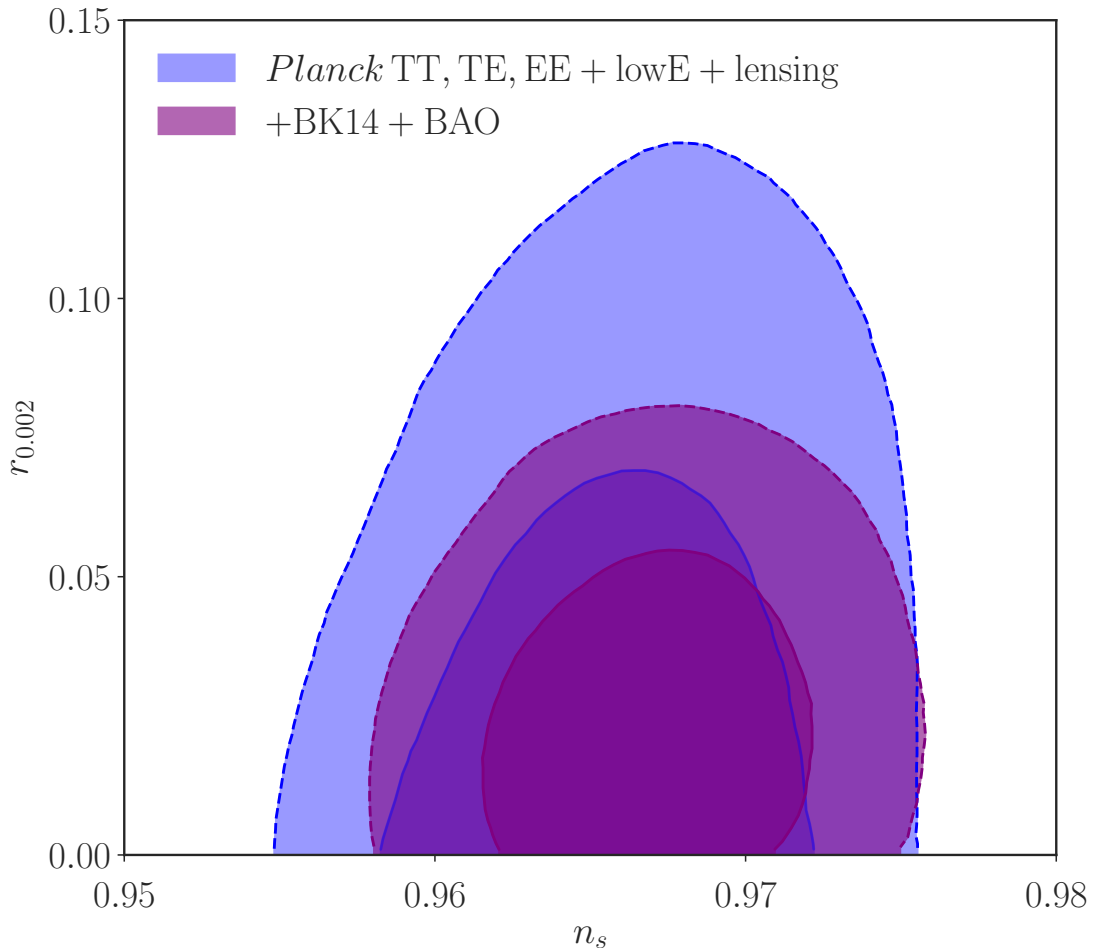


**Figure 2.2:** Constraints in the  $r$  vs  $n_s$  plane using *Planck* 2018 data, reproduced from [1].  $2\sigma$  ( $1\sigma$ ) constraints are indicated by dashed (solid) lines respectively.

and using the limit of  $r \lesssim 0.07$  this imposes a limit of

$$V \lesssim 7.6 \times 10^{64} \text{ GeV}^4. \quad (2.138)$$

Throughout this section we have presumed the perturbation fields are well represented by Gaussian random fields and treated them as a statistical ensemble. It is also possible to constrain the primordial non-Gaussianities. That is, the measured deviance from a Gaussian distribution of the temperature anisotropies in the CMB. We have only introduced slow-roll, single-field models which predict a vanishing amount of non-Gaussianity,  $f_{NL}$ , but more complex inflationary

models such as multi-field models generally predict higher levels of  $f_{NL}$ . In this way, measurements of  $f_{NL}$  allow us to distinguish between different families of inflationary models. The constraints on  $f_{NL}$  vary depending on the cosmological model in question but generally accept non-Gaussianities to be minimal. Ref. [1] considers  $f_{NL}$  constraints in a few common extensions to cold, single-field inflation.

We have about exhausted the CMB of observational constraints for models of inflation. There are a few technical extensions to those presented here, such as polarisation of the CMB but we do not utilise them here and so direct the reader to [3] for an overview. Instead, we move now to consider building an inflationary model.

## 2.5 Inflationary Model Building

Section 2.4 outlined the requirements for a scalar field to drive an accelerated expansion of the Universe and laid out the slow-roll assumptions and the observables that allow us to distinguish between inflationary models. There are three main cosmological observations that models of inflation need to satisfy; the amplitude of the power spectrum of scalar curvature perturbations, the scalar spectral index and the tensor-to-scalar ratio, which we define in Section 2.4.5.

As discussed in Section 2.4.5, the observables are compared at the pivot scale. The power spectrum is only well constrained for scales close to  $k_*$ , because Eq. (2.130) is an expansion in  $k$ . The power spectrum may look very different at smaller scales, something which is often assumed in primordial black hole research, which is mentioned further in Chapter 6.

Ref. [54] conducted a Bayesian analysis of a plethora of existing slow-roll, single-field inflation models after the publication of the Planck 2013 results [55] to place constraints on the shape of the inflationary potential and found strong Bayesian preference for a plateau inflationary potential. This interpretation of the Planck results is widely accepted and shapes the inflationary models described in the original research in this thesis. We also point out the special mention Ref. [54] gives to the  $\alpha$ -attractor models of inflation, developed from Ref. [56], which we

utilise to develop a novel model of quintessential inflation (see Section 2.8.2) in the original research in Chapter 7.

In addition to the observational constraints detailed in Section 2.4.5, theoretical considerations also exist and the two most relevant for the research presented here are the  $\eta$  problem in supergravity and the question of super-Planckian field excursions.

### 2.5.1 Global and Local Supersymmetry

As we favour a scalar field for the driving mechanism of inflation, global supersymmetry (SUSY) is an attractive theory in which to embed an inflationary model because it provides a host of additional scalar fields to the standard model with many flat directions, ideal for inflation [57]. SUSY posits that fermions and bosons are different states of a single object, known as a supermultiplet. It provides an answer to the hierarchy problem of particle physics by stabilising against radiative corrections, improves the unification of the coupling constants of the electromagnetic, weak and strong interactions and provides a host of particle candidates for CDM [58].

The observed particles of the standard model are not supermultiplets of one another and so the theory predicts new particles, known as ‘superpartners’. The particles arise from symmetries generated by quantum mechanical operators which exchange the fermionic and bosonic states, hence the name supersymmetry. If these symmetries were unbroken, we would observe the new particles with exactly the same mass as their partners. Particle physics experiments have found no trace of the superpartners so we believe the symmetry is broken, allowing superpartners to have different masses.

Lagrangians which are invariant under supersymmetric transformations include two auxiliary fields, termed ‘F’ and ‘D’ which respectively represent the chiral and vectorial sectors of the supersymmetric theory [3]. If SUSY is unbroken the potential vanishes in the vacuum [59]. It is most common to spontaneously break the symmetry via the F-term which provides the scalar potential with the

following term

$$V_F = \sum_i \left| \frac{\partial W}{\partial \phi_i} \right|^2, \quad (2.139)$$

where  $W$  is the superpotential, a function of the superfields present in the theory. We could also invoke a soft SUSY-breaking term, with the form

$$V_{\text{soft}} = \pm m_{\text{soft}}^2 |\phi|^2, \quad (2.140)$$

which is added to the scalar field potential by hand. Solving the hierarchy problem requires  $m_{\text{soft}} \simeq \mathcal{O}(1\text{TeV})$ .

Supergravity (SUGRA) is supersymmetry including gravity. Extending SUSY to depend on spacetime co-ordinates effectively makes it a local symmetry, which is why it is often referred to as local SUSY. In SUGRA the F-term also depends on the Kähler potential,  $K$ , and has a more complicated form [60, 60–62]

$$V_F = e^{\frac{K}{m_{\text{Pl}}^2}} \left[ \sum_{i,j} \left( \frac{\partial^2 K}{\partial \phi_i^* \partial \phi_j} \right)^{-1} \left( \frac{\partial W}{\partial \phi_i} + \frac{W}{m_{\text{Pl}}^2} \frac{\partial K}{\partial \phi_i} \right) \left( \frac{\partial W}{\partial \phi_i} + \frac{W}{m_{\text{Pl}}^2} \frac{\partial K}{\partial \phi_i} \right)^* - \frac{3|W|^2}{m_{\text{Pl}}^2} \right]. \quad (2.141)$$

The Kähler potential is equivalent to a metric in field space and is dimensionless.

SUSY (and SUGRA) may also be broken via the D-term but this is less common. It is more often assumed to be a flat direction which is negligible during inflation. If D-terms are present in the scalar field potential they are quartic, an example is used in the research in Chapter 3.

### 2.5.2 The $\eta$ Problem of Supergravity

The kinetic term in the Lagrangian depends on the Kähler potential as

$$\mathcal{L}_{\text{kin}} = \frac{\partial^2 K}{\partial \phi_i \partial \phi_j^*} \partial_\mu \phi_i \partial^\mu \phi_j^*, \quad (2.142)$$

where  $\mu$  is a spacetime index. Canonically normalised fields therefore require Kähler potentials of the form

$$K = \sum_i |\phi_i|^2 + \dots, \quad (2.143)$$

which is called a minimal Kähler potential.

As we saw in Eq. (2.77) the second slow-roll parameter,  $\eta$ , depends on the second derivative of the scalar potential with respect to the field, which from the exponential in Eq. (2.141) will always be proportional to

$$\eta \propto K'' + \dots. \quad (2.144)$$

For the minimal Kähler potential<sup>1</sup>,  $K'' = 1$ , meaning  $\eta > 1$ . This seemingly prohibits successful slow-roll inflation which, as discussed in Section 2.4.3, requires  $|\eta| < 1$ . This is the  $\eta$  problem of supergravity. If a more complicated form of the Kähler potential is used this can be avoided but this is often highly non-trivial.

## 2.6 Models of Inflation

The easiest inflationary models to formulate are cold, meaning there is no source of radiation present, and minimally coupled to gravity, as per the EH action (Eq. (2.7)). They are single and small-field, meaning the model only consists of one scalar field and it does not extend to super-Planckian distances in field space.

However there are many ways to extend these simple approaches, each with their own motivations, merits and potential drawbacks. One notable example relevant to this thesis is discussed in Section 2.6.5 but first we introduce the difference between large and small field models, which are of historical relevance, and hybrid inflation, which bridges the gap between the two and forms the basis of the research in Chapter 4.

---

<sup>1</sup>Pre-factors disappear with suitable redefinitions in configuration space to represent the superfields in terms of their component scalar fields.

### 2.6.1 Large Field vs Small Field Inflation

The first inflation model to be formulated<sup>1</sup> was that of Guth in 1981 [65], which relied on a scalar field being trapped in a local minimum of its potential to provide an effective cosmological constant description for inflation. Guth suggested that the field would eventually quantum tunnel to its global minimum, thereby ending inflation. However, the first order phase-transition that is required to terminate inflation in this manner generates ‘bubbles’ of true vacuum which are unable to coalesce because of the rapid expansion of the regions outside of the bubbles. This is the ‘graceful exit’ problem of ‘old inflation’.

The inflationary theory was developed by Linde [66] and Albrecht & Steinhardt [67] to involve the field slowly rolling from an unstable maximum to the minimum of its potential, which was able to generate promising density perturbations. Without the violent first-order phase transition the models produced viable Universes and were termed ‘new inflation’. However, both old and new inflation rely upon cosmological phase transitions which depend on thermal equilibrium.

Linde was the first to drop the assumption of thermal equilibrium with his proposal of ‘chaotic inflation’ [68]. Chaotic inflation removes the restrictions on the initial conditions of the scalar field, instead allowing any initial condition which may incorporate an inflationary regime. The simplest example of chaotic inflation has the potential

$$V(\phi) = \frac{1}{2}m^2\phi^2, \quad (2.145)$$

where  $m$  is a mass scale. If the field finds itself initially at large field values then the Friedmann equation, Eq. (2.63), tells us  $H$  is also large. As we saw in Section 2.2 the Klein-Gordon equation for the evolution of a scalar field features a ‘friction’ term due to the expansion of the Universe,  $3H\dot{\phi}$ . For large  $H$  the scalar field is moving very slowly in field space and all of the slow-roll assumptions detailed in Section 2.4.3 hold.

---

<sup>1</sup>Starobinsky [63, 64] provides an earlier example of an inflationary model but without the cosmological motivations of Guth.

Chaotic inflation models with generic potentials of the form

$$V(\phi) = M^4 \left( \frac{\phi}{m_{\text{Pl}}} \right)^n, \quad (2.146)$$

are referred to as large-field models, due to the displacement of the field from the stable minimum of its potential in field space:

$$\text{Large field : } \quad \Delta\phi \gg m_{\text{Pl}}, \quad (2.147)$$

$$\text{Small field : } \quad \Delta\phi < m_{\text{Pl}}. \quad (2.148)$$

As Linde himself emphasises [69], chaotic inflation marks a departure from an assumption about initial conditions for inflation, rather than aligning itself with any one inflationary model.

Small-field models which feature an unstable maximum in the potential, as per new inflation but without the assumption of a thermal phase transition to give rise to inflation, can also support slow-roll inflation, as long as the potential is sufficiently flat. Slow-roll inflation takes place in the small vicinity of the maximum and so we can express the potential generically via a Taylor expansion about this maximum point as

$$V(\phi) = M^4 \left[ 1 - \left( \frac{\phi}{\mu} \right)^n \right] + \dots. \quad (2.149)$$

where ‘ $\dots$ ’ represent stabilising terms. The shape of the potential away from the origin is unimportant for the dynamics of inflation and potentials of this form arise naturally in spontaneous symmetry breaking models. The key observational difference between large and small field models lies in their predictions for the tensor-to-scalar ratio.

## 2.6.2 The Lyth Bound

It was first noticed by Lyth [70] that the field-excursion of the inflaton could be related to the tensor-to-scalar ratio via Eq. (2.84), by replacing  $\sqrt{\epsilon_H}$  with  $\sqrt{r}/4$ :

$$\Delta\phi \approx \sqrt{\frac{r}{8}} m_{\text{Pl}} |\Delta N|, \quad (2.150)$$

where  $\Delta\phi$  corresponds to the inflaton variation and Eq. (2.150) is valid for approximately constant  $\epsilon$ . We cannot assume that  $\epsilon$  is constant during the entire duration of slow-roll inflation, but we can be confident that the assumption holds around the pivot scale.

Ref. [70] estimates that approximately 4.6 e-folds pass between the pivot scale and scales corresponding to the first peak on the CMB map leaving the horizon. Using this as a heavily conservative minimum (of course, we expect inflation to last at least 30 e-folds, even if subsequent periods of thermal inflation take place, see Section 2.6.5) we can find a lower limit on the inflaton's variation of:

$$\Delta\phi \geq \sqrt{2r} m_{\text{Pl}}. \quad (2.151)$$

Sizeable tensor predictions thus require sizeable inflaton field variations. The current bound of  $r < 0.07$  [1] means that chaotic inflation models are largely ruled out because of their high  $r$  predictions, a necessary by-product of large field models. A detection of the order of  $r \approx 0.01$  would mean

$$\Delta\phi \gtrsim 0.1 m_{\text{Pl}}, \quad (2.152)$$

where we stress again this is only modelled using  $\Delta N \simeq 5$  around the pivot scale, increasing this to  $\Delta N \simeq 30$  the bound becomes

$$\Delta\phi \gtrsim m_{\text{Pl}}, \quad (2.153)$$

which is still a conservative estimate for most inflationary models. Looking at a maximum constraint, with the current bound of  $r \leq 0.07$ , using a maximum

e-folding number of  $\Delta N = 60$ , we see

$$\Delta\phi \lesssim 6m_{\text{Pl}}, \quad (2.154)$$

which shows the best way to view the Lyth bound is not as a constraint on either  $r$  or  $\Delta\phi$ , but an inescapable relationship between the two. If a tensor signal is found of the order of  $r \simeq 0.01$ , field displacements during inflation will have to be approximately Planckian to accommodate the observation. Conversely, if the upper bound on  $r$  is reduced below  $r \simeq 0.01$  then models with super-Planckian field displacements will be ruled out.

### 2.6.3 Super-Planckian Field Variations

If a significant tensor perturbation is detected, requiring a super-Planckian field variation, extra considerations for the scalar potential are introduced. Higher order terms in the effective potential, arising from couplings between the inflaton and other fields (necessary, even in minimal models, for most reheating mechanisms) are expected to be suppressed for  $\Delta\phi \ll m_{\text{Pl}}$ . For field excursions  $\Delta\phi \approx m_{\text{Pl}}$  this cannot be assumed and the effective potential will be different.

Often, higher order non-renormalisable terms act to lift the potential, jeopardising its flatness and suitability for generating a period of accelerating inflation. If negative terms are introduced the potential may even be unbounded from below, as is the case for fermionic couplings such as the Coleman-Weinberg loop correction - discussed in detail as part of the research in Chapter 5 which utilises an effective potential with self-interacting higher order terms to develop a step in the potential suitable for inflation. Maintaining sub-Planckian field excursions is not a major concern for the inflationary models presented in Chapters 3 and 4 but it motivates the work in Chapters 7 and 8 where the super-Planckian field-excursions must be controlled in quintessential inflation models.

Recently, a new conjecture in string theory prompted a flurry of activity into the constraints imposed upon scalar field potentials if they are embedded in string theory, distinguishing a ‘swampland’ outside of the string theory landscape where seemingly robust effective field theories may not actually be compatible with

quantum gravity [71]. The new conjecture imposes a minimum on the derivative of the scalar field potential:

$$|\nabla V| \geq \frac{cV}{m_{\text{Pl}}}, \quad (2.155)$$

where  $c > 0$  is a constant  $\mathcal{O}(1)$ . This has very interesting consequences for  $\Lambda$ CDM which we address in more detail in Section 2.8.2, because it appears to forbid de-Sitter minimum and indicate a preference within string theory for quintessence models of dark energy.

The conjecture also prompted a re-emergence of the swampland distance conjecture [72] which states an effective field theory is only valid for a finite scalar field variation, beyond a certain distance an infinite tower of states becomes light, a distance thought to be of the order of the Planck mass. Ref [73] gives a review of recent developments in the field. We do not discuss it further here except to say it is a conjecture within string theory, which may or may not be the correct ‘theory of everything’.

### 2.6.4 Hybrid Inflation

The original manifestation of hybrid inflation [74], coined the name as a ‘hybrid’ theory between chaotic inflation and new inflation. In hybrid inflation the inflaton field slowly evolves along a flat direction, but it is also coupled to a secondary field,  $\sigma$ , called the waterfall field, initially held at  $\sigma = 0$ . The inflaton field evolves in slow-roll along the  $\sigma = 0$  plateau and inflation ensues until a critical value,  $\phi_c$ , when the symmetry is broken. The  $\sigma$  field evolves from an unstable maximum at zero to its true minimum, thereby ending inflation. A diagram of this behaviour is shown in Fig. 2.3.

The symmetry breaking which ends inflation in this model may lead to the formation of topological defects, with interesting repercussions. As mentioned in Section 2.3.4, the energy density of topological defects is heavily constrained, however their existence depends on the symmetry group of the GUT in which the model is embedded. If the GUT is semi-simple then the defects formed are cosmic strings, upon which there are stringent constraints. These constraints arise because cosmic strings affect structure formation and produce different observable

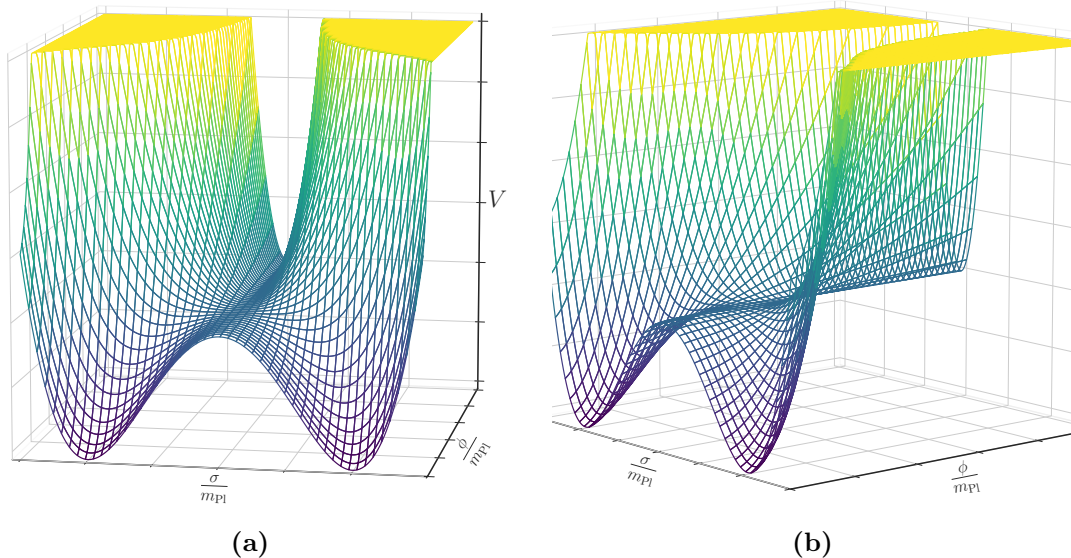


**Figure 2.3:** A sketch of the potential in hybrid inflation using arbitrary units, shown from two different perspectives.

signals in the CMB. The greater the influence of the cosmic strings, the more the acoustic peaks are suppressed. The higher the energy scale of the symmetry breaking, the greater the effect of cosmic strings on structure formation. As such, cosmic string constraints impose an upper limit on the energy scale of symmetry breaking, which corresponds to a reduction in the e-folds of inflation. This effect should be considered if one is presuming the symmetry group of the GUT is semi-simple. If it is not, the situation is more complicated. Either there are no defects formed, in which case there are no constraints, or monopoles or domain walls are formed which are very heavily constrained [75], as discussed in Section 2.3.4. We refer the interested reader to Refs. [76–78] for further details.

The original theory predicted a blue-tilted spectrum for the primordial scalar perturbations at odds with recent observations. The model was later revived in supergravity, a version of the model which predicts a red spectrum. It is a very successful example of a scalar field model embedded in SUGRA managing to avoid the  $\eta$  problem, described in Section 2.5.2, without resorting to a complex Kähler potential. An accidental cancellation from the higher order terms allows  $\eta \ll 1$  and saves the model. Unfortunately, the most recent Planck observations [1] rule out the minimal SUGRA version of hybrid inflation, as it predicts  $n_s \geq 0.980$ ,

but the original research in Chapter 4 presents a way to save minimal hybrid inflation in SUGRA.

### 2.6.5 Thermal Inflation

Thermal inflation is a short period of inflation following primordial inflation, driven by a second scalar field called the flaton field [79]. A flaton field has an almost flat potential and a large VEV and they naturally arise in many particle field theories. Thermal inflation occurs at lower energies than primordial inflation to avoid spoiling the primordial density perturbation spectrum. Thermal inflation was originally investigated with the intention of solving the problem of moduli generated after primordial inflation.

A flaton field is strongly coupled to the thermal bath and has a potential of the form

$$V = V_0 - \frac{1}{2}m^2\theta^2 + \frac{\lambda}{[2(n+2)]!} \frac{\theta^{2(n+2)}}{m_{\text{Pl}}^{2n}} + \frac{1}{2}g^2T^2\theta^2, \quad (2.156)$$

where  $n > 0$ ,  $\theta$  is the flaton field<sup>1</sup>,  $g$  is the coupling to the thermal bath and  $T$  is the temperature of the thermal bath. Directly after primordial inflation the flaton potential is dominated by the final term, controlled by the temperature of the thermal bath, and the flaton field is trapped in a quadratic potential at the origin. This is possible because the quartic self-interaction term is negligible for flaton fields [79], allowing the potential to be flattened.

At  $\theta = 0$  the potential energy density is  $V_0$  and when  $V_0 > \rho_r$  (the energy density of radiation, the dominant component of the Universe after inflation) another period of inflation occurs. Thus, from the relationship between the density of the thermal bath and its temperature in Eq. (2.94), the temperature at the onset of thermal inflation is

$$T_1 = \left( \frac{30}{\pi^2 g_*} \right)^{1/4} V_0^{1/4} \simeq V_0^{1/4}. \quad (2.157)$$

As thermal inflation ensues, the temperature of the thermal bath drops expo-

---

<sup>1</sup>In the literature the flaton field is most commonly denoted by  $\phi$  but we use  $\theta$  here in an effort to distinguish it from the many scalar fields denoted by  $\phi$  in this thesis.

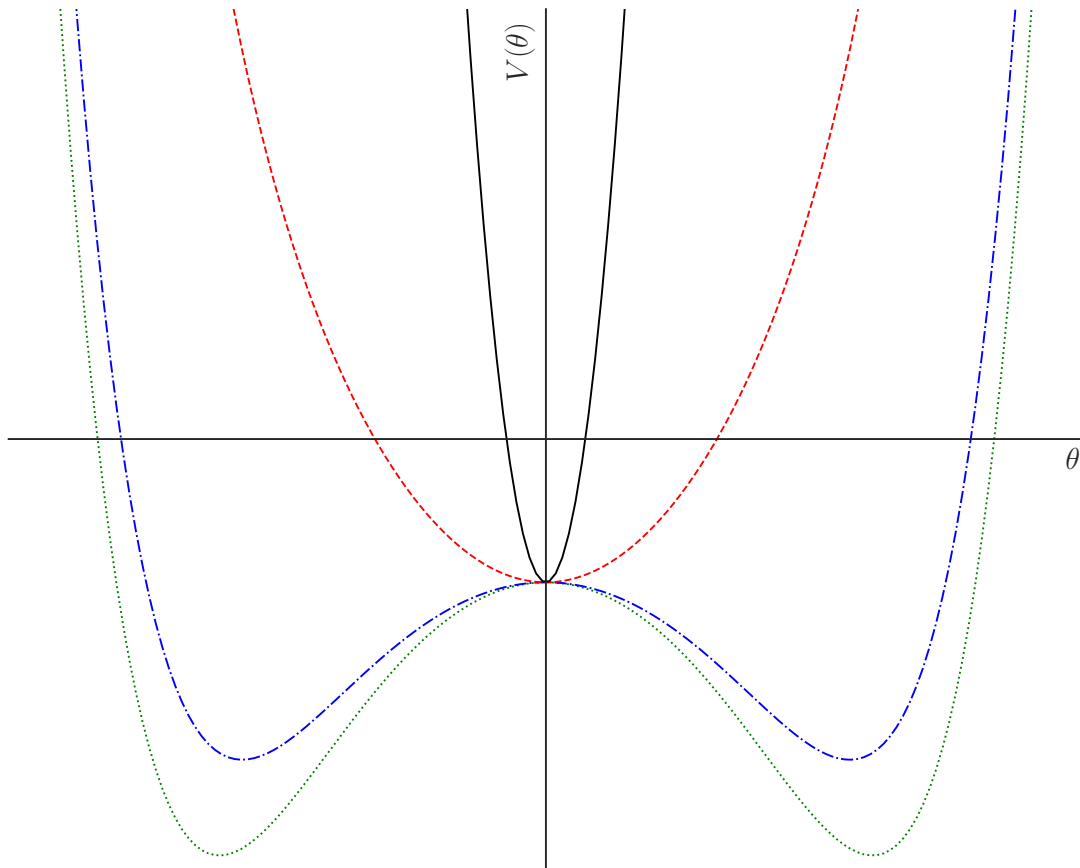


**Figure 2.4:** A sketch of the thermal inflation flaton potential using arbitrary units. As the temperature drops the potential opens up, allowing the flaton to move towards its VEV. The black (solid) line indicates the highest temperature, with the red (dashed), blue (dot-dashed) and green (dotted) lines at respectively lower temperatures.

nentially and so very quickly the dominant term in the potential is no longer the thermal interaction term. A phase transition occurs and the flaton is released towards its VEV, terminating thermal inflation. This occurs at the temperature

$$T_2 = \frac{m}{g}, \quad (2.158)$$

where  $m$  is the mass of the flaton field and this behaviour is demonstrated in Fig. 2.4.

It is the third term in Eq. (2.156) which controls the magnitude of the flaton

VEV,  $\langle\theta\rangle$ , and we see that a larger VEV requires a larger<sup>1</sup>  $n$

$$\langle\theta\rangle = \left[ \frac{\lambda}{(2n+3)!} \right]^{-\frac{1}{2(n+1)}} (m_{\text{Pl}}^n m)^{\frac{1}{n+1}}, \quad (2.159)$$

and as  $n \rightarrow \infty$ ,  $\langle\theta\rangle \rightarrow m_{\text{Pl}}$ . We have defined the minimum to be the vacuum and so from  $V(\langle\theta\rangle) = 0$  we find

$$V_0 = \frac{m^2 \langle\theta\rangle^2 (n+1)}{2 (n+2)}, \quad (2.160)$$

meaning the energy scale for thermal inflation is

$$V_0^{1/4} \simeq \sqrt{m \langle\theta\rangle}. \quad (2.161)$$

From the definition of the e-folding number in Eq. (2.88) and the fact that the scale factor is inversely proportional to the temperature of the thermal bath,  $a \propto T^{-1}$ , we can see the e-folds of thermal inflation correspond to

$$N_T = \ln \left( \frac{T_1}{T_2} \right) \simeq \frac{1}{2} \ln \left( \frac{g^2 \langle\theta\rangle}{m} \right). \quad (2.162)$$

Thermal inflation is interesting because it allows the number of e-folds of primordial inflation to vary, which is a feature of the original research in Chapters 3 and 4. For a perturbative coupling constant  $g \leq 1$ , maximum VEV corresponding to  $\langle\theta\rangle \leq m_{\text{Pl}}$  and  $m \geq 1\text{TeV}$  (because flaton particles have not been observed in any particle accelerators) we obtain a maximum of

$$N_T \simeq 17, \quad (2.163)$$

possible e-folds of thermal inflation.

---

<sup>1</sup>Which presumes the preceding terms are suppressed and  $\lambda$  is not equal for all  $n$ .

### 2.6.6 Eternal Inflation

The discussion of inflation so far, especially in Section 2.4.5, has focused on the e-folds of inflation during which observable scales left the horizon, because those are the e-folds of inflation which have an impact on the observational signatures of inflation. However, there is theoretically no maximum limit on the duration of inflation before this point. The slow-roll description of inflation has an unspoken caveat, in that we are assuming the classical dynamics of the scalar field dominate over the quantum fluctuations. Section 2.4.5 demonstrates how quantum fluctuations modify the classical slow-roll dynamics slightly to generate the density perturbations in the late Universe, but if they dominate the Universe undergoes what is known as eternal inflation.

During slow-roll the classical variation of the field is

$$|\dot{\phi}| \simeq \frac{V'}{3H} \simeq \frac{m_{\text{Pl}} V'}{\sqrt{3V}}, \quad (2.164)$$

and the amplitude of the quantum fluctuations, as introduced in Section 2.4.5, is given by

$$\left| \frac{\delta\phi}{\delta t} \right| \simeq \frac{H^2}{2\pi} \simeq \frac{V}{6\pi m_{\text{Pl}}^2}. \quad (2.165)$$

We therefore see that when

$$\frac{V^3}{12\pi^2 m_{\text{Pl}}^6 V'^2} > 1, \quad (2.166)$$

eternal inflation ensues.

This description of eternal inflation appears intuitive for very flat parts of the potential, such as on a hilltop in large-field models [80, 81]. Whereas classically we expect the field to roll down to the minimum, there is a vanishing quantum probability that it remains on the hilltop. Eternal inflation is also present in chaotic inflation models [82] leading to the idea of the ‘multiverse’, whereby pockets of the Universe inflate forever, causally distinct from one another, which supports the string landscape hypothesis, because it provides a mechanism to populate the landscape of string vacua, Ref. [83] provides an overview.

### 2.6.7 $f(R)$ Theories

If a field is non-minimally coupled to gravity there is an extra coupling term in the Lagrangian which alters the dynamics of inflation. They are not expressly examined in this thesis but it is worth mentioning that a conformal transformation shows that a non-minimally coupled scalar field in GR can be dynamically equivalent to an  $f(R)$  theory of gravity.  $f(R)$  theories of gravity swap the Ricci scalar in the Einstein-Hilbert action for a function of the Ricci scalar,  $f(R)$

$$S = \frac{m_{\text{Pl}}^2}{2} \int d^4x \sqrt{-g} f(R), \quad (2.167)$$

An example of this degeneracy is Starobinsky inflation and  $R+R^2$  gravity [64], and the framework of Gauss-Bonnet gravity used in the original research in Chapter 8 is related to  $f(R)$  gravity.

## 2.7 Reheating the Universe after Inflation

During inflation anything present in the Universe such as radiation and matter is diluted away by the expansion<sup>1</sup>. However, we know the Universe today is hot and filled with matter so we need a mechanism to (re)create this scenario. This process is called reheating, whereby the inflaton passes its energy density into other particle species of the SM via decay processes. For this to happen, the inflaton has to be coupled to other fields of the standard model and interaction terms are introduced to the Lagrangian of the theory. Interaction terms are additional terms in the Lagrangian, which are derived from particle physics and take forms similar to

$$\mathcal{L}_{\text{int}} = -\sigma\nu\phi\chi^2 - h\phi\bar{\psi}\psi - \frac{1}{2}g^2\phi^2\chi^2, \quad (2.168)$$

where  $\chi$  is a generic scalar field and  $\psi$  is a generic fermionic field, both assumed to be decay products of the inflaton,  $\phi$ .  $\nu$  is a mass scale,  $\sigma$  is the VEV of  $\phi$  and

<sup>1</sup>Except in the case of Warm Inflation [84].

$g$  and  $h$  are dimensionless coupling constants.

We define the reheating temperature of the Universe,  $T_{\text{reh}}$ , to be the temperature when this process has completed and radiation domination begins; temperature only has meaning when there is a particle species to be described by it. The longer reheating takes the more the reheating temperature decreases because of the continued expansion of the Universe.

Prompt reheating means almost immediate radiation domination and barely any time passes to dilute the energy. We know the energy scale at the end of simple, single-field inflation is approximately the GUT scale,  $T_{\text{reh}} \simeq 10^{16}\text{GeV}$ . The reheating temperature is a parameter in Eq. (2.97) for the number of e-folds of inflation remaining when observable scales left the horizon. As such, it strongly affects observables and hence should be thoroughly understood.

Before addressing the decay of the inflaton to other species, we first investigate the behaviour of the inflaton itself at this time. It is most common in inflationary models for the inflaton to oscillate in a minimum of its potential after inflation ends. Taylor expanding around the minimum, the potential can be well approximated by a quadratic

$$V(\phi) \approx \frac{1}{2}m_\phi^2\phi^2, \quad (2.169)$$

where  $m_\phi$  is the mass of the inflaton, meaning the KG equation becomes

$$\ddot{\phi} + 3H\dot{\phi} + m_\phi^2\phi = 0, \quad (2.170)$$

which is the equation of a damped harmonic oscillator, with solutions resembling

$$\phi \propto e^{\int \lambda(t) dt}. \quad (2.171)$$

Substituting solutions of this form into Eq. (2.170) we find

$$\lambda(t) \simeq \frac{-3H(t) \pm \sqrt{9H(t)^2 - 4m_\phi^2}}{2}, \quad (2.172)$$

where the motion of the oscillator has three behaviours, depending on the level of damping. The behaviour of interest to us for reheating is when the oscillator is under-damped, meaning it approaches zero very quickly and then oscillates about it. This occurs when  $9H^2 - 4m_\phi^2 < 0$  which translates to

$$m_\phi > \frac{3H}{2}. \quad (2.173)$$

Using this, the form of the damped oscillator can be approximated by an exponentially decaying sinusoid

$$\phi \approx \Phi(t) \sin(m_\phi t), \quad (2.174)$$

where

$$\Phi \propto e^{-\frac{1}{2} \int 3H dt}. \quad (2.175)$$

At this point the energy density of the inflaton (and hence its oscillation amplitude) is decaying due to only the expansion of the Universe.

The simplest description of reheating is perturbative reheating, whereby the inflaton transfers its energy to the standard model via single-body decays. If quantum enhancements are taken into account, due to the coherent nature of the inflaton field, preheating (or *instant* preheating if the decay particle decays quickly enough) also occurs. If the inflaton is not directly coupled to the SM particles, then reheating will proceed via gravitational reheating. These are addressed in detail in the following sections.

### 2.7.1 Perturbative Reheating

Perturbative reheating is in many respects the simplest description of reheating and has a classical description. It is often superseded by other reheating mechanisms, described in subsequent sections, which take into account the quantum effects of the decay, such as resonance. However, if these are incomplete or ineffective for some reason, the classical description of reheating persists.

A homogeneous scalar field oscillating about the minimum of its potential can be thought of as a collection of particles with zero momenta. If the inflaton is coupled to other fields, as it oscillates about the minimum of its potential it decays into the other fields, governed by the interactions in the Lagrangian. In perturbative reheating, individual inflaton particles are treated independently, with each having a finite probability of decaying.

When the inflaton field is coupled to other fields, the interaction terms in the Lagrangian (Eq. (2.168)) introduce corrections to the inflaton mass, so that the KG equation now looks like

$$\ddot{\phi} + (3H + \Gamma)\dot{\phi} + V'(\phi) = 0, \quad (2.176)$$

where  $\Gamma$  is the decay rate of the inflaton to other species. The solution for  $\phi$  becomes

$$\phi = \phi_0 e^{-\frac{1}{2} \int (3H + \Gamma) dt} \sin(m_\phi t), \quad (2.177)$$

and we can see that when  $\Gamma > 3H$  the decrease in inflaton energy due to particle decay dominates over the decrease due to the expansion of the Universe. This can also be seen from the continuity equation, taking the derivative of the energy density of the scalar field we see

$$\dot{\rho} = \dot{\phi}\ddot{\phi} + V'(\phi)\dot{\phi} = \dot{\phi}(\ddot{\phi} + V') = -\dot{\phi}^2(3H + \Gamma), \quad (2.178)$$

where in the last equality we have substituted in a rearranged form of Eq. (2.176), leading to

$$\dot{\rho} + (3H + \Gamma)\rho = 0, \quad (2.179)$$

where we have used the fact that the average kinetic energy is equal to the average potential energy for the oscillating field, hence  $\rho = \dot{\phi}^2$ . This also explains why  $p$  no longer features in the continuity equation here, because  $p = 0$  for the oscillating field and it behaves as matter. We have replicated the continuity equation from Eq. (2.23) for pressureless matter but now with an extra term accounting for the decays of the particles.

The decay rates for the interactions in Eq. (2.168) are [3]:

$$\Gamma_{\phi \rightarrow \chi\chi} = \frac{\sigma^2 \nu^2}{8\pi m_\phi}, \quad (2.180)$$

$$\Gamma_{\phi \rightarrow \bar{\psi}\psi} = \frac{h^2 m_\phi}{8\pi}, \quad (2.181)$$

$$\Gamma_{\phi\phi \rightarrow \chi\chi} = \frac{g^2 \phi^2}{8\pi m_\phi}. \quad (2.182)$$

When  $\Gamma \approx H$  the decay products accumulate faster than they can be diluted away by the expansion of the Universe. Different decay channels occur over different timescales, for example the last decay process in the above is proportional to  $t^{-2}$  whereas  $H \propto t^{-1}$ , as such it never reaches  $\Gamma \approx H$  and is not a dominant contribution to perturbative reheating<sup>1</sup>.

After inflation we know  $m_\phi \gg H$  (see Eq. (2.81)) and so the inflaton is completing many oscillations in one Hubble time. It is because the oscillating inflaton behaves as matter with  $w = 0$  that the length of reheating and hence the value of  $T_{\text{reh}}$  has such an effect on the observables, because the expansion rate of the Universe is altered. As we saw in Section 2.2.3, when  $w = 0$ ,  $a \propto t^{2/3}$ , in contrast with radiation domination, when  $w = 1/3$ , which behaves as  $a \propto t^{1/2}$ . This explains why a lower value for  $T_{\text{reh}}$  translates to a lower  $N_*$ , because the Universe has been able to expand more within a given time.

The evolution equation for the energy density of the decay products follows from energy conservation and is given by

$$\dot{\rho}_r + 4H\rho_r - \Gamma_\phi \rho_\phi = 0, \quad (2.183)$$

where we use the subscript ‘ $r$ ’ because the decay products are relativistic and will decay to the standard model radiation bath. The final term is a source term from the decay of the inflaton. Whilst the inflaton is oscillating and  $\rho_r$  is subdominant,

---

<sup>1</sup>Also the first process is only present if there is a symmetry breaking present, so  $\sigma \neq 0$ . Hence, without symmetry breaking the 2nd decay is the dominant one.

an approximate solution to Eq. (2.183) is [85]

$$\rho_r \simeq \frac{m_{\text{Pl}}^2 \Gamma}{10\pi t} \left[ 1 - \left( \frac{t}{t_{\text{end}}} \right)^{-5/3} \right], \quad (2.184)$$

where ‘end’ refers to the end of inflation. During matter domination  $t \propto a^{3/2}$  so  $\rho_r \propto a^{-3/2}$  and relating the radiation energy density to the temperature,  $\rho_r \propto T^4$  (via Eq. (2.94)) we see that during the oscillations the temperature behaves as  $T \propto \rho_r^{1/4} \propto a^{-3/8}$ .

This means the reheating temperature, defined at the point radiation domination begins, is not the maximum temperature attained during this period, which instead occurs at the onset of the oscillations. It is important not to discount the presence of the subdominant radiation bath during the oscillatory phase. For example, the original research presented in Chapter 6 considers the impact on black hole formation rates during this primordial epoch. When the Universe is radiation dominated we can estimate the temperature of the radiation via

$$\rho_r \approx \frac{\pi^2 g_* T^4}{30}, \quad (2.185)$$

where  $g_*$  are the number of relativistic degrees of freedom.

As mentioned, the Universe is continuing to expand during this process, so the quicker reheating completes, whereby radiation comes to dominate the energy density budget of the Universe, the higher the reheating temperature, denoted by  $T_{\text{reh}}$  is. At the end of the oscillatory period, the decay products accumulate more quickly than the expansion dilutes them and the reheating temperature can be calculating by substituting the Friedmann equation, which by definition is  $3m_{\text{Pl}}^2 H^2 = \rho_r$  at reheating, into  $3H = \Gamma$ :

$$T_{\text{reh}} = \left( \frac{10}{\pi^2 g_*} \right)^{\frac{1}{4}} \sqrt{m_{\text{Pl}} \Gamma} \approx \sqrt{m_{\text{Pl}} \Gamma}. \quad (2.186)$$

## 2.7.2 Preheating

In the previous description we considered the inflaton particles decaying individually through single particle decay processes. However, if the inflaton field is treated as a condensate composed of many inflaton quanta all oscillating with the same phase, rather than individual particles, there is an effect called parametric resonance which must be considered, which enhances particle production.

We consider that the inflaton is again coupled to a scalar field, but we now use a quantum treatment and express the coupled field,  $\hat{\chi}$ , as a sum of its creation and annihilation operators

$$\hat{\chi} = \frac{1}{(2\pi)^3} \int [\hat{a}(\mathbf{k})\chi_k(t) + \hat{a}^\dagger(-\mathbf{k})\chi_k^*(t)]e^{i\mathbf{k}\cdot\mathbf{x}} d^3k, \quad (2.187)$$

and the Fourier modes in this expansion obey the wave equation

$$\ddot{\chi}_k + 3H\dot{\chi}_k + \left(\frac{k^2}{a^2} + m_{\chi,\text{eff}}^2\right)\chi_k = 0, \quad (2.188)$$

where

$$m_{\chi,\text{eff}} = m_{\chi,0} + m_{\chi,\text{int}}, \quad (2.189)$$

represents the bare mass of the  $\chi$  field plus the correction to its mass arising from the interaction term.  $m_{\chi,\text{eff}}$  has a dependence on  $\phi$  through  $m_{\chi,\text{int}}^2 \equiv V''_{\text{int}}(\phi)$  and hence the frequency of this quantum harmonic oscillator is now time dependent:

$$\omega^2(t) = \frac{k^2}{a^2(t)} + m_{\chi,\text{eff}}^2(t). \quad (2.190)$$

One will notice the frequency also depends on the scale factor of the Universe, but after inflation we know  $m_\phi \gg H$  (see Eq. (2.81)) and so the inflaton is completing many oscillations in one Hubble time. As such, we can normalise  $a = 1$  and the frequency is simply

$$\omega^2(t) = k^2 + m_{\chi,\text{eff}}^2(t). \quad (2.191)$$

The dominant decay channel for parametric resonance effects is the third one in

Eq. (2.168), which gives  $m_{\chi,\text{int}}^2 = g^2\phi^2$  and presuming  $m_{\chi,0} \ll m_{\chi,\text{int}}$  (which we will see is valid momentarily) we use this now to demonstrate:

$$\ddot{\chi}_k + (k^2 + g^2\phi^2)\chi_k = 0. \quad (2.192)$$

In the previous section (Eq. (2.174)) we found

$$\phi = \Phi \sin(m_\phi t), \quad (2.193)$$

where  $\Phi$  is the amplitude of the oscillating inflaton field, which allows us to rewrite the equation of motion as

$$\ddot{\chi}_k + (k^2 + g^2\Phi^2 \sin^2(m_\phi t))\chi_k = 0. \quad (2.194)$$

A change of variables ( $m_\phi t = z$ ) allows us to write this in the form

$$\chi_k'' + (A_k - 2q \cos(2z))\chi_k = 0, \quad (2.195)$$

where

$$A_k = \frac{k^2}{m_\phi^2} + 2q \quad q = \frac{g^2\Phi^2}{4m_\phi^2}, \quad (2.196)$$

$q$  is the ‘quality factor’ and a prime represents a derivative with respect to  $z$ . The motivation for this representation is that this is the well-known Mathieu equation, whose solutions can be stable or unstable depending on the parameter space  $\{A_k, q\}$ . For a given mode an instability corresponds to exponential growth of the occupation number

$$n_k \propto \exp(2\mu_k^{(n)} z), \quad (2.197)$$

where  $\mu_k$  is the Floquet exponent, calculated numerically but generally taken to be approximately  $0 < \mu \lesssim 0.3$  [86] and  $n$  is the particular resonance band. This growth of occupation numbers is interpreted as particle production and the instability bands are shown in Fig. 2.5

The value of  $q$  determines the width of instability mode bands, when  $q < 1$  it is

called narrow resonance and otherwise, broad resonance. The wider the resonance bands the more efficient the reheating is. During broad resonance the  $\chi_k$  field oscillates much more quickly than the  $\phi$  field and for most of the oscillation the effective mass of  $\chi_k$  is larger than that of  $\phi$  and particle production is suppressed due to the adiabatic nature of the oscillations. However, at points during the oscillation the adiabaticity constraint is violated, meaning

$$\frac{|\dot{\omega}|}{\omega^2} \gg 1, \quad (2.198)$$

and bursts of exponential particle production occur. For the coupling here, this occurs for  $k$  values

$$k^2 < (g^2 \phi m_\phi \Phi)^{2/3} - g^2 \phi^2, \quad (2.199)$$

where we have used that  $|\dot{\phi}_0| = m_\phi \Phi$  near the minimum of the effective potential. Finding the maximum of Eq. (2.199) allows us to find a range of  $k$  values which undergo particle production

$$0 \leq 2k \leq \sqrt{g m_\phi \Phi}, \quad (2.200)$$

and specifying  $k > 0$  in Eq. (2.199) gives a region in field space where the adiabaticity constraint is violated (Eq. (2.198)):

$$-\sqrt{\frac{m_\phi \Phi}{g}} \lesssim \phi \lesssim \sqrt{\frac{m_\phi \Phi}{g}}. \quad (2.201)$$

The general equation for the occupation number of produced particles is [86]

$$n_k = \exp\left(-\frac{\pi(k^2 + m_\chi^2)}{g|\dot{\phi}_{\min}|}\right), \quad (2.202)$$

where we allow the  $\chi$  field to be massive and reinstate  $\dot{\phi}$  rather than assuming its value at the minimum, defined by the subscript ‘min’ here. Integrating over

all values of  $k$  gives the total number density of  $\chi$  particles [87, 88]

$$n_\chi = \frac{1}{2\pi^2} \int_0^\infty k^2 n_k dk = \frac{(g|\dot{\phi}_{\min}|)^{3/2}}{8\pi^3} \exp\left(\frac{-\pi m_\chi^2}{g|\dot{\phi}_{\min}|}\right). \quad (2.203)$$

As long as  $m_\chi^2 < g|\dot{\phi}_{\min}|$  the number density is not exponentially suppressed and simplifies to

$$n_\chi \simeq \frac{(g|\dot{\phi}_{\min}|)^{3/2}}{8\pi^3}, \quad (2.204)$$

with no dependence on  $m_\chi$ . However, if  $m_\chi^2 \simeq g|\dot{\phi}_{\min}|$  for oscillations after the first, particle production will be exponentially suppressed due to the decrease occurring in  $\dot{\phi}$  for a constant  $m_\chi$ .

As preheating proceeds the amplitude of the  $\phi$  oscillations decreases and so the resonance moves from the broad to the narrow regime. However, we have neglected the possible effect the produced  $\chi$  particles might have on the dynamics of  $\phi$ . The effective mass of  $\phi$  now receives a contribution from the newly created particles

$$m_\phi^2 = g^2 \langle \chi^2 \rangle, \quad (2.205)$$

where we use the Hartree approximation

$$\langle \chi^2 \rangle = \int_0^\infty \frac{k^2 dk}{2\pi^2} |\chi_k(t)|^2. \quad (2.206)$$

The addition of this backreaction term to the KG equation acts to suppress the resonance and so to ensure it does not spoil the mechanism  $g^2 \langle \chi^2 \rangle < m^2$  should be imposed which acts as a constraint on the coupling constant,  $g$ . However, because  $\langle \chi^2 \rangle$  grows during this process, preheating never fully completes and energy density remaining in the inflaton is dissipated via perturbative reheating.

### 2.7.3 Instant Preheating

Instant preheating is another non-perturbative process but uniquely does not require oscillations about a minimum. Preheating via parametric resonance relies on multiple crossings of  $\phi = 0$  to exponentially increase the energy density of

$\chi$  whereas *instant* preheating focuses on the first oscillation only [87]. Instant preheating utilises the same coupling as that in preheating but  $\chi$  is also coupled to a fermion,  $\psi$ , as:

$$\mathcal{L} = -\frac{1}{2}g^2\phi^2\chi^2 - h\bar{\psi}\psi\chi, \quad (2.207)$$

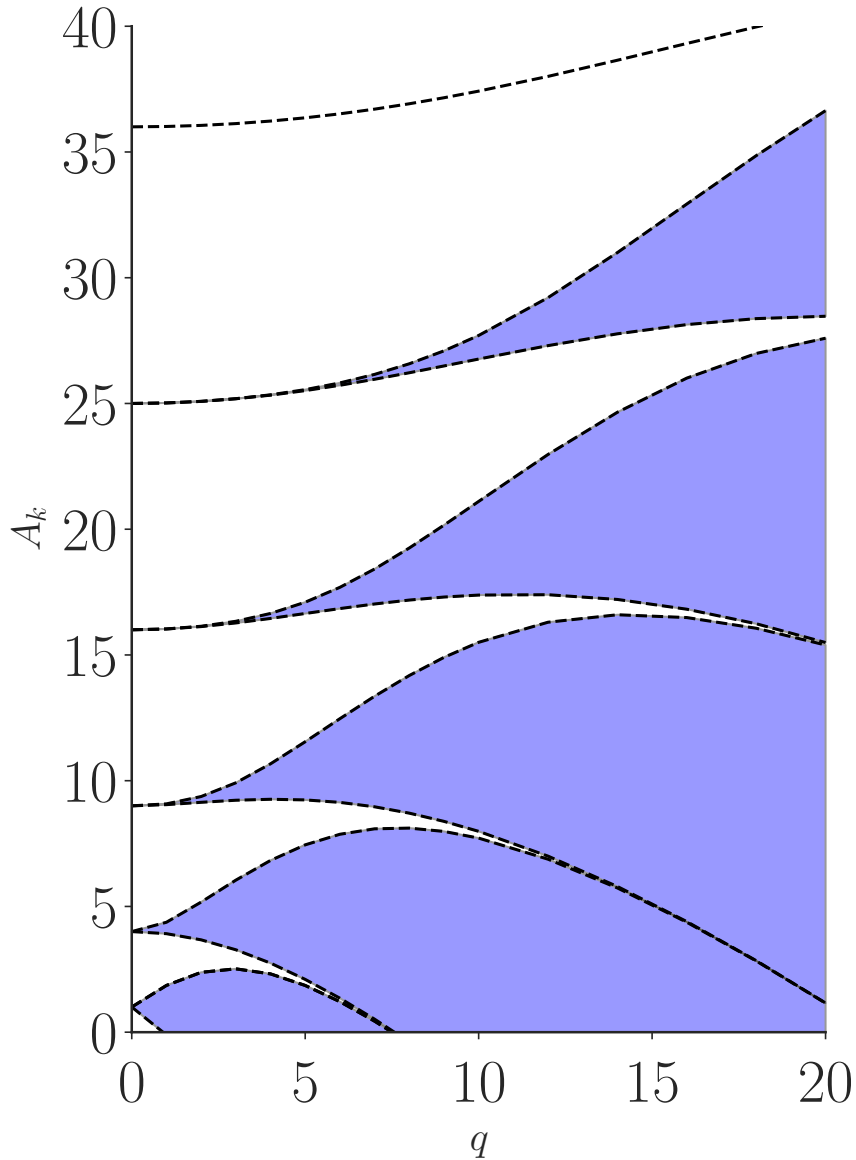


**Figure 2.5:** Mathieu instability bands (blue regions) which are interpreted as exponential particle production.

where  $g$  and  $h$  are dimensionless coupling constants.

As  $\phi$  crosses the origin the number density of produced  $\chi$  particles suddenly increases and then remains approximately constant for the duration of the inflaton's oscillation, as per the broad resonance regime of preheating seen previously. However, the effective mass of  $\chi$  is

$$m_\chi^2 = g^2 \phi^2, \quad (2.208)$$

which grows as  $\phi$  moves to larger values. As such, if  $\chi$  decays to  $\psi$  at the point where its mass is maximised, the energy density of produced particles is enhanced.

The decay rate for the produced  $\chi$  particles is

$$\Gamma_{\chi \rightarrow \bar{\psi} \psi} = \frac{h^2 m_\chi}{8\pi}, \quad (2.209)$$

presuming the bare mass of the  $\chi$  particle is negligible to the interaction mass, given in Eq. (2.208), this equates to

$$\Gamma_{\chi \rightarrow \bar{\psi} \psi} = \frac{h^2 g \phi}{8\pi}, \quad (2.210)$$

where  $\phi$  is evaluated at the point of decay. As  $\phi$  is growing as it moves to the extremum of its oscillation, the decay rate is also growing, indicating that  $\chi$  is predisposed to decay at the maximum amplitude of  $\phi$ . Depending on the values of  $g$  and  $h$ ,  $\chi$  may decay before it reaches  $\phi_{\max}$  but there is a lower limit arising from the requirement that

$$m_\chi = g|\phi| \geq 2m_\psi, \quad (2.211)$$

whatever the mass of the fermions may be, otherwise the decay is kinematically forbidden.

If the model in question has a minimum and the  $\chi$  particles do not decay before subsequent oscillations of the inflaton, reheating will proceed via parametric resonance. Because instant preheating does not rely on bosonic amplification to enhance the energy density of the decay particle the inflaton is able to decay directly to fermions as well as bosons.

The important distinction of instant preheating, that the theory does not require any oscillation of the inflaton about a minimum, means it is an excellent candidate for reheating in theories of quintessential inflation and will feature heavily in the research in Chapters 7 and 8.

We find the density of the produced  $\chi$  particles by combining Eq. (2.204) with the  $\chi$  particle effective mass [87, 88]

$$\rho_{\chi}^{\text{IP}} = \frac{g^{5/2} |\dot{\phi}_{\text{IP}}|^{3/2} \phi_{\text{IP}}}{8\pi^3}. \quad (2.212)$$

The instant preheating efficiency is maximised when  $\phi$  is near the final edge of the production window because, even though we expect a continuous contribution to  $n_{\chi}$  whilst  $\phi$  is in this region, the produced  $\chi$ -particles are diluted by the expansion of the Universe. Therefore, we expect only the ones produced near the end of the particle production regime to contribute significantly to  $\rho_{\chi}^{\text{IP}}$ . From Eq. (2.201), re-instating  $\dot{\phi}$  we set

$$\phi_{\text{IP}} = \sqrt{\frac{\dot{\phi}_{\text{IP}}}{g}}, \quad (2.213)$$

which simplifies Eq. (2.212) to

$$\rho_r^{\text{IP}} = \rho_{\chi}^{\text{IP}} = \frac{g^2 \dot{\phi}_{\text{IP}}^2}{8\pi^3}, \quad (2.214)$$

where we have assumed the decay of the  $\chi$ -particles to radiation is instantaneous.

### 2.7.4 Gravitational Reheating

If, for some reason, the inflaton is not explicitly coupled to other fields, or the reheating mechanism is ineffective, the Universe will still progress into radiation domination (as we know it must) via gravitational reheating [89]. Gravitational reheating is in most cases sub-dominant to another form of reheating mechanism because it is very inefficient, but it is always present and in the absence of other mechanisms it reheats the Universe. As discussed in Section 2.4.1, the cosmological horizon during periods of accelerated expansion is an event horizon.

Quantum fluctuations of the vacuum can heuristically be thought of as pairs of virtual particles and anti-particles constantly popping into existence and subsequently annihilating with one another. When there is an event horizon, pairs of virtual particles are unable to annihilate if they are outside of causal contact, meaning they become real particles.

Particles produced in this manner during inflation are inflated away but are being constantly replenished, meaning that at the end of inflation a sub-dominant thermal<sup>1</sup> bath will exist that, given time, may come to dominate the energy density of the Universe and initiate a radiation dominated epoch [89]. All non-conformally invariant light fields ( $m < H$ ) produce particles gravitationally because they are coupled to the metric via gravity and the temperature of the thermal bath generated by gravitational reheating is

$$T = \frac{H}{2\pi}, \quad (2.215)$$

which is the Hawking temperature of de Sitter space. As such, it is an appropriate choice for quasi-de Sitter inflation but we note the pre-factor changes for other types of inflation, e.g. power-law inflation. As we first saw in Eq. (2.94), the energy density of radiation is related to its temperature via

$$\rho_r = \frac{\pi^2 g_*}{30} T^4, \quad (2.216)$$

which in this case gives

$$\rho_r = \frac{q g_*}{480 \pi^2} H^4, \quad (2.217)$$

where we have introduced an efficiency factor,  $q \approx 1$ , to encapsulate the produced radiation not necessarily being thermalised.

---

<sup>1</sup>The radiation is not exactly thermal, which is why Eq. (2.217) features an efficiency factor,  $q$ .

### 2.7.5 Constraints on Reheating

The main constraints that must be considered for reheating are the timescales involved. BBN commences at energy levels of approximately 100 keV, when photons in the thermal bath no longer have enough energy to photo-disintegrate the nuclei of light elements, meaning they start to form in measurable quantities for the first time. Reheating quantifies the moment at which the Universe is dominated by thermalised radiation, so this necessarily must occur at energy levels higher than 100 keV. As such, an ultimate lower bound on the reheating temperature of the Universe is

$$T_{\text{reh}} > 1 \text{ MeV} . \quad (2.218)$$

Another possible constraint on the reheating temperature exists if the inflation model in question is embedded in a supergravity theory (see Section 2.5.1). In supergravity models the graviton has a ‘super partner’ called the gravitino. If they exist, gravitinos are expected to have a mass of approximately the TeV scale which presents a constraint on their abundance if they are a stable particle contributing to dark matter. Alternatively, if they are unstable and decay to other particles the decay channels will produce energetic particles capable of disrupting BBN. Gravitinos only decay via gravitationally suppressed interactions which means they have a long lifetime and would survive past the time of BBN if they were produced in the early Universe. As such, the abundance of gravitinos either needs to be heavily constrained or avoided completely.

Production mechanisms for gravitinos are either thermal (produced via scatterings in the thermal bath) or non-thermal (direct inflaton decay [90–92]). For thermal production their relative abundance has a strong dependence on the reheating temperature; to avoid an excess of stable gravitinos contributing to dark matter and over-closing the Universe requires

$$T_{\text{reh}} < \mathcal{O}(10^7) \text{ GeV} . \quad (2.219)$$

Alternatively, to avoid an excess of unstable gravitinos’ decay products destabil-

ising BBN requires

$$T_{\text{reh}} < \mathcal{O}(10^6 - 10^9) \text{ GeV}. \quad (2.220)$$

As is evident from the constraints, thermal production of gravitinos is more important for a higher  $T_{\text{reh}}$ . However, production via inflaton decay is more effective with a lower reheating temperature. Therefore, constraining the thermal production naturally enhances the non-thermal production. The non-thermal production of gravitinos is already effective for a reheating temperature satisfying either Eq. (2.219) or Eq. (2.220) [91], meaning it does not present as a constraint on  $T_{\text{reh}}$  but rather the details of the supergravity model. For the purposes of this thesis we take a bound of [90–92]

$$T_{\text{reh}} < 10^9 \text{ GeV}. \quad (2.221)$$

After reheating, the Universe is radiation dominated, but as we know the energy density of radiation scales as  $\rho_r \propto a^{-4}$  whilst the energy density of matter scales as  $\rho_m \propto a^{-3}$ . This means the Universe reaches a point where they are approximately equal, the time of matter-radiation equality. From this point on the Universe is matter dominated. However, as briefly mentioned in Section 2.1.3, in the 1990s two separate teams of researchers made the discovery that the current expansion of the Universe is actually accelerating [30, 31]. This means the Universe has transitioned from matter domination into a period now known as dark energy domination. The late-time (present day) evolution of the Universe is investigated in detail in the next section.

## 2.8 Dark Energy and Quintessential Inflation

As we saw in Section 2.4.3, to have accelerated expansion, namely  $\ddot{a} > 0$ , requires a fluid with equation of state  $w < -\frac{1}{3}$  to be the dominant component of the Universe. This unknown fluid which acts to accelerate the expansion of the Universe in the modern day is given the name ‘Dark Energy’, Ref. [93] provides a comprehensive review. The nature of dark energy is undetermined but observations of the accelerating expansion have constrained the density parameter and

the equation of state of dark energy to be<sup>1</sup> [4]

$$\Omega_{\text{DE}} = 0.685 \pm 0.007, \quad (2.222)$$

$$w_{\text{DE}} = -1.03 \pm 0.03. \quad (2.223)$$

Constraining the details of dark energy is an active research area. Whilst  $\Lambda$ CDM is the foremost theoretical description for dark energy it has its downfalls and discrepancies which competing models are able to alleviate, the most prominent of which is quintessence. We introduce both of these in the following sections.

### 2.8.1 $\Lambda$ CDM

The simplest explanation for dark energy is the ‘Cosmological Constant’ (CC),  $\Lambda$ . The CC was first introduced by Einstein to his field equation to enable it to describe a static, matter-filled Universe, as he believed the Universe to be at the time. As soon as Hubble observed that our Universe was, in fact, not static, Einstein retracted the CC as ‘the greatest blunder of his life’<sup>2</sup>.

Einstein introduced a carefully balanced form of  $\Lambda$  to result in a static Universe, but a slightly larger value,  $\Lambda \geq m_{\text{Pl}}^2/2$  would produce an accelerated expansion<sup>3</sup>. The cosmological constant can be modelled as a perfect fluid with  $\rho_\Lambda \equiv m_{\text{Pl}}^2 \Lambda$  and an unchanging equation of state parameter,  $w_\Lambda = -1$ . For a positive CC,  $\Lambda > 0 \leftrightarrow \rho_\Lambda > 0$  and so we see that the pressure is negative and the cosmological constant satisfies the criteria to explain dark energy - as long as it is the dominant contribution to the energy density of the Universe at present.

By definition, explaining dark energy in this way requires a component of the Universe whose energy density remains constant eternally, regardless of the expansion. One physical explanation put forth for the CC is vacuum energy, a quantum effect which could adequately describe our observations. However, attempts to derive a value for the vacuum energy produce wildly different values

<sup>1</sup>In Ref. [4]  $\Omega_{\text{DE}}$  is referred to as  $\Omega_\Lambda$  but as we discuss quintessence here we reserve  $\Omega_\Lambda$  for when we specifically refer to the cosmological constant explanation of dark energy.

<sup>2</sup>According to George Gamow in his memoirs [94].

<sup>3</sup>A smaller value for  $\Lambda$  leads to collapse.

to the critical density of the Universe we observe today, a quirk known as the ‘Cosmological Constant Problem’.

### 2.8.1.1 The Cosmological Constant Problem

The vacuum energy density has not been accurately computed in quantum field theory, but a natural value would be the cut-off scale of existing theories, the Planck energy density:

$$\langle \rho \rangle_{\text{vac}} \simeq \frac{E_{Pl}}{l_{Pl}^3} \simeq m_{Pl}^4 \simeq 10^{72} \text{ GeV}^4. \quad (2.224)$$

The observed critical energy density of the Universe today is  $\rho_c \approx 10^{-48} \text{ GeV}^4$  and  $\rho_{DE} \simeq 0.7\rho_c$ . Hence, comparing the observed with the predicted

$$\frac{\rho_c}{m_{Pl}^4} \approx 10^{-120}, \quad (2.225)$$

we see there is a separation of approximately 120 orders of magnitude between the vacuum energy density we expect from quantum field theory and the observed dark energy density.

Clearly something is amiss here and so it is typical to assume the vacuum energy density is zero, due to an unknown symmetry, and then the cosmological constant explains the energy density of the dark energy

$$\rho_\Lambda \equiv m_{Pl}^2 \Lambda \simeq (10^{-12} \text{ GeV})^4, \quad (2.226)$$

$$\Lambda \approx (10^{-42} \text{ GeV})^2, \quad (2.227)$$

and takes a value which is almost, but not exactly, zero, differing at the 84th decimal place. The cosmological constant problem has hence been described<sup>1</sup> as the ‘worst fine-tuning problem in Physics’.

---

<sup>1</sup>By Laurence Krauss.

### 2.8.1.2 Future Horizons Problem of $\Lambda$ CDM

The question of why  $\Lambda$  should be so small but not exactly zero is sometimes answered using anthropic arguments<sup>1</sup> in string theory because the string landscape provides a plethora of de-Sitter vacua at varying energies [96]. However,  $\Lambda$ CDM in string theory suffers from the future horizons problem.

In  $\Lambda$ CDM, the Universe transitions into a period of total  $\Lambda$  domination which never ends, the Universe expansion accelerates forever and in the distant future all unbound matter will become infinitely diluted, separated outside of causal contact with anything else - there will be future horizons that prevent the communication of information. This is incompatible with string theory, which requires future asymptotic states to be well defined in order for an S-matrix to be formulated [97, 98].

This can either be viewed as a problem of models resulting in eternal cosmic acceleration, or a problem of string theory as a viable mathematical description of the Universe. We do not comment too much either way except to point out the second swampland conjecture, detailed in Section 2.6.3, which brings the very existence of de-Sitter vacua in string theory into question.

We therefore move on, taking the conservative viewpoint that eternal periods of cosmic acceleration are best avoided if possible, but remain agnostic as to the Theory of Everything.

## 2.8.2 Quintessence

An alternative to  $\Lambda$ CDM is quintessence, so named [99] as a ‘fifth element’ after baryons, CDM, photons and neutrinos. Quintessence is a dynamic scalar field which can generate the observed accelerated expansion if it is slowly rolling along a flat part of its potential and is the dominant component of the energy density budget of the Universe at present [100]. Utilising a scalar field does not remove the need to explain why the theoretical vacuum energy density does not

---

<sup>1</sup>The anthropic principle considers fine-tuning questions to be unremarkable because fundamental constants (etc...) necessarily take the values required for human life to then evolve and question them. From a continuum of possible values, we witness the one we do out of nothing more remarkable than coincidence [95].

match observations, as it must still be set to zero due to some unknown symmetry. However, it reduces the levels of fine-tuning because we do not have to arbitrarily assign a tiny, and seemingly unnatural, value to a constant, instead the quintessence field naturally evolves to provide the correct energy density for dark energy at the correct time. The dynamical nature of the quintessence field, with  $\dot{w} \neq 0$ , also means it does not suffer from the future horizons problem if  $V \rightarrow 0$  eventually, giving quintessence models two clear advantages over  $\Lambda$ CDM. However, quintessence models suffer from problems of their own.

Firstly, in many cases a quintessence field features an exponential potential of the form [101]

$$V(\phi) \propto e^{-\lambda\phi/m_{\text{Pl}}}, \quad (2.228)$$

for which the mass-squared is  $m^2 \approx \frac{\lambda^2 V(\phi)}{m_{\text{Pl}}^2}$ . By necessity, we need the potential energy density to match the dark energy observations,  $V(\phi) = 0.7\rho_c = 3m_{\text{Pl}}^2 H_0^2$ , which means  $m \approx \lambda H_0$  and the mass of a quintessence scalar field is approximately of the order of the present Hubble constant value,  $H_0 \approx 1.43 \times 10^{-42}$  GeV. This means its Compton wavelength, which is  $1/m$ , is of the order of the size of the horizon and a long-range interaction force might exist, which would violate the Equivalence Principle and has never been observed. As such, the interaction terms between the quintessence scalar field and other standard model fields in the Lagrangian must be suppressed somehow. This is known as the ‘fifth force problem’.

Secondly, quintessence introduces another source of fine-tuning, that of the initial conditions. To ensure the energy density of the quintessence field matches the observations we see today, it is necessary to tune the initial conditions of the scalar field. Reducing the fine-tuning of  $\Lambda$ CDM is one of the motivations for quintessence so this must be kept under control. In a similar way, it is important to ensure quintessence models do not feature scales similar to  $\Lambda$ ; introducing scales of the order of the cosmological constant by hand does not reduce the fine-tuning.

Finally, quintessence models generally require the scalar field to travel over Planckian distances in field space. However, as explained in Section 2.6.3, super-Planckian field excursions in field space mean we cannot guarantee the flatness of

the potential any more, due to radiative corrections. Ref. [102] gives a summary of the difficulties facing quintessence models with  $\phi \gg m_{\text{Pl}}$ , and finds them unviable.

### 2.8.3 Quintessential Inflation

If the mechanism of quintessence is a slowly rolling scalar field, reminiscent of the inflaton field, the question ‘could the quintessence field be the same scalar field as drives primordial inflation?’ naturally arises. Combining the two scalar fields into one in this way is called quintessential inflation (QI) [103] and naturally improves on quintessence alone in two key ways. Firstly, using a single unified theoretical framework, as well as seeming economical, keeps the theory more minimal with fewer degrees of freedom than two separate scalar fields. Secondly, uniting the two phases of Universe evolution eliminates the initial conditions problem of quintessence, because the initial conditions are now fixed by the attractor of inflation.

Forming a successful model of quintessential inflation has its challenges. The energy density scales in question are staggeringly different, with inflation at the order of  $10^{64} \text{ GeV}^4$  and late-time accelerated expansion approximately  $10^{-48} \text{ GeV}^4$ , a difference of approximately 112 orders of magnitude, which a successful scalar field potential will need to bridge. Secondly, both periods of accelerated expansion require a flat potential for the accelerated expansion to be viable in the minimal versions of the theory<sup>1</sup>, two *plateaus* separated by 112 orders of magnitude is suddenly much more difficult to formulate, running the risk of forming an artificial potential.

Presuming such a potential is justifiable, there is now a hugely steep drop between the two plateau regions, regardless of the formulation of the theory. As the field crosses this point, the Klein-Gordon equation becomes dominated by the kinetic terms and the field traverses large distances in field space, regardless of the potential. If the field crosses Planckian distances the flatness of the potential is thrown into question and radiative corrections must be considered. If the second,

---

<sup>1</sup>Warm inflation [84], as an example, does not require a flat potential but is no longer a minimal theory.

late-time, plateau region cannot be guaranteed, then the potential's suitability for quintessential inflation is all but negated. However, if the inflaton's motion is restricted to sub-Planckian field distances, the potential is likely to be too curved at early times for inflation to progress in a manner that matches observations, which is the 'η-problem of quintessential inflation' [104].

Quintessential inflation models also still suffer from the fifth force problem and must somehow suppress their interactions to the other standard model fields at large distances.

A final obstacle in a model of quintessential inflation is how to successfully reheat the Universe after inflation, with a scalar field potential which by necessity does not have a minimum for traditional perturbative reheating to occur at. The field must also retain some trace of its energy density at late times to explain dark energy, and so it cannot decay completely.

#### 2.8.4 Early-time Kinematics of Quintessential Inflation

When inflation ends and the field reaches the very steep part of its potential, its EoM is dominated by the influence of the kinetic terms and the motion of the field is oblivious to the shape of the potential. The Klein-Gordon equation (Eq. (2.62)) simplifies to

$$\ddot{\phi} + 3H\dot{\phi} \simeq 0, \quad (2.229)$$

and the dynamics of the field during this regime can be treated in a model independent way.

Solutions to Eq. (2.229) take different forms depending on the background dynamics. If the kinetically dominated inflaton is dominating the energy budget of the Universe the solutions to Eq. (2.229) are<sup>1</sup>

$$\dot{\phi} = \sqrt{\frac{2}{3}} \frac{m_{\text{Pl}}}{t}, \quad (2.230)$$

---

<sup>1</sup>This analytical treatment presumes immediate kination directly after the end of inflation, which may introduce slight inaccuracies to the calculation but any intermediate period can only be traced numerically.

$$\phi = \phi_{\text{end}} + \sqrt{\frac{2}{3}} m_{\text{Pl}} \ln \left( \frac{t}{t_{\text{end}}} \right), \quad (2.231)$$

where ‘end’ denotes the end of inflation. If the background is dominated by radiation energy density, the solutions are

$$\dot{\phi} = \sqrt{\frac{2}{3}} \frac{m_{\text{Pl}} \sqrt{t_{\text{reh}}}}{t^{3/2}}, \quad (2.232)$$

$$\phi = \phi_{\text{reh}} + \sqrt{\frac{2}{3}} m_{\text{Pl}} \left( 1 - \sqrt{\frac{t_{\text{reh}}}{t}} \right), \quad (2.233)$$

where ‘reh’ denotes reheating, the onset of radiation domination.

When the dominant energy density in the Universe is the inflaton, driven purely by its kinetic energy density, the Universe is in a period of ‘kination’. Typically in QI models, a period of kination will commence at the end of inflation, with the inflaton obeying Eqs. (2.230) and (2.231), but at some point before BBN kination has to end to allow the history of the HBB to proceed as normal, with a radiation dominated Universe. The inflaton is still kinetically dominated and oblivious of the potential for some time, obeying Eqs. (2.232) and (2.233) until its variation ceases and the field freezes until late times. We define the point in field space at which this occurs by  $\phi_F$ , at  $t \gg t_{\text{reh}}$ , when Eq. (2.233) can be approximated by

$$\phi_F \simeq \phi_{\text{reh}} + \sqrt{\frac{2}{3}} m_{\text{Pl}}. \quad (2.234)$$

A period of kination is a non-standard extension to the typical Universe history which progresses from inflation into radiation domination and matter domination to the present day, with possible scope for an effective matter dominated regime during slow perturbative reheating after inflation. Including a period of kination changes the dynamics of the expansion of the Universe in such a way that is reflected in observable quantities.

### 2.8.4.1 Gravitational Waves During Kination

During kination the pressure and energy density of the scalar field are also oblivious of the potential and so the equation of state parameter of the Universe is  $w = 1$ . The equation for estimating the e-folds of primordial inflation, Eq. (2.96), has a dependence on the equation of state parameter of the Universe in the interval between the end of inflation and the completion of reheating. If there is a period of kination, with  $w = 1$ , the number of e-folds of inflation since observable scales left the horizon is increased.

Whilst  $N_*$  is not an observable quantity in its own right, the spectral index of scalar curvature perturbations and the tensor-to-scalar ratio are both affected by a change in  $N_*$ . More drastically however, the spectrum of gravitational waves may be severely altered in a model with kination compared to one without. As seen in Section 2.4.5, gravitational waves have constant amplitude whilst their wavelengths are super-horizon but undergo damped oscillations as they re-enter the horizon, of the form

$$h_{+,x} \propto \frac{1}{a} \sin\left(\frac{k}{a}\right). \quad (2.235)$$

The energy density of gravitational waves is given by

$$\rho_{\text{GW}} = \frac{m_{\text{Pl}}^2}{4} \langle \dot{h}_{+,x}^2 \rangle, \quad (2.236)$$

where  $\langle \rangle$  denotes an average over several wavelengths. For modes which have re-entered the horizon this gives

$$\rho_{\text{GW}} \propto a^{-4}. \quad (2.237)$$

The density fraction of gravitational waves is

$$\Omega_{\text{gw}} = \frac{\rho_{\text{GW}}}{\rho_b}, \quad (2.238)$$

so during a period of kination we see  $\Omega_{\text{GW}} \propto a^2$ , in contrast to radiation domination when  $\Omega_{\text{GW}} \simeq \text{const}$ . This behaviour is shown in Fig. 2.6.

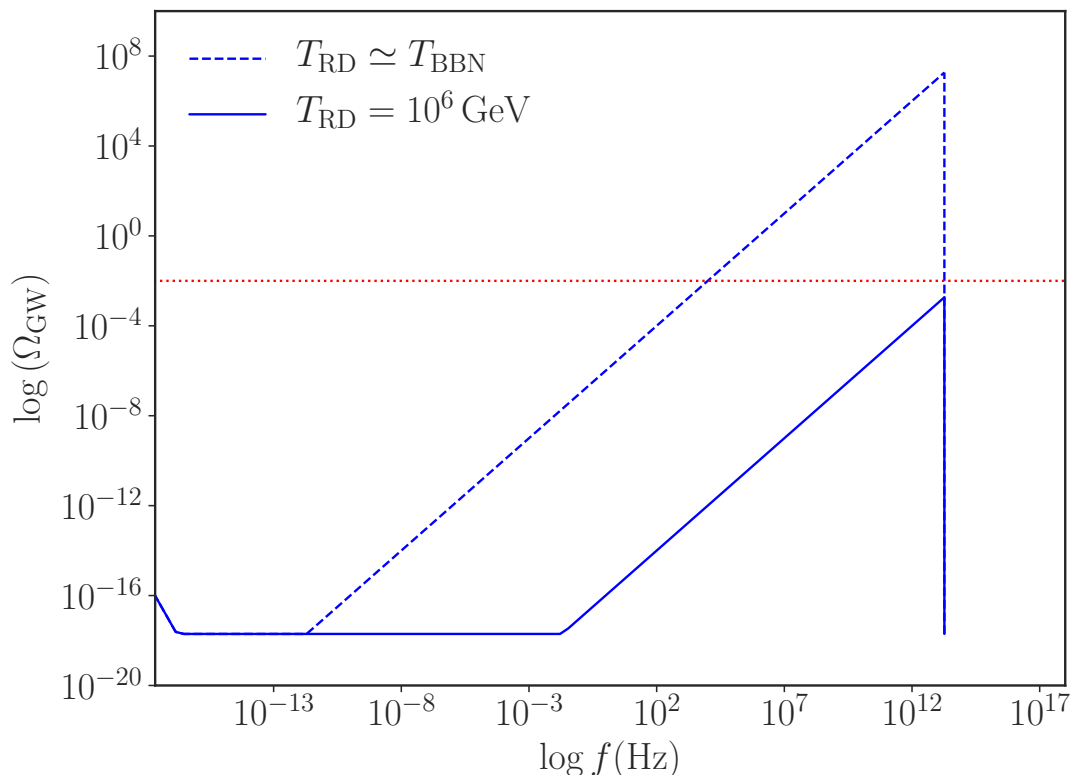


**Figure 2.6:** A spike in gravitational waves appears at high frequencies when there is a period of kination, the reheating temperature determines the length of kination and therefore the magnitude of the spike. N.B. This is an example sketch to show the behaviour and should not be used as a representative reference for particular values etc...

The expansion rate at the time of BBN is highly constrained by measurements, meaning the relative energy densities of the Universe at that point are highly constrained. Gravitational waves contribute to the radiation energy density and increase the rate of expansion, meaning gravitational waves at high frequencies (re-entering the horizon before BBN) are heavily constrained. The upper bound at the onset of radiation domination is [105]

$$\Omega_{\text{GW}}^{\text{reh}} \leq 10^{-2}. \quad (2.239)$$

For models with a period of kination, this bound imposes constraints on the

duration of kination which translates to a bound on the reheating temperature in each model.

### 2.8.5 Late-time Kinematics of Quintessential Inflation

For quintessential inflation models, the late time evolution of the scalar field is in many cases modelled by an exponential potential tail of the form of Eq. (2.228), for which there exist two attractor solutions to the full KG equation. The steepness of the exponential potential tail determines which attractor solution the inflaton follows, parametrised by  $\lambda$  in the exponential. After the field has frozen for a time it unfreezes and briefly oscillates around the attractor before settling to it. The models are known as thawing quintessence models [106]. An example of the behaviour of the scalar field is depicted in Fig. 2.7.

For accelerated expansion we need the scalar field to become the dominant component to the energy density of the Universe at late times. This is not always the case, depending on which attractor solution the field follows when it unfreezes and begins to evolve again. The energy density of the quintessence field can be dominant or sub-dominant to the background. If it is dominant the Universe moves into a period of eternal accelerated expansion but if it is sub-dominant there may be a period of transient accelerated expansion, as it oscillates before settling to the attractor. Copeland et al [101] used a phase-plane analysis and found for constant values of  $\lambda$ , the dominant quintessence attractor solution is a stable node when  $\lambda < \sqrt{3}$ . For  $\sqrt{3} < \lambda < \sqrt{6}$  and  $\lambda > \sqrt{6}$  the subdominant quintessence attractor solution is a stable node and a stable spiral respectively.

To find both attractor solutions we start from the KG equation

$$\ddot{\phi} + 3H\dot{\phi} + V'(\phi) = 0, \quad (2.240)$$

and remember the following definition from Section 2.2.3:

$$H = \frac{2}{3(1 + w_{\text{dom}})t}. \quad (2.241)$$

We use the unusual notation ‘dom’ to refer to the dominant energy density in the Universe, the reason for which will become clear when we investigate the two attractor solutions momentarily. The KG equation then becomes

$$\ddot{\phi} + \frac{2}{1 + w_{\text{dom}}} \frac{\dot{\phi}}{t} - \frac{\lambda V}{m_{\text{Pl}}^2} = 0, \quad (2.242)$$

where we use the exponential potential in Eq. (2.228). We rearrange the equation

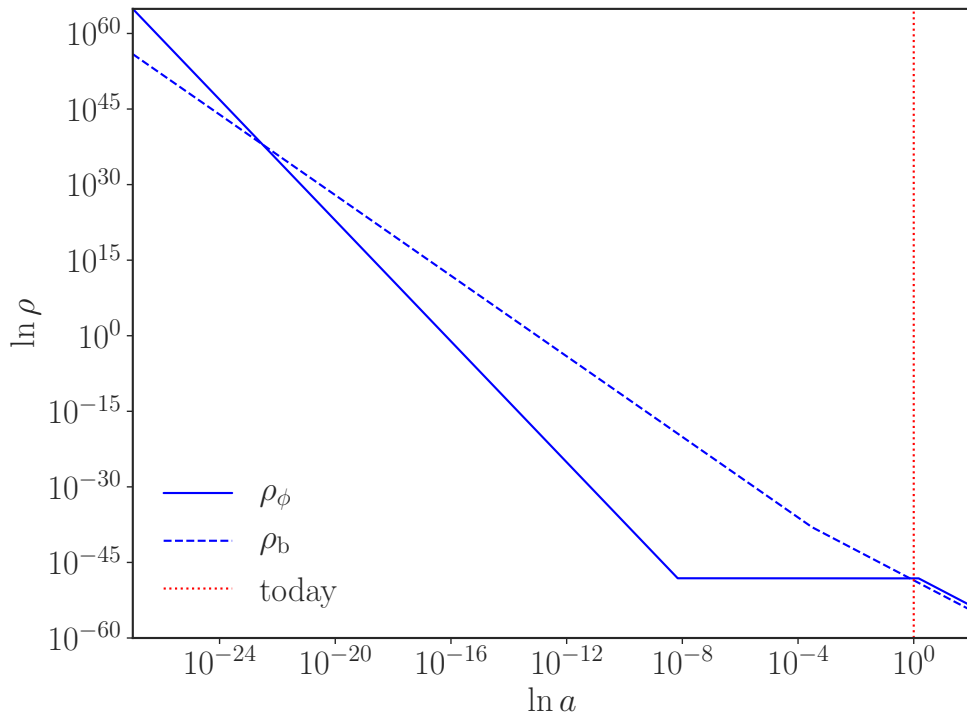


**Figure 2.7:** Log-log plot depicting the evolution of the energy density of the scalar field,  $\rho_\phi$  (solid line), compared the energy density of the background,  $\rho_b$  (dashed line), which initially evolves as radiation ( $\rho \propto a^{-4}$ ) and then matter ( $\rho \propto a^{-3}$ ). The scalar field is kinetically dominated ( $\rho \propto a^{-6}$ ) until it freezes, when its energy density becomes constant. The red dotted line indicates the present time, when the scalar field has recently become the dominant energy density of the Universe again. This plot shows the scalar field following the dominant attractor solution.

of state parameter for the scalar field to see

$$V = \frac{\dot{\phi}^2 (1 - w_\phi)}{2 (1 + w_\phi)}, \quad (2.243)$$

which substitutes into Eq. (2.242) to leave

$$\ddot{\phi} + \frac{2}{1 + w_{\text{dom}}} \frac{\dot{\phi}}{t} - \frac{\lambda}{m_{\text{Pl}}} \frac{(1 - w_\phi) \dot{\phi}^2}{(1 + w_\phi) 2} = 0. \quad (2.244)$$

For both attractor solutions we assume all three terms in the KG equation are approximately equal in magnitude, which leads to the ansatz  $\dot{\phi} = \frac{C}{t}$  and therefore  $\ddot{\phi} = \frac{-C}{t^2}$  which leaves the KG equation in the form

$$-1 + \frac{2}{(1 + w_{\text{dom}})} - \frac{\lambda C}{2 m_{\text{Pl}}} \frac{(1 - w_\phi)}{(1 + w_\phi)} = 0, \quad (2.245)$$

where we have divided through by  $C/t^2$  to simplify.

For the sub-dominant case, the energy density of the scalar field tracks that of the background [101] and so  $w_\phi = w_{\text{dom}}$ . For the dominant case the scalar field itself *is* the dominant energy density in the Universe and so again  $w_\phi = w_{\text{dom}}$ . Hence, in both cases we can solve Eq. (2.245) to find  $C = \frac{2m_{\text{Pl}}}{\lambda}$  and  $\dot{\phi} = \frac{2m_{\text{Pl}}}{\lambda t}$ . Eq. (2.243) then leads immediately to the solution:

$$V = \frac{2m_{\text{Pl}}^2 (1 - w_\phi)}{\lambda^2 t^2 (1 + w_\phi)}. \quad (2.246)$$

For the sub-dominant case, this is the final solution because we do not know the value of  $\lambda$ . We simply take advantage of the relationship  $w_\phi = w_{\text{dom}}$  as a final step:

$$V = \frac{2m_{\text{Pl}}^2 (1 - w_{\text{dom}})}{\lambda^2 t^2 (1 + w_{\text{dom}})}. \quad (2.247)$$

However, for the dominant attractor we can take the derivation further using the Friedmann equation. When the scalar field is the dominant component of the

Universe energy density we can write

$$3m_{\text{Pl}}^2 H^2 = \frac{1}{2}\dot{\phi}^2 + V, \quad (2.248)$$

which, using Eq. (2.243), rearranges to

$$H = \frac{\dot{\phi}}{m_{\text{Pl}}\sqrt{3(1+w_\phi)}}. \quad (2.249)$$

Equating this with  $H = \frac{2}{3(1+w_{\text{dom}})t}$  and reusing the ansatz  $\dot{\phi} = C/t$  results in another equation for  $C$ :

$$C = \frac{2m_{\text{Pl}}}{\sqrt{3+3w_\phi}}, \quad (2.250)$$

where we again set  $w_\phi = w_{\text{dom}}$ . We equate Eq. (2.250) with the previous solution of  $C = \frac{2m_{\text{Pl}}}{\lambda}$  to determine a relationship between  $\lambda$  and  $w_\phi$  in the dominant attractor:

$$\lambda^2 = 3(1+w_\phi). \quad (2.251)$$

This allows us to simplify the attractor solution in the dominant case to

$$V = \frac{2(6-\lambda^2)m_{\text{Pl}}^2}{\lambda^4 t^2}. \quad (2.252)$$

The attractor solutions differ with regard to the evolution of  $\rho_\phi$  compared to  $\rho_m$ , which is fixed at  $\rho_m \propto a^{-3}$ . For sub-dominant quintessence,  $\rho_\phi \propto a^{-3}$ , meaning  $\rho_\phi/\rho_m$  stays constant and for this reason the sub-dominant attractor case is sometimes referred to as a scaling solution. The value of  $\lambda = \sqrt{3}$  (since  $w_b = 0$ ) represents the boundary between the two attractor solutions, i.e. as  $\lambda$  increases toward  $\sqrt{3}$ , the evolution of  $\rho_\phi$  increasingly moves towards that of  $\rho_\phi \propto a^{-3}$ . For  $\lambda < \sqrt{3}$ , Eq. (2.251) shows  $w = -1 + \lambda^2/3$  on the dominant attractor, meaning  $\rho_\phi \propto a^{-\lambda^2}$  and  $\lambda < \sqrt{2}$  results in  $w < -1/3$ , leading to eternal accelerated expansion.

An analysis of the late-time dynamics of a quintessential inflation model is presented in Chapter 7, where we analyse the parameter space of  $w_\phi$  which allows

late-time accelerated expansion. Novel models of quintessential inflation are presented as part of the original research in Chapters 7 and 8, where care is taken to remain at sub-Planckian field values and an in-depth analysis of reheating in QI models is detailed.

The first part of Chapter 2 provided a whirlwind tour of the more well understood aspects of the history of the Universe, from the HBB through RD and MD. Section 2.2 then introduced the mathematical formalisms to describe an expanding Universe such as ours, which describes the Universe we observe exceptionally well. However, Section 2.3 went on to detail a few shortcomings of the HBB model, where it is ‘rough around the edges’ so to speak. Section 2.4 then introduced cosmic inflation as a means to overcome the problems, including inflation’s greatest strength - a description of how inflation seeds the primordial inhomogeneities which grow to become the structure of the Universe we are familiar with, predicting an almost scale invariant spectrum of perturbations which has since been confirmed. This contributed to the inflationary paradigm becoming an accepted description of the early Universe. Inflation is a ‘paradigm’ because it is a theoretical description without an agreed-upon model; indeed, this thesis presents five separate models of inflation.

We progress now into original research; introducing two new inflationary models in Chapters 3 and 5, saving an exciting pre-existing inflationary model in Chapter 4, investigating PBH production rates in Chapter 6 and combining primordial and late-time accelerating expansion in Chapters 7 and 8.

# Chapter 3

## Power-law Plateau Inflation: A New Family of Inflationary Models

*This chapter is based on the original research by the author, in collaboration with Konstantinos Dimopoulos, published in Physical Review D [107].*

### 3.1 Introduction

The research presented in this chapter is the first of several motivated by the observations of the Planck satellite [1], namely of the spectral index of curvature perturbations and the upper bound on the ratio of the power spectra of the tensor-to-scalar perturbations, which strongly suggest that primordial inflation is single-field with a concave scalar potential, featuring an inflationary plateau. The fact that non-Gaussian and isocurvature perturbations have not been observed only serves to strengthen the evidence for a single-field inflationary model. The origins of these inflationary observables are detailed in Section 2.4.5 and the

constraints are repeated here for ease of reference:

$$n_s = 0.965 \pm 0.004, \quad (3.1)$$

$$r_{0.002} < 0.07. \quad (3.2)$$

Planck also finds a vanishing running for the spectral index, of

$$\frac{dn_s}{d \ln k} = -0.0045 \pm 0.0067. \quad (3.3)$$

Different classes of inflationary models produce wildly varying predictions for these observables and the recent advances in the precision of cosmic microwave background observations have resulted in some models being ruled out. Most notably, the minimal versions of chaotic and hybrid inflation (see Section 2.6) are incompatible with the constraints in Eqs. (3.1) and (3.2) (though the research in Chapter 4 revives minimal hybrid inflation in supergravity). As such, models with an inflationary plateau (e.g. Starobinsky  $R^2$  Inflation [64], or Higgs Inflation [108]) are now receiving enormous attention. More recent models such as  $\alpha$ -attractors [109, 110] (an important part of the research in Chapter 7 and so fully introduced there) have developed a wider family of plateau inflation models, but in all of these the approach to the inflationary plateau is exponential, meaning distinguishing between models is difficult [111, 112].

The research in this chapter introduces a new family of single-field inflationary models called power-law plateau inflation<sup>1</sup>. This research develops the idea of a power-law approach to the inflationary potential from Refs. [115, 116], which use a deceptively simple but highly non-perturbative superpotential in global supersymmetry; here we remove the need for the exotic superpotential.

Power-law plateau inflation has a simple potential which features an inflationary plateau for large inflaton field values but at small field values, after inflation, reduces to an approximately monomial potential. The family of models have two mass scales, parametrised by observations.

---

<sup>1</sup>This should not be confused with plateau inflation in Refs. [113, 114].

## 3.2 Power-law Plateau Inflation

The potential we propose is the following:

$$V = V_0 \left( \frac{\phi^n}{\phi^n + m^n} \right)^q, \quad (3.4)$$

where  $m$  is a mass scale,  $n$  and  $q$  are real parameters restricted to integer values and  $\phi$  is a canonically normalised, real scalar field.  $V_0$  is a constant density scale and we assume  $\phi \geq m$  to avoid replicating monomial inflation with  $V \propto \phi^{nq}$ , which is disfavoured by observations. The potential can be re-expressed in terms of  $\left(\frac{m}{\phi}\right)$  as

$$V = V_0 \left[ 1 + \left( \frac{m}{\phi} \right)^n \right]^{-q}, \quad (3.5)$$

which allows us to represent the slow-roll parameters (introduced in Section 2.4.5) as

$$\epsilon = \frac{m_{\text{Pl}}^2}{2} \left( \frac{V'}{V} \right)^2 \simeq \frac{n^2 q^2}{2a^2} \left( \frac{m}{\phi} \right)^{2(n+1)} \left[ 1 - 2 \left( \frac{m}{\phi} \right)^n \right], \quad (3.6)$$

$$\eta = m_{\text{Pl}}^2 \left( \frac{V''}{V} \right) \simeq -\frac{n(n+1)q}{a^2} \left( \frac{m}{\phi} \right)^{n+2} \left[ 1 - \frac{(nq + 2n + 1)}{(n+1)} \left( \frac{m}{\phi} \right)^n \right], \quad (3.7)$$

where

$$a \equiv \frac{m}{m_{\text{Pl}}}. \quad (3.8)$$

Slow-roll inflation ends when the slow-roll constraints in Eq. (2.78) are violated, from  $\eta \simeq 1$  we see this occurs at

$$\frac{\phi_e}{m} = \left[ \frac{n(n+1)q}{a^2} \left( 1 - \frac{(nq + 2n + 1)}{(n+1)} \left( \frac{m}{\phi_e} \right)^n \right) \right]^{\frac{1}{n+2}}. \quad (3.9)$$

The e-folds of slow-roll inflation, defined in Eq. (2.85), are found to be

$$N_* \simeq \frac{a^2}{nq} \left[ \frac{1}{n+2} \left( \frac{\phi_*}{m} \right)^{n+2} + \frac{1}{2} \left( \frac{\phi_*}{m} \right)^2 - \frac{1}{n+2} \left( \frac{\phi_e}{m} \right)^{n+2} - \frac{1}{2} \left( \frac{\phi_e}{m} \right)^2 \right], \quad (3.10)$$

where  $\phi_* \equiv \phi(t_*)$  denotes the time when observable scales left the horizon. This

rearranges to

$$\left(\frac{\phi_*}{m}\right) = K^{\frac{1}{n+2}} \left(1 - \frac{1}{2} K^{\frac{-n}{n+2}}\right), \quad (3.11)$$

where

$$K = \frac{n(n+2)q}{a^2} \left(N_* + \frac{n+1}{n+2}\right), \quad (3.12)$$

and we use the zeroth order simplification of Eq. (3.9), substituting in the zeroth order solution to Eq. (3.10) during the derivation. This now enables us to find the following expressions for the tensor-to-scalar ratio and the spectral index of the curvature perturbation as a function of slow-roll e-folding number:

$$r = 16\epsilon \simeq \frac{8n^2q^2}{a^2} K^{\frac{-2(n+1)}{(n+2)}} \left(1 + (n-1)K^{\frac{-n}{n+2}}\right), \quad (3.13)$$

$$n_s = 1 + 2\eta - 6\epsilon \simeq 1 - \frac{2n(n+1)q}{a^2 K} \left(1 + \frac{n(n-2q-1)}{2(n+1)} K^{\frac{-n}{n+2}}\right), \quad (3.14)$$

where the  $\epsilon$  term in Eq. (3.14) is omitted as negligible. We also find the running of the spectral index to be

$$\frac{dn_s}{d \ln k} = -2 \frac{(n+1)}{(n+2)} \left(N_* + \frac{n+1}{n+2}\right)^{-2} \left[1 + \frac{n^2 - 2nq - n}{n+2} K^{\frac{-n}{n+2}}\right]. \quad (3.15)$$

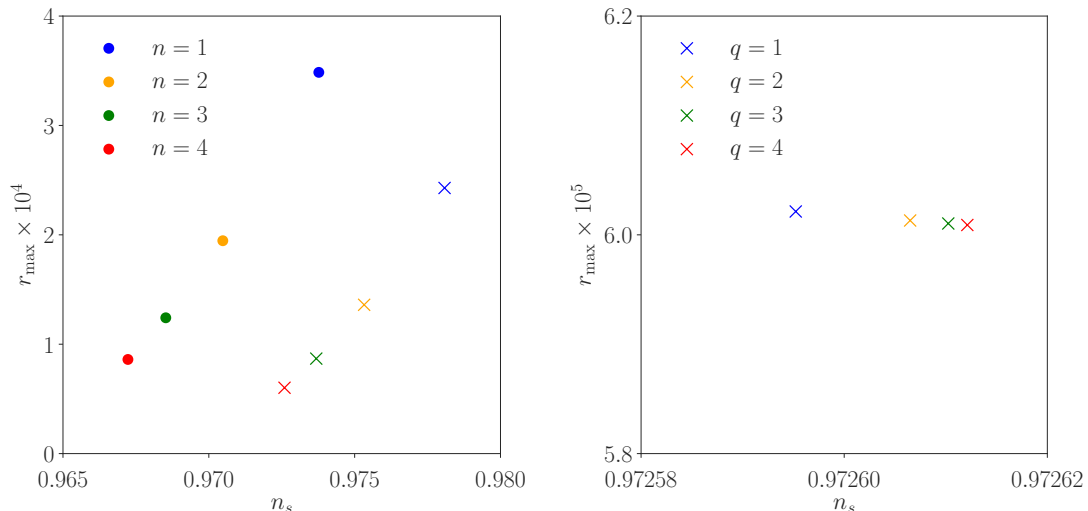
From Eq. (3.11) we can see the constraint  $\phi \geq m$  can be converted to an upper limit on  $a$ , which to zeroth order in Eq. (3.11) is

$$a \leq \sqrt{X}, \quad (3.16)$$

where we define

$$X \equiv n(n+2)q \left(N_* + \frac{n+1}{n+2}\right), \quad (3.17)$$

for ease in the following equations. Eq. (3.16) does not invoke a particularly stringent limit on the values  $a$  can take. As an example, with  $n = 2$ ,  $q = 1$ ,  $N = 50$  we find  $a \leq 20$ . However, we also initially impose sub-Planckian values of  $\phi$  to compare with perturbative models and avoid supergravity (SUGRA) corrections.



(a) Maximum  $r$  values arising from maximum allowed  $a$  values for  $N_* = 50$  (circles) and  $N_* = 60$  (crosses). Small variations from  $q$  values are detailed in window (b).

(b) The  $n = 4$  ( $N_* = 60$ ) result from window (a) is shown in detail. Varying  $q$  has little effect on  $r$  or  $n_s$ , with variations only at the fifth decimal place.

**Figure 3.1:**  $n_s$  and  $r$  for maximum  $a$  values for each  $n$  and  $q$  combination.

This translates to a much more stringent bound on  $a$  of

$$a \leq X^{-1/n} \left( 1 + \frac{(n+2)}{2nX} \right), \quad (3.18)$$

where the second term in the bracket is the first order correction. Using  $n = 2$ ,  $q = 1$ ,  $N_* = 50$  again, we find  $a_{\max} \leq 0.05$ .

We find changes to the observables,  $n_s$  and  $r$ , are minimal for varying  $q$  values (see Fig. 3.1), but for a given  $n$  and  $N_*$  a lower  $q$  value increases  $a_{\max}$ . To this end we consider  $q = 1$  in the following unless stated otherwise. For  $n = 1$ ,  $q = 1$  we find  $a_{\max} = 0.007$  which gives a spectral index of  $n_s = 0.974$  lying well outside of the Planck bounds, as can be seen in Fig. 3.1. At this stage, the  $n = 1$  form of power-law plateau inflation is ruled out. Table 3.1 details the limits on  $a$  for  $n > 1$  and the associated predictions for the spectral index, tensor-to-scalar ratio and the running of the spectral index using 50 e-folds of inflation since the observable scales left the horizon.

From Eq. (3.18) we see raising  $N_*$  reduces the  $a$  parameter space which is

$n$	$q$	$a_{\max}$	$n_s$	$r \times 10^4$	$\frac{dn_s}{d \ln k} \times 10^4$
2	1	0.050	0.970468	1.95	-5.82
3	1	0.110	0.968504	1.24	-6.20
4	1	0.169	0.967202	0.86	-6.45

**Table 3.1:** Maximum  $a$  values with  $q = 1$ ,  $N_* = 50$ , whilst  $\phi$  remains sub-Planckian and the corresponding values of  $n_s$ ,  $r$  and  $\frac{dn_s}{d \ln k}$ .

already limited. Also, to first order Eq. (3.13) shows

$$r \propto N_*^{\frac{-2(n+1)}{(n+2)}}, \quad (3.19)$$

meaning a lower value of  $N_*$  is more likely to produce a sizeable tensor-to-scalar ratio which could make contact with future observations. This can be seen in Fig. 3.1 which also highlights lower  $N_*$  seeming to match the Planck  $n_s$  parameter space more readily. Considering  $N_* = 50$  e-folds of slow-roll inflation implies a low reheating temperature, we assess the validity of this in Section 3.3.1. Furthermore, the results could be improved if we had an even lower value for the number of inflationary e-folds, the possibility of this is investigated in Section 3.3.2.

### 3.3 A Low e-folding Number

In this section we justify the choice of assuming a low reheating temperature and  $N_* \simeq 50$ . We also investigate if a period of thermal inflation (a second period of inflation which may occur after primordial inflation has ended, introduced in Section 2.6.5), can lower the e-folds of primordial inflation further to possibly bring the results into the sweet spot of the Planck results.

#### 3.3.1 The Reheating Temperature

Section 2.4.4 derived Eq. (2.97) which allows a determination of inflationary e-folding number, given a value for the reheating temperature and the potential energy density at the end of inflation, as well as the equation of state parameter

of the Universe during reheating. To start, we assume that between the end of inflation and reheating the Universe is dominated by the inflaton condensate coherently oscillating in a quadratic potential around its vacuum expectation value (VEV), meaning  $w = 0$ . For simplicity we also take the number of relativistic degrees of freedom at reheating to be  $g_* = 106.75$  and equate  $V_* \simeq V_{\text{end}}$  which leaves Eq. (2.97) as

$$N_* = 60.6 + \frac{1}{3} \ln \left( \frac{T_{\text{reh}}}{V_{\text{end}}^{1/4}} \right) + \ln \left( \frac{V_{\text{end}}^{1/4}}{m_{\text{Pl}}} \right), \quad (3.20)$$

where  $V_{\text{end}}$  is the potential energy density at the end of inflation and  $T_{\text{reh}}$  is the reheating temperature. The potential energy density at the end of inflation can be found by combining Eq. (3.5) with Eq. (3.9)

$$V_{\text{end}} = V_0 \left( 1 + \left( \frac{m}{\phi_e} \right)^n \right)^{-q}, \quad (3.21)$$

which requires knowledge of the inflationary scale,  $V_0$ .  $V_0$ , is determined by the COBE constraint, detailed in Eq. (2.136), which for this model rearranges to

$$V_0 \simeq \frac{3\pi^2 m_{\text{Pl}}^4 A_s r}{2} \left( 1 + \left( \frac{m}{\phi_*} \right)^n \right)^q, \quad (3.22)$$

where we substitute  $V_* \equiv V(\phi_*)$  from Eq. (3.5) and  $r$  is given in Eq. (3.13). For all  $n$  and  $q$  combinations considered thus far, we find  $V_0^{1/4} \simeq 3 \times 10^{15}$  GeV, meaning  $V_{\text{end}}^{1/4} \simeq 3 \times 10^{15}$  GeV. Assuming that  $T_{\text{reh}}$  is greater than the electroweak scale (to allow EW-baryogenesis), we have:

$$N_* \geq 45, \quad (3.23)$$

which validates our choice to use the  $N_* = 50$  value.

The analytical approach (taking only zeroth order terms in the equations) to find  $V_{\text{end}}$  may have introduced inaccuracies, to determine  $N_*$  accurately a full analysis would require iterative techniques. However, from Eq. (2.138),  $V_*^{1/4}$  is constrained to be  $V_* < 1.7 \times 10^{16}$  GeV. Assuming  $V_* \approx V_{\text{end}}$  and using this in

Eq. (3.20) also gives the same result for  $N_*$ .

Alternatively, for higher  $n$  values it is not valid to use  $w = 0$  for a field oscillating in a quadratic potential. For  $n = 4$  the field oscillates in a quartic potential which gives  $w = 1/3$  instead [117]. Using this the e-folding number calculation simplifies to

$$N_* = 60.4 + \ln\left(\frac{V_{\text{end}}^{1/4}}{m_{\text{Pl}}}\right), \quad (3.24)$$

and we see the dependence on the reheating temperature cancels out. As such, the e-folding number takes a single value of  $N_* = 54$ .

### 3.3.2 Thermal Inflation

It was shown in Section 2.6.5 that for a flaton field controlling thermal inflation, the larger the VEV of the flaton field, the more e-folds of thermal inflation occur due to the relationship:

$$N_T \simeq \frac{1}{2} \ln\left(\frac{g^2 \langle \theta \rangle}{m}\right), \quad (3.25)$$

where  $\theta$  is the flaton field, which is maximised for maximum  $\langle \theta \rangle$  (the VEV of the flaton field) and minimum  $m$  (the mass of the flaton field). A flaton field has not been observed at any particle physics accelerator, which are capable of observing particles of approximately the EW scale, hence  $m > m_{\text{EW}}$  which is approximately 1 TeV. The maximum VEV for a flaton field is  $\langle \theta \rangle \simeq m_{\text{Pl}}$  and so we find

$$N_T \leq \frac{1}{2} \ln\left(\frac{m_{\text{Pl}}}{m_{\text{EW}}}\right) \simeq 17. \quad (3.26)$$

Considering that 17 e-folds of thermal inflation occurred, we may lower the value of  $N_*$  down to 33 or so<sup>1</sup>. However, this will affect the combinations of  $n$ ,  $q$  and  $a$  that are still able to maintain sub-Planckian  $\phi$ .

As mentioned earlier and noted in Fig. 3.1,  $q$  has a limited effect on  $n_s$  and  $r$  and so for simplicity we maintain  $q = 1$ . Varying  $a$  has limited effect on  $n_s$ , but increasing  $a$  increases  $r$ , and so we continue to use the maximum allowed  $a$

<sup>1</sup>Presuming 50 e-folds of primordial inflation, the average of the  $N_*$  values found in Section 3.3.1.

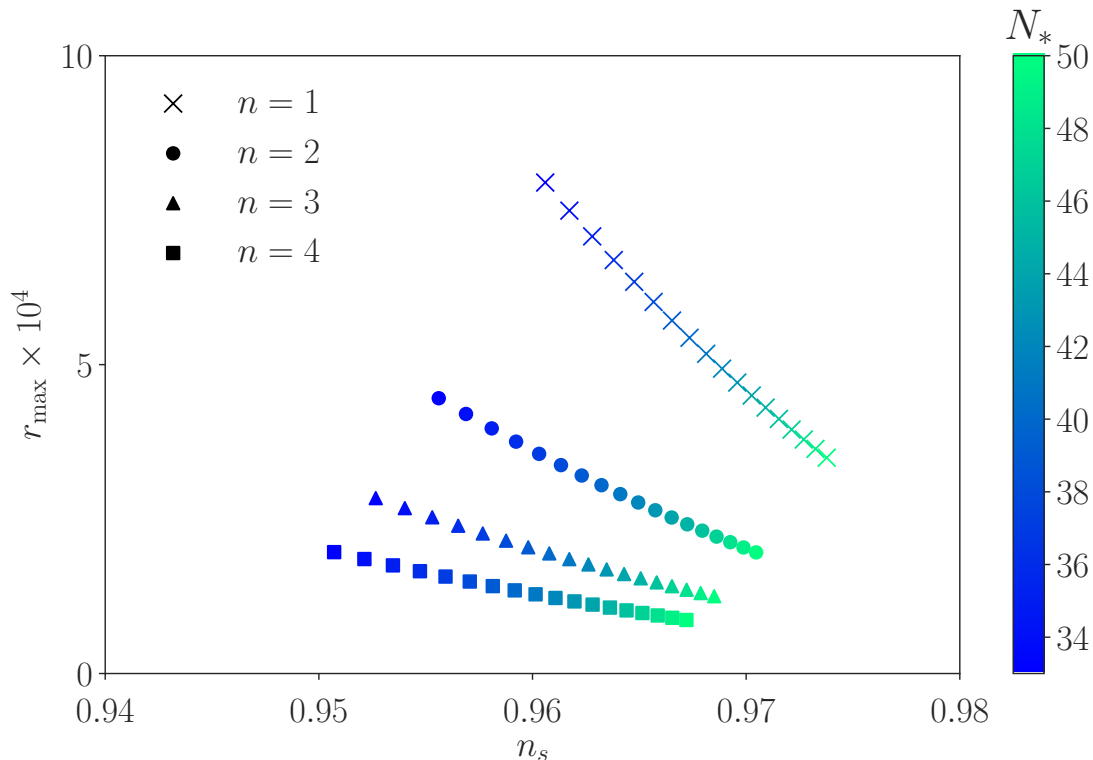


**Figure 3.2:**  $n_s$  and  $r$  for  $q = 1$  and the maximum allowed  $a$  value from Eq. (3.18) for  $1 \leq n \leq 4$  and  $33 \leq N_* \leq 50$ .  $N_*$  is shown on the colour map.

values. We now allow  $N_*$  to vary from 33 to 50 and examine the effects. We are able to reinstate  $n = 1$  because the lowering of  $N_*$  may bring the  $n_s$  predictions back within the Planck parameter space for a limited range of  $a$  values. The full results are shown in Fig. 3.2 and Table 3.2 details the parameter space matching the Planck results [1]. We find the maximum  $a$  value is  $a \equiv \frac{m}{m_{\text{Pl}}} \simeq 0.18$ , meaning the mass scale,  $m$ , takes a maximum value of  $m_{\text{max}} \simeq \mathcal{O}(10^{17} \text{ GeV})$ , which could be associated with the string energy scale. Section 3.4 investigates a more minimal version of the model with only one mass scale, assuming  $m \simeq V_0^{1/4}$  and Section 3.6 investigates the model when it is embedded into a super-symmetric theory, which could feature such energy scales.

$n$	$r_{\max} \times 10^4$	$a_{\max}$	$N_{*,\min}$
1	7.49	0.010	34
2	3.37	0.057	38
3	1.85	0.118	41
4	1.22	0.177	42

**Table 3.2:** The maximum values of  $r$ , for which  $n_s$  is within the Planck  $1\sigma$  bounds, and the corresponding maximum  $a$  (obtained using Eq. (3.18)) and minimum  $N_*$  values for the  $n$  values shown in Fig. 3.2.

### 3.4 A Single Mass Scale

In Section 3.3 the inflationary energy scale was found to be of the order of the GUT scale, whereas in Section 3.3.2 the second mass scale in our theory,  $m$ , was found to be an order of magnitude or so higher. In an attempt to make the model more economic, constrained and predictive, we consider that a single mass scale,  $M$ , characterises the model, such that  $M \equiv m \equiv V_0^{1/4}$ . We rewrite the scalar potential as

$$V = M^4 \left( 1 + \left( \frac{M}{\phi} \right)^n \right)^{-q}. \quad (3.27)$$

Re-using the COBE constraint from Eq. (2.136) we obtain

$$\left( \frac{M}{m_P} \right) = (2\sqrt{3}\pi n q \sqrt{A_s})^{\frac{n+2}{n+4}} \left[ n(n+2)q \left( N_* + \frac{n+1}{n+2} \right) \right]^{-\frac{n+1}{n+4}}. \quad (3.28)$$

Remembering  $M \equiv V_0^{1/4}$  and  $V_0^{1/4} \simeq 10^{15}$  GeV from Section 3.3, we expect our values for  $a$  are now lower. Eq. (3.13) shows  $r \propto a^{\frac{2n}{n+2}}$  and so we expect the  $r_{\max}$  values to drop by approximately two orders of magnitude ( $m$  was previously found to be of the order of  $10^{17}$  GeV for the largest  $r$  values).

Using Eq. (3.28) for  $a = M/m_{\text{Pl}}$  in the equations for  $n_s$  and  $r$  we find the results shown in Fig. 3.3. As expected, whilst  $n_s$  is still within the Planck bounds, the values for  $r$  have dropped considerably due to the reduction in  $a = M/m_{\text{Pl}} \ll 1$ . Note that we find  $M \sim 10^{15}$  GeV, which is close to the scale of grand unification as expected.

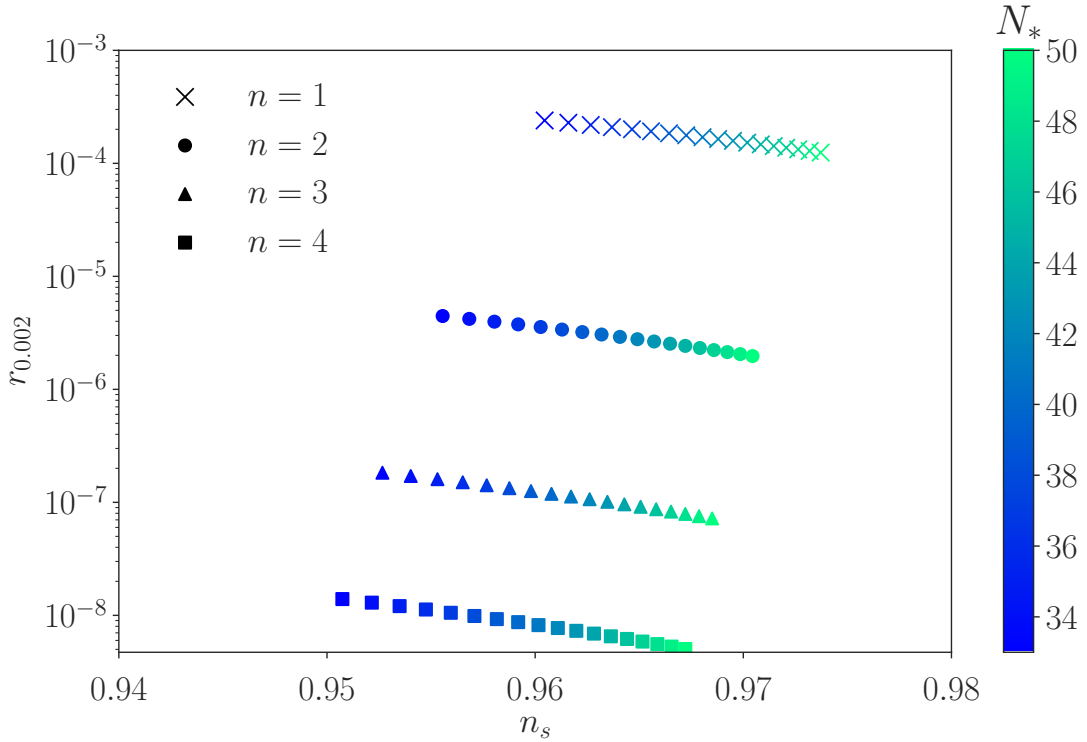


**Figure 3.3:** Values for  $n_s$  and  $r$  in the case of a single mass scale. Using the  $a$  value from Eq. (3.28) for  $1 \leq n \leq 4$ ,  $q = 1$  and  $33 \leq N_* \leq 50$ .  $N_*$  is shown on the colour map.

### 3.5 Large-field Power-law Plateau Inflation

Combining the two mass scales into one in the previous section had only limited benefits so we now reinstate both  $m$  and  $V_0$  and instead investigate the predictions for the inflationary observables in a large-field inflationary set-up, whereby we remove the constraint  $\phi < m_P$  and therefore the upper limit on  $a$ . Higher  $a$  values produce higher  $r$  values but also higher  $n_s$  values so we must be wary our  $n_s$  results do not migrate outside of the Planck bounds. To mitigate this, a lower  $N_*$  value is again better, so we consider values down to 33. We consider  $a = 1.0$  and  $a = 5.0$  as two example cases, both of which still satisfy the bound  $(\phi/m)^n > 1$  from Eq. (3.16) for all values of  $n$ . Fig. 3.4 shows the Planck results being satisfied for a wide range of our model parameters meaning the model is successful without any fine tuning, reinforced by the fact both mass scales assume

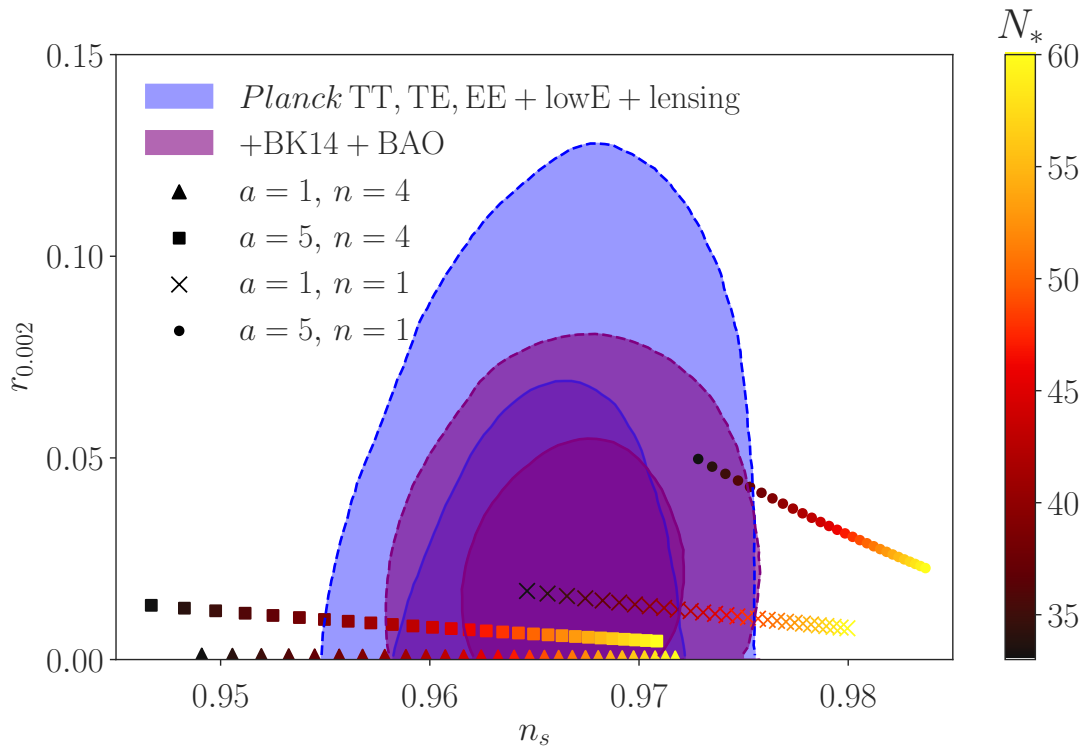


**Figure 3.4:** Values for  $n_s$  and  $r$  with  $q = 1$ ,  $1 \leq n \leq 4$  when super-Planckian field displacements are allowed. E-folding number varies between  $33 \leq N_* \leq 60$ , as shown on the colour map.

natural values;  $m \simeq m_{\text{Pl}}$  and  $V_0^{1/4}$  is of the scale of grand unification.

The model is successful for sub-Planckian field values, but if potentially observable  $r$  values are appealing, the large-field set-up predicts  $r$  values as large as a few percent. In light of this, in the next section we embed the model in supersymmetry and develop this to supergravity (SUGRA) in Section 3.6.2 to examine the effects of SUGRA corrections when the field is super-Planckian.

### 3.6 Supersymmetric Power-law Plateau Inflation

In this section we present a toy-model of power-law plateau inflation in supersymmetry. We first derive the scalar potential in global supersymmetry (SUSY), where we require  $M < m < \phi < m_{\text{Pl}}$ , where  $M$  is the scale of a grand unified

theory (GUT). Given that  $\log(m_{\text{Pl}}/M) \simeq 2$ , the available parameter space is not a lot. However, generalising the derivation into local supersymmetry (SUGRA) may allow super-Planckian values for the inflaton, while  $m \simeq m_{\text{Pl}}$ .

We follow the approach of Ref. [118] but only in form, not assuming the same theoretical framework (hence, we only consider a toy model) and with an important difference: we consider a minimal Kähler potential so that we can avoid producing too large  $n_s$ , but retain the successes of the power-law plateau inflation model.

### 3.6.1 Global Supersymmetry

At first, we consider only global supersymmetry (SUSY) and sub-Planckian fields. We introduce the non-renormalisable superpotential:

$$W = \frac{S^2(\Phi_1^2 - \Phi_2^2)}{2m}, \quad (3.29)$$

where  $S, \Phi_1, \Phi_2$  are chiral superfields and  $m$  is a large, but sub-Planckian, scale. Using the definitions in Section 2.5.1 we then find the F-term scalar potential to be

$$V_F = \frac{|S|^2}{m^2} \left[ |\Phi_1^2 - \Phi_2^2|^2 + |S|^2(|\Phi_1|^2 + |\Phi_2|^2) \right]. \quad (3.30)$$

The above potential is minimised when  $\Phi_1 = \Phi_2$ . Rotating the fields in configuration space (assuming a suitable R-symmetry) we can introduce a canonically normalised, real scalar field,  $\phi$ , such that  $|\Phi_1| = |\Phi_2| \equiv \frac{1}{2}\phi$ . Then the scalar potential becomes

$$V_F = \frac{|S|^4 \phi^2}{2m^2}. \quad (3.31)$$

We consider that there is also a D-term contribution to the scalar potential. Mirroring Ref. [118], we take

$$V_D = \frac{1}{2}(|S|^2 - \sqrt{2}M^2)^2. \quad (3.32)$$

Thus, in total, the scalar potential reads

$$V = \frac{|S|^4 \phi^2}{2m^2} + \frac{1}{2}(|S|^2 - \sqrt{2}M^2)^2. \quad (3.33)$$

Minimising the potential in the  $S$  direction requires

$$\frac{\partial V}{\partial |S|} = 0 \Rightarrow \langle |S|^2 \rangle = \frac{\sqrt{2}M^2}{1 + \phi^2/m^2}. \quad (3.34)$$

Inserting the above in Eq. (3.33) we obtain

$$V = \frac{M^4 \phi^2}{m^2 + \phi^2}, \quad (3.35)$$

which is the  $n = 2, q = 1$  power-law plateau inflation model.

### 3.6.2 Local Supersymmetry

In SUGRA, we continue to consider the superpotential in Eq. (3.29) and we will also consider a minimal Kähler potential

$$K = |\Phi_1|^2 + |\Phi_2|^2 + |S|^2. \quad (3.36)$$

Again, using the definitions from Section 2.5.1, the F-term scalar potential is

$$V_F = \exp\left(\frac{|\Phi_1|^2 + |\Phi_2|^2 + |S|^2}{m_{\text{Pl}}^2}\right) \times \left[ \frac{|S|^2 |\Phi_1^2 - \Phi_2^2|^2}{m^2} \left(1 + \frac{2|S|^2}{m_{\text{Pl}}^2} + \frac{|S|^4}{4m_{\text{Pl}}^4}\right) + \frac{|S|^4 (|\Phi_1|^2 + |\Phi_2|^2)}{m^2} \left(1 + \frac{|\Phi_1^2 - \Phi_2^2|^2}{4m_{\text{Pl}}^4}\right) - 3 \frac{|S|^4 |\Phi_1^2 - \Phi_2^2|^2}{4m^2 m_{\text{Pl}}^2} \right]. \quad (3.37)$$

Considering that  $|S|$  is sub-Planckian, since  $\langle |S|^2 \rangle < \sqrt{2}M^2$ , we have

$$V_F \simeq \exp\left(\frac{|\Phi_1|^2 + |\Phi_2|^2}{m_{\text{Pl}}^2}\right) \left[ \frac{|S|^2 |\Phi_1^2 - \Phi_2^2|^2}{m^2} + \frac{|S|^4 (|\Phi_1|^2 + |\Phi_2|^2)}{m^2} \left(1 + \frac{|\Phi_1^2 - \Phi_2^2|^2}{4m_{\text{Pl}}^4}\right) \right]. \quad (3.38)$$

Again, the potential is minimised when  $\Phi_1 = \Phi_2$ . Writing  $|\Phi_1| = |\Phi_2| \equiv \frac{1}{2}\phi$ , we obtain

$$V_F = e^{\frac{1}{2}(\phi/m_P)^2} \frac{|S|^4 \phi^2}{2m^2}. \quad (3.39)$$

We consider the same D-term contribution to the scalar potential, given in Eq. (3.32). The total scalar potential is now

$$V = e^{\frac{1}{2}(\phi/m_P)^2} \frac{|S|^4 \phi^2}{2m^2} + \frac{1}{2}(|S|^2 - \sqrt{2}M^2)^2. \quad (3.40)$$

Minimising the above along the  $S$  direction, we find

$$\langle |S|^2 \rangle = \frac{\sqrt{2}M^2}{1 + e^{\frac{1}{2}(\phi/m_P)^2} (\phi/m)^2}. \quad (3.41)$$

Inserting this into Eq. (3.40) we obtain

$$V = \frac{M^4 \phi^2}{e^{-\frac{1}{2}(\phi/m_P)^2} m^2 + \phi^2}. \quad (3.42)$$

Eq. (3.42) is almost an exact match for power-law plateau inflation but not exactly because of the exponential in the denominator. First, we point out that when  $m < \phi < m_{\text{Pl}}$ , the exponential goes to unity and we recover the power-law plateau inflation potential from Eq. (3.4) with  $n = 2$ ,  $q = 1$ , as we found in the SUSY derivation.

To have an idea of the value of the observables in this toy model, we can investigate the slow-roll parameters, which are found to be

$$\epsilon = \frac{2}{x} \frac{a^4}{(a^2 + e^{\frac{1}{2}x} x)^2} \left(1 + \frac{1}{2}x\right)^2, \quad (3.43)$$

$$\eta = \frac{1}{x} \frac{2a^2}{a^2 + e^{\frac{1}{2}x}} \left[ \frac{a^2(1+2x) - 3x}{a^2 + e^{\frac{1}{2}x}} \left( 1 + \frac{1}{2}x \right) - \frac{1}{2}x^2 \right], \quad (3.44)$$

where  $x \equiv (\phi/m_{\text{Pl}})^2$  and we remind the reader that  $a = m/m_{\text{Pl}}$ . At this point we can check that we recover the power-law plateau inflation predictions in the small-field limit. As an example, Eq. (3.14) with  $n = 2$ ,  $q = 1$  is

$$\epsilon = \frac{2a^4}{x^3} \left( 1 - \frac{a^2}{x} \right) \simeq \frac{2a^4}{x^3}. \quad (3.45)$$

Taking these limits ( $m < \phi < m_{\text{Pl}} \rightarrow a < x, a \ll 1, x \ll 1$ ) in Eq. (3.43), the SUGRA toy-model replicates this.

Following on from Eqs. (3.43) and (3.44), the spectral index and tensor-to-scalar ratio in the SUGRA toy model are therefore

$$n_s - 1 = 2\eta - 6\epsilon = \frac{4}{x} \frac{a^4}{(a^2 + e^{\frac{1}{2}x})^2} \left[ \frac{a^2(\frac{1}{2}x - 2) - 3x}{a^2 + e^{\frac{1}{2}x}} \left( 1 + \frac{1}{2}x \right) - \frac{1}{2}x^2 \right], \quad (3.46)$$

$$r = 16\epsilon = \frac{32}{x} \frac{a^4}{(a^2 + e^{\frac{1}{2}x})^2} \left( 1 + \frac{1}{2}x \right)^2, \quad (3.47)$$

In the opposite limit of super-Planckian field excursions, with  $\phi > m_{\text{Pl}} \rightarrow x \gg 1$  and taking  $a \sim 1$  the slow-roll parameters in Eqs. (3.43) and (3.44) are simplified considerably to

$$\epsilon \simeq \frac{a^4}{2xe^x} \quad \text{and} \quad \eta \simeq -a^2 e^{-\frac{1}{2}x}. \quad (3.48)$$

At this point we see the SUGRA version of the model evades the  $\eta$ -problem of SUGRA inflation (see Section 2.5.2) because  $|\eta| \ll 1$ .

In this limit, it is easy to find

$$N_* = \frac{1}{4} \int_{x_{\text{end}}}^x \frac{a^2 + e^{\frac{1}{2}x}}{a^2(1 + \frac{1}{2}x)} dx \rightarrow a^2 N_* \simeq \exp(x/2), \quad (3.49)$$

where we have taken  $x \gg x_{\text{end}}$ . Then, the observables become

$$n_s \simeq 1 + 2\eta \simeq 1 - \frac{2}{N_*} \quad \text{and} \quad r = 16\epsilon \simeq \frac{4}{\ln(a^2 N_*) N_*^2}. \quad (3.50)$$

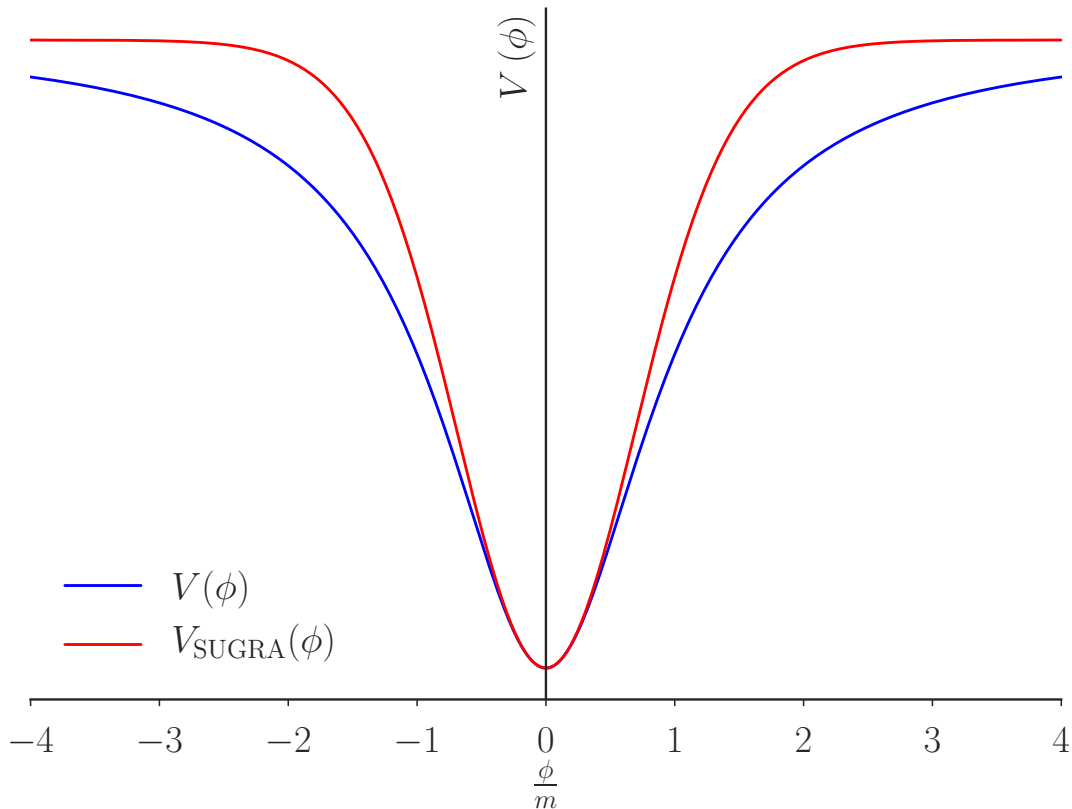


**Figure 3.5:** A comparison of the scalar field potentials for the power-law plateau inflation model with  $n = 2$ ,  $q = 1$ , and the SUGRA potential Eq. (3.42)

The prediction for the spectral index of scalar curvature perturbations in the SUGRA toy-model for  $x \gg 1$  reproduces the result obtained in  $\alpha$ -attractor models [119], which are introduced fully in Chapter 7, where we embed a model of quintessential inflation in the framework. The  $\alpha$ -attractors are a class of models which always produce the same predictions for the observables, independently of the details of the scalar field potential. The origin of  $\alpha$ -attractors is explained more fully in Section 7.2 but Fig. 3.5 shows the difference in the scalar field potential between the original power-law plateau inflation model with  $n = 2$ ,  $q = 1$  and the potential derived in SUGRA. The SUGRA potential approaches the plateau more rapidly in field space and mimics a T-model  $\alpha$ -attractor potential with  $\alpha \ll 1$ , as seen in Ref. [120].

We can contrast with the predictions of power-law plateau inflation given by

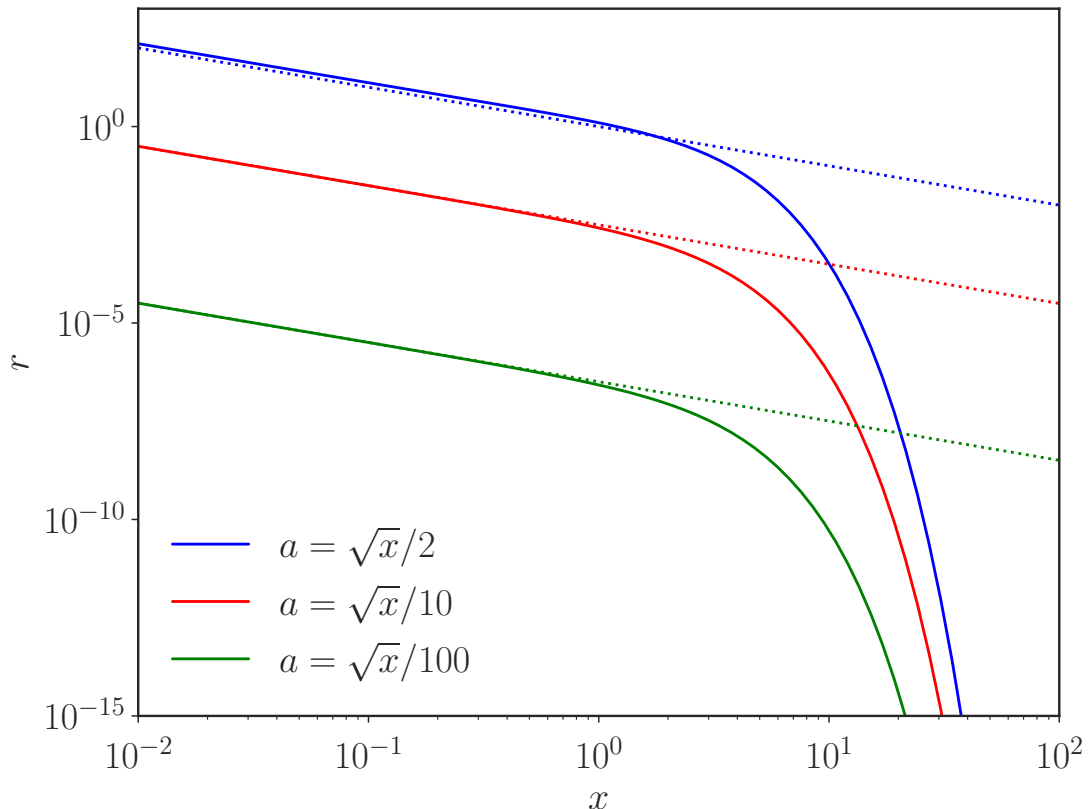


**Figure 3.6:** A comparison of the  $r$  predictions for the typical power-law plateau inflation potential (Eq. (3.4), dotted line) and the potential derived in SUGRA (Eq. (3.42), solid line), for varying  $a$  values.

Eqs. (3.13) and (3.14) (the small-field limit), which for  $n = 2$ ,  $q = 1$ , at lowest order and taking  $N_* \gg 1$  are

$$n_s \simeq 1 - \frac{3}{2N_*} \quad \text{and} \quad r \simeq \frac{\sqrt{2}a}{N_*^{3/2}}. \quad (3.51)$$

We see that the predictions of our SUGRA toy-model in the large-field limit are more pronounced with respect to  $N_*$ , with both the spectral index and the tensor-to-scalar ratio smaller. We also note the dependence of  $r$  on  $a$  is more prominent in the original, small-field case.

Realistically, we expect the inflaton field values to lie somewhere between these two extremes, where  $\phi \sim m_{\text{Pl}} \sim m$  (i.e.  $x \sim 1$ ). This means we would expect  $n_s$

and  $r$  to lie in between the values given by Eqs. (3.50) and (3.51). Note that the predicted values are well in agreement with the Planck data, in all cases.

In Section 3.5 we saw an enhancement of  $r$  in the large-field scenario. This occurred because relaxing the constraint  $\phi \ll m_{\text{Pl}}$  meant the upper limit on  $a$  Eq. (3.18) was relaxed. As discussed in Section 3.4,  $r \propto a^{\frac{2n}{n+2}}$  so a higher  $a$  means a higher prediction for  $r$ . If the model is rooted in supergravity as we have it here, we expect the  $r$  predictions to be enhanced for mildly super-Planckian field values before the field feels the full effect of the SUGRA corrections. This is demonstrated in Fig. 3.6 which plots  $r$  in the case of the  $n = 2$ ,  $q = 1$  power-law plateau inflation model and the slightly different SUGRA toy-model. We can see the  $r$  values being boosted for higher  $a$  values, which are now allowed in the large-field set-up. Starting at approximately  $x \simeq 1$  we then see the SUGRA corrections begin to damp the  $r$  value. We also note that the solutions match better at small-field values for lower  $a$  values, which we assumed in the derivation of Eq. (3.45), where the two solutions coalesce.

## 3.7 Discussion

The research in this chapter presents a new family of inflationary models called power-law plateau inflation, analysed in detail. The models feature an inflationary plateau, which is approached in a power-law manner, in contrast to the popular Starobinsky/Higgs inflation models (and their variants). We show that power-law plateau inflation is in excellent agreement with the Planck observations. Predicted values for  $r$  and  $n_s$  fall comfortably within the  $1\sigma$  bounds of the Planck observations, for all variations of the family of models, whilst individual models are clearly distinguishable by future observations (see Figs. 3.2 and 3.4).

In the basic set-up of the model we find unobservably small predictions for  $r$ . This may or may not be a problem but we find the prediction for  $r$  is enhanced for a lower  $N_*$  value, prompting an investigation into a low reheating temperature and a period of thermal inflation. Utilising  $N_*$  values as low as 33 increases the prediction to  $r \simeq 7 \times 10^{-4}$  which might be observable in the future (see Table 3.2). We find the energy scale of inflation to be  $V_0^{1/4} \simeq 10^{15}$  GeV and in the interests

of minimality present the model with a single-mass scale in Section 3.4. Whilst being economical this further reduces  $r$  to unobservable levels and so does not add much beyond being economical.

We then construct a toy model realisation in supersymmetry, following Ref. [118] but crucially considering canonically normalised fields (i.e. minimal Kähler potential) which exactly produces the power-law plateau inflation model with  $n = 2$ ,  $q = 1$ , one of the most preferred for predictions compatible with observations. If potentially observable  $r$  values are required, the model predicts much larger  $r$  values if the field is allowed to travel to Planckian field values. Values as large as a few percent (up to 5%, see Fig. 3.4) are achieved without fine-tuning for natural values of the mass scales (Planck and GUT scale). As such, we extend the toy-model realisation to supergravity and investigate the SUGRA corrections, which reduce both the  $n_s$  and the  $r$  predictions. For mildly super-Planckian field values we expect the  $r$  predictions to be enhanced before feeling any suppression effects. The level of success of power-law plateau inflation, and the fact that it offers distinct and testable predictions makes it a worthy candidate for primordial inflation.

This first chapter of original research is an exciting foray into the world of inflationary model building which is extended in the following chapters. The utilisation of a period of thermal inflation used herein prompts the research presented in the next chapter: utilising a period of thermal inflation to revive hybrid inflation in the minimal supergravity set-up.

# Chapter 4

## How Thermal Inflation Can Save Minimal Hybrid Inflation in Supergravity

*This chapter is based on the original research by the author in collaboration with Konstantinos Dimopoulos, published in the Journal of Cosmology and AstroParticle Physics [121].*

### 4.1 Introduction

The latest observational data from the Planck satellite is so precise that it excludes several families of well motivated and thoroughly explored inflationary models [4]. A prominent example is minimal hybrid inflation.

Hybrid inflation was introduced by Linde [74] to employ sub-Planckian field values whilst avoiding ‘unnaturally’ tiny couplings. The model is introduced in Section 2.6.4 and Fig. 2.3 details the scalar field potentials of the inflaton,  $\phi$ , and the waterfall field,  $\sigma$ . As introduced in Section 2.6.4, the first embodiment of the model predicts a blue spectrum of scalar curvature perturbations,  $n_s > 1$ , which is now ruled out by observations. When hybrid inflation is realised in

supergravity (SUGRA) the predictions move to  $n_s < 1$  and more into alignment with the Planck results. However, with the recent advances in the precision of CMB observations, the  $n_s$  predictions of the minimal version of SUGRA hybrid inflation are now also outside of the Planck bounds.

It is disappointing that the minimal version of SUGRA hybrid inflation is ruled out because it is able to side-step the  $\eta$  problem of supergravity whilst maintaining its minimality, a feat which is unusual for inflationary models realised in SUGRA. The  $\eta$  problem is introduced in Section 2.5.2 and revolves around the fact that in SUGRA  $\eta \propto K''$  where  $K$  is the Kähler potential (see Section 2.5.1 for a brief introduction to supergravity), and for canonical fields  $K'' = 1$  meaning slow-roll is unachievable. In minimal SUGRA hybrid inflation there is an accidental cancellation in the higher order terms of  $K''$  which allows  $\eta \ll 1$  during inflation without the need for any complex additions to the theoretical set-up or a symmetry.

Many authors have put forward modifications which are able to save hybrid inflation, producing observables within the allowed ranges, but at the expense of the above accidental cancellation, meaning elaborate Kähler constructions have to be introduced to ensure slow-roll (e.g. see Refs. [122–124] and references therein). This undermines one of the attractive facets of the theory to start with - its minimality.

The research in this chapter proposes a mechanism to render the model compatible with observations whilst retaining the neat feature of the accidental cancellation of minimal hybrid inflation in SUGRA. Inspired by the research in Chapter 3, we consider that there is a period of thermal inflation due to some flaton scalar field. The acts to lower the e-folds of primordial inflation which elapse since observable scales leave the horizon, a key parameter in the inflationary observables. We first derive the hybrid inflation scalar potential in SUGRA and then we investigate the effect of a period of thermal inflation, introduced in Section 2.6.5.

## 4.2 Minimal Hybrid Inflation in Supergravity

Hybrid inflation in SUGRA is achieved with the superpotential

$$W = \kappa\Phi(S\bar{S} - M^2) + \dots \quad (4.1)$$

where the dots denote Planck-suppressed non-renormalisable operators,  $\Phi$  is a gauge singlet superfield which acts as the inflaton and  $S$  and  $\bar{S}$  are a pair of superfields, assumed to be oppositely charged under some gauge group. The flatness of the inflationary trajectory is guaranteed by a U(1) R-symmetry on  $\Phi$ . The parameters  $\kappa$  and  $M$  are made positive with field redefinitions, where  $M \sim 10^{16}$  GeV is the scale of a grand unified theory (GUT) and  $\kappa \leq 1$  is a dimensionless coupling constant. The supersymmetric minimum is at  $\langle S \rangle = \langle \bar{S} \rangle = M$  and  $\langle \Phi \rangle = 0$ . We also consider a minimal Kähler potential for the fields:

$$K = |S|^2 + |\bar{S}|^2 + |\Phi|^2. \quad (4.2)$$

Using Eq. (2.141) the F-term scalar potential is then

$$V_F = \kappa^2 |M^2 - S\bar{S}|^2 + \kappa^2 |\Phi|^2 (|S|^2 + |\bar{S}|^2) + \dots, \quad (4.3)$$

where the dots denote Planck-suppressed terms and we assume that the fields are sub-Planckian.

When  $|\langle S \rangle| = |\langle \bar{S} \rangle|$ , the D-terms vanish. Since the soft-breaking terms are negligible near the inflation scale (the GUT scale), the scalar potential is  $V = V_F + \Delta V$ , where  $\Delta V$  is the Coleman-Weinberg (CW) one-loop radiative correction:

$$\Delta V \simeq \frac{\kappa^4 M^4}{16\pi^2} \ln \frac{\kappa^2 |\Phi|^2}{\Lambda^2}, \quad (4.4)$$

where  $\Lambda$  is some renormalisation scale. As we will see, it is the CW term that lifts the potential for the inflaton field to roll slightly. By suitable rotations in field space [125] we write  $\Phi = \phi/\sqrt{2}$  and  $S = \bar{S} = \sigma/2$ , where  $\phi$  and  $\sigma$  are canonically

normalised real scalar fields. Using these variables the scalar field potential is

$$V(\phi, \sigma) = \kappa^2 \left( M^2 - \frac{\sigma^2}{4} \right)^2 + \frac{\kappa^2 \phi^2 \sigma^2}{4} + \frac{\kappa^4 M^4}{8\pi^2} \ln \left( \frac{\kappa \phi}{\sqrt{2}\Lambda} \right), \quad (4.5)$$

which is first introduced in Section 2.6.4 and depicted in Fig. 2.3, where we can see the the inflaton field  $\phi$  rolls along a valley until at a particular point the field opens up in the  $\sigma$  direction and inflation ends as the  $\sigma$  field moves to its vacuum expectation value (VEV). We can find

$$\frac{\partial V}{\partial \sigma} = \kappa^2 \sigma \left( \frac{\sigma^2}{4} + \frac{\phi^2}{2} - M^2 \right), \quad (4.6)$$

so the potential is extremised for either  $\sigma = 0$  or  $\sigma = \sqrt{4M^2 - 2\phi^2}$ . We find the mass-squared for  $\sigma$ , from  $m_\sigma^2 \simeq \partial^2 V / \partial \sigma^2$ , to be

$$m_\sigma^2 = \kappa^2 \left( \frac{3\sigma^2}{4} + \frac{\phi^2}{2} - M^2 \right). \quad (4.7)$$

At  $\sigma = 0$ , we see the potential is a minimum for  $\phi > \phi_c \equiv \sqrt{2}M$  and inflation is driven by the false vacuum density  $\kappa^2 M^4$ . However, when  $\phi < \phi_c \equiv \sqrt{2}M$ , the waterfall field becomes tachyonic and  $\sigma = 0$  is no longer a minimum but a maximum,  $\sigma$  moves to its VEV and inflation ends abruptly. From the second solution to Eq. (4.6), with  $\phi \ll \sqrt{2}M$ , we find the VEV to be

$$\langle \sigma \rangle \simeq 2M. \quad (4.8)$$

During inflation, the potential is

$$V = \kappa^2 M^4 + \frac{\kappa^4 M^4}{8\pi^2} \ln \left( \frac{\kappa \phi}{\sqrt{2}\Lambda} \right), \quad (4.9)$$

where the second term is subdominant but provides a slope along the inflationary valley, necessary for slow-roll.

The slow-roll parameters are

$$\epsilon = \frac{m_{\text{Pl}}^2}{2} \left( \frac{V'}{V} \right)^2 = \frac{\kappa^4}{128\pi^4} \left( \frac{m_{\text{Pl}}}{\phi} \right)^2, \quad (4.10)$$

$$\eta = m_{\text{Pl}}^2 \frac{V''}{V} = -\frac{\kappa^2}{8\pi^2} \left( \frac{m_{\text{Pl}}}{\phi} \right)^2, \quad (4.11)$$

where the prime denotes derivative with respect to the inflaton  $\phi$ .

For the spectral index of the density perturbations we have

$$n_s = 1 + 2\eta - 6\epsilon = 1 - \frac{\kappa^2}{4\pi^2} \left( 1 + \frac{3\kappa^2}{16\pi^2} \right) \left( \frac{m_{\text{Pl}}}{\phi} \right)^2, \quad (4.12)$$

while the tensor-to-scalar ratio is given by the consistency condition,  $r = 16\epsilon$ .

The remaining e-folds of slow-roll inflation when observable scales leave the horizon, defined in Eq. (2.85), are found to be

$$N_* = \frac{(\phi^2 - \phi_e^2)}{m_{\text{Pl}}^2} \left[ \frac{4\pi^2}{\kappa^2} + \frac{1}{2} \ln \left( \frac{\kappa\phi}{\sqrt{2}\Lambda} \right) - \frac{1}{4} \right], \quad (4.13)$$

which rearranges to express the field as a function of e-folding number as

$$\left( \frac{\phi}{m_{\text{Pl}}} \right)^2 = \frac{2M^2}{m_{\text{Pl}}^2} + \frac{\kappa^2 N_*}{4\pi^2}, \quad (4.14)$$

where we use  $\phi_{\text{end}} = \phi_c = \sqrt{2}M$  for the integration limit. This allows us to express the observational parameters as

$$n_s = 1 - \frac{\kappa^2 m_{\text{Pl}}^2}{8\pi^2 M^2} \left( 1 + \frac{3\kappa^2}{16\pi^2} \right) \left( 1 + \frac{\kappa^2 m_{\text{Pl}}^2 N_*}{8\pi^2 M^2} \right)^{-1} \simeq 1 - \frac{1}{N_*}, \quad (4.15)$$

and

$$r = \frac{\kappa^2 m_{\text{Pl}}^2}{16\pi^4 M^2} \left( 1 + \frac{\kappa^2 m_{\text{Pl}}^2 N_*}{8\pi^2 M^2} \right)^{-1} \simeq \frac{\kappa^2}{2\pi^2} \frac{1}{N_*}. \quad (4.16)$$

Eqs. (4.15) and (4.16) with  $\kappa = 0.1$  and  $N_* = 60$  (50) give  $r = 8 \times 10^{-6}$  ( $1 \times 10^{-5}$ )

and  $n_s = 0.983$  (0.980). Whilst  $r$  is well beneath the Planck upper bound, but as yet unobservable,  $n_s$  is clearly above the upper  $2\sigma$  bound of the Planck observations [1]. Therefore, as expected, the model appears to be excluded. However, as we saw in Chapter 3, a lower value of  $N_*$  can bring  $n_s$  within the Planck bounds. Furthermore, it may also increase  $r$  to the point of observability.

### 4.3 Thermal Inflation to Reduce $N_*$

Thermal inflation is introduced in Section 2.6.5 and the research in Chapter 3 utilises it in a similar manner to the purpose here, to lower the number of e-folds of primordial inflation since observable scales left the horizon,  $N_*$ . The remaining number of e-folds of inflation when the cosmological scales exit the horizon is given in Eq. (2.97), which we reproduce here with an additional term indicating a reduction in  $N_*$  if there is a subsequent period of thermal inflation:

$$N_* = 60.6 + \frac{1}{3} \ln \left( \frac{T_{\text{reh}}}{V_{\text{end}}^{1/4}} \right) + \ln \left( \frac{V_{\text{end}}^{1/4}}{m_{\text{Pl}}} \right) - N_T, \quad (4.17)$$

where we take  $g_* = 106.75$ , equate  $V_* \simeq V_{\text{end}}$  and  $N_T$  represents the e-folds of thermal inflation. We have also assumed that the equation of state parameter during reheating is  $w = 0$ , which is applicable for a field oscillating in a quadratic minimum.

When there is a period of thermal inflation, reheating from primordial inflation completes before the thermal inflation initiates. As such,  $T_{\text{reh}} \geq V_0^{1/4}$  where  $V_0$  is the energy scale of thermal inflation. The flaton potential is given in Eq. (2.156) and the energy scale is calculated in Eq. (2.161) to be  $V_0^{1/4} \simeq \sqrt{m\langle\theta\rangle}$  where  $m$  is the mass of the flaton field and  $\langle\theta\rangle$  its vacuum expectation value (VEV). This is therefore the minimum reheating temperature and inserting this into Eq. (4.17) we see

$$N_* = 60.6 + \frac{1}{3} \ln \left( \frac{\sqrt{m\langle\theta\rangle}}{V_{\text{end}}^{1/4}} \right) + \ln \left( \frac{V_{\text{end}}^{1/4}}{m_{\text{Pl}}} \right) - N_T, \quad (4.18)$$

and we substitute  $N_T$  from Section 2.6.5 to obtain

$$N_* = 60.6 + \frac{1}{3} \ln \left( \frac{\sqrt{m \langle \theta \rangle}}{V_{\text{end}}^{1/4}} \right) + \ln \left( \frac{V_{\text{end}}^{1/4}}{m_{\text{Pl}}} \right) - \frac{1}{2} \ln \left( \frac{g^2 \langle \theta \rangle}{m} \right) \quad (4.19)$$

$$\simeq 60.6 + \ln \left( \frac{V_{\text{end}}^{1/4}}{m_{\text{Pl}}} \right) + \frac{1}{3} \ln \left( \frac{m^2}{V_{\text{end}}^{1/4} \langle \theta \rangle} \right), \quad (4.20)$$

where in the final equality we presume  $g \simeq 1$ , where  $g$  is the coupling between the flaton field and the thermal bath. We see that a larger flaton VEV will reduce  $N_*$  more.

The VEV of the flaton field is calculated in Eq. (2.159), which we repeat here:

$$\langle \theta \rangle = \left[ \frac{\lambda_n}{(2n+3)!} \right]^{-\frac{1}{2(n+1)}} (m_{\text{Pl}}^n m)^{\frac{1}{n+1}}, \quad (4.21)$$

where increasing  $n$  corresponds to higher order non-renormalisable terms in the flaton potential, given in Eq. (2.156), and  $\lambda_n$  is the coupling constant for a respective value of  $n$ . Both  $\lambda_n$  and  $n$  can vary which means the value of the flaton VEV falls on a continuum. As such, we keep  $\langle \theta \rangle$  in Eq. (4.20) and investigate it as a free parameter.

## 4.4 Results

Table 4.1 shows the results of varying  $\langle \theta \rangle$ , thereby determining the range of  $N_*$  from Eq. (4.20) which can be used to calculate  $n_s$  from Eq. (4.15) and  $r$  from Eq. (4.16). The results are plotted in Fig. 4.1, where the Planck [1] constraints on  $n_s$  are indicated, namely:

$$n_s = 0.965 \pm 0.004 \quad 68\% \text{ CL}, \quad (4.22)$$

$$n_s = 0.965 \pm 0.009 \quad 95\% \text{ CL}. \quad (4.23)$$

All results for  $r$  are still safely below the upper bound from Planck [1] but are enhanced and so may be observable in the future. The results for the spec-

tral index of scalar curvature perturbations are improved with respect to the Planck bounds for larger values of the flaton VEV. This corresponds to  $n \geq 1$  in Eq. (4.21).

The flaton mass-squared is found from  $V''(\langle\theta\rangle)$  where the prime denotes a derivative with respect to  $\theta$  (not  $\phi$  as it denoted earlier) and the flaton potential is defined in Eq. (2.156). We find the mass-squared to be

$$m_{\text{flaton}}^2 = 2(n+1)m^2, \quad (4.24)$$

so for  $n = 2$ , assuming  $m \geq 1$  TeV (typical for a supersymmetric flat direction lifted by a soft mass), we find

$$m_{\text{flaton}} \geq 2.4 \text{ TeV}, \quad (4.25)$$

which is safely above the latest LHC bounds.

We also calculate  $M$  using the COBE constraint in Eq. (2.136) and find

$$M^4 = \frac{3m_{\text{Pl}}^4 \kappa^2 A_s}{16\pi^2} \left( \frac{m_{\text{Pl}}}{\phi} \right)^2 = \frac{3m_{\text{Pl}}^4 A_s}{4N_*} \left( 1 + \frac{8\pi^2 M^2}{m_{\text{Pl}}^2 \kappa^2 N_*} \right)^{-1} \simeq \frac{3m_{\text{Pl}}^4 A_s}{4N_*}, \quad (4.26)$$

where we use Eq. (4.14) in the middle equality and the final equality shows the zeroth-order solution, presuming the second term in the bracket of the middle equality to be small. For  $\kappa = 0.1$  we expect this to be true and solving iteratively we see the assumption is valid. For  $\kappa = 0.1$  and  $N_* = 50$  we find

$\langle\theta\rangle$ (GeV)	$N_*$	$n_s$	$r_{\text{max}} \times 10^3$
$10^{10}$	39.7	0.975	1.27
$10^{12}$	38.2	0.974	1.33
$10^{14}$	36.7	0.973	1.38
$10^{16}$	35.2	0.972	1.44
$10^{18}$	33.6	0.970	1.51

**Table 4.1:**  $\langle\theta\rangle$ ,  $N_*$ ,  $n_s$  and  $r_{\text{max}}$  (using  $\kappa = 1$ ) values.

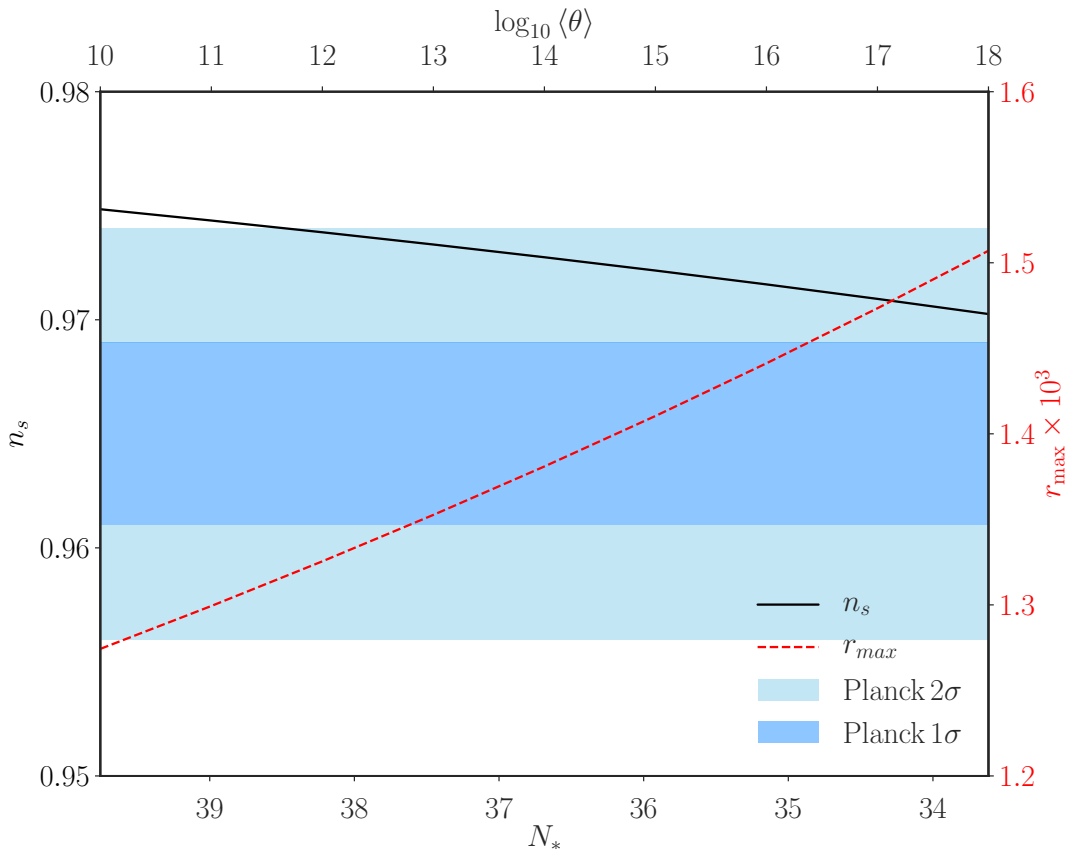


**Figure 4.1:**  $n_s$  and  $r_{\max}$  in hybrid inflation as a function of  $\langle\theta\rangle$  and therefore  $N_*$ . The solid, black line depicts the values of  $n_s$ . The dashed, red line depicts the maximum allowed value for  $r$ , which corresponds to  $\kappa = 1$ . The Planck 2018  $1\sigma$  and  $2\sigma$  bounds are indicated by the horizontal shaded regions.

$M \simeq 6 \times 10^{15}$  GeV, which is approximately the GUT scale, as expected. This may lead to the assumption that the symmetry breaking which ends inflation is the GUT phase transition, allowing us to identify the waterfall field with the GUT Higgs field. However, if it is the GUT Higgs field this could be a concern because it is not appropriate to take the lowest possible reheating temperature of  $T_{\text{reh}} \simeq \sqrt{m\langle\theta\rangle}$ . Whether or not the waterfall field is in fact the GUT Higgs field, it is instructive to consider the effect of a higher reheating temperature, because a higher reheating temperature increases the e-folds of inflation and so acts in opposition to the thermal inflation mechanism.

To quantify this, in the analysis so far, when the reheating temperature takes

its lowest possible value it results in a reduction of between 3.5 to 6.5 e-folds, depending on the VEV of the flaton field (from the second term in Eq. (4.17)). In contrast, if we take the reheating temperature to equal the energy scale of inflation, the second term in Eq. (4.17) simply goes to zero. Without the extra reduction provided by a low reheating temperature, predictions for  $n_s$  in agreement with the Planck results require  $\langle\theta\rangle \gtrsim 10^{16}$  GeV, which limits the parameter space.

However, just as the flaton VEV falls on a continuum, so too does the reheating temperature. As such,  $\langle\theta\rangle \gtrsim 10^{16}$  GeV is the most stringent constraint on the flaton VEV when prompt reheating ( $T_{\text{reh}} \simeq M$ ) is presumed. Alternatively, Table 4.1 and Fig. 4.1 represent the least stringent constraints on  $\langle\theta\rangle$  from  $T_{\text{reh}} \simeq V_0^{1/4}$ , resulting in the lowest predictions for  $N_*$  for a given  $\langle\theta\rangle$ .

## 4.5 Discussion

The research in this chapter brings the observational predictions of hybrid inflation in minimal SUGRA into alignment with the Planck 2018 constraints on  $n_s$  and  $r$ . We derive the cosmological observational parameters in minimal SUGRA hybrid inflation and show they enter the parameter space of the Planck results, at the  $2\sigma$  level for lower e-foldings of primordial inflation since observable scales left the horizon. Following on from the last chapter we obtain a reduction in  $N_*$  by invoking a period of thermal inflation after reheating from primordial inflation completes.

The value of  $N_*$  is increasingly reduced for larger vacuum expectation values of the flaton field which drives thermal inflation. For values of the VEV larger than approximately  $10^{12}$  GeV the predictions in this model match observations. As can be seen in Fig. 4.1, the tensor-to-scalar ratio,  $r$ , is also significantly increased for lower  $N_*$  values. We find  $r \simeq \mathcal{O}(10^{-3})$  which may be observable in the near future.

Scalar fields abound in supersymmetric theories, any of which could play the role of the flaton field, meaning a period of thermal inflation is a natural thing to consider. The mechanism used herein does not alter the theoretical

framework in any way so the accidental calculation in the higher order terms of the Kähler potential which solves the  $\eta$  problem is maintained whilst the model stays minimal.

Using the lower values of  $N_*$  allowed by a late period of thermal inflation, successfully improves the minimal hybrid inflation model in the SUGRA scenario. The fact that  $r$  is increased to potentially observable levels also means the model is predictive, and could be confirmed by the next data release from cosmological observing experiments.

The research in this chapter differs from the previous in that we do not present a new model to describe inflation, instead we improve an old model by utilising a new idea. This theme is continued in the next chapter, which investigates a realisation of inflection-point inflation with a simpler set-up than that seen in the literature previously.

# Chapter 5

## Loop Inflection-Point Inflation

*This chapter is based on research by the author, in collaboration with Konstantinos Dimopoulos and Antonio Racioppi, published in the Journal of AstroParticle Physics [126].*

### 5.1 Introduction

As stressed in the introduction to Chapter 3, the latest CMB observations suggest that the scalar potential of the inflaton features an inflationary plateau. Many of the mechanisms put forward to generate an inflationary plateau involve exotic constructions in the context of elaborate, beyond-the-standard-model theories. Simple theoretical set-ups are preferable and with this in mind we introduce the research presented in this chapter - a model of inflection-point inflation generated using only the stabilising loop corrections to an unbounded (from below) inflaton potential.

In inflection-point inflation the inflationary plateau exists due to the interplay of opposing contributions in the scalar potential, which (almost) cancel each other out, generating a step on the otherwise steep potential wall. The original model is called A-term inflation, because it employs the A-term of a supersymmetric theory [127, 128], or MSSM inflation, because it considered a flat direction in MSSM [129–132] as the inflaton. However, other models of inflection-point infla-

tion have also been constructed [133–141]. Most of these also consider an elaborate setup in the context of supersymmetry, string theory or other extensions of the Standard Model.

In this chapter we introduce a simpler set-up, without any physics more exotic than simple field theory in curved spacetime, which provides such an impressive description of the inflationary scenario itself. The research in this chapter is similar to the work in Refs. [138–141]. However, in Refs. [138–141] the authors consider a rather complicated running of the inflaton self-coupling, where many particles are contributing to it, this is not necessary in the model we present here.

## 5.2 Loop Inflection-point Inflation

To study an inflection point model of inflation we first take a scalar field potential which is unbounded from below and stabilise it with the addition of higher order terms. In previous works care was taken so that loop corrections do not spoil the stability of the potential [142–148]. In contrast, we consider the unstable Coleman-Weinberg potential and recover stability by introducing a Planck-suppressed effective operator.

Taking a quartic tree-level potential and the Coleman-Weinberg (CW) one-loop potential we obtain

$$V_{\text{eff}}(\phi) = \left[ \lambda - \xi \ln \left( \frac{y^2 \phi^2}{\mu^2} \right) \right] \phi^4, \quad (5.1)$$

where  $y$  is a Yukawa coupling which we presume to be the dominant contribution to the CW potential,  $\lambda$  is a self-coupling constant,  $\xi = y^4/32\pi^2$  and  $\mu$  is some renormalisation scale. We can incorporate a running expression for  $\lambda$  which takes the form

$$\lambda(\mu) = \lambda(M) - 2\xi \ln \left( \frac{\mu}{M} \right), \quad (5.2)$$

where  $M$  is the scale at which we impose the boundary condition on the running of  $\lambda$ .

Eq. (5.2) has three unknown parameters:  $\xi$ ,  $\mu$  and  $M$ , but for an appropriately chosen  $\mu$  there is a value of  $M$  given by

$$\mu = M \exp\left(\frac{\lambda(M)}{2\xi}\right), \quad (5.3)$$

which results in another energy scale,  $M_0$ , for which<sup>1</sup>  $\lambda(M_0) = 0$ . This allows us to write the coupling in Eq. (5.2) in the simpler form:

$$\lambda(\mu) = -2\xi \ln\left(\frac{\mu}{M}\right), \quad (5.4)$$

which is always valid for an appropriate combination of  $\mu$  and  $M$ .

This is a convenient parametrisation, rather than anything physical, for any other choice of  $\lambda(M^*) = 0$  we would simply have  $M^* = M \exp(\frac{\lambda(M)}{2\xi})$  at which to impose the boundary condition. The physicality of the choice arises when a choice for any of the parameters is made. We will see momentarily that the scalar field potential actually loses any dependence on  $\mu$ , leaving only  $\beta$  and  $M$ . As we discuss, we make a sensible choice for  $M$  for this first analysis and  $\beta$  is constrained from CMB observations. A full analysis would be improved by considered all possible values of  $M$ , but this is beyond the scope of the research presented here.

Using the simplification  $\lambda(M) = 0$  and inserting Eq. (5.2) into Eq. (5.1) we find

$$V_{\text{eff}}(\phi) = -\xi \ln\left(\frac{y^2 \phi^2}{M^2}\right) \phi^4, \quad (5.5)$$

which as expected is unbounded from below. We introduce non-renormalisable Planck-suppressed effective operators to stabilise it

$$V = -\xi \ln\left(\frac{y^2 \phi^2}{M^2}\right) \phi^4 + \lambda_n \frac{\phi^{2n+4}}{m_{\text{Pl}}^{2n}}, \quad (5.6)$$

where the first term is the 1-loop effective potential obtained in Eq. (5.5) and

---

<sup>1</sup>Assuming that  $\xi$  is large enough for Eq. (5.3) to be satisfied for a reasonable value of  $\mu$ , consistent with the range of validity of the theory.

the second term is the dominant non-renormalisable operator, with  $\lambda_n \ll 1$  and  $n \geq 1$ .

The values of  $M$  and  $y$  are not restricted but it is reasonable to expect new physics to happen around the scale of grand unification (GUT-scale), therefore we expect  $M \sim 10^{15-16}$  GeV. The Yukawa coupling should be small enough ( $y < 1$ ) to preserve perturbativity but also large enough to give rise to the relevant corrections, therefore we expect to find  $y \simeq 10^{-2} - 10^{-3}$ . Combining these we obtain that  $y/M$  is around  $1/m_{\text{Pl}}$ , therefore for a first analysis we choose to study the model where

$$\frac{y^2}{M^2} = \frac{1}{m_{\text{Pl}}^2}. \quad (5.7)$$

For a first analysis we focus on  $n = 1$ , we consider higher  $n$  values in Section 5.5. Noting that the slow-roll formalism is independent of the potential normalisation, we hence re-parametrise the potential as

$$V = \xi \left[ -\ln \left( \frac{\phi^2}{m_{\text{Pl}}^2} \right) \phi^4 + \alpha \frac{\phi^6}{m_{\text{Pl}}^2} \right], \quad (5.8)$$

where<sup>1</sup>  $\alpha = \lambda_n/\xi$ . An example plot of the potential is shown in Fig. 5.1 where the inflection-point can clearly be seen.

A flat inflection point is defined to be the point  $\phi_f$ , where  $V'' = V' = 0$  is satisfied, using Eq. (5.6) we find

$$V' = 2\xi\phi^3 \left[ \frac{3\alpha\phi^2}{m_{\text{Pl}}^2} - 2\ln \left( \frac{\phi^2}{m_{\text{Pl}}^2} \right) - 1 \right], \quad (5.9)$$

and

$$V'' = 2\xi\phi^2 \left[ \frac{15\alpha\phi^2}{m_{\text{Pl}}^2} - 6\ln \left( \frac{\phi^2}{m_{\text{Pl}}^2} \right) - 7 \right]. \quad (5.10)$$

Setting Eqs. (5.9) and (5.10) equal to zero and solving the resulting simultaneous equations we see the potential has a flat inflection point at

$$\phi_f = e^{1/4} m_{\text{Pl}}. \quad (5.11)$$

---

<sup>1</sup>Please note that  $\alpha$  in this chapter has no relation to the  $\alpha$  of the  $\alpha$ -attractors which feature in Chapter 7, it is simply a parameter to ease notation.

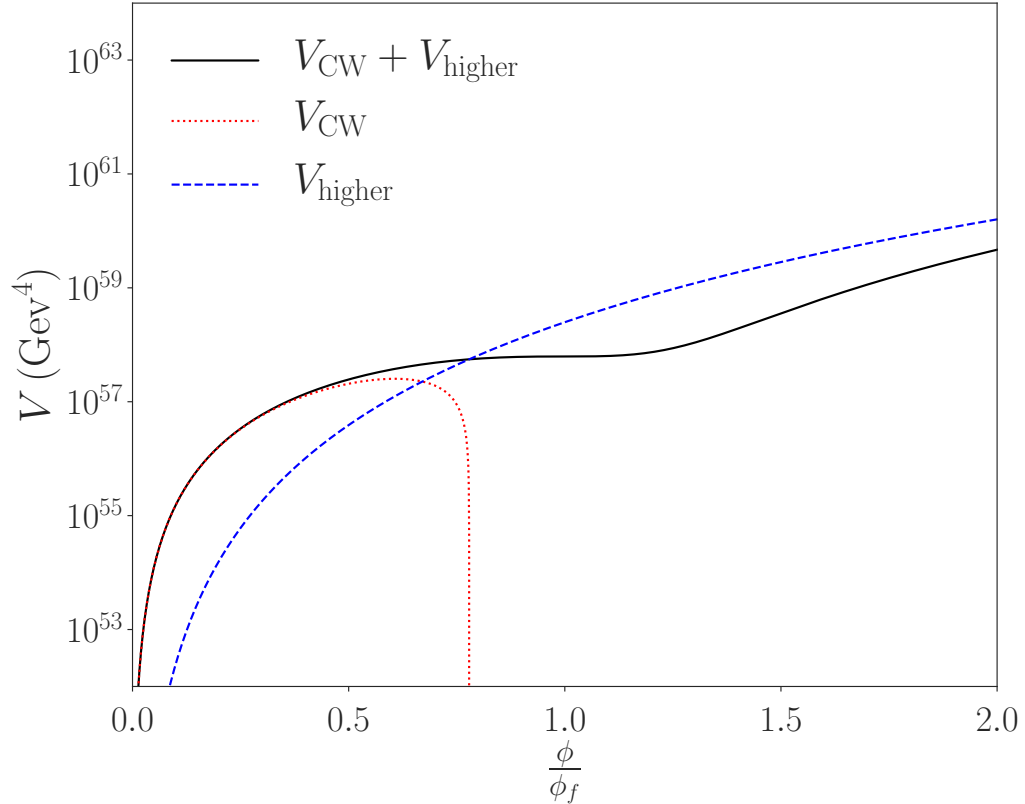


**Figure 5.1:** The scalar field potential with  $n = 1$ .  $V_{\text{CW}}$  and  $V_{\text{higher}}$  refer to the first and second terms in Eq. (5.8) respectively. This example is plotted for  $\delta = 10^{-5.95}$ , defined in Eq. (5.13), with  $\xi$  calculated via the iteration process detailed in Section 5.3.

Setting either Eq. (5.9) or Eq. (5.10) to zero and re-inserting Eq. (5.11) allows us to determine the parameter  $\alpha$  at the inflection point, which we find to be

$$\alpha_f \equiv \frac{2}{3\sqrt{e}}. \quad (5.12)$$

However, we do not need to have a completely flat inflection point for slow-roll inflation to be viable and so to study the inflationary predictions for values of  $\alpha$  around  $\alpha_f$ , we parametrise:

$$\alpha = (1 + \delta)\alpha_f, \quad (5.13)$$

and use  $\delta$  as a free parameter. Varying  $\delta$  allows us to find the range of allowed

slopes of the plateau around the flat inflection point. Increasing  $\delta$  increases the slope of the plateau and decreasing  $\delta$  to negative values introduces a local maximum (see Fig. 5.6).

To constrain acceptable  $\delta$  values for the model, we compute predictions for the inflationary observables, namely the spectral index of the scalar curvature perturbations,  $n_s$ , its running,  $n'_s \equiv \frac{dn_s}{d \ln k}$  and the tensor-to-scalar ratio,  $r$ , and contrast them with the Planck constraints, as per the approach of Chapters 3 and 4. However, in the past two chapters we have used the e-folds of inflation given by Eq. (2.85) to obtain the field value when observable scales left the horizon, using only the end of inflation as a boundary condition. This may not be appropriate in this chapter.

The inflationary models in Chapters 3 and 4 had infinitely long inflationary plateaus, as long as  $\phi > \phi_e$ . The same is not true in this model, which has a limited plateau to accommodate slow-roll inflation. It cannot be guaranteed that  $N_{\text{tot}} > N_*$  *a priori* in this model, where  $N_{\text{tot}}$  are the total e-foldings of slow-roll inflation along the length of the plateau, so we investigate the relationship between  $N_*$  and  $N_{\text{tot}}$  in the next section.

### 5.3 Computing $N_*$ and $\xi$

We first calculate  $N_*$  for the model and then find  $N_{\text{tot}}$  to constrain the parameter space with the requirement  $N_* > N_{\text{tot}}$ . As in Chapters 3 and 4 we use the typical equation for the number of e-folds of observable inflation,  $N_*$ , presented in Eq. (2.97) but there is a crucial difference between this model and the two in the previous chapters which presumed  $w \simeq 0$  in the calculation, for the inflaton oscillating in a quadratic minimum of its potential (see Section 2.7.1). This model, in contrast, has the inflaton oscillating in a *quartic* minimum of its potential, which we can see from Eq. (5.8):

$$\lim_{\phi \rightarrow 0} \left[ -\xi \ln \left( \frac{\phi^2}{m_{\text{Pl}}^2} \right) \phi^4 \right] = \frac{1}{2} \xi \phi^4. \quad (5.14)$$

The average density of a scalar field coherently oscillating in a quartic potential scales as  $\rho_\phi \propto a^{-4}$  [117], just as the density of a radiation dominated Universe. Therefore, we use  $w = 1/3$  in this model which simplifies Eq. (2.97) to

$$N_* = 59.7 + \frac{1}{4} \ln \left( \frac{g_* \pi^2}{60} \right) + \ln \left( \frac{V_*^{1/4}}{m_{\text{Pl}}} \right) + \ln \left( \frac{V_*^{1/4}}{T_{\text{reh}}} \right) + \ln \left( \frac{T_{\text{reh}}}{V_*^{1/4}} \right), \quad (5.15)$$

where  $g_*$  is the effective number of relativistic degrees of freedom.  $V_* \equiv V(\phi_*)$  and  $V_{\text{end}} = V(\phi_{\text{end}})$  and we expect  $V_* \simeq V_{\text{end}}$ . Equating the two makes  $N_*$  independent of  $T_{\text{reh}}$ , leaving

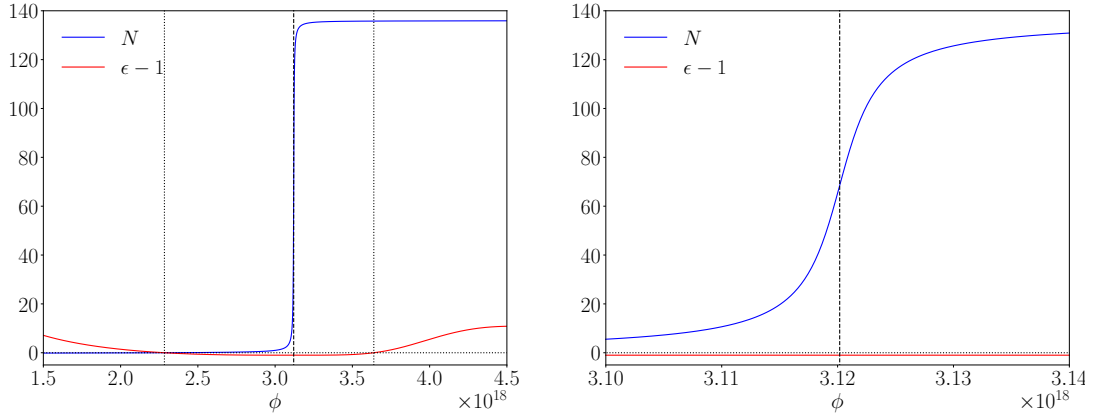
$$N_* = 60.4 + \ln \left( \frac{V_{\text{end}}^{1/4}}{m_{\text{Pl}}} \right), \quad (5.16)$$

where we have taken  $g_* = 106.75$ .

For a first approximation we take  $V_{\text{end}}^{1/4} \approx 10^{16}$  GeV in Eq. (5.16) and obtain  $N_* \simeq 54.9$ . From this point, we embark upon a numerical iteration of  $\phi_*$ ,  $\xi$ ,  $V_{\text{end}}$  and  $N_*$  in turn, to obtain precise values. Inspecting the slow-roll parameters (defined in Eqs. (2.76) and (2.77)), it is  $\epsilon < 1$  which is violated first and so we calculate the end of inflation from  $\epsilon = 1$ . Armed with  $\phi_e$  we can then invert Eq. (2.85) to find  $\phi_*$  for the estimated value of  $N_*$ .

The equations are unfortunately too complicated to solve analytically, but we present them graphically in Fig. 5.2 to help with an intuitive understanding of the iteration process. As soon as  $\phi_*$  has been determined we calculate the energy scale of inflation,  $\xi$ , from the COBE constraint in Eq. (2.136), which allows an accurate determination of  $V_{\text{end}}$  to be made from Eq. (5.8) (which features  $\xi$  and  $\phi_e$ ). From there, we make a more accurate calculation of  $N_*$  from Eq. (5.16) and repeat the process until the values converge.

$N_{\text{tot}}$  is easier to find and depends mainly on the initial conditions of the inflaton. We determine the beginning and end of inflation by  $\epsilon = 1$  and calculate the total number of e-folds of slow-roll inflation numerically, by integrating between the two values of  $\phi$  that result in  $\epsilon = 1$ . If  $N_* \simeq N_{\text{tot}}$  we may need to investigate the initial conditions of  $\phi$  to assess whether or not slow-roll does start at  $\epsilon = 1$ .



(a) The dashed vertical line denotes the inflection point and the dotted lines either side indicate the beginning and end of slow-roll inflation, coinciding with  $\epsilon = 1$ .

(b) Zooming into the region in Fig. 5.2a where  $N$  varies, we see there are an approximately even number of e-folds of inflation either side of the inflection point.

**Figure 5.2:**  $\epsilon - 1$  and  $N$  for varying  $\phi$ . In the iteration process we first find  $\epsilon = 1$ , denoted by the dotted vertical lines, the smaller of which allows us to find  $\phi_e$ . Using  $\phi_e$  as the lower integration limit and  $\phi$  for the higher,  $N$  is then plotted from Eq. (2.85). The point at which  $N = N_*$  then allows  $\phi_*$  to be determined. The dashed vertical line indicates the inflection point.

This will depend on whether or not the inflaton is kinetically dominated when it reaches the plateau. Upon inspection of the results we see it is valid to use  $N_* = N_{\text{tot}}$  as an upper bound for  $\delta$  because the inflationary observables associated with these  $N$  values are well outside the Planck bounds [1], meaning the range of  $\delta$  we will constrain in the following sections will be safe from any questions of the initial conditions of the inflaton arising from  $N_* \simeq N_{\text{tot}}$ . The maximum value for  $\delta$  with this first constraint is

$$\delta < 10^{-5.14}. \quad (5.17)$$

The true bound is likely to be slightly less tight than Eq. (5.17) but the iteration method becomes less trustworthy as  $N_* \simeq N_{\text{tot}}$  is approached because the slow-roll assumptions are implicit in the calculation of  $N_*$ ;  $\delta = 10^{-5.14}$  is the last value for which the computation converges without devoting any additional computational resources. The fact that the constraints in the following sections are all tighter allows us to leave Eq. (5.17) in its current form and not investigate the region

$\delta$	$N_*$	$N_{\text{tot}}$	$n_s$	$r/10^{-9}$	$n'_s/10^{-3}$
$10^{-5.80}$	51.38	121.0	0.974	7.96	-2.86
$10^{-5.85}$	51.35	128.2	0.967	6.90	-2.66
$10^{-5.90}$	51.32	135.8	0.962	6.10	-2.50
$10^{-5.95}$	51.29	143.8	0.957	5.47	-2.36

**Table 5.1:**  $\delta$  values producing  $n_s$  within the Planck  $2\sigma$  bounds.

$N_* \simeq N_{\text{tot}}$ .

## 5.4 Inflationary Observables

We investigate the spectral index and tensor-to-scalar ratio predictions for this model for varying positive  $\delta$  values satisfying the bound in Eq. (5.17). We use the Planck 2018  $2\sigma$  constraint of  $n_s = 0.965 \pm 0.009$  [1], to find limits on  $\delta$  of:

$$10^{-5.96} \leq \delta \leq 10^{-5.79}. \quad (5.18)$$

The parameter space satisfying the Planck results is presented in Table 5.1. It is clear that, for the region where the spectral index and tensor-to-scalar ratio values match observations,  $\delta$  is within the constraint of Eq. (5.17) such that  $N_* < N_{\text{tot}}$  and we do not need to worry about initial conditions. The model's predictions for the inflationary observables are shown in Fig. 5.3.

## 5.5 Higher-order Non-renormalisable Terms

We now extend the analysis to higher orders of the the non-renormalisable operator in Eq. (5.6). Keeping  $n$  as a free parameter we generalise Eqs. (5.11) and (5.12) to

$$\phi_f = m_{\text{Pl}} \exp\left(\frac{2-n}{4n}\right), \quad (5.19)$$

$$\alpha_f = \frac{2}{n(n+2)} \exp\left(\frac{n-2}{2}\right). \quad (5.20)$$

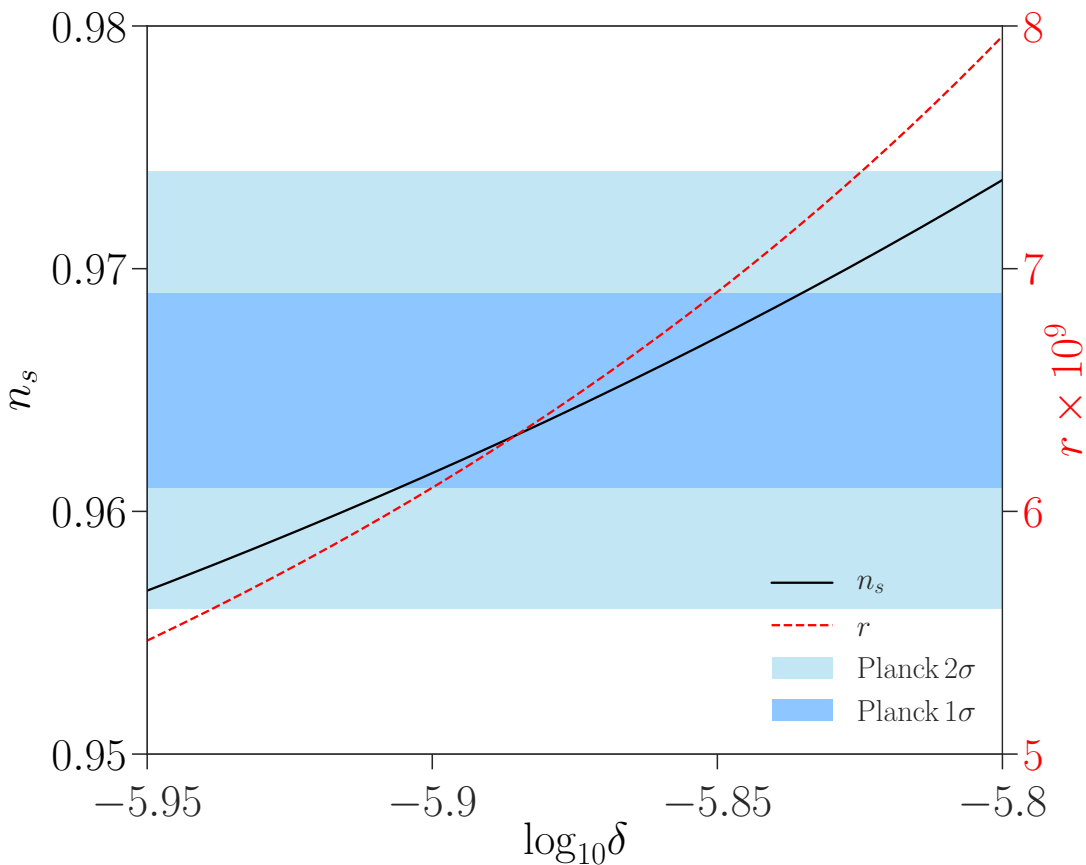


**Figure 5.3:** Values of  $\delta$  for which  $n_s$  (solid black line) and  $r$  (dashed red line) fall within the Planck bounds for  $n_s$  depicted with the shaded horizontal bands (light:  $2\sigma$  and dark:  $1\sigma$ ).

The value of the field at the inflection point,  $\phi_f$ , reduces somewhat for larger  $n$ , as shown in Table 5.2 and we find that  $(\phi_f/m_{\text{Pl}})^{2n} \lesssim 0.1$  for  $n \geq 4$ . When the cosmological scales exit the horizon at  $\phi_*$  the inflaton has already travelled past the inflection point to smaller field values and so for our analysis of the observables we expect higher-order non-renormalisable terms ( $n > 4$ ) to be suppressed. Thus, it is unlikely that the dominant, stabilising, non-renormalisable operator would correspond to  $n > 4$ .

To constrain the parameter space we follow the process outlined in Section 5.3 and again constrain  $\delta$  values to align with the Planck results. The range for  $\delta$  remains about the same size for all  $n$  values but shifts to smaller values for larger  $n$  values. This behaviour can be seen in Fig. 5.4 where we present a comparison

$n$	1	2	3	4
$(\phi_f/m_{\text{Pl}})^{2n}$	1.65	1.00	0.61	0.37

**Table 5.2:** Values of  $(\phi_f/m_{\text{Pl}})^{2n}$  for  $n \geq 1$ .

$\delta$	$N_*$	$N_{\text{tot}}$	$n_s$	$r(\times 10^{10})$	$n'_s(\times 10^3)$
$10^{-5.90}$	50.87	123.60	0.970	9.57	-2.79
$10^{-5.95}$	50.84	130.93	0.964	8.38	-2.62
$10^{-6.00}$	50.81	138.70	0.959	7.45	-2.47

**Table 5.3:** Results for  $\phi^8$ .

$\delta$	$N_*$	$N_{\text{tot}}$	$n_s$	$r(\times 10^{10})$	$n'_s(\times 10^3)$
$10^{-5.85}$	50.67	118.55	0.975	4.16	-2.96
$10^{-5.90}$	50.63	125.58	0.968	3.60	-2.75
$10^{-5.95}$	50.60	133.03	0.962	3.17	-2.58
$10^{-6.00}$	50.57	140.92	0.957	2.83	-2.44

**Table 5.4:** Results for  $\phi^{10}$ .

$\delta$	$N_*$	$N_{\text{tot}}$	$n_s$	$r(\times 10^{10})$	$n'_s(\times 10^3)$
$10^{-5.85}$	50.50	121.21	0.972	2.13	-2.88
$10^{-5.90}$	50.47	128.40	0.965	1.86	-2.69
$10^{-5.95}$	50.44	136.01	0.960	1.65	-2.53
$10^{-6.00}$	50.50	144.08	0.955	1.48	-2.40

**Table 5.5:** Results for  $\phi^{12}$ .

of the  $n_s$  predictions for  $n = 1, 2, 3, 4$ . The results for  $n = 2, 3, 4$  are tabulated in Tables 5.3 to 5.5 and our findings from the  $n = 1$  case are largely unchanged.

We find  $r \simeq 10^{-10}$ , with very small differences for varying  $n$ , and changes in  $n_s$  for varying  $n$  are at the  $10^{-3}$  level. It should not be a surprise that our results are robust and largely independent of  $n$ , as is shown in Fig. 5.4; by the time the cosmological scales leave the horizon the field has rolled passed the inflection point and the scalar potential is dominated by the CW-term in Eq. (5.5), which is  $n$  independent.

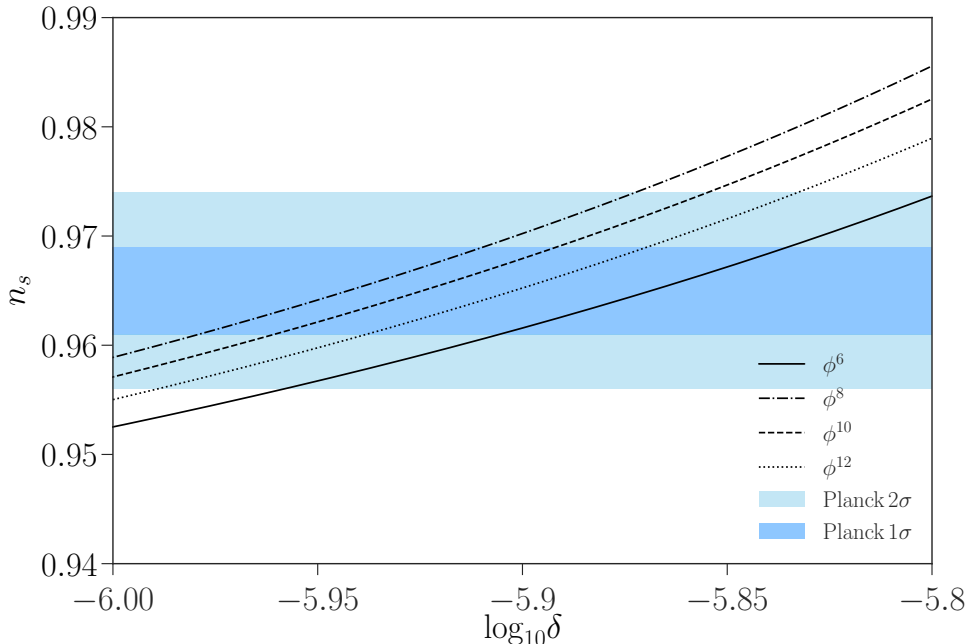


**Figure 5.4:** A comparison of the  $n_s$  predictions for varying orders of the non-normalisable term,  $n$ , focusing on the  $\delta$  values for which  $n_s$  falls within the Planck bounds depicted by the shaded horizontal bands (light:  $2\sigma$  and dark:  $1\sigma$ ).

It is interesting to see that  $n_s$  appears first to increase for larger  $n$ , before decreasing again. This is not intuitive to explain without a detailed analytical solution for  $n_s$ , but from the competing powers of the polynomials in Eqs. (5.9) and (5.10) it is not unexpected. Fig. 5.5 shows the behaviour of  $n_s$  for varying  $n$  and we see the same pattern observed in Fig. 5.4.

## 5.6 The Inflationary Energy Scale and Reheating Temperature

As discussed in Section 5.3, we determine the inflationary energy scale numerically via the COBE constraint in Eq. (2.136). For all  $n$  and  $\delta$  values considered we find  $V^{1/4} \sim 10^{14}$  GeV and  $\xi \sim 10^{-16}$  GeV. In Section 5.2 we define  $\xi = y^4/32\pi^2$  so from this we find  $y \simeq 4 \times 10^{-4}$  for the Yukawa coupling, obeying the perturbativity requirement,  $y \ll 1$ , as expected. In the minimal setup where the Weyl fermion is

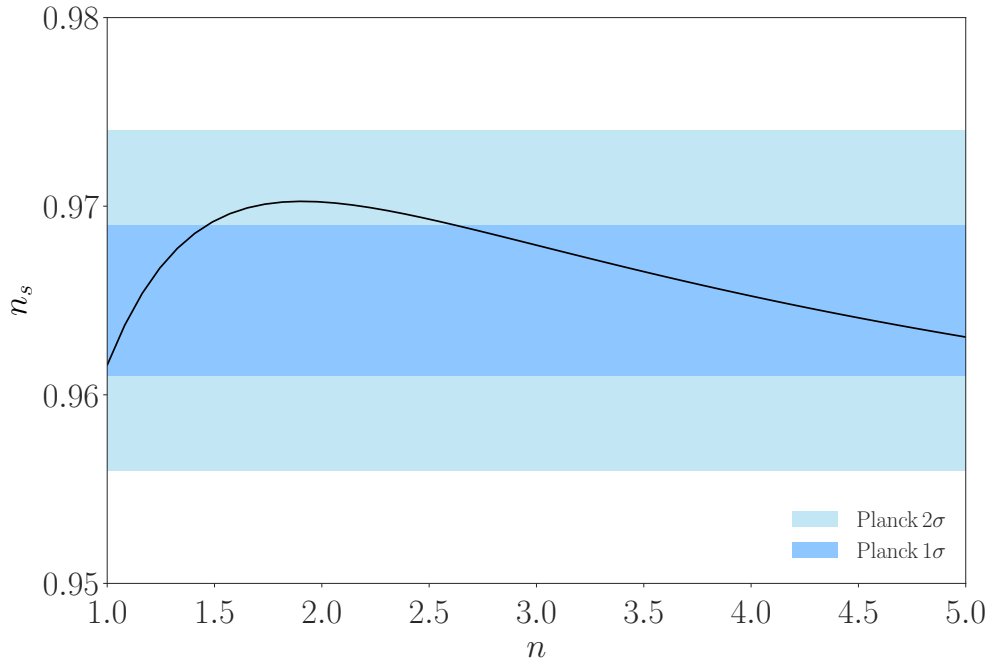


**Figure 5.5:** Predictions of  $n_s$  for  $\delta = 10^{-5.9}$  with varying  $n$  in the potential in Eq. (5.6).

only coupled to  $\phi$ , the running of the coupling  $y$  has a beta function  $\beta_y \approx y^3$ . The running is negligible for  $y \ll 1$  meaning we are justified to treat  $y$  as a constant. Through Eq. (5.7), we then determine  $M = 2\sqrt{\pi}(2\xi)^{1/4}m_{\text{Pl}} \simeq 10^{15}$  GeV; near the grand unification scale and sub-Planckian as expected.

The decay rate of the inflaton particles to the Weyl fermions they couple to is given in Eq. (2.180), which in the variables of this chapter is  $\Gamma = y^2 m_\phi / 8\pi$ . As we saw in Section 5.3, oscillations in a quartic potential mimic a radiation background, with  $\rho \propto a^{-4}$  [117], so after inflation when the inflaton is oscillating about its potential minimum, using Eq. (2.34) with a radiation background, we see  $H \propto a^{-2}$ . The decay rate,  $\Gamma$ , is proportional to the mass and from  $m_\phi^2 \simeq V''(\phi)$  we see  $m \propto \phi$  meaning  $\Gamma \propto \phi$ . For a field oscillating in a quartic minimum  $\Phi \propto 1/a$  [117]. Therefore,  $\Gamma/H \propto a$ , increasing with time as we expect, until  $\Gamma \sim H$ ; the decay becomes efficient, decay products accumulate and reheating completes.

The temperature and energy density of the produced radiation bath are related via Eq. (2.94). At reheating the energy density of the oscillating condensate

is transferred to the radiation bath, and so we need to find  $\rho_{\text{reh}}$ . For the density of the oscillating condensate we have

$$\rho_{\text{reh}} = \rho_{\text{end}} \left( \frac{a_{\text{end}}}{a_{\text{reh}}} \right)^4, \quad (5.21)$$

and from  $\Gamma/H \propto a$  we find

$$\frac{a_{\text{reh}}}{a_{\text{end}}} \sim \frac{H_{\text{end}}}{\Gamma_{\text{end}}} \simeq \frac{1}{\sqrt{\xi}} \frac{8\pi H_{\text{end}}}{y^2 \phi_{\text{end}}}, \quad (5.22)$$

which leaves us with

$$\rho_{\text{reh}} = \rho_{\text{end}} \frac{\xi^2 y^8 \phi_{\text{end}}^4}{8^4 \pi^4 H_{\text{end}}^4}. \quad (5.23)$$

Using  $\rho_{\text{end}} \sim V_{\text{end}} \sim \xi \phi_{\text{end}}^4$  and  $H_{\text{end}}^2 = \rho_{\text{end}}/3m_{\text{Pl}}^2$  gives

$$\rho_{\text{reh}} = \frac{9\xi m_{\text{Pl}}^4 y^8}{8^4 \pi^4}, \quad (5.24)$$

and equating this with the radiation bath temperature via Eq. (2.94) we see

$$T_{\text{reh}} \sim \left( \frac{270}{\pi^2 g_*} \right)^{1/4} \frac{y^2 \xi^{1/4}}{8\pi} m_{\text{Pl}} \sim 0.03 y^2 \xi^{1/4} m_{\text{Pl}}, \quad (5.25)$$

where we take  $g_* = 106.75$  in the second approximation. For the parameter values found earlier:  $y \simeq 4 \times 10^{-4}$  and  $\xi \sim 10^{-16}$ , we get  $T_{\text{reh}} \sim 10^6$  GeV, which is comfortably higher than the temperature at BBN ( $\sim 1$  MeV).

We do not rule out the possibility that the scalar potential also contains a quadratic term, of the form of  $m^2 \phi^2$  but if such a term is present it must be negligible during inflation meaning  $m^2 < \xi \phi^2$ . Using  $\xi \sim 10^{-16}$  and  $\phi \sim \phi_f \sim m_{\text{Pl}}$ , we find the bound  $m < 10^{10}$  GeV.

In order not to influence reheating, which will have a knock on effect on the analysis of the rest of this chapter via the e-folding number, the bound on  $m$  is much more stringent. We need the quadratic term in the potential to remain subdominant until the decay of the inflaton condensate, meaning  $m^2 < \xi \phi_{\text{reh}}^2$ .

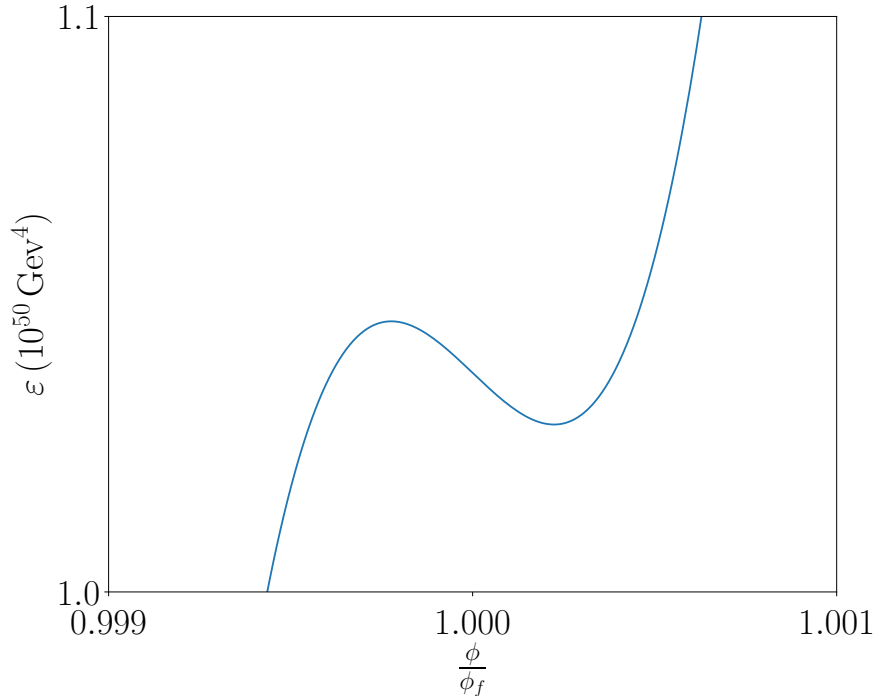


**Figure 5.6:** The scalar field potential when  $\delta$  takes negative values, showing the appearance of a local maximum and minimum. In this example  $\delta = -10^{-7}$ . Due to the scales involved we define  $V(\phi) = V_0 + \varepsilon$  where  $V_0 = 2.507017 \times 10^{57} \text{GeV}^4$ .

Earlier we saw  $\phi \propto 1/a$ , so using Eq. (5.22) we find

$$\phi_{\text{reh}} \simeq \frac{y^2 \sqrt{\xi}}{8\pi} \frac{\phi_{\text{end}}^2}{H_{\text{end}}}, \quad (5.26)$$

which translates to the bound

$$m < \sqrt{3\xi} \frac{y^2}{8\pi} m_{\text{Pl}}, \quad (5.27)$$

where we again consider that  $H_{\text{end}}^2 \simeq \rho_{\text{end}}/3m_{\text{Pl}}^2 \simeq \xi\phi_{\text{end}}^4/3m_{\text{Pl}}^2$ . Putting the numbers in, we obtain  $m < 300 \text{ GeV}$  or so, which does not leave a huge parameter space but it also means it might be observable in the LHC in the near future. It also means that if  $m \sim 1 \text{ TeV}$ , the influence on the value of  $N_*$  would be of the order  $\Delta N_* \simeq \frac{1}{6} \ln(m^2 - \xi\phi_{\text{reh}}^2) < 1$ , which would have minimal impact on our results.

## 5.7 Additional Considerations

### 5.7.1 Negative $\delta$ Values

It is possible for  $\delta$  to take negative values, in which case the potential develops a local minimum and maximum in place of a flat plateau, an example of which is shown in Fig. 5.6. The inflaton will oscillate about the local minimum until it quantum tunnels to the far side of the local maximum. When the inflaton tunnels through the local maximum, it may be in a position to slow-roll on the other side of the peak, hopefully for enough e-folds to generate  $n_s$  and  $r$  in accordance with observations.

From the definition of  $V'$  given in Eq. (5.9) we can find the stationary points in the usual way from  $V' = 0$  which gives

$$\frac{3\alpha\phi^2}{m_{\text{Pl}}^2} = 2 \ln \left( \frac{\phi^2}{m_{\text{Pl}}^2} \right) + 1. \quad (5.28)$$

We re-write this as

$$\exp \left( \frac{3\alpha\phi^2}{m_{\text{Pl}}^2} \right) = \frac{\phi^4 e}{m_{\text{Pl}}^4}, \quad (5.29)$$

and rearrange to

$$\frac{-3\alpha\phi^2}{2m_{\text{Pl}}^2} \exp \left( \frac{-3\alpha\phi^2}{2m_{\text{Pl}}^2} \right) = \frac{-3\alpha}{2e^{1/2}}, \quad (5.30)$$

allowing us to use the Lambert W function, which satisfies  $x = W(x)e^{W(x)}$ , to solve and find:

$$\left( \frac{\phi}{m_{\text{Pl}}} \right)^2 = \frac{-2}{3\alpha} W \left( \frac{-3\alpha}{2e^{1/2}} \right). \quad (5.31)$$

Since  $\phi^2 > 0$  this implies  $W \left( \frac{-3\alpha}{2e^{1/2}} \right) < 0$ . The Lambert W function is depicted in Fig. 5.7 and we see  $W(x) < 0$  is true for  $x < 0$ , meaning we require  $\left( \frac{-3\alpha}{2e^{1/2}} \right) < 0$  and this imposes a bound of  $\alpha > 0$  and hence  $\delta > -1$  (from Eq. (5.13)).

The Lambert W function is only real for  $x > \frac{-1}{e}$  leading to a second bound of

$$\alpha < \frac{2}{3e^{1/2}}. \quad (5.32)$$

Remembering the relationship between  $\alpha$  and  $\delta$  given in Eq. (5.13) and combining both bounds this translates to a constraint on  $\delta$  of

$$-1 \leq \delta \leq 0. \quad (5.33)$$

These do not provide useful bounds for us, but the upper bound, whilst being trivial, reinforces the idea that we require negative  $\delta$  values to form the local minimum and maximum. We find two solutions to Eq. (5.31), corresponding to the minimum and maximum, from the  $W_0$  and  $W_{-1}$  branches of the Lambert W function in the region  $\frac{-1}{e} < x < 0$ .

Once the location of the local minimum is known (which will be the larger of the two solutions to Eq. (5.31)) we are able to find the corresponding point on the far side of the maximum which the inflaton will quantum tunnel to, using the fact that  $V(\phi_{\text{entry}}) \simeq V(\phi_{\text{exit}})$ .

We then use  $\phi_{\text{exit}}$  to calculate the total number of slow-roll e-folds from the exit point of the quantum tunnelling and find that they satisfy  $N_{\text{tot}} > N_*$  only for  $\delta \geq -10^{-6.6}$ . For  $|\delta|$  values larger than this there are not enough e-foldings of slow-roll available after the quantum tunnelling event. This makes sense because a larger  $|\delta|$  value will result in a deeper minimum, meaning after quantum tunnelling the inflaton will emerge further down the potential, with less of the inflection point plateau to roll along. For all negative  $\delta$  values we find  $N_* \simeq 51.05$ . Even though this is a similar e-folding number to our result in the positive  $\delta$  case (see Section 5.4), the differing  $\delta$  value means the predictions for the spectral index are not compatible with the Planck 2018 bounds.

### 5.7.2 A Diffusion Zone Around $\phi_f$

Returning to positive  $\delta$  values, when  $\delta$  is very small and the potential very flat around the inflection point, a diffusion zone may exist. A diffusion zone is a region where the quantum fluctuations of the inflaton dominate over its classical motion.

During slow-roll inflation we presume the slow-roll assumptions in Eqs. (2.72) and (2.73) are valid and the KG equation tells us the classical evolution of the

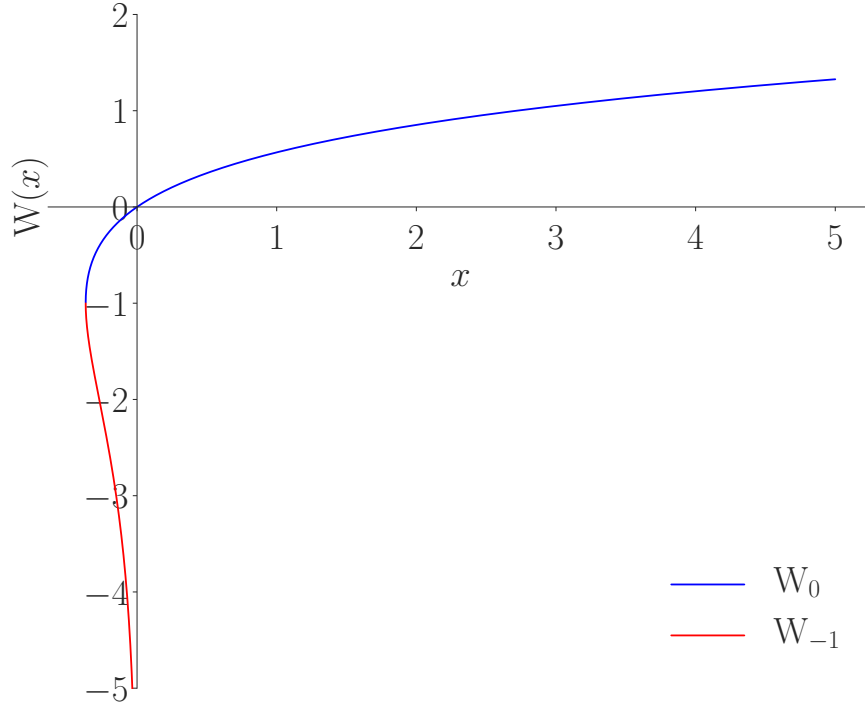


**Figure 5.7:** The Lambert W function

field is

$$|\dot{\phi}| \simeq \frac{V'}{3H}, \quad (5.34)$$

which for  $\delta \ll 1$  may be very small. On the other hand, the amplitude of a quantum fluctuation of the scalar field is given by

$$\left| \frac{\delta\phi}{\delta t} \right| \simeq \frac{H^2}{2\pi} \simeq \frac{V}{6\pi m_{\text{Pl}}^2}. \quad (5.35)$$

As introduced in Section 2.6.6, if the quantum fluctuations of the field overwhelm its classical evolution the field becomes impervious to the potential and eternal inflation ensues. This will happen if  $|\frac{\delta\phi}{\delta t}| > |\dot{\phi}|$ , so to avoid a diffusion zone we need

$$\frac{V}{6\pi m_{\text{Pl}}^2} < \frac{V'}{3H}. \quad (5.36)$$

Using the definitions in Eqs. (5.8) and (5.9), with  $\phi_f$ , which is the flattest part

of the potential for positive  $\delta$  values, we obtain a cubic inequality:

$$\frac{\xi e^3}{48\pi^2} \left[ \alpha^3 - \left( \frac{3\pi^2}{2e^{1/2}} + \frac{432\pi^2}{\xi e^2} \right) \alpha^2 + \left( \frac{576\pi^2}{\xi e^{5/2}} + \frac{1}{2e} + \frac{4}{8e^{3/2}} \right) \alpha + \frac{192\pi^2}{\xi e^3} \left( 1 + \frac{\xi e^{3/2}}{1536\pi^2} \right) \right] \geq 0, \quad (5.37)$$

and we can find the minimum allowed  $\alpha$  value by setting the inequality equal to zero and using  $\xi \simeq 10^{-16}$ , for which we see

$$\alpha_{\min} = 0.404354. \quad (5.38)$$

From the definition of  $\alpha$  in Eq. (5.13) this translates to

$$\delta_{\min} = \frac{3e^{1/2}a_{\min}}{2} - 1 = 5.61 \times 10^{-7} \simeq 10^{-6.25}. \quad (5.39)$$

Eq. (5.39) is the minimum value  $\delta$  can take in order to avoid a diffusion zone existing around the inflection point. From the inflationary observable constraints on  $\delta$  in Section 5.4 we see a diffusion zone does not exist for our model and we do not need to concern ourselves with the constraints it would impose. However, we point out that the existence of a diffusion zone does not invalidate inflation, it simply imposes that  $\phi_*$  exists outside of the diffusion zone, requiring  $N_* < N_{\text{SR}}$  where  $N_{\text{SR}}$  is the total e-folds of slow-roll inflation that can occur from the edge of the diffusion zone.

### 5.7.3 Ultra Slow-roll Inflation

The slow-roll assumptions (Eqs. (2.72) and (2.73)) may not always be valid in models of inflection-point inflation, if a period of Ultra Slow Roll (USR) exists [149]. We use the terminology of Ref. [149] which labels  $\ddot{\phi}$ ,  $3H\dot{\phi}$  and  $V'(\phi)$  in the KG equation as the acceleration, friction and slope terms respectively. The first slow-roll assumption says

$$\ddot{\phi} \ll 3H\dot{\phi}, \quad (5.40)$$

leaving the friction term coupled to the slope term in the KG equation. However, in very flat sections of the potential we may see the opposite behaviour, where the slope becomes negligible and we have the acceleration term locked to the slope term.

We can intuitively see the behaviour from the Hubble parameters defined in Section 2.4.3, especially  $\eta_H$ :

$$\eta_H = -\frac{\dot{\epsilon}_H}{H\epsilon_H}, \quad (5.41)$$

where  $\epsilon_H$  is the first Hubble slow-roll parameter, defined in Eq. (2.64). Following Ref. [149], Eq. (5.41) can be written as

$$\eta_H = \frac{2\ddot{\phi}}{H\dot{\phi}} + 2\epsilon_H, \quad (5.42)$$

which for traditional slow-roll, with  $\epsilon_H \ll 1$ , is very small. However, in USR the first term in Eq. (5.42) is not negligible, instead approaching a constant value as the acceleration and friction terms become comparable. Hence, when we are in the USR regime we find

$$\eta_H \simeq -6, \quad (5.43)$$

which means that slow-roll is no longer an appropriate assumption. This leads to very different predictions for the inflationary observables because the field is rolling much quicker during USR and calculations of  $N_*$  assuming slow-roll will result in an overestimate for  $N_*$ .

Ref. [149] shows that the danger from USR can be averted as long as the inflaton's kinetic energy is capped at

$$\rho_{\text{kin}} \leq \frac{(m_{\text{Pl}}V')^2}{6V}, \quad (5.44)$$

when it approaches the inflection point. For our model this results in a bound of

$$\rho_{\text{kin}} \lesssim 16m_{\text{Pl}}^4 \xi e^{1/4} \delta^2, \quad (5.45)$$

which for the parameter values found in Section 5.4 gives a maximum kinetic

energy of

$$\rho_{\text{kin,max}}^{1/4} \simeq 10^{12} \text{ GeV} . \quad (5.46)$$

In Section 5.6 we found the energy scale of inflation to be approximately  $V^{1/4} \simeq 10^{14} \text{ GeV}$  and so requiring  $\rho_{\text{kin}}^{1/4}$  be three orders of magnitude smaller is not unreasonable, we do not consider the initial conditions further.

## 5.8 Discussion

This chapter presents a model of inflection-point inflation which does not rely on an embedding in a beyond-the-standard-model theory. We simply stabilise an unbounded CW potential with loop corrections to form the inflationary plateau and hence name the model ‘loop inflection-point inflation’. Due to the nature of inflection-point inflation, whereby terms in the scalar potential almost, but not quite, cancel each other out, the model necessarily involves an element of tuning.

The level of tuning in the model is of the order of  $\mathcal{O}(10^{-6})$ , which is much reduced compared to typical realisations in the literature, for example tuning in A-term inflation is of the order of  $\mathcal{O}(10^{-20})$  [128] and the merits of relying on physics no more exotic than the standard model should not be overlooked.

The parameter we constrain in the model is  $\delta$ , which quantifies the scalar potential’s deviation from a perfectly flat inflection point. We use the inflationary observables,  $n_s$  and  $r$ , to constrain its magnitude and find it is necessary to restrict its values to  $10^{-5.96} \leq \delta \leq 10^{-5.79}$ .

We find the energy scale of inflation to be  $V^{1/4} \simeq 10^{14} \text{ GeV}$ , and  $M \simeq 10^{15} \text{ GeV}$ , near the GUT scale as expected. The model incorporates a Yukawa coupling in the CW loop term, which takes a value of  $y \simeq 4 \times 10^{-4}$ , as is typical.

Due to the extremely flat nature of the inflection point, we verify that a diffusion zone does not exist in the model and owing to the shorter than usual plateau in the model we check that the total e-foldings of inflation support the required e-foldings of slow-roll inflation. We also have a constraint on the inflaton’s initial kinetic density of  $\rho_{\text{kin}}^{1/4} \lesssim 10^{12} \text{ GeV}$ . A study of reheating in this model finds the

number of e-folds of inflation after observable scales leave the horizon is independent of the reheating temperature when the inflaton is oscillating in a quartic minimum. This is also found in Chapter 3.

Due to the complexity of the equations in this model, this chapter demonstrates the first example of a numerical approach for calculating the specifics of inflation. This is developed in following chapters, where coupled differential equations require numerical integration techniques. In the next chapter we take a brief interlude from models of inflation and present research on primordial black holes.

# Chapter 6

## Primordial Black Hole Formation During Slow Reheating After Inflation

*This chapter is based on research by the author, in collaboration with Bernard Carr, Konstantinos Dimopoulos and Tommi Tenkanen, published in Physical Review D [150].*

### 6.1 Introduction

Overdensities in the early Universe eventually grow into the rich structure formation we see today. However, it is also possible that an overdensity may collapse to a black hole instead; black holes forming in the early Universe are called Primordial Black Holes (PBHs) [151]. Black holes emit radiation and eventually evaporate on a timescale proportional to their size [152], so only PBHs with mass greater than  $10^{15}g$  will have survived to the present day. PBHs form with masses of the order of the particle horizon mass at the time of their formation, meaning they are able to form with a large range of masses [151, 153]. Black holes which have not evaporated before the current epoch are a possible CDM candidate,

but there are stringent constraints on their allowed masses and abundances from observations, Ref. [154] provides a good overview of the current constraints and we direct the reader there for further references. There is no direct evidence for the existence of PBHs but the recent observations by LIGO provide the first direct evidence for non-primordial black holes in the Universe [155] and PBHs are a robust theoretical prediction. Their formation allows the power spectrum of inflation to be probed at much smaller scales than can be observed directly. This presumes the collapse of overdensities which originated as fluctuations during inflation to be the foremost formation mechanism of PBHs. There are several other notable formation mechanisms for which Refs. [156, 157] give a useful review and further references.

Provided there are no other forces, a large enough density contrast will gravitationally collapse to form a PBH. However, during radiation dominated eras of the Universe, the thermal energy of the radiation background provides a restorative force, opposing gravitational collapse. The Jeans length,  $R_J$ , defines the length scale for which gravitational energy and restorative pressure are balanced. Only overdensities larger than the Jeans length are unstable to gravitational collapse. In a matter dominated Universe this is negligible and overdensities of any size may grow large enough to collapse to a PBH, though only if they are sufficiently spherically symmetric to avoid disc formation or fragmentation.

During reheating after inflation, an oscillating inflaton behaves as a matter dominated Universe. Radiation pressure is minimal and this era is generally taken to be a prime PBH formation era until radiation domination begins and the increased Jeans length suppresses their formation again. During the reheating process there is a radiation bath being produced which is quickly diluted away for most of the oscillating period. However, as we approach the completion of reheating the radiation bath starts to accumulate. It is still sub-dominant but it has an effect on the effective equation of state parameter, as the latter grows to become  $w_r = 1/3$  at radiation domination.

This is pertinent to the study of primordial black holes (PBHs) because their formation rates are calculated assuming either matter domination or radiation domination. In this chapter, we investigate the intervening transition period and

how the varying equation of state parameter affects the formation rate and mass function of PBHs.

## 6.2 PBH Production

For an overdense region in the early Universe to collapse and form a PBH, there are three constraints it should satisfy:

- (i) It must be larger than the Jeans length at maximum expansion,
- (ii) It must be sufficiently spherically symmetric,
- (iii) It must be spinning sufficiently slowly.

A density contrast is defined by

$$\delta = \frac{\rho - \bar{\rho}}{\bar{\rho}}, \quad (6.1)$$

and we assume the fluctuations have a Gaussian distribution with variance  $\sigma^2(k)$  at horizon crossing. During RD, overdensities satisfying constraint (i), whereby  $\delta > \delta_c$ , where  $\delta_c$  is some critical value to be determined, lie on the Gaussian tail of the density fluctuation distribution. Overdensities on the Gaussian tail are expected to be spherically symmetric [158, 159], so satisfying (i) during RD automatically satisfies (ii). Constraint (iii) is also satisfied during RD because the Jeans length is of the order of the size of the horizon, meaning the overdensity does not evolve much between entering the horizon and collapsing to a PBH.

Therefore, during RD it is the size of an overdensity which controls whether or not it collapses to form a PBH. The fraction of the energy density of the Universe collapsing to form PBHs is found from the probability of an overdensity meeting constraint (i) [160]:

$$\begin{aligned} \beta(M) &= \frac{2}{\sqrt{2\pi}\sigma(M)} \int_{\delta_c}^{\infty} d\delta \exp\left(-\frac{\delta^2}{\sigma(M)^2}\right) \\ &= \text{Erfc}\left(\frac{\delta_c}{\sqrt{2}\sigma(M)}\right), \end{aligned} \quad (6.2)$$

where  $\text{Erfc}$  is the complementary error function and  $\sigma$  is the rms fluctuation amplitude. As only density fluctuations on the tail of the distribution are large enough to form PBHs, we see the production rate is exponentially suppressed.

Alternatively, for a MD Universe the probability of (i) being satisfied is close to unity because the Jeans length becomes very small. However, now we move away from the Gaussian tail of the density fluctuation distribution, spherical symmetry cannot be assumed. Constraint (ii) becomes the limiting factor for the fraction of the total energy density in the Universe collapsing to form PBHs, given by [161–163]

$$\beta(M) \simeq 0.056\sigma(M)^5. \quad (6.3)$$

For smaller density contrasts the effect of any rotation of the collapsing region becomes more apparent, the fraction of overdensities satisfying (iii) becomes smaller than Eq. (6.3) and the limiting factor on their production is then [164]

$$\beta(M) \simeq 2 \times 10^{-6} f_q(q_c) \mathcal{J}^6 \sigma(M)^2 \exp\left(-0.147 \frac{\mathcal{J}^{4/3}}{\sigma(M)^{2/3}}\right), \quad (6.4)$$

where  $f_q$  is the fraction of masses for which  $q \leq q_c$  where  $q$  is the dimensionless quadrupole moment and  $q_c = \sqrt{2}$  [164].  $\mathcal{J}$  is a complicated ratio of integrals which arises in the calculation of the angular momentum, but it is approximately unity, as shown in Ref. [165], so we take  $\mathcal{J} = 1$ . Ref. [164] also states “we assume  $f_q(q_c)$  is not too small” - decreasing  $f_q(q_c)$  suppresses the formation rate further, but does not affect the behaviour we discuss from here onwards so we set  $f_q(q_c) = 1$  without loss of generality. For comparison, Eqs. (6.2) to (6.4) are plotted in Fig. 6.1.

After inflation, the inflaton oscillates about a quadratic minimum of its potential and its equation of state is  $w = 0$ , as in a MD era of the Universe (see Section 2.7). The assumption of Eqs. (6.2) to (6.4) is that there is a discontinuous transition from MD to RD after reheating completes. However, during a period of slow reheating after inflation the value of  $w_{\text{eff}}$  transitions smoothly from  $w_{\text{eff}} = 0$  to  $w_{\text{eff}} = 1/3$  as the decay products of the inflaton slowly accumulate. Taking a sharp cut-off between these two regions is not a natural way of modelling the PBH production and so we trace the behaviour of  $w_{\text{eff}}$  in the intermediary regime.

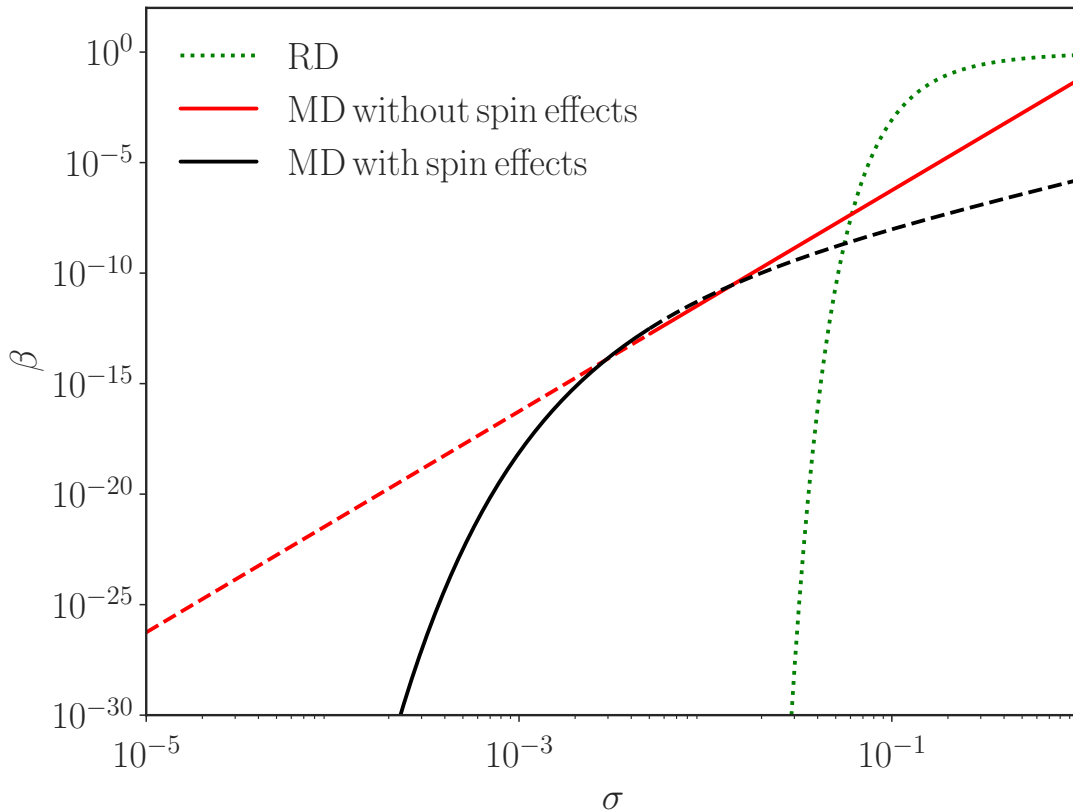


**Figure 6.1:** The fraction of the total energy density collapsing into PBHs,  $\beta$ , as a function of  $\sigma(M)$ . During radiation domination and matter domination different considerations control  $\beta$ . The green dotted line shows  $\beta$  in a radiation dominated Universe, given by Eq. (6.2) with  $\delta_c = w_r$ . The red line shows  $\beta$  in a matter dominated Universe when the limiting factor controlling  $\beta$  is the fraction of overdensities which are sufficiently spherically symmetric, Eq. (6.3), valid for  $0.005 < \sigma < 0.2$ . The black line shows  $\beta$  in a matter dominated Universe when the limiting factor controlling  $\beta$  is the angular momentum of the region and Eq. (6.4) is appropriate, when  $\sigma < 0.005$ . When the red (black) line is solid rather than dashed, this indicates the red (black) line is the limiting factor controlling  $\beta$  in the matter dominated regime.

We expect that the growing thermal bath will increase the Jeans length to a size whereby (i) limits the production rate of PBHs even before reheating completes. Put another way, the fraction of overdensities with sufficient spherical symmetry to collapse is likely to be larger than the fraction of overdensities which are of sufficient size to collapse, meaning (i) becomes the dominant constraint on PBH production before radiation domination is achieved.

### 6.3 The Effect of a Slow Reheating Period

Whilst the inflaton is oscillating in the quadratic minimum the produced (subdominant) radiation has an energy density [85]

$$\rho_r = \frac{\rho_\phi}{4} \frac{\Gamma}{H}, \quad (6.5)$$

where  $\rho_r$  is the energy density of the produced radiation,  $\rho_\phi$  is the energy density of the inflaton and  $\Gamma$  is its decay rate. Using this, the effective equation of state parameter can be written as

$$w_{\text{eff}} = \frac{p_\phi + p_r}{\rho_\phi + \rho_r} = w_r \frac{\Gamma}{4H} \left( 1 + \frac{\Gamma}{4H} \right)^{-1} \simeq \frac{w_r}{4} \frac{\Gamma}{H}, \quad (6.6)$$

where  $p_\phi \simeq 0$  is the pressure of the inflaton,  $p_r$  the pressure of the radiation,  $w_r = 1/3$  is the equation of state parameter of radiation and we take  $\rho_r \ll \rho_\phi$  in the last equality.

A precise expression for the critical size required for a density contrast to collapse against any radiative pressure is derived in [166]:

$$\delta_c = \frac{3(1+w)}{5+3w} \sin^2 \left( \frac{\pi\sqrt{w}}{1+3w} \right), \quad (6.7)$$

which applies in the co-moving gauge; the appropriate choice if we wish to compare to the production fraction in a matter dominated scenario. We simplify  $\delta_c \simeq 6w_{\text{eff}}$  which is true for  $w_{\text{eff}} \ll 1$  and combining Eqs. (6.2), (6.6) and (6.7) see that the fraction of overdensities large enough to collapse is

$$\beta(M) = \text{Erfc} \left( \frac{3w_r}{\sqrt{8}\sigma(M)} \frac{\Gamma}{H} \right). \quad (6.8)$$

We rearrange for  $\Gamma/H$  and find

$$\frac{\Gamma}{H} \simeq \frac{\sqrt{8}\sigma(M)}{3w_r} \text{Erfc}^{-1}(\beta(\sigma)). \quad (6.9)$$

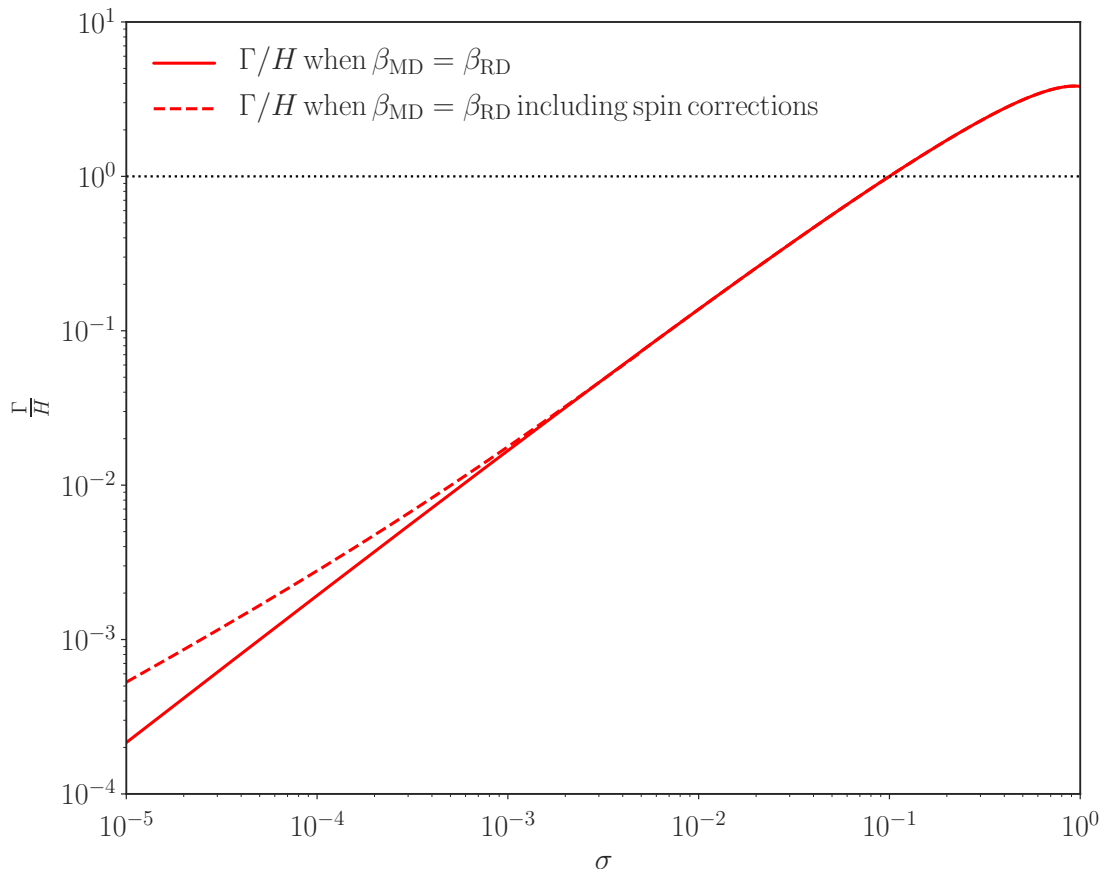


**Figure 6.2:** Solutions to Eq. (6.9); the solid red line uses  $\beta(M)$  defined in Eq. (6.3) for the complete range of  $\sigma$  values, the dashed red line uses  $\beta(M)$  defined in Eq. (6.4) in the region  $\sigma < 0.005$ . The dotted horizontal line denotes  $\Gamma/H = 1$ .

This allows us to replace  $\beta(\sigma)$  with Eq. (6.3) or Eq. (6.4) as appropriate to find the value of  $\Gamma/H$  when the different PBH formation rates coincide. For smaller  $\Gamma/H$  values we expect the matter-domination considerations to constrain the fraction more, but as  $\Gamma/H$  increases and we approach radiation domination, we expect the sub-dominant radiation bath to have an effect on the fraction of overdensities satisfying  $\delta > \delta_c$  and for this to become the limiting constraint on  $\beta$ . Effectively we are using  $\Gamma/H$  as a time co-ordinate; if we assume  $\Gamma \simeq \text{constant}$  then  $\Gamma/H \propto H^{-1}$  and using the relationship in Eq. (2.34) we see  $\Gamma/H \propto t$ . The times when the PBH formation rates in MD and RD coincide vary for different  $\sigma$  values, which can be seen in Fig. 6.2. We immediately see that the sub-dominant radiation bath has no effect on fluctuations above a threshold size, meaning the

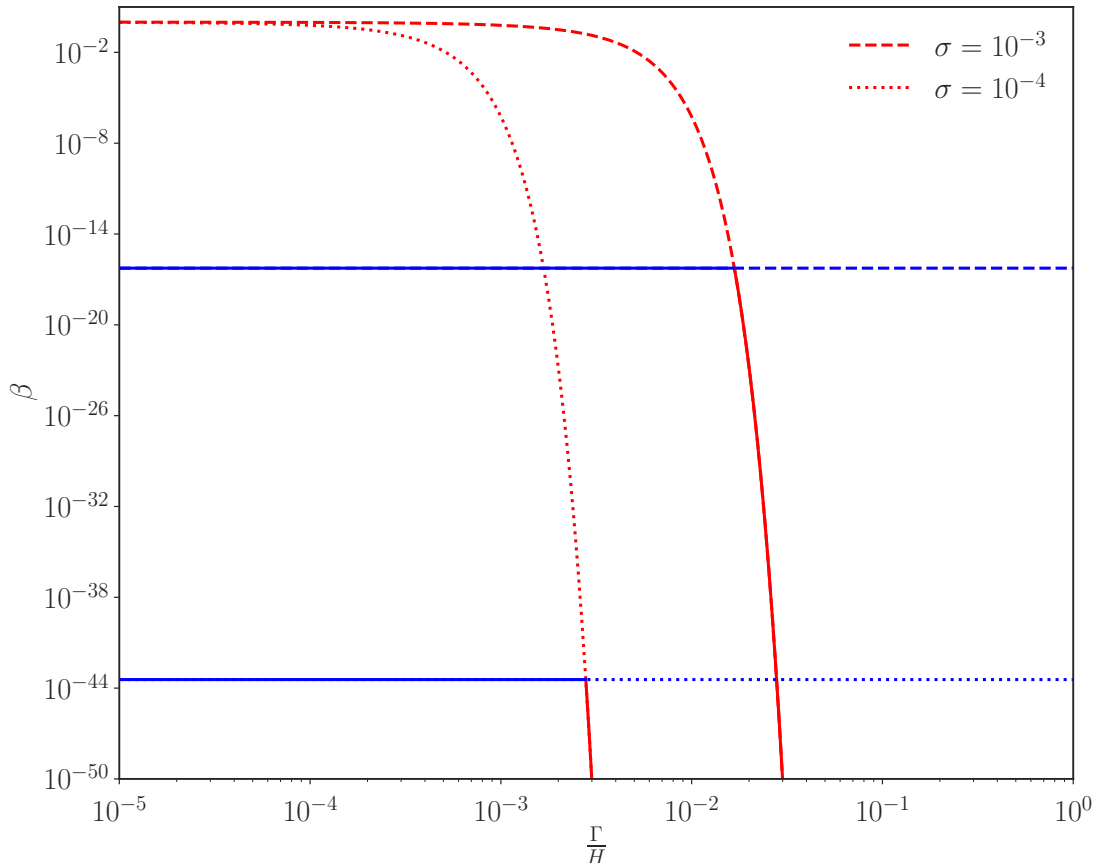


**Figure 6.3:** The fraction of overdensities able to collapse from Eq. (6.2) in red and Eq. (6.3) in blue. For  $\Gamma/H \ll 1$ , when  $w_{\text{eff}} \simeq 0$ , the fraction of overdensities with  $\delta > \delta_c$  is almost unity but the fraction which are sufficiently spherical is much lower, hindering the PBH formation rate. As  $\Gamma/H$  increases the fraction with  $\delta > \delta_c$  drops drastically as  $w_{\text{eff}} \rightarrow 1/3$  and limits the PBH formation rate. The solid line indicates the limiting factor affecting formation rate at any time. Two example values of  $\sigma$  are shown via the dashed and dotted lines.

transition between production fractions never occurs during slow-reheating and Eq. (6.3) applies throughout. We find the threshold value of  $\sigma_c \simeq 0.05$ .

We see that the solutions coincide at earlier times for smaller fluctuations. This makes sense because smaller fluctuations will fall below the (growing) Jeans length sooner. This can be seen in Fig. 6.3 where we plot the probability of an overdensity satisfying constraints (i) and (ii), as a function of time ( $\Gamma/H$ ). We see that at a certain time the limiting probability switches from constraint (ii),

to constraint (i), and (for  $\sigma < \sigma_c$ ) this does not coincide with the beginning of radiation domination ( $\Gamma \simeq H$ ) as previously assumed in the literature.

We can calculate the e-folds of effective MD for PBH formation in the early Universe to quantify the effect we are discussing. From Eq. (2.88) we find the e-folds of reheating to be

$$N_{\text{reh}} = \ln \left( \frac{a_{\text{reh}}}{a_{\text{end}}} \right), \quad (6.10)$$

where ‘reh’ denotes the moment of reheating and ‘end’ denotes the end of inflation. During MD  $a \propto H^{-2/3}$  so we see

$$N_{\text{reh}} = \frac{2}{3} \ln \left( \frac{H_*}{\Gamma} \right), \quad (6.11)$$

where we have used  $H_{\text{end}} \simeq H(\phi_*)$  and  $H_{\text{reh}} \simeq \Gamma$ .

However, as we have seen, the transition between production mechanisms (which we denote by subscript ‘x’) occurs before reheating. We can calculate how many e-folds of effective MD occur before this takes places as

$$N_x = \frac{2}{3} \ln \left( \frac{H_* \Gamma}{\Gamma H_x} \right) = \frac{2}{3} \ln \left( \frac{H_* \sqrt{8\sigma}(M)}{\Gamma 3w_r} \text{Erfc}^{-1}(\beta(\sigma)) \right), \quad (6.12)$$

which reduces Eq. (6.11) by

$$\Delta N = N_{\text{reh}} - N_x = \frac{2}{3} \ln \left( \frac{3w_r}{\sqrt{8\sigma} \text{Erfc}^{-1}(\beta(\sigma))} \right). \quad (6.13)$$

The reduction is  $\mathcal{O}(10\%)$ , independent of  $\Gamma$ . This makes sense because a change in  $\Gamma$  changes both when the suppression occurs and when reheating completes.

This behaviour is shown in Fig. 6.4 where we plot the point where the sub-dominant radiation bath affects the formation rate,  $N_x$ , the onset of radiation domination,  $N_{\text{reh}}$ , and the difference between them,  $\Delta N$ . We see  $N_x$  increasing for larger  $\sigma$  as we would expect because larger overdensities resist the growing Jeans length for longer - the sub-dominant thermal bath has less of an impact on larger overdensities.

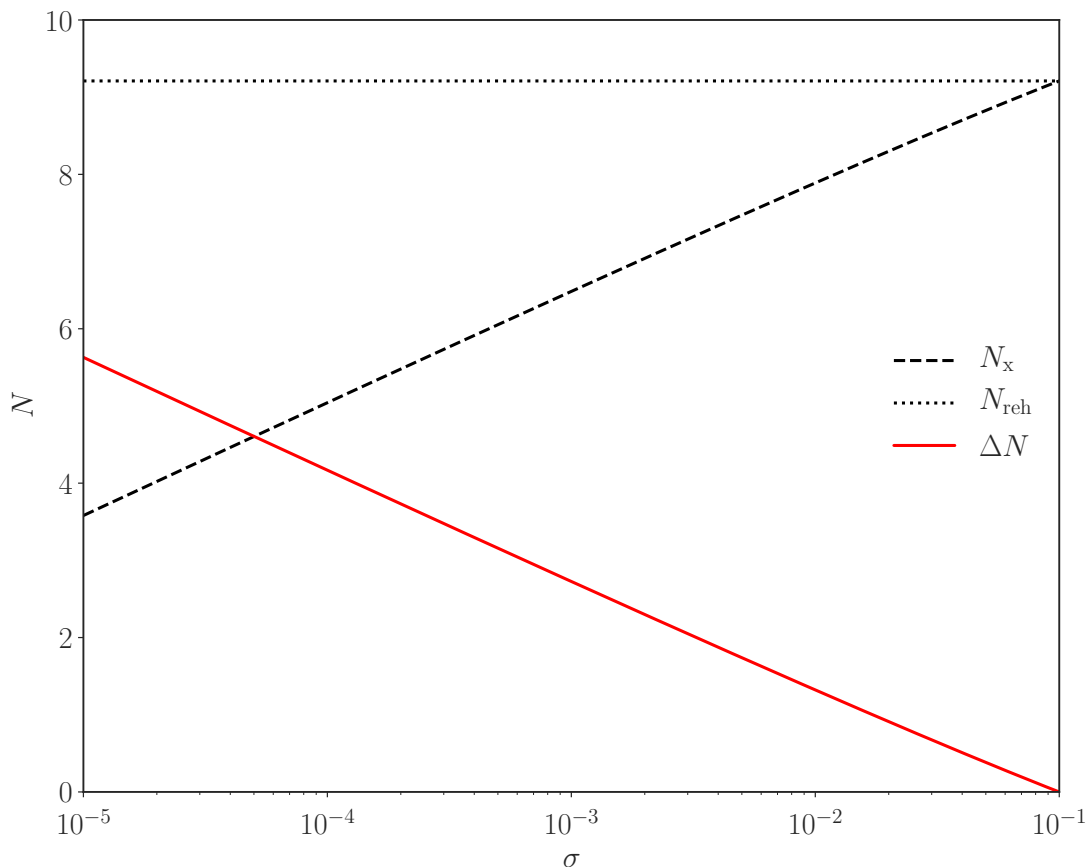


**Figure 6.4:** The duration of effective MD when  $\Gamma \simeq H$  signifies an immediate transition to RD (dotted, black line) and calculated  $\Gamma/H$  from Eq. (6.9), taking into account the growing thermal bath (dashed, black line). The red line shows the difference between the two calculations.

## 6.4 Primordial Black Hole Mass Function

Presuming that an overdensity satisfies the spherical symmetry and angular momentum requirements of (ii) and (iii), when it re-enters the horizon during effective matter domination it will eventually collapse to form a PBH, regardless of its initial amplitude because density contrasts grow linearly with scale factor and the restorative radiation pressure is negligible.

PBHs are expected to form with roughly the mass of the horizon when they first entered. The particle horizon during periods of matter domination is calculated in Section 2.3.2 and given by  $D_H(t) = 3t = 2/H$ , so we find the mass

contained within the horizon to be

$$M_{D_H} = \frac{32\pi m_{\text{Pl}}^2}{H}, \quad (6.14)$$

where we use  $\rho_{\text{tot}} = 3m_{\text{Pl}}^2 H^2$ . Therefore the minimum mass a PBH can have is given by

$$M_{\text{min}} = \frac{32\pi m_{\text{Pl}}^2}{H_{\text{end}}}, \quad (6.15)$$

where ‘end’ denotes the end of inflation, i.e. for the first scales to enter the horizon in the effective matter dominated era after inflation ends.

An overdensity collapses to a PBH when it reaches  $\delta \simeq \sigma \simeq 1$ , but this must happen before it feels the effect of the building radiation bath which will prevent its collapse. Perturbations inside the horizon grow linearly with the scale factor during a matter dominated regime, so from  $\sigma \propto a$  we can write

$$\frac{\sigma_{\text{col}}}{\sigma_{\text{entry}}} = \frac{a_{\text{col}}}{a_{\text{entry}}} = \left( \frac{H_{\text{entry}}}{H_{\text{col}}} \right)^{2/3}, \quad (6.16)$$

where ‘col’ denotes the moment of overdensity collapse and we use  $a \propto H^{-2/3}$  in a matter dominated Universe (see Eqs. (2.33) and (2.34)). We set  $\sigma_{\text{col}} = 1$ , so in following equations we suppress the subscript on  $\sigma_{\text{entry}}$ . We therefore need to ensure  $H_{\text{col}} > H_x$  where ‘x’ signifies the point at which the thermal bath has grown enough that constraint (i) is the limiting factor in the collapse of an overdensity. Therefore the minimum value of  $H$  (largest value of  $a$ ) which satisfies this for a given  $\sigma$  will be

$$H_{\text{entry,min}} = \frac{H_x}{\sigma^{3/2}}. \quad (6.17)$$

Rearranging Eq. (6.9) we find

$$H_x = \frac{3w_r \Gamma}{\sqrt{8\sigma} \text{Erfc}^{-1}(\beta(\sigma))}, \quad (6.18)$$

and so combining Eqs. (6.14), (6.17) and (6.18) provides the maximum mass

possible for a PBH formed with<sup>1</sup>  $\sigma < \sigma_c$

$$M_{\max} = \frac{32\pi m_{\text{Pl}}^2 \sigma^{3/2}}{H_x} = \frac{64\sqrt{2}\pi m_{\text{Pl}}^2 \sigma^{5/2}}{3w_r \Gamma} \text{Erfc}^{-1}(\beta(\sigma)). \quad (6.19)$$

We define reheating to be at  $\Gamma \simeq H$  and at reheating  $3m_{\text{Pl}}^2 H^2 = \rho_r$  so we see

$$3m_{\text{Pl}}^2 \Gamma^2 = \frac{g_* \pi^2 T_{\text{reh}}^4}{30}, \quad (6.20)$$

where we have used the relationship between the temperature and energy density of the thermal bath given in Eq. (2.94). From here we obtain

$$\Gamma = \frac{\sqrt{g_*} \pi T_{\text{reh}}^2}{3\sqrt{10} m_{\text{Pl}}}, \quad (6.21)$$

which we use to rewrite Eq. (6.19) as

$$M_{\max} = \frac{128\sqrt{5} m_{\text{Pl}}^3 \sigma^{5/2}}{w_r \sqrt{g_*} T_{\text{reh}}^2} \text{Erfc}^{-1}(\beta(\sigma)). \quad (6.22)$$

In PBH research, because of the masses involved it is more typical to use  $M_\odot$  as a mass scale, where  $M_\odot \simeq 4.53 \times 10^{38} m_{\text{Pl}}$  is the mass of the Sun. Using  $w_r = 1/3$  and  $g_* = 106.75$ , we find a final expression

$$\frac{M_{\max}}{M_\odot} \simeq 20\sigma^{5/2} \text{Erfc}^{-1}(\beta(\sigma)) \left( \frac{T_{\text{reh}}}{\text{GeV}} \right)^{-2}. \quad (6.23)$$

Rewriting Eq. (6.15) in a similar format we see

$$\begin{aligned} M_{\min} &\simeq 3.52 \times 10^{-18} \left( \frac{H_{\text{end}}}{\text{GeV}} \right)^{-1} M_\odot, \\ M_{\max} &\simeq \begin{cases} 20\sigma^{5/2} \text{Erfc}^{-1}(\beta(\sigma)) \left( \frac{T_{\text{reh}}}{\text{GeV}} \right)^{-2} M_\odot & \text{for } \sigma < \sigma_c, \\ 0.4\sigma^{3/2} \left( \frac{T_{\text{reh}}}{\text{GeV}} \right)^{-2} M_\odot & \text{for } \sigma > \sigma_c, \end{cases} \end{aligned} \quad (6.24)$$

<sup>1</sup>For  $\sigma > \sigma_c$ ,  $H_x \equiv H_{\text{reh}}$  and the standard result holds.

where in the third expression overdensities with  $\sigma > \sigma_c$  are unaffected by the sub-dominant radiation bath, meaning  $H_x = H_{\text{reh}}$  as is the usual case in the literature.

The fraction of the dark matter made up of PBHs can be expressed as [167]

$$f_{\text{PBH}} \equiv \frac{\Omega_{\text{PBH}}}{\Omega_{\text{DM}}} = \frac{1}{\rho_{\text{DM}}} \int \psi(M) \, dM, \quad (6.25)$$

where  $\psi(M)$  is the mass function and  $\rho_{\text{DM}}$  is the energy density of dark matter in the Universe. With appropriate normalisation  $\rho_{\text{DM}}$  can be absorbed into  $\psi(M)$  so that the PBH DM fraction within a particular mass range  $(M, M + dM)$  can be expressed as

$$f = \frac{\rho_{\text{PBH}}}{\rho_{\text{DM}}} = \int \psi(M) \, dM. \quad (6.26)$$

Inverting this we can find the mass function

$$\psi(M) = \frac{df}{dM} = \frac{1}{M} \frac{d}{d \ln M} \left( \frac{\rho_{\text{PBH}}}{\rho_{\text{DM}}} \right), \quad (6.27)$$

where we use the substitution  $\frac{d}{dM} \equiv \frac{1}{M} \frac{d}{d \ln M}$  because the definition of  $\beta(M)$  is

$$\beta(M) = \frac{1}{\rho_{\text{tot}}} \frac{d\rho_{\text{PBH}}(M)}{d \ln M}, \quad (6.28)$$

which allows us to simplify Eq. (6.27) to

$$\psi(M) = \frac{\rho_{\text{tot}}}{\rho_{\text{DM}}} \frac{\beta(M)}{M}. \quad (6.29)$$

During matter dominated epochs of Universe expansion the ratio  $\rho_{\text{PBH}}/\rho_{\text{DM}}$  is constant, because they both evolve as  $a^{-3}$ . This means  $f$  today is equal to  $f$  at matter-radiation equality (denoted by ‘eq’). It also means the fraction of the Universe in PBHs during their formation is equivalent to the fraction at reheating. However, after reheating the Universe becomes radiation dominated and evolves

as  $\rho_{\text{tot}} \propto a^{-4}$ . This means

$$\frac{\rho_{\text{tot}}}{\rho_{\text{DM}}}\bigg|_{\text{reh}} = \frac{\rho_{\text{tot}}}{\rho_{\text{DM}}}\bigg|_{\text{eq}} \frac{a_{\text{eq}}}{a_{\text{reh}}}. \quad (6.30)$$

At matter-radiation equality  $\rho_{\text{tot}} \simeq \rho_{\text{DM}}$  which means the current PBH dark matter fraction in the mass range  $(M, M + dM)$  is

$$\begin{aligned} \psi(M) dM &= \frac{a_{\text{eq}}}{a_{\text{reh}}} \frac{\beta}{M} dM, \\ &\simeq \left( \frac{g_*(T_{\text{reh}})}{g_*(T_{\text{eq}})} \right)^{1/3} \frac{T_{\text{reh}}}{T_{\text{eq}}} \frac{\beta(M)}{M} dM, \end{aligned} \quad (6.31)$$

where  $g_*(T_{\text{eq}}) = 3.909$ ,  $g_*(T_{\text{reh}}) = 106.75$  and  $T_{\text{eq}} \simeq 10^{-10}$  GeV. The precise value of  $T_{\text{eq}}$  used in this thesis is given in Table 1.1.

We can now use Eq. (6.31) to calculate the mass function of the produced PBHs in the refined scenario of a continuous transition between the formation fractions given in Eqs. (6.2) and (6.3), using the boundary masses derived in Eq. (6.24) for the integration limits.

The resulting mass functions for three  $\sigma$  values are plotted in Fig. 6.5, showing the predictions when the sub-dominant radiation bath is taken into account and the previous predictions when it was not. Fig. 6.5 is plotted using Eq. (6.3) for  $\sigma > 0.005$  and Eq. (6.4) otherwise. In Fig. 6.6 we plot both for comparison and demonstrate the effect angular momentum considerations have on the mass spectrum when  $\sigma < 0.005$ . Ignoring the angular momentum considerations does not affect the results we present here, culminating in the truncation of the mass spectrum as demonstrated in Fig. 6.5, but it results in a serious overestimate of the mass function for  $\sigma < 0.005$ .

The total dark matter fraction in PBHs can be obtained from Eq. (6.26), using Eq. (6.24) as integration limits. Observational constraints on the PBH abundance can then be analysed. The research presented here aims to demonstrate how a sub-dominant radiation bath from a period of slow reheating truncates the PBH mass function, so we do not analyse the constraints on the PBH abundance, which are many and varied. Ref. [154] describes the procedure and current constraints.

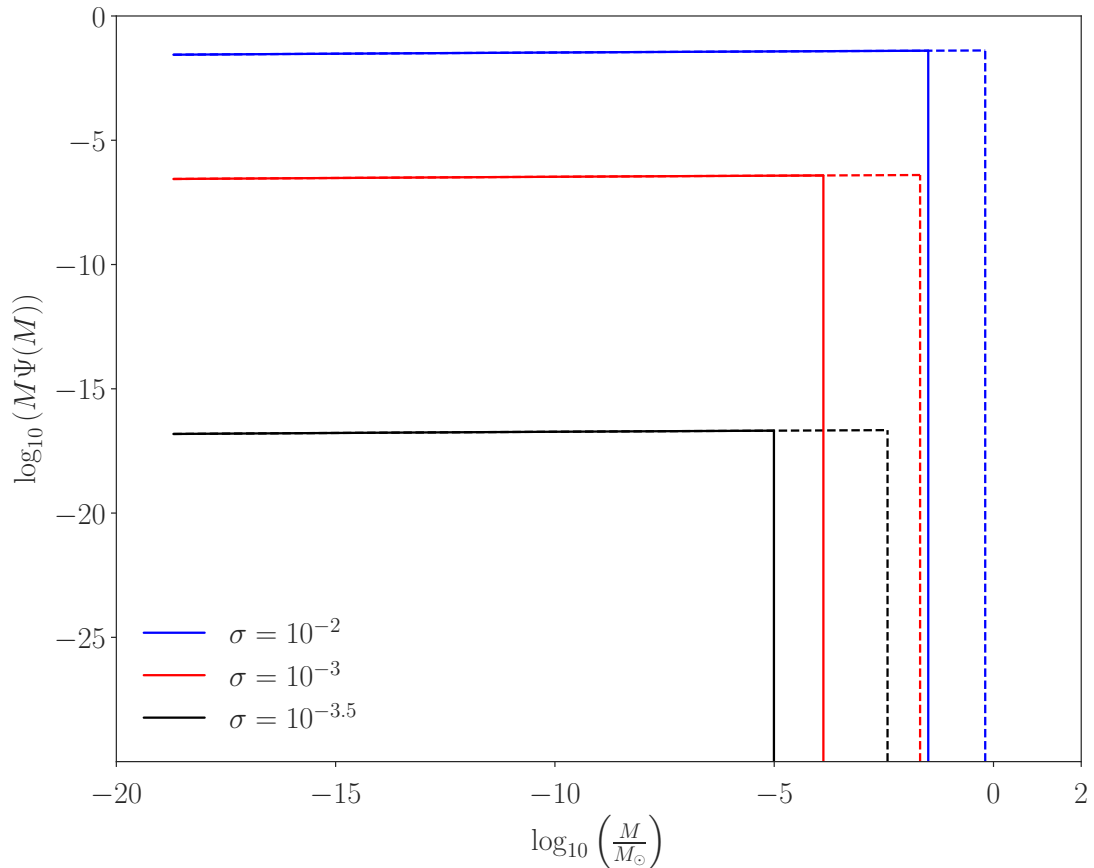


**Figure 6.5:** The PBH mass function for three example  $\sigma$  values (all below  $\sigma_c$ ). The solid lines represent the new cut-off taking into account the sub-dominant radiation bath, the dashed lines show the standard result in the literature where the mass cut-off occurs at  $H_{\text{reh}}$ . The minimum mass used here is  $M_{\text{evap}} \simeq 2 \times 10^{-19}$  GeV, the mass of PBHs evaporating today [2].

We find a maximum cut-off for the PBH mass at around  $100 M_{\odot}$ , for  $\sigma \simeq \sigma_c$ , the maximum  $\sigma$  for which the effect of the sub-dominant radiation bath changes the analysis from that in the literature. Observations of the CMB constrain the power spectrum of the primordial curvature fluctuations. Eq. (2.135) gives the 2018 Planck constraint on the amplitude of the power spectrum, which is the variance of the field, meaning we find  $\sigma \simeq 10^{-5}$ . The power spectrum is also constrained to be almost exactly scale invariant at the scales observed by Planck, which uses a pivot scale of  $k_* = 0.05 \text{ Mpc}^{-1}$ . The mass spectrum for  $\sigma = 10^{-5}$  is heavily suppressed to  $\mathcal{O}(10^{-145})$  and it is clear that there is not a

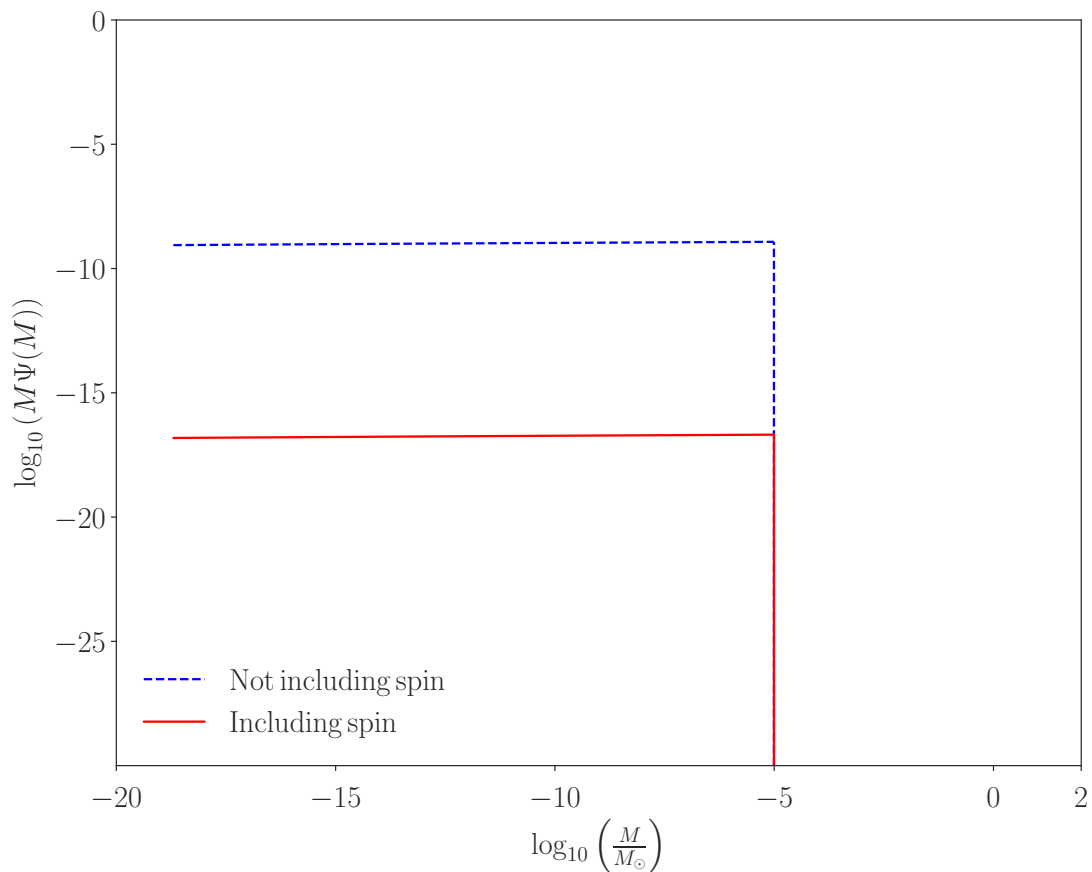


**Figure 6.6:** The mass function for  $\sigma = 10^{-3.5}$  with (solid, red line) and without (dashed, blue line) taking spin effects into consideration.

significant fraction of the CDM made up by PBHs. However, it is not necessary to assume that the power spectrum of curvature fluctuations follows the pattern of the CMB at smaller scales. Special features in the power spectrum [154, 168] or a blue spectrum [169] at smaller scales could increase  $\sigma$ . In fact, PBH formation necessarily provides constraints on the shape of the power spectrum at smaller scales and is therefore a predictive theory.

## 6.5 Discussion

This chapter presents a detailed analysis of the effect of a sub-dominant radiation bath, due to slow reheating, on the formation rate of PBHs. We show that the presence of the sub-dominant radiation bath has an effect on the formation rate of primordial black holes and so must be taken into account. The influence of the thermal bath slowly grows throughout the reheating period, resulting in a gradual transition from effective matter-domination to the HBB radiation domination, in contrast to the sharp cut-off between the two which is normally assumed in the literature. The radiation bath affecting the formation rate earlier results in a truncation of the mass function of the produced PBHs.

This chapter does not consider the specifics of any particular inflationary model, but simply assumes a quadratic minimum in the scalar field potential, which is typical. This demonstrates the far-reaching consequences the little-understood reheating epoch has on not just models of inflation but cosmological and astrophysical predictions in general.

Chapters 7 and 8 investigate different reheating mechanisms but it is important to stress that the reheating epoch is poorly constrained and open to interpretation. The results presented herein are generic for any model with a period of effective matter domination and a growing sub-dominant thermal bath.

# Chapter 7

## Quintessential Inflation with $\alpha$ -attractors

*This chapter is based on the original research by the author, in collaboration with Konstantinos Dimopoulos, published in the Journal of Cosmology and AstroParticle Physics [170] and Leonora Donaldson Wood, published in Physical Review D [171].*

### 7.1 Introduction

The research in this chapter is the first example, in this thesis, of a model of quintessential inflation. As introduced in Section 2.8, the observed dynamics of the late Universe, namely the current epoch of accelerating expansion, can only be explained within General Relativity (GR) via the introduction of some hypothetical substance called dark energy.  $\Lambda$ CDM, the currently accepted concordance model of cosmology, fits the dark energy (DE) observations remarkably well but suffers from an incredible fine-tuning problem, (see Section 2.8.1) which motivates the search for other explanations for the mechanism of dark energy.

Quintessential inflation (QI) is introduced in Section 2.8.3 and presents a neat alternative to  $\Lambda$ CDM which manages to avoid the fine-tuning problem. QI is a minimal extension to the standard model of particle physics (SM) because it uses

a single theoretical framework to describe both inflation and dark energy, namely a dynamical scalar field. However, as mentioned in Section 2.8.3, building QI models is not easy because of the vast difference in energy densities between primordial inflation and late-time dark energy. The research presented in this chapter manages to generate a scalar field potential of the requisite form by embedding the model in the  $\alpha$ -attractors framework of inflationary model building [56, 109, 110, 119, 120, 172–188]. The use of the  $\alpha$ -attractors for a period of late-time accelerated expansion was investigated in Ref. [189] and we extend this idea to form a model of quintessential inflation.

In Section 7.2 we introduce the  $\alpha$ -attractors framework and present the model. Section 7.3 calculates predictions for the inflationary observables which are in excellent agreement with the Planck 2018 results. As we will see, this is a generic feature of all  $\alpha$ -attractor models. The inflationary observables provide the first constraints on model parameters. Section 7.4 then analyses the regime of kination - present in all QI models, and the eventual freezing of the scalar field, as introduced in Section 2.8.4. We see it is heavily dependent on when radiation domination begins, which is controlled by the reheating mechanism. We proceed to investigate gravitational reheating and instant preheating in Sections 7.6 and 7.8 respectively. Before doing so we remain agnostic as to the reheating mechanism and present an analysis of the late-time quintessence requirements imposed upon the model which provide the tightest constraints on model parameters.

For natural values of the parameters, the model attains accelerated expansion whilst maintaining a mildly sub-Planckian field displacement such that the flatness of the quintessential tail is not lifted by radiative corrections (see Section 2.6.3) and violations of the equivalence principle (see Section 2.8.2) are under control.

## 7.2 The Potential and its Embedding in $\alpha$ -Attractors

The  $\alpha$ -attractors framework, pioneered by Linde and Kallosh [56, 109, 110, 188, 190–192] involves modifying the kinetic term in an otherwise simple inflation

model to the form

$$\mathcal{L}_{\text{kin}} = \frac{\frac{1}{2}\partial_\mu\varphi\partial^\mu\varphi}{\left(1 - \frac{\varphi^2}{6\alpha m_{\text{Pl}}^2}\right)^2}, \quad (7.1)$$

where  $\alpha$  is a dimensionless, positive constant. The kinetic term features poles at  $\varphi = \pm\sqrt{6\alpha}m_{\text{Pl}}$ , which  $\varphi$  cannot traverse in field space [56, 109, 180, 183]. Such a kinetic term is well motivated in supergravity (SUGRA) [56, 109, 180, 183] where a non-trivial Kähler manifold corresponds to a non-canonical kinetic term in the Lagrangian. Returning to canonical variables via a transformation

$$\varphi = \sqrt{6\alpha}m_{\text{Pl}} \tanh\left(\frac{\phi}{\sqrt{6\alpha}m_{\text{Pl}}}\right), \quad (7.2)$$

transposes the poles to infinity and means any scalar field potential present in the theory now takes the form

$$V(\varphi) = V\left[\tanh\left(\frac{\phi}{\sqrt{6\alpha}m_{\text{Pl}}}\right)\right], \quad (7.3)$$

which generates a plateau in the potential. In effect, the canonical potential  $V(\phi)$  is stretched as the non-canonical field,  $\varphi$ , approaches the poles [193]. By adding a simple exponential scalar potential (possibly due to gaugino condensation [194–196]), which naturally features one plateau already, we are able to construct a model of quintessential inflation featuring two plateaus, forming the second from this ‘stretching’ effect of  $\alpha$ -attractors.

The full Lagrangian is

$$\mathcal{L}_{\text{kin}} = \frac{\frac{1}{2}\partial_\mu\varphi\partial^\mu\varphi}{\left(1 - \frac{\varphi^2}{6\alpha m_{\text{Pl}}^2}\right)^2} - V_0 e^{-\kappa\varphi/m_{\text{Pl}}} + \Lambda, \quad (7.4)$$

where  $\kappa$  is a dimensionless, positive constant.  $V_0$  is a constant density scale and  $\Lambda$  is the cosmological constant. Two plateaus exist in the model, with  $V \rightarrow V_0 e^{\pm n}$  where we introduce the notation

$$n \equiv \kappa\sqrt{6\alpha}, \quad (7.5)$$

for ease in subsequent equations. It is necessary to introduce  $\Lambda$  because we presume the vacuum density in the Universe is zero, due to some unknown symmetry. However, because of the second pole in the model,  $\varphi$  cannot go to infinity in the vacuum and is instead capped at the energy density of the second plateau in the model,  $V = V_0 e^{-n}$  as  $\varphi \rightarrow \sqrt{6\alpha} m_{\text{Pl}}$ . To obtain zero vacuum energy density hence requires  $\Lambda = V_0 e^{-n}$ . Substituting this back into Eq. (7.4), the Lagrangian becomes

$$\mathcal{L} = \frac{\frac{1}{2}(\partial\varphi)^2}{\left(1 - \frac{\varphi^2}{6\alpha m_{\text{Pl}}^2}\right)^2} - V_0 e^{-n} \left[ e^{n\left(1 - \frac{\varphi}{\sqrt{6\alpha} m_{\text{Pl}}}\right)} - 1 \right]. \quad (7.6)$$

It is now evident that as  $\frac{\varphi}{m_{\text{Pl}}} \rightarrow \sqrt{6\alpha}$  the potential density disappears. Incorporating a  $\Lambda$  scale might, at first glance, seem to undermine the motivations of quintessence but we will show that our  $\Lambda$  scale is quite natural, motivated by zero vacuum energy density. Therefore it solves the fine-tuning problem of  $\Lambda$ CDM, introduced in Section 2.8.1.1. Incorporating  $\Lambda$  in this way means the plateaus in the model are now altered and the stretching at  $\frac{\varphi}{m_{\text{Pl}}} \rightarrow \pm\sqrt{6\alpha}$  now corresponds to  $V \rightarrow V_0 e^{-n}(e^{2n} - 1)$  or  $V \rightarrow 0$ .

In canonical variables, the scalar potential is

$$V(\phi) = e^{-2n} M^4 \left\{ \exp \left[ n \left( 1 - \tanh \frac{\phi}{\sqrt{6\alpha} m_{\text{Pl}}} \right) \right] - 1 \right\}, \quad (7.7)$$

where we have defined the inflationary energy scale,  $M$ , such that  $M^4 \equiv e^n V_0$ . Note, therefore, that  $\Lambda = e^{-2n} M^4$ .

When we switch from  $\varphi$  to  $\phi$  the poles in the kinetic term are transposed to infinity, meaning  $\phi$  in the canonical Lagrangian is unbounded:  $-\infty < \phi < +\infty$ . The effect of the scalar potential,  $V(\phi)$ , becoming “stretched” as  $\varphi$  approaches the poles allows our new canonical field,  $\phi$ , to take any value whilst our non-canonical degree of freedom,  $\varphi$ , remains sub-Planckian at all times, as long as  $\alpha \lesssim \frac{1}{6}$ . In fact, loop corrections and interactions are both suppressed in the region of the poles in  $\alpha$  attractor theories (this is discussed in more detailed in Section 7.10.1) meaning it is not imperative to maintain  $\varphi < m_{\text{Pl}}$ , but to be conservative and use a natural value for  $\alpha$ , we impose a soft bound of  $\sqrt{6\alpha} < 5$ .

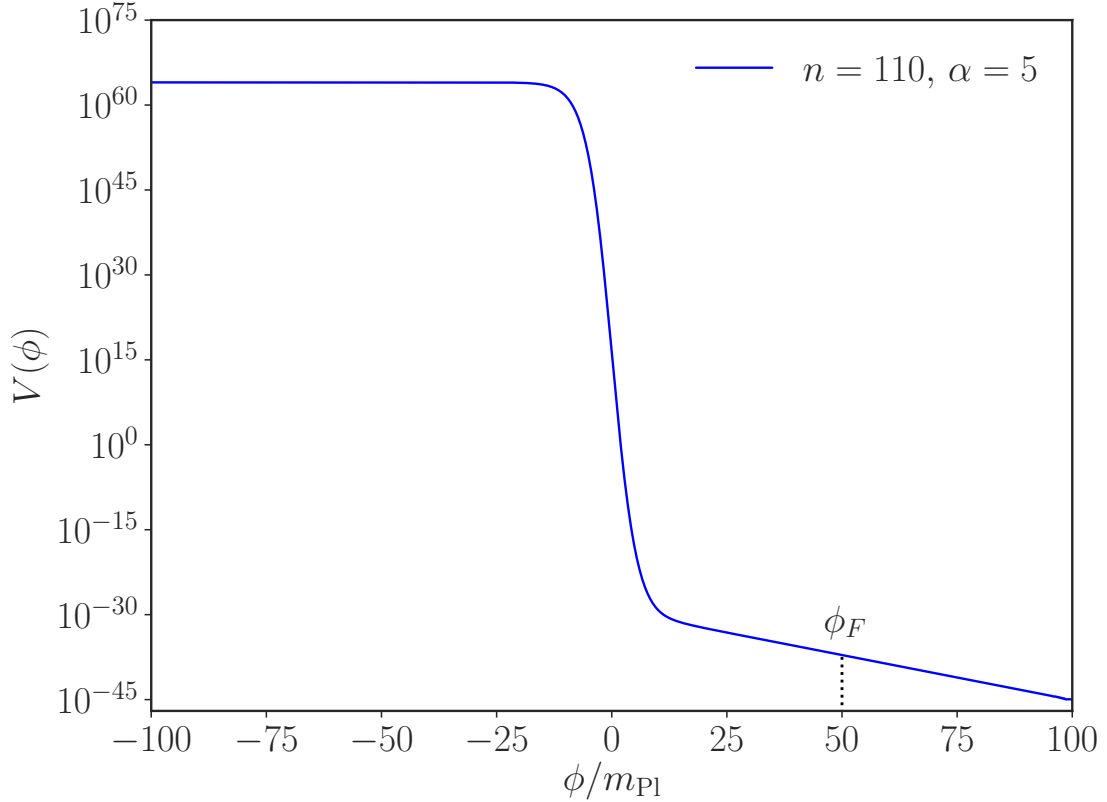


**Figure 7.1:** The potential in Eq. (7.7). It features two flat regions for  $|\phi| \gg \sqrt{6\alpha} m_{\text{Pl}}$ ; the inflationary plateau and the quintessential tail, with a steep dip between them. An example freezing value for the field is indicated by  $\phi_F$ , defined in Eq. (7.33).

As  $\tanh(\phi/\sqrt{6\alpha}m_{\text{Pl}})$  approaches a constant value when  $|\phi|$  is very large, the potential becomes asymptotically constant, featuring plateaus. At the locations of these plateaus the field slow rolls and accelerated expansion occurs. At early times ( $\phi \rightarrow -\infty, \varphi \rightarrow -\sqrt{6\alpha} m_{\text{Pl}}$ ), the potential in Eq. (7.7) can be simplified to

$$V(\phi) \simeq M^4 \exp\left(-2ne^{\frac{2\phi}{\sqrt{6\alpha}m_{\text{Pl}}}}\right), \quad (7.8)$$

which gives rise to the inflationary plateau. In the opposite limit, towards late times ( $\phi \rightarrow +\infty, \varphi \rightarrow +\sqrt{6\alpha} m_{\text{Pl}}$ ), the potential in Eq. (7.7) becomes

$$V \simeq 2ne^{-2n} M^4 \exp(-2\phi/\sqrt{6\alpha} m_{\text{Pl}}), \quad (7.9)$$

which corresponds to the quintessential tail. It is evident that the potential density asymptotes to zero as  $\phi \rightarrow +\infty$ . The potential is shown in Fig. 7.1. In the following sections we examine these two periods and the evolution between them.

### 7.2.1 Initial Conditions

To be a successful quintessential inflation model the initial value of  $\varphi$  needs to be between the poles in the potential. If  $\varphi$  is initially too small ( $\varphi < -\sqrt{6\alpha}$ ) then the field would roll down to  $\varphi = -\sqrt{6\alpha}$  only and the required  $\Lambda$  for zero vacuum density would have been  $\Lambda = V_0 e^{\kappa\sqrt{6\alpha}}$ . In this case, we have inflation with an exponential potential, which is power-law and contradicts observations (plus, it never ends). If  $\varphi$  is initially too large ( $\varphi > \sqrt{6\alpha}$ ) then it would roll down to infinity and the vacuum density would be zero without the introduction of  $\Lambda$ . We would have inflation near the pole but the exponential tail is not steep enough to allow for successful quintessence. We refer the interested reader to Ref. [197].

We do not consider either case and because the initial conditions are not a testable facet of the theory we consider the discussion of them to be largely academic, as per the no-hair theorem.

## 7.3 Inflation

In the limit  $\phi \rightarrow -\infty$  ( $\varphi \rightarrow -\sqrt{6\alpha}$ ), the potential Eq. (7.7) simplifies to the form in Eq. (7.8) and we find the inflationary slow-roll parameters (Eqs. (2.76) and (2.77)) to be

$$\epsilon = \frac{m_{\text{Pl}}^2}{2} \left( \frac{V'}{V} \right)^2 = \frac{4n^2}{3\alpha} e^{\frac{4\phi}{\sqrt{6\alpha}m_{\text{Pl}}}}, \quad (7.10)$$

$$\eta = m_{\text{Pl}}^2 \frac{V''}{V} = -\frac{4n}{3\alpha} e^{\frac{2\phi}{\sqrt{6\alpha}m_{\text{Pl}}}} \left( 1 - 2ne^{\frac{2\phi_*}{\sqrt{6\alpha}m_{\text{Pl}}}} \right), \quad (7.11)$$

where a prime denotes derivative with respect to  $\phi$ . From the usual condition denoting the end of inflation,  $\epsilon = 1$ , we find:

$$\phi_{\text{end}} = \frac{\sqrt{6\alpha}}{2} m_{\text{Pl}} \ln \left( \frac{\sqrt{3\alpha}}{2n} \right). \quad (7.12)$$

The slow roll parameters are better expressed as functions of the number of remaining e-folds of inflation at horizon crossing of cosmological scales,  $N_*$ , defined in Eq. (2.85), through which we obtain:

$$\phi_* = \frac{\sqrt{6\alpha}}{2} m_{\text{Pl}} \ln \left[ \frac{3\alpha}{4n} \left( N_* + \frac{\sqrt{3\alpha}}{2} \right)^{-1} \right], \quad (7.13)$$

which can be negative if  $\alpha$  is small. Using this, the slow-roll parameters become

$$\epsilon = \frac{3\alpha}{4} \left( N_* + \frac{\sqrt{3\alpha}}{2} \right)^{-2}, \quad (7.14)$$

$$\eta = - \left( N_* + \frac{\sqrt{3\alpha}}{2} \right)^{-1} \left[ 1 - \frac{3\alpha}{2} \left( N_* + \frac{\sqrt{3\alpha}}{2} \right)^{-1} \right], \quad (7.15)$$

which are both independent of  $\kappa$ . They only depend on  $N_*$  and  $\alpha$ , which is the recognisable parameter of all  $\alpha$ -attractor theories and controls the size of the region between the poles in non-canonical field space.

We then obtain the tensor-to-scalar ratio and the spectral index of the scalar curvature perturbation:

$$r = 16\epsilon = 12\alpha \left( N_* + \frac{\sqrt{3\alpha}}{2} \right)^{-2}, \quad (7.16)$$

$$n_s = 1 + 2\eta - 6\epsilon = 1 - \frac{2}{\left( N_* + \frac{\sqrt{3\alpha}}{2} \right)} - \frac{3\alpha}{2 \left( N_* + \frac{\sqrt{3\alpha}}{2} \right)^2} \simeq 1 - \frac{2}{N_*}, \quad (7.17)$$

where the last equality in Eq. (7.17) corresponds to small  $\alpha$ . As expected, we

see that  $n_s$  has the same form of all  $\alpha$ -attractors inflationary models. In fact, most plateau inflationary models, like Starobinsky [64, 198] and Higgs [108] inflation, which are favoured by the latest CMB observations [1, 199], make these predictions, including the SUGRA toy model of power-law plateau inflation in Chapter 3.

We also calculate the running of the spectral index which is

$$\begin{aligned} n_s' \equiv \frac{dn_s}{d \ln k} &= -\frac{1}{\left(N_* + \frac{\sqrt{3\alpha}}{2}\right)} \frac{2\left(N_* + \frac{\sqrt{3\alpha}}{2}\right) + 3\alpha}{\left(N_* + \frac{\sqrt{3\alpha}}{2}\right)^2 - 2\left(N_* + \frac{\sqrt{3\alpha}}{2}\right) - \frac{3}{2}\alpha} \\ &\simeq -\frac{2}{N_*^2 - 2N_*}, \end{aligned} \quad (7.18)$$

where again the last equality corresponds to small  $\alpha$ .

As briefly mentioned,  $\alpha$  is the parameter which controls the size of the region between the poles. When  $\alpha \rightarrow 0$  then the region between the poles is shrinking, so it becomes increasingly unlikely that  $\varphi$  initially finds itself there. In the opposite limit,  $\alpha \rightarrow \infty$ , the poles are transposed to infinity and  $\varphi$  becomes canonically normalised. In this latter case, there are no plateaus to consider and we end up with either power-law inflation that never ends, or with no inflation at all (depending on how big  $\kappa$  is in Eq. (7.6)). Barring the extremes  $\alpha = 0$  or  $\alpha \rightarrow \infty$ , the natural value of  $\alpha$  is close to unity. Also, as demonstrated in Fig. 7.2, when  $\alpha \lesssim 0.1$  or so the value of the spectral index gradually becomes insensitive to  $\alpha$  meaning there is no benefit in considering incredibly small (fine-tuned)  $\alpha$  values.

### 7.3.1 Inflationary Energy Scale and e-folding Number

The number of remaining e-folds of inflation when the cosmological scales exit the horizon,  $N_*$ , depends on the expansion history of the Universe, as explained in Section 2.4.4. QI models generally contain a period of kination, where the kinetic energy density of the inflaton is, for a time, the dominant energy density in the Universe and controls its evolution. This model is no exception.

Kination is introduced in Section 2.8.4 (and is investigated for this model in Section 7.4), where we state that the equation of state parameter of the Universe

during a period of kination is  $w = 1$ ; this means the Universe expansion rate is altered compared to a scenario without kination, because the expansion rate in kination behaves as  $a \propto t^{1/3} \propto \rho^{-1/6}$ . This has the effect of increasing the number of inflationary e-folds since the observable scales left the horizon via the terms with pre-factors including  $w$  in Eq. (2.97), repeated here for ease of reference:

$$N_* = 59.7 + \frac{1}{3(1+w)} \ln \left( \frac{g_* \pi^2}{60} \right) + \ln \left( \frac{V_*^{1/4}}{m_{\text{Pl}}} \right) + \ln \left( \frac{V_*^{1/4}}{T_{\text{reh}}} \right) + \frac{4}{3(1+w)} \ln \left( \frac{T_{\text{reh}}}{V_{\text{end}}^{1/4}} \right). \quad (7.19)$$

For a period of kination with  $w = 1$  Eq. (7.19) becomes

$$N_* = 59.9 + \ln \left( \frac{V_*^{1/4}}{m_{\text{Pl}}} \right) + \ln \left( \frac{V_*^{1/4}}{T_{\text{reh}}} \right) + \frac{2}{3} \ln \left( \frac{T_{\text{reh}}}{V_{\text{end}}^{1/4}} \right), \quad (7.20)$$

where we have used  $g_* = 106.75$  and  $V_* \equiv V(\phi_*)$ ,  $V_{\text{end}} \equiv V(\phi_{\text{end}})$  which we find by combining Eqs. (7.12) and (7.13) with Eq. (7.8) as

$$V_* = M^4 \exp \left[ \frac{-3\alpha}{2} \left( N_* + \frac{\sqrt{3\alpha}}{2} \right)^{-1} \right], \quad (7.21)$$

$$V_{\text{end}} = M^4 e^{-\sqrt{3\alpha}}. \quad (7.22)$$

The energy scale of inflation can be calculated from the COBE constraint, introduced in Section 2.4.5 as

$$\sqrt{A_s} = \frac{1}{2\sqrt{3\pi}} \frac{V^{3/2}}{m_{\text{Pl}}^3 |V'|}, \quad (7.23)$$

where  $A_s = (2.101_{-0.034}^{+0.031}) \times 10^{-9}$ , is the amplitude of the scalar curvature perturbation.

bation [1]. Using Eq. (7.8) and Eq. (7.13) we find:

$$\left(\frac{M}{m_{\text{Pl}}}\right)^2 = 3\pi\sqrt{2\alpha A_s} \left(N_* + \frac{\sqrt{3\alpha}}{2}\right)^{-1} \exp\left[\frac{3\alpha}{4} \left(N_* + \frac{\sqrt{3\alpha}}{2}\right)^{-1}\right]. \quad (7.24)$$

We can hence find  $N_*$  for a particular value of  $\alpha$  by solving Eqs. (7.20) and (7.24) iteratively. This requires knowledge of the reheating temperature,  $T_{\text{reh}}$ . As mentioned in Section 2.7.5, there are constraints on the reheating temperature arising from reheating having completed before BBN, from the overproduction of gravitinos (if the model is embedded in supergravity) and from the spike in gravitational waves produced from a prolonged period of kination. There are also specific constraints such as the size of coupling constants and the effect of backreaction, depending on the mechanism of reheating. These are addressed in detail in subsequent sections of this chapter.

Initially we use two extremal values of  $T_{\text{reh}} = 10^4(10^{14})$  GeV to obtain  $N_* \simeq 63(56)$  for  $\alpha = 1$ . Particular values of  $M$  for various  $\alpha$  values are shown in Table 7.1 for  $N_* = 55$  and  $N_* = 65$ . Final e-folding numbers for each  $\alpha$  are solved iteratively once the reheating temperature has been fully analysed in subsequent sections. Eq. (7.24) shows that  $M$  is independent of  $n$  and, as expected, is near the scale of grand unification  $\approx 10^{16}$  GeV.

$N_*$	$\alpha$	$M(\text{GeV})$
55	0.01	$2.56 \times 10^{15}$
	0.10	$4.55 \times 10^{15}$
	1	$8.09 \times 10^{15}$
	10	$1.50 \times 10^{16}$
	100	$4.29 \times 10^{16}$
65	0.01	$2.35 \times 10^{15}$
	0.10	$4.18 \times 10^{15}$
	1	$7.44 \times 10^{15}$
	10	$1.37 \times 10^{16}$
	100	$3.68 \times 10^{16}$

**Table 7.1:** Values of  $M$  calculated from Eq. (7.24) for various  $\alpha$  values.

### 7.3.2 Parameter Space from Observational Constraints

The constraint on the tensor-to-scalar ratio from observations by the Planck satellite [1],  $r < 0.07$ , allows us to constrain the allowed values of  $\alpha$ :

$$120\alpha < \left(N_* + \frac{\sqrt{3\alpha}}{2}\right)^2. \quad (7.25)$$

Taking  $N_* = 65$  as an upper bound results in a bound of  $\alpha \leq 28$ . Currently we have no lower bound on  $r$  and hence no lower bound on  $\alpha$ , but (as shown later) it should not get too small. Requiring the mass scale which suppresses the non-canonical  $\varphi$  in the kinetic term not to be too small compared to  $M$ , we have  $\sqrt{6\alpha} m_{\text{Pl}} \gtrsim M$ , which results in  $\alpha \gtrsim 10^{-7}$ . However, as mentioned previously the spectral index becomes insensitive to  $\alpha$  much below 0.1.

The corresponding bounds on  $n_s$  are

$$0.9626 \lesssim n_s \leq 0.9692, \quad (7.26)$$

and are well contained within the Planck bounds. Fig. 7.2 shows the parameter space for  $n_s$  and  $r$  in our model using the range  $10^{-7} \leq \alpha \leq 28$ . However, because of the field redefinition in Eq. (7.2), to avoid super-Planckian values of  $\varphi$  we impose  $\alpha \simeq \mathcal{O}(1)$  which places us firmly within the constraints of the tensor-to-scalar ratio.

At this point we must highlight a quirk in the behaviour of  $\alpha$ . It turns out that as  $\alpha$  goes to small values, the  $r - n_s$  line curves back on itself, which can be seen in Fig. 7.2 (and in more detail in Fig. 7.7) and once noticed, is immediately evident in the form of Eq. (7.17). This means that the maximum value of  $n_s$  is not obtained for either of the extremes of the allowed  $\alpha$  values. Instead, using  $\frac{dn_s}{d\alpha} = 0$  we find the maximum  $n_s$  value is obtained for

$$\alpha = \frac{N_*^2}{3(N_* - 0.5)^2}, \quad (7.27)$$

which for both  $N_* = 55$  and  $N_* = 65$  gives  $\alpha \simeq 0.34$ . Using  $\alpha = 0.34$  as the

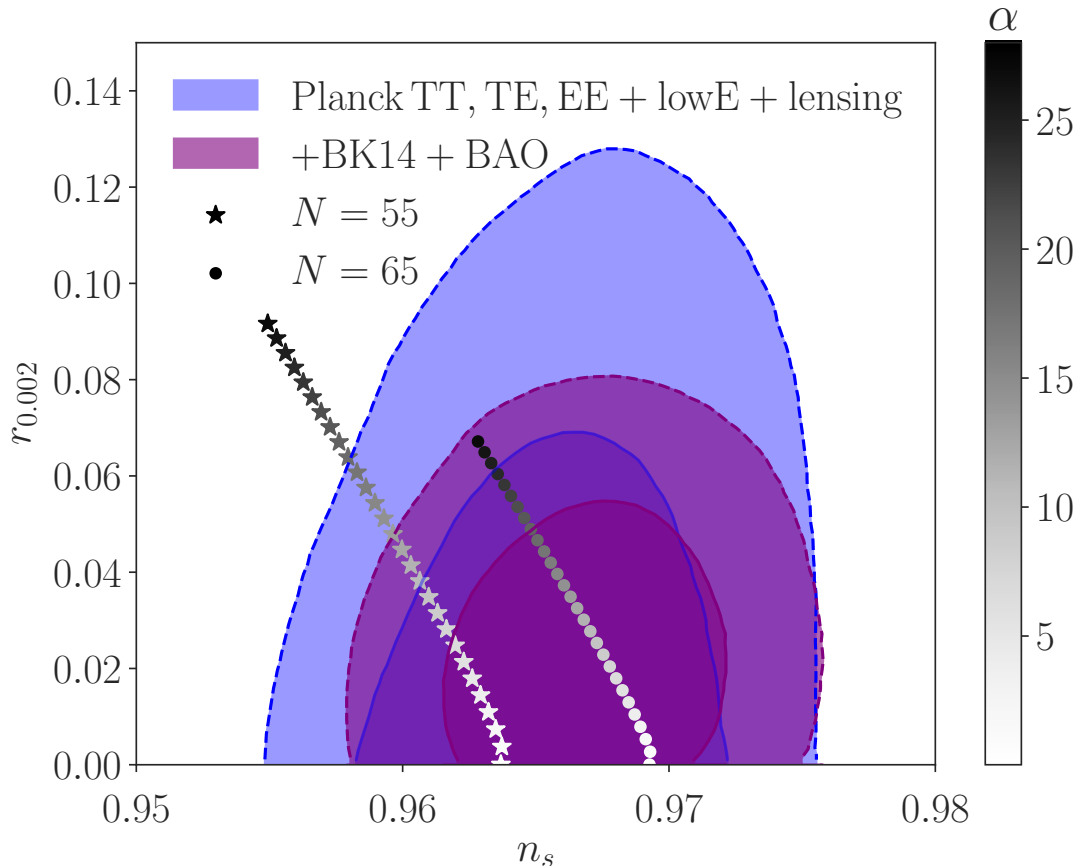


**Figure 7.2:** The tensor-to-scalar ratio,  $r$ , versus the spectral index,  $n_s$  for our model is displayed overlaying the Planck 2018 results.  $\alpha$  varies from 0 to 28 according to the colour map on the right, stars represent  $N = 55$  and circles represent  $N = 65$ . The slope of the line for large values of  $\alpha$  is understood as  $n_s \rightarrow 0$  when  $\alpha \gg 1$  (cf. Eq. (7.17)). Note that the line corresponding to the values of  $n_s$  and  $r$  curves back on itself for small  $\alpha$  (values of  $\alpha \lesssim 0.1$  or so) so that the spectral index becomes insensitive to  $\alpha$  when it is small. This region is shown in more detail in Fig. 7.7.

upper bound and maintaining  $10^{-7}$  as the lower, for a single value of  $N_*$ ,  $n_s$  is almost constant, as noted previously. So instead we present the final parameter space for  $n_s$  with these initial constraints using the range  $55 \leq N_* \leq 65$  as

$$0.9636 \lesssim n_s \leq 0.9693, \quad (7.28)$$

which corresponds to a line joining the very lowest data points in Fig. 7.2, well inside the Planck  $1\sigma$  contour.

Inflation ends when the potential is no longer flat enough for the kinetic energy of the inflaton to be suppressed compared to its potential energy. This occurs at the edge of the inflationary plateau when the scalar field potential has a sharp, steep drop down to the quintessence plateau, shown in Fig. 7.1. For a time the energy density of the scalar field is dominated by its new-found kinetic energy but at some point this runs out and the field effectively freezes in field space. We now investigate this period of evolution.

## 7.4 Freezing of the Scalar Field

As we know, after inflation there is a period of kination before reheating completes and radiation domination ensues. This is a non-oscillatory model of inflation, so reheating must occur without the decay of the inflaton field which is required to survive until the present and become quintessence. Since the inflaton is not oscillating after inflation, reheating of the Universe cannot occur through the perturbative decay of the inflaton field. Alternative options for reheating are introduced in Section 2.7 and in this chapter we utilise gravitational reheating and instant preheating.

Soon after inflation ends, the inflaton energy density is completely dominated by the kinetic part. As introduced in Section 2.8.4, this allows the KG equation, which governs the evolution of the scalar field, to be simplified by omitting the potential term. The EoM and its solutions are shown in Eqs. (2.229) to (2.231). When reheating completes, kination necessarily ends but the field is still dominated by its kinetic energy for some time. Solutions to the EoM in a radiation background are given in Eqs. (2.232) and (2.233) where  $\phi_F$  is introduced, which is the value of the field when its motion in field space freezes.

The value of  $\phi_F$  depends on the efficiency of reheating. We can define the radiation density parameter as

$$\Omega_r \equiv \rho_r / \rho. \quad (7.29)$$

Gravitational reheating represents the lowest possible value of the radiation density parameter at the end of inflation which can, in principle, approach unity. Thus, in general we have

$$(\Omega_r^{\text{end}})_{\text{gr}} \lesssim \Omega_r^{\text{end}} \lesssim 1. \quad (7.30)$$

During kination  $\rho = \rho_{\text{kin}} \equiv \frac{1}{2}\dot{\phi}^2 \propto a^{-6}$  but radiation density scales as  $\rho_r \propto a^{-4}$ . This means that once the thermal bath is created, it will eventually take over, but furthermore, the density parameter of radiation scales as  $\Omega_r \propto a^2$  during kination. Relating this to  $t$  (see Section 2.2.3) we find

$$\Omega_r^{\text{end}} = \Omega_r^{\text{reh}} \left( \frac{a_{\text{end}}}{a_{\text{reh}}} \right)^2 = \left( \frac{t_{\text{end}}}{t_{\text{reh}}} \right)^{\frac{2}{3}}, \quad (7.31)$$

which when inserted into the EoM solution during kination (Eq. (2.231)) provides the field value at reheating

$$\phi_{\text{reh}} = \phi_{\text{end}} - \sqrt{\frac{3}{2}} m_{\text{Pl}} \ln \Omega_r^{\text{end}}. \quad (7.32)$$

The EoM solution during radiation domination, Eq. (2.233), takes  $\phi_{\text{reh}}$  as an initial condition, so inputting Eq. (7.32) shows the field eventually freezes (for  $t \gg t_{\text{reh}}$ ) at the value

$$\phi_F = \phi_{\text{end}} + \sqrt{\frac{2}{3}} m_{\text{Pl}} \left( 1 - \frac{3}{2} \ln \Omega_r^{\text{end}} \right). \quad (7.33)$$

For instant preheating, in contrast to gravitational reheating, the thermal bath is not produced immediately when inflation ends. Instead it is produced when the field crosses an enhanced symmetry point, so we cannot define the radiation density parameter,  $\Omega_r$ , until this time. The instant preheating mechanism is introduced in Section 2.7.3 and is investigated in detail for this model in Section 7.8, but we define the moment of radiation production as  $t_{\text{IP}}$ , at the field value  $\phi_{\text{IP}} \equiv \phi(t_{\text{IP}})$ . Solving the EoM for  $\phi_F$  is then the same procedure as for gravitational reheating with  $\phi_{\text{end}} \rightarrow \phi_{\text{IP}}$  in Eq. (7.33).

It should be stressed here that these results are model independent because

whilst  $\phi$  is kinetically dominated it is oblivious of the potential<sup>1</sup>. We include the equations here for ease of reference and to facilitate the discussion of the variation in the point at which the thermal bath is created in the two reheating mechanisms and our ability to distinguish it. The physics is the same, independent of the model parameters and the evolution of  $\rho_\phi$  is shown in Fig. 2.7.

From Eq. (7.33), we see that to maximise the value of  $\phi_F$ , in order to achieve a low residual potential density, we have to consider the minimum possible value of  $\Omega_r$  at  $t_{\text{end}}$  ( $t_{\text{IP}}$ ) for gravitational reheating (instant preheating).

As suggested by Eq. (7.30), gravitational reheating can provide a much smaller value for  $\Omega_r$  (at the instant of its creation) than instant preheating. Gravitational reheating ensures the field retains enough kinetic density to roll to a low potential density, to align with observations of dark energy today. It also promotes economy in the model because it avoids introducing any additional scalar fields which would be required for other reheating mechanisms. However, the trade-off of such an economical approach is that the notoriously low reheating temperature of gravitational reheating ( $T_{\text{reh}} \approx 10^6$  GeV) produces a spike in gravitational waves at low frequencies, which could interfere with BBN (see Section 2.8.4.1). For this reason, we also investigate instant preheating which is much more efficient and avoids this problem.

However, before investigating reheating we investigate the constraints on  $\alpha$  arising from the quintessence epoch. It is  $\alpha$  which controls the steepness of the quintessential tail and ultimately, whether quintessence is successfully achieved, therefore there are further constraints on the values  $\alpha$  can take than those examined in Section 7.3.2.

---

<sup>1</sup>Of course, just before freezing we have  $\rho_{\text{kin}} \lesssim V$ . However, the subsequent variation of  $\phi$  is exponentially suppressed, so  $\phi \simeq \phi_F = \text{constant}$ .

## 7.5 Quintessence

As noted in Eq. (7.9) but repeated again here for ease of reference, in the limit  $\phi \rightarrow +\infty$  ( $\varphi \rightarrow \sqrt{6\alpha}m_{\text{Pl}}$ ), the potential simplifies to

$$V \simeq 2ne^{-2n}M^4 e^{-\frac{2\phi}{\sqrt{6\alpha}m_{\text{Pl}}}}, \quad (7.34)$$

which is a representation of the standard exponential quintessential tail, which is written as

$$V = V_Q \exp(-\lambda\phi/m_{\text{Pl}}), \quad (7.35)$$

where

$$V_Q = 2ne^{-2n}M^4, \quad (7.36)$$

and

$$\lambda = \frac{2}{\sqrt{6\alpha}} \equiv \frac{2\kappa}{n}. \quad (7.37)$$

The parameter  $n$  controls the energy density of the quintessence plateau. Enforcing the requirement that the energy density of quintessence,  $V(\phi_F)$ , must be comparable with the energy density of the Universe at present,  $\rho_0$ , (coincidence requirement) gives

$$\frac{\rho_{\text{inf}}}{\rho_0} \simeq \frac{V_{\text{inf}}}{V_F} \simeq \frac{e^{\lambda\phi_F/m_{\text{Pl}}}}{2ne^{-2n}} \sim 10^{108}, \quad (7.38)$$

where we used  $V_{\text{inf}} = (1 - e^{-2n})M^4 \simeq M^4 \sim (10^{15} \text{ GeV})^4$  (we will find  $n \gg 1$ ),  $\rho_0 \sim 10^{-48} \text{ GeV}^4$  and  $V_F = V_Q \exp(-\lambda\phi_F/m_{\text{Pl}})$ , where  $\phi_F$  is the point in field space at which the inflaton freezes when it runs out of kinetic energy, defined in Eq. (7.33). In order to achieve a low residual potential density it is beneficial to maximise  $\phi_F$  but this depends on the particulars of reheating and so we keep  $\phi_F$  as a free parameter for now.

Eq. (7.38) rearranges to

$$2n - \ln(2n) \simeq 108 \ln 10 - \frac{2}{\sqrt{6\alpha}} \frac{\phi_F}{m_{\text{Pl}}}, \quad (7.39)$$

where we used  $\lambda = 2/\sqrt{6\alpha}$ . For an allowed range of  $\alpha$  values we can now calculate

the allowed  $n$  range for a given  $\phi_F$  (after a detailed investigation of reheating).

At late-times the field unfreezes and follows an attractor solution to the KG equation, detailed in Section 2.8.5. Depending on the slope of the quintessential tail, controlled by  $\lambda$  the energy density of the field will either be dominant or sub-dominant to the background. For successful quintessence we require the scalar field to dominate the energy budget of the Universe whilst slow-rolling, meaning it must follow the dominant attractor solution, Eq. (2.252) meaning  $\lambda < \sqrt{3}$ . However, as noted in Section 2.8.5, when the field unfreezes it briefly oscillates about the attractor before settling to it.

This brief oscillation of the field could result in a bout of transient accelerated expansion for the sub-dominant attractor, if the field oscillates above the background for a time [104, 200–203]. This is an exciting possibility because transient accelerated expansion has a clear merit over eternal accelerated expansion, as in  $\Lambda$ CDM. Section 2.8.1.2 introduces the future horizons problem of string theory, which is unavoidable in eternal accelerated expansion. This may be just a problem of string theory and not a no-go theorem of nature but it is still very attractive to consider models which avoid eternal acceleration if possible. The next section investigates the particular late time dynamics of this model to see if a period of transient accelerated expansion is possible during the oscillation of  $\rho_\phi$  above the background energy density. We also point out that future states may be well defined in QI models where the eventual value of the vacuum density is zero, because the future event horizon increases to infinity. Therefore, the future horizon problem is overcome even without a period of transient accelerated expansion.

To explore the late Universe dynamics of the model we assume the Universe can be described by an FLRW metric, that the effects of  $\rho_r$  are negligible and that  $\rho_\Lambda = 0$ . Therefore, the content of the Universe is modelled as two perfect fluid components; the scalar field  $\phi$ , and a non-relativistic background matter fluid, denoted by subscript ‘ $m$ ’. We use the evolution equations detailed in Section 2.2.2 with the addition of our scalar field,  $\phi$ , to numerically explore the cosmological dynamics of the quintessence model for all cosmological parameters. We use the Planck 2015 observations to constrain the range of  $\lambda$  for which any current transient or eternal accelerated expansion is present.

### 7.5.1 Observational Constraints on Quintessence

The 2015 Planck observations [204] suggest that the density parameter of dark energy is  $\Omega_{\text{DE}} = 1 - \Omega_{\text{K}} - \Omega_m$ , where  $\Omega_{\text{K}} = 0.000 \pm 0.005$ , and  $\Omega_m = 0.308 \pm 0.012$ . This results in  $\Omega_{\text{DE}} = 0.692 \pm 0.017$ .

As  $w_\phi$  is time-varying, we model a Taylor expansion of  $w_\phi$  to first order

$$w_\phi = w_{\text{DE}} + \left(1 - \frac{a}{a_0}\right) w_a, \quad (7.40)$$

where  $w_a = -(dw_\phi/da)_0$ , the subscript ‘0’ denotes values today, when  $a = a_0$  and  $w_\phi(a_0) = w_{\text{DE}}$ . We use the Planck bounds [204] of  $w_{\text{DE}} = -1.023^{+0.091}_{-0.096}$  at  $2\sigma$  in our constraint on possible ranges of values for  $\lambda$ . This translates to  $w_0 = -0.7112 \pm 0.0821$ , where  $w_0$  is the barotropic parameter of the Universe at present,  $w_0 = (p_\phi/\rho)_0$ .

Demanding that our model satisfies these observational requirements, the Universe today has to lie within the range  $(\rho_\phi/\rho_m)_0 = \Omega_{\text{DE}}/\Omega_m = 2.2523 \pm 0.1429$ . We start with the frozen field, where  $\dot{\phi}_F = 0$  and  $(\rho_\phi/\rho_m)_F \ll 1$  and investigate any current eternal or transient accelerated expansion found.

Only a change in the value of  $\lambda$  affects the evolution of our model once the field is unfrozen. A relative decrease (increase) in the value of  $\rho_\phi^F = V(\phi_F)$ , for a given  $\rho_m^F$ , only increases (decreases) the evolution time of the model until  $a_0$  today, i.e. the model is extended backwards (forwards) to an earlier (later) time when  $\phi$  is frozen. Similarly, any change in the value of  $\phi_F$  can be expressed as a change in  $V_Q$  and so, for a given value of  $\lambda$ , also has no effect on the dynamics. Conversely, since  $\Omega_{\text{DE}}$  is fixed by observations, changes in  $\phi_F$  without a change in  $V_Q$  must instead be accompanied with corresponding changes in  $\lambda$ , such that the contribution of quintessence to the density budget at present remains fixed.

#### 7.5.1.1 Transient Accelerated Expansion

For brief periods of transient accelerated expansion with  $w < -1/3$ , we find a range of numerically valid  $\lambda$  values bridging the dominant and subdominant

quintessence regimes

$$\sqrt{2} \leq \lambda < \sqrt{3.38}. \quad (7.41)$$

However, the values for  $w$  that we find in this scenario are incompatible with the Planck constraints for the entire range of  $\lambda$  values above. As the minimum value of  $w$  reached during any period of evolution increases with increasing  $\lambda$ , we only need to look at  $\lambda = \sqrt{2}$  to illustrate our findings. This is shown in Fig. 7.3, where we use  $\lambda = \sqrt{2}$ . It can be clearly seen that the minimum value of  $w$  is not nearly small enough to match the Planck observational bounds, and so all higher values of  $\lambda$  are also ruled out. Fig. 7.3 also highlights the requirement  $\lambda < \sqrt{2}$  for eternal accelerated expansion from Eq. (2.251), as we can clearly see  $w = -1/3$  in the attractor limit where  $\lambda = \sqrt{2}$ . We can also see  $w_\phi$  moving toward the same value because we are in the dominant quintessence regime.

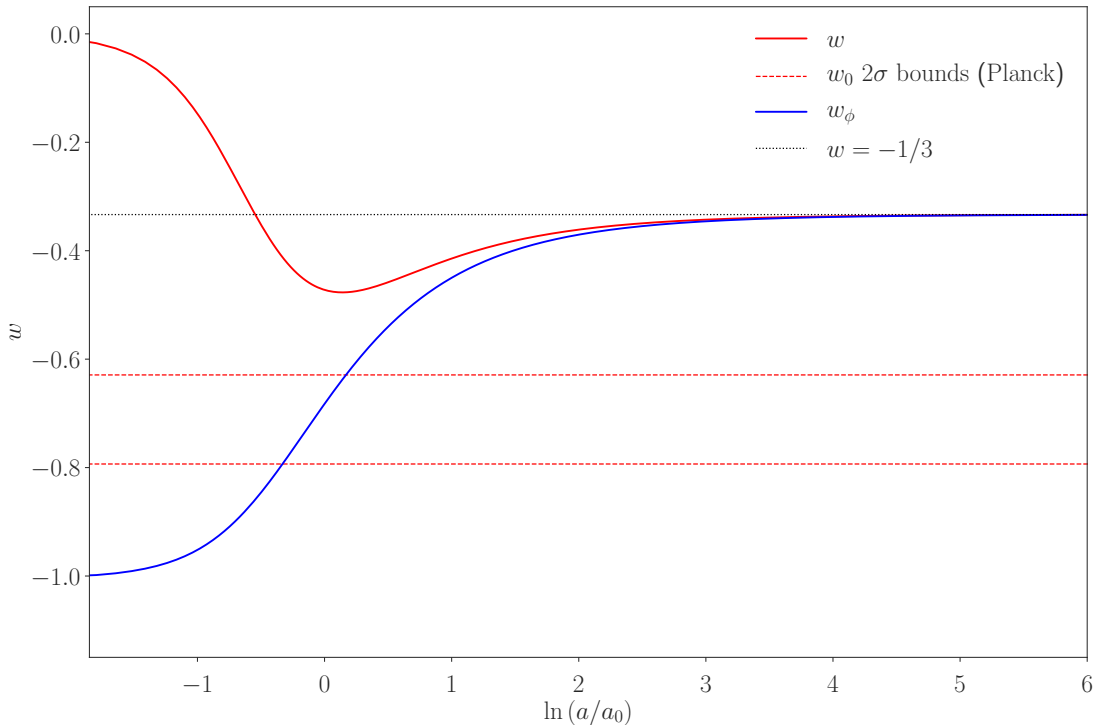


**Figure 7.3:** Transient accelerated expansion for  $\lambda = \sqrt{2}$ . We find  $w < -1/3$ , but the minimum value of  $w$  is well outside of the Planck bounds.

### 7.5.1.2 Eternal Accelerated Expansion

We know theoretically that  $w < -1/3$  for  $\lambda < \sqrt{2}$ . Applying the Planck constraints we find the cosmologically viable range is reduced to  $\lambda < \sqrt{0.46}$ . We find that, in all cases, the scalar field at present has unfrozen but is yet to settle on the attractor solution. This is illustrated in Fig. 7.4 for  $\lambda = \sqrt{0.4}$ . It can also clearly be seen that the present day values at  $\ln(a/a_0) = 0$  are within the Planck bounds. We find that it is the bound for  $w_{\text{DE}} = -1.023_{-0.096}^{+0.091}$  that constrains our possible range of values to  $\lambda < \sqrt{0.46}$  (rather than the  $w_0$  bound), which can be seen in Fig. 7.4, where the value of  $w_{\text{DE}}$  is closer to the upper Planck bound for  $w_{\text{DE}}$  compared to the value for  $w_0$ , which is further within the upper Planck bound for  $w_0$ . When increasing  $\lambda$ , we find that  $w_{\text{DE}}$  exits the upper Planck bound for  $w_{\text{DE}}$  before  $w_0$  exits the upper Planck bound for  $w_0$ . If we ignore this constraint and just demand that  $w_0 = -0.7112 \pm 0.0821$  today, then our range of possible values for  $\lambda$  extends to  $\lambda < \sqrt{0.68}$ . Using our Taylor expansion of  $w_\phi$  to first order,

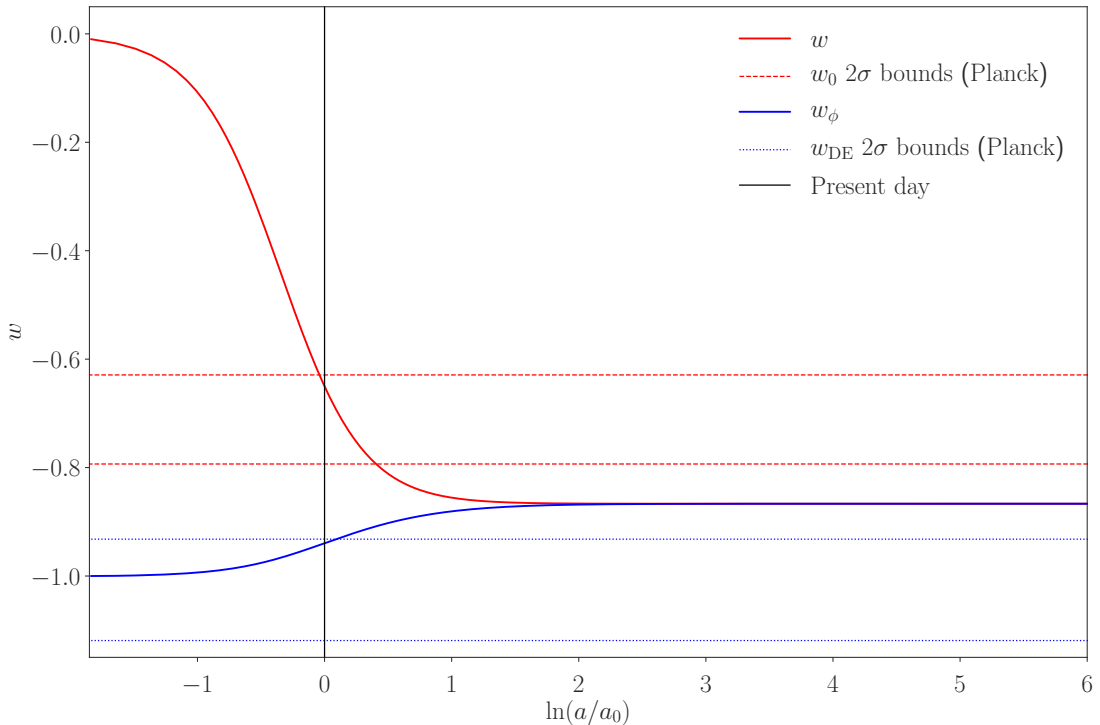


**Figure 7.4:** Eternal accelerated expansion for  $\lambda = \sqrt{0.4}$ . The scalar field has unfrozen, but is yet to settle on the attractor solution.

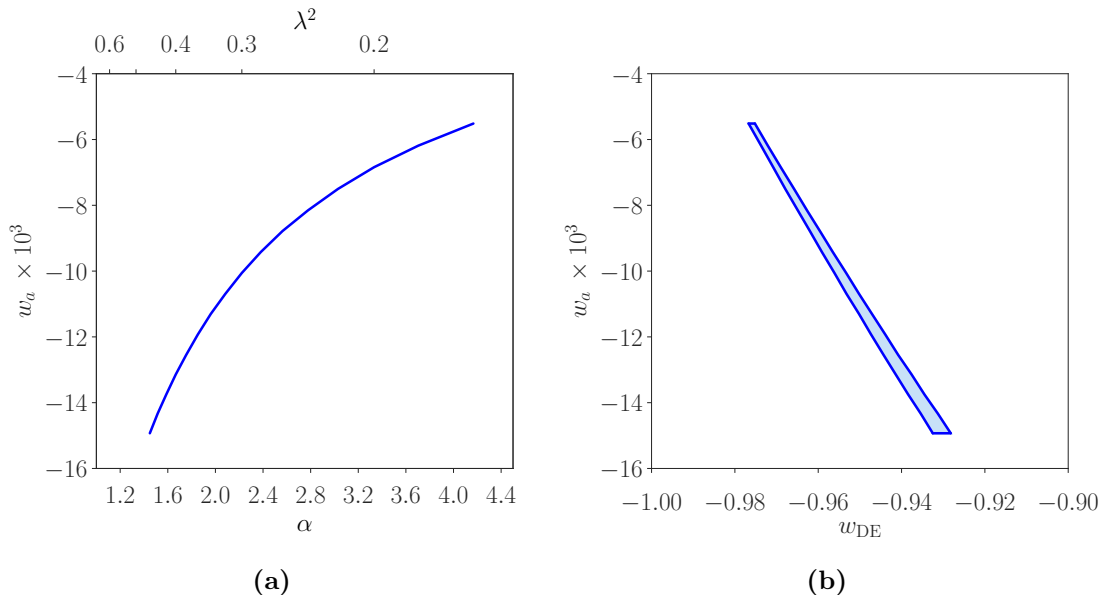


**Figure 7.5:** Time dependence of  $w_\phi$  as modelled by the Taylor expansion in Eq. (7.40). The allowed parameter space depicted lies well within the  $1\sigma$  Planck contour for  $\lambda^2 < 0.46 \Leftrightarrow \alpha > 1.45$ .

(cf. Eq. (7.40)), we obtain a range of values for  $|w_a|$  that are of  $\mathcal{O}(10^{-2}) - \mathcal{O}(10^{-3})$ . These values easily lie within current Planck bounds [204], but can be potentially observable in the near future, e.g. by EUCLID. This is illustrated in Figs. 7.5a and 7.5b.

The results so far only constrain  $\lambda$ , and are therefore valid for any exponential quintessence model. We now apply our findings to the  $\alpha$ -attractors QI model. We convert from  $\lambda$  to  $\alpha$  using  $\alpha = 2/3\lambda^2$  (cf. Eq. (7.9)), and restate all our findings in terms of  $\alpha$ . This upper bound on  $\lambda$  results in only a lower bound on  $\alpha$ . We can obtain an upper bound on  $\alpha$  by avoiding super-Planckian values for the non-canonical field,  $\varphi$ . The motivation for this is to suppress radiative corrections and the 5th-force problem, which plague quintessence models, as mentioned in Sections 2.6.2 and 2.8.2. However, the bound is soft, as both loop corrections and interactions are suppressed near the poles of  $\alpha$ -attractor theories [187, 193] as we discuss in Section 7.10.1. Still, being conservative, we choose to avoid a super-Planckian non-canonical inflation field. Therefore, the relevant range for  $\alpha$

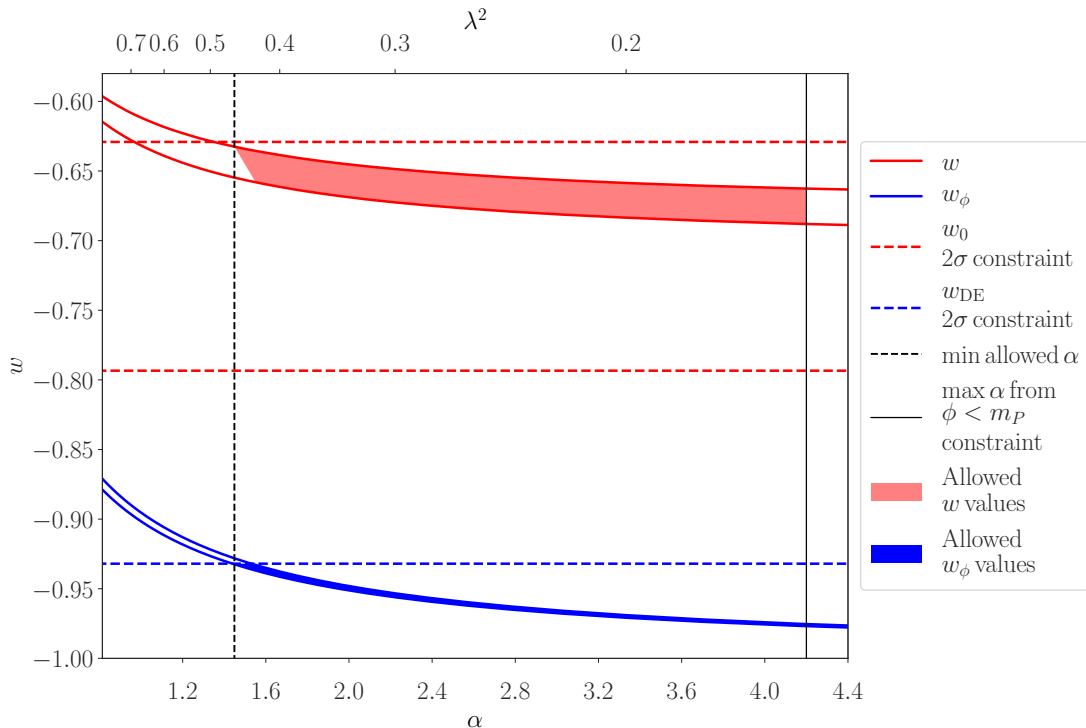


**Figure 7.6:** Possible range of values for  $\alpha$  and  $\lambda^2$ , from the Planck constraints on  $w$ . It is shown that the  $2\sigma$  upper bound on  $w_{DE}$  is satisfied only for  $\lambda^2 < 0.46$  or equivalently  $\alpha = 2/3\lambda^2 > 1.45$ . The allowed ranges of  $w$  and  $w_\phi$  reflect the observed range in  $\Omega_{DE}/\Omega_m$ . Values in the text are quoted to 2 s.f.

is the following:

$$3 \lesssim \sqrt{6\alpha} \lesssim 5 \quad \Leftrightarrow \quad 1.5 \leq \alpha \leq 4.2. \quad (7.42)$$

These results are plotted in Fig. 7.6, which is labelled in terms of  $\lambda^2$  and  $\alpha$  for comparison. Armed with our allowed  $\alpha$  range we can now investigate the reheating epoch to determine  $\phi_F$  and hence (finally) the constraints on the model parameter,  $n$ .

## 7.6 Gravitational Reheating

In the interests of keeping the model minimal and avoiding the introduction of extra degrees of freedom we first consider gravitational reheating, detailed in

Section 2.7.4, for which the radiation density is

$$\rho_r^{\text{gr}} = \frac{q g_*}{480\pi^2} H^4, \quad (7.43)$$

where  $g_*$  is the number of effective relativistic degrees of freedom,  $q \sim 1$  is an efficiency factor and the produced thermal bath is at the Hawking temperature of de Sitter space,  $T = H/2\pi$ .

Reheating is defined as the moment radiation domination begins, so  $\rho_r^{\text{reh}} = \rho_\phi^{\text{reh}}$ . During kination the energy density of the scalar field scales as  $\rho_\phi \propto a^{-6}$  so we can write  $\rho_\phi^{\text{reh}} = \rho_\phi^{\text{end}} \left(\frac{a_{\text{end}}}{a_{\text{reh}}}\right)^6$ . From Eq. (7.31) we see that  $\left(\frac{a_{\text{end}}}{a_{\text{reh}}}\right)^2 = \Omega_r^{\text{end}}$  because  $\Omega_r^{\text{reh}} = 1$  by definition. This results in

$$\rho_r^{\text{reh}} = \rho_\phi^{\text{end}} (\Omega_r^{\text{end}})^3, \quad (7.44)$$

and using this in Eq. (7.43) shows the reheating temperature is

$$T_{\text{reh}} = \left[ \frac{30}{q\pi^2 g_*^{\text{reh}}} (\Omega_r^{\text{end}})^3 \rho_\phi^{\text{end}} \right]^{1/4}. \quad (7.45)$$

In view of Eq. (7.43), the density parameter of radiation for gravitational reheating at the end of inflation is

$$(\Omega_r^{\text{end}})_{\text{gr}} \equiv \frac{\rho_r^{\text{gr}}}{\rho} \Big|_{\text{end}} = \frac{q g_*^{\text{end}}}{1440\pi^2} \left( \frac{H_{\text{end}}}{m_{\text{Pl}}} \right)^2. \quad (7.46)$$

Combining this with Eqs. (7.30) and (7.45), we find

$$T_{\text{reh}} \geq \frac{\sqrt{q}}{\pi^2} \left( \frac{15}{2g_*^{\text{reh}}} \left( \frac{g_*^{\text{end}}}{1080} \right)^3 \right)^{1/4} \frac{V_{\text{end}}}{m_{\text{Pl}}^3}, \quad (7.47)$$

where the equality corresponds to gravitational reheating. Taking  $g_*^{\text{end}} = \mathcal{O}(10^5)$  and  $g_*^{\text{reh}} = 106.75$ , we find  $T_{\text{reh}} \gtrsim \frac{V_{\text{end}}}{m_{\text{Pl}}^3} \simeq 10^6$  GeV, which is safely much higher than the temperature at BBN.

Now that we have a value for  $\Omega_r^{\text{end}}$  we are able to find  $\phi_F$  from Eq. (7.33),

which in turn allows us to find the constraints on  $n$  from Eq. (7.39). This is done iteratively because  $\Omega_r^{\text{end}}$  is a function of  $N_*$  via  $M$  in  $V_{\text{end}}$ , which itself depends on  $\Omega_r^{\text{end}}$  through  $T_{\text{reh}}$ . As a first approximation we equate  $V_{\text{end}} \simeq V_*$  and see from Eq. (7.20) that

$$N_* \simeq 59.9 + \ln \left( \frac{V_{\text{end}}^{1/4}}{m_{\text{Pl}}} \right) - \frac{1}{3} \ln \left( \frac{T_{\text{reh}}}{V_{\text{end}}^{1/4}} \right). \quad (7.48)$$

It turns out that for gravitational reheating

$$\left( \frac{T_{\text{reh}}}{V_{\text{end}}^{1/4}} \right)^{1/3} \propto \left( \frac{V_{\text{end}}^{1/4}}{m_{\text{Pl}}} \right), \quad (7.49)$$

leaving a constant value for  $N_*$  of 61.5. Reinstating  $V_*$  and iterating fully we find

$$62.54 \leq N_* \leq 63.23, \quad (7.50)$$

for the values of  $\alpha$  given in Eq. (7.42).

Hence, when gravitational reheating is the mechanism responsible for producing the thermal bath of the hot big bang, for the range  $1.5 \leq \alpha \leq 4.2$  we find a range of values for  $\phi_F$  and  $n$ :

$$45.6 \leq \frac{\phi_F}{m_{\text{Pl}}} \leq 52.3, \quad (7.51)$$

$$108 \leq n \leq 115. \quad (7.52)$$

These two parameters are inextricably linked in the model.  $\alpha$  controls the slope of the quintessential tail, so different  $\alpha$  values allow the field to traverse different distances in field space. To ensure the energy density of the field matches observations of dark energy, the  $n$  parameter which controls the height of the plateau is constrained.

For comparison, and also for reference in the next section, the corresponding field values at the end of inflation are

$$7.1 \leq \frac{\phi_{\text{end}}}{m_{\text{Pl}}} \leq 13.4. \quad (7.53)$$

Using the values in Eq. (7.52), since  $\kappa \equiv n/\sqrt{6\alpha}$ , we readily obtain

$$23 \lesssim \kappa \leq 36. \quad (7.54)$$

Thus, because  $\kappa \approx 30$ , the non-canonical  $\varphi$  in the exponent of the scalar potential in Eq. (7.1) is suppressed by the mass-scale  $m_{\text{Pl}}/\kappa \simeq 8 \times 10^{16} \text{ GeV} \sim M$ .

In view of the above range, we also obtain  $V_0^{1/4} = e^{-n/4}M = 10^{3-4} \text{ GeV}$ , which is the electroweak energy scale. We also find that the scale of the cosmological constant is  $\Lambda^{1/4} = e^{-n/2}M \sim 10^{-5} \text{ GeV}$  which is much larger than the value of  $\simeq 10^{-3} \text{ eV}$  required in  $\Lambda\text{CDM}$  and is discussed in more detail at the end of this chapter. We will see in the next section that these values are compatible with inefficient instant preheating, in which case gravitational reheating (which is always present) takes over the reheating process.

As both the tensor-to-scalar ratio and the spectral index are independent of  $n$ , we simply use the constraints on  $\alpha$  in Eq. (7.42) to update our results. For the spectral index we find

$$0.9677 \leq n_s \leq 0.9680. \quad (7.55)$$

For the running of the spectral index, we find the value  $n'_s = -5.3 \times 10^{-4}$ . Finally, we find the following range of values for the tensor-to-scalar ratio:

$$4.4 \times 10^{-3} \lesssim r \leq 1.2 \times 10^{-2}, \quad (7.56)$$

which can be potentially observable in the near future. These results are plotted in Fig. 7.7.

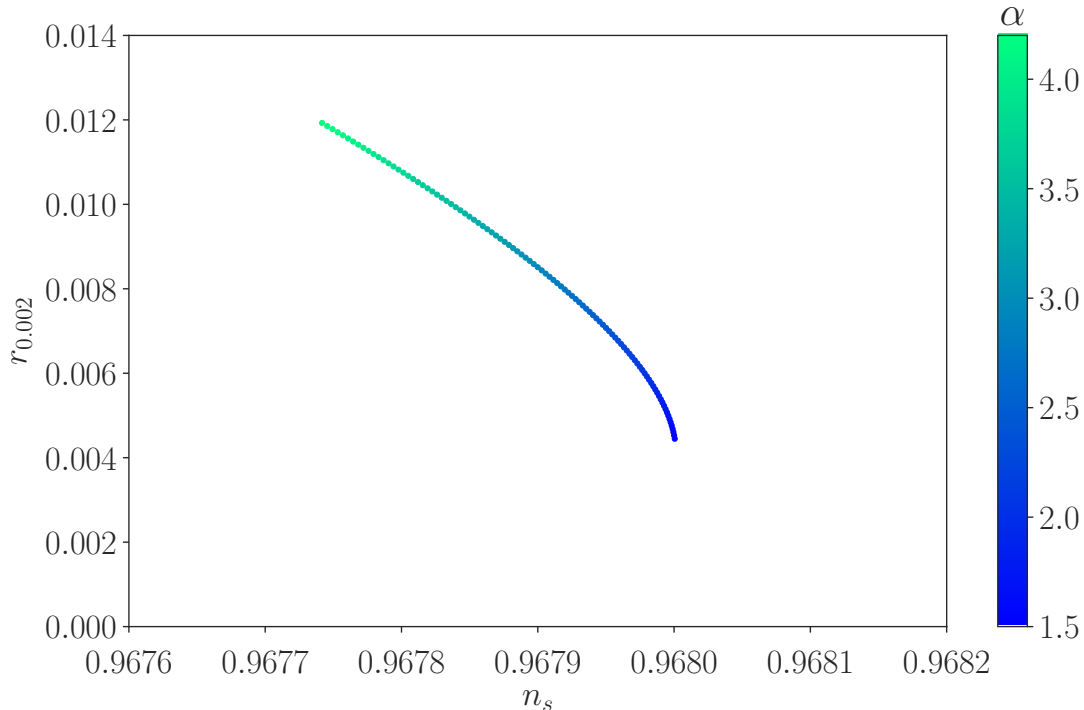


**Figure 7.7:** The tensor-to-scalar ratio,  $r$ , versus the spectral index,  $n_s$  for  $\alpha$  varying from 1.5 to 4.2 according to the colour map on the right. All of these results are well within the Planck  $1\sigma$  range. Values of  $r$  are potentially observable in the near future.

## 7.7 Considerations for Gravitational Reheating

### 7.7.1 Overproduction of Gravitinos

The  $\alpha$ -attractors framework arises naturally in supergravity. Therefore, one limitation which should be taken into account is the overproduction of gravitinos, the super-partner of the graviton. Section 2.7.5 outlines the potential problems arising from the presence of gravitinos and the constraints imposed on their abundance.

In our model the inflaton does not oscillate around its VEV, so we are only concerned with the thermal production of gravitinos - their creation via scatterings in the thermal bath produced via gravitational reheating. The relative abundance of produced gravitinos depends strongly on the reheating temperature,

$T_{\text{reh}}$ , and for ease of reference we repeat the constraint from Section 2.7.5:

$$T_{\text{reh}} \lesssim 10^9 \text{ GeV} . \quad (7.57)$$

The reheating temperature for gravitational reheating is derived in Eq. (7.47) and found to be  $T_{\text{reh}} \simeq 10^6 \text{ GeV}$ . The reheating temperature we find is thus below the upper-bound to avoid gravitino overproduction, as expected because of the inefficiency of gravitational reheating.

### 7.7.2 Overproduction of Gravitational Waves

As introduced in Section 2.8.4.1, a cosmological model involving a period of kination naturally produces a spike in the spectrum of gravitational waves at high frequencies. In order to ensure the generated gravitational waves do not destabilise BBN, an upper bound is imposed on their density fraction [105]:

$$\left( \frac{\rho_g}{\rho_r} \right)_{\text{reh}} \lesssim 10^{-2} , \quad (7.58)$$

where

$$\left( \frac{\rho_g}{\rho_r} \right)_{\text{reh}} = \frac{64}{3\pi} h_{\text{GW}}^2 \left( \frac{\rho_\varphi}{\rho_r} \right)_{\text{end}} . \quad (7.59)$$

Using the relations

$$h_{\text{GW}}^2 = \frac{H_{\text{end}}^2}{8m_{\text{Pl}}^2} \quad \text{and} \quad H_{\text{end}}^2 \simeq \frac{V_{\text{end}}}{3m_{\text{Pl}}^2} , \quad (7.60)$$

we can re-express this as

$$\left( \frac{\rho_g}{\rho_r} \right)_{\text{reh}} = \frac{8}{9\pi} \frac{V_{\text{end}}}{m_{\text{Pl}}^4} \frac{1}{\Omega_r^{\text{end}}} \lesssim 10^{-2} . \quad (7.61)$$

This rearranges to a constraint on the density parameter of radiation at the end of inflation

$$\Omega_r^{\text{end}} \geq \frac{800V_{\text{end}}}{9\pi m_{\text{Pl}}^4} , \quad (7.62)$$

and we can use this minimum value of  $\Omega_r^{\text{end}}$  in Eq. (7.45) to obtain a lower bound on the reheating temperature

$$T_{\text{reh}} \geq \left( \frac{10240 \times 10^6}{243\pi^5 g_*^{\text{reh}}} \right)^{1/4} \frac{V_{\text{end}}}{m_{\text{Pl}}^3} \simeq \frac{V_{\text{end}}}{m_{\text{Pl}}^3}. \quad (7.63)$$

Using  $V_{\text{end}} = e^{-\sqrt{3\alpha}} M^4 \simeq 10^{60} \text{ GeV}$  from Eqs. (7.8) and (7.12) gives a lower bound on the reheating temperature of:

$$T_{\text{reh}} \geq 10^6 \text{ GeV}. \quad (7.64)$$

This bound on  $T_{\text{reh}}$  is of the same magnitude as the values found in the previous section. Gravitational reheating, by not invoking any additional fields or couplings is the most minimal reheating mechanism we could use to generate the thermal bath of the HBB, which is aligned with the motivations behind quintessential inflation theories. However, its minimalistic approach is also its downfall in this instance. In the absence of inflaton decays to other fields, the gravitational reheating mechanism is very inefficient and results in a very low reheating temperature for the model. This would not be a problem in many other theories but because quintessential inflation models contain a period of kination which generates a spike in the gravitational wave spectrum at high energies, the reheating temperature is capped from below. This may rule out gravitational reheating as a viable mechanism in this model and in the next section we investigate instant preheating as an alternative.

## 7.8 Instant Preheating

To investigate instant preheating we again need to find how far the inflaton rolls in field space, to be able to constrain  $n$  via Eq. (7.39).

This is not as straightforward as it was for gravitational reheating because we need to determine the point at which instant preheating occurs,  $\phi_{\text{IP}}$ , in Eq. (7.33). To do this we evolve the equations of motion numerically, in order to determine

exactly when instant preheating occurs and how this affects the variables we need to constrain. The equations of motion used are:

$$3m_{\text{Pl}}^2 H^2 = \frac{1}{2}\dot{\phi}^2 + V(\phi), \quad (7.65)$$

$$\dot{H} = -\frac{\dot{\phi}^2}{2m_{\text{Pl}}^2}, \quad (7.66)$$

$$\ddot{\phi} = -3H\dot{\phi} - V'(\phi), \quad (7.67)$$

where the prime denotes differentiation with respect to  $\phi$  and dots denote differentiation with respect to time.

For instant preheating we presume the inflaton  $\varphi$  is coupled to another scalar field,  $\chi$ , as detailed in Section 2.7.3. In particular, we consider an interaction at an enhanced symmetry point (ESP) at  $\varphi = \varphi_0$ . The Lagrangian density near the ESP is

$$\mathcal{L} = \mathcal{L}(\varphi_0) + \mathcal{L}_{\text{int}}, \quad (7.68)$$

where  $\mathcal{L}(\varphi_0)$  is determined by Eq. (7.6) evaluated at  $\varphi_0$ . We repeat the interaction Lagrangian density from Eq. (2.207) for clarity as

$$\mathcal{L} = -\frac{1}{2}g^2(\varphi - \varphi_0)^2\chi^2 - h\bar{\psi}\psi\chi, \quad (7.69)$$

where we have introduced a shift symmetry to indicate the presence of the ESP, which does not necessarily need to be at the origin.

The careful reader may have noticed that the interaction involves  $\varphi$ , the original non-canonically normalised field. Hence, we will need to convert from  $\phi$  in the simulation to  $\varphi$  in the calculations. We can find  $\varphi$  using Eq. (7.2) from which we readily obtain

$$\dot{\varphi} = \text{sech}^2\left(\frac{\phi}{\sqrt{6}\alpha m_{\text{Pl}}}\right)\dot{\phi}, \quad (7.70)$$

where we obtain  $\phi$  and  $\dot{\phi}$  from the computation, but for completeness:

$$\phi = \sqrt{6\alpha}m_{\text{Pl}} \tanh^{-1} \left( \frac{\varphi}{\sqrt{6\alpha}m_{\text{Pl}}} \right) \quad (7.71)$$

$$\dot{\phi} = \frac{\dot{\varphi}}{1 - \frac{\varphi^2}{6\alpha m_{\text{Pl}}^2}}, \quad (7.72)$$

which are analytically cyclic.

Following the procedure in Section 2.7.3, for the interaction terms used here, with  $m_\chi^2 = g^2(\varphi - \varphi_0)^2$  we find particle production takes place when

$$|\dot{\varphi}| > g(\varphi - \varphi_0)^2, \quad (7.73)$$

which gives the following range for  $\varphi$

$$\varphi_0 - \sqrt{\frac{|\dot{\varphi}|}{g}} \leq \varphi \leq \varphi_0 + \sqrt{\frac{|\dot{\varphi}|}{g}}. \quad (7.74)$$

The above is the window of  $\varphi$  in which particle production occurs and is identical to that obtained from the general treatment in Section 2.7.3, with the additional freedom of the location of the ESP.

It is clear from Eq. (7.74) that the region where  $\dot{\varphi}$  is maximised and particle production occurs is very close to  $\varphi = 0$  (we take  $\varphi_0 \simeq 0$ ), meaning  $\varphi \simeq \phi$  (c.f. Eq. (7.2)) and  $\varphi$  is almost canonical. This can be seen clearly in Fig. 7.8. This is because, when the non-canonical  $\varphi$  is near the poles it hardly varies, even when the canonical  $\phi$  changes substantially. Thus, it is not possible to violate the adiabaticity condition as in Eq. (2.198) in this region. Therefore, there may be many ESPs along the  $\phi$  direction, but only near  $\varphi \simeq \phi \simeq 0$  can we have particle production. Henceforth, we return to the notation of the canonical  $\phi$ .

We know the energy density of produced  $\chi$  particles is

$$\rho_\chi^{\text{IP}} = \frac{g^{5/2} |\dot{\phi}_{\text{IP}}|^{3/2} \phi_{\text{IP}}}{8\pi^3}. \quad (7.75)$$

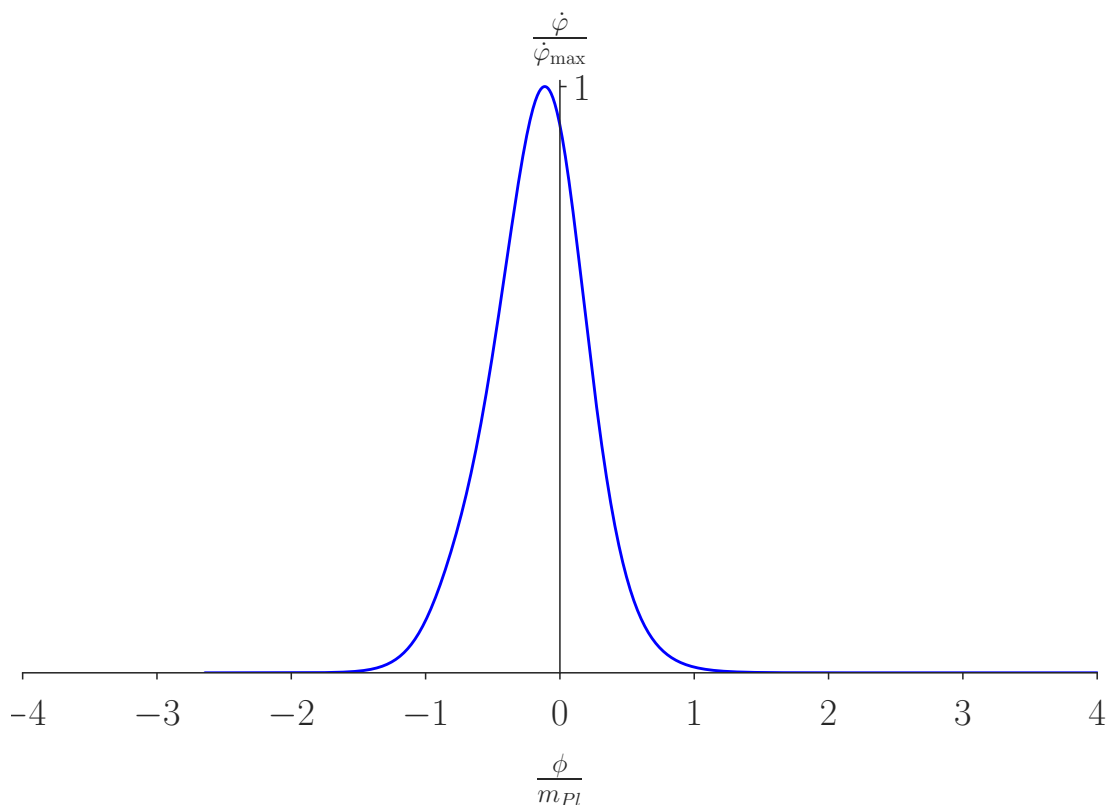


**Figure 7.8:**  $\dot{\phi}$  is maximised very close to  $\phi \simeq 0 \simeq \dot{\phi}$ .

The instant preheating efficiency is maximised when  $\phi$  is near the final edge of the production window in Eq. (7.74) because, even though we expect a continuous contribution to  $n_\chi$  whilst  $\phi$  is in this region, the produced  $\chi$ -particles are diluted by the expansion of the Universe. Therefore, we expect only the ones produced near the end of the particle production regime to contribute significantly to  $\rho_\chi^{\text{IP}}$ . As such, from Eq. (7.74), taking  $\varphi_0 \simeq 0$ , we set

$$\phi_{\text{IP}} = \sqrt{\frac{\dot{\phi}_{\text{IP}}}{g}}, \quad (7.76)$$

which simplifies Eq. (7.75) to

$$\rho_r^{\text{IP}} = \rho_\chi^{\text{IP}} = \frac{g^2 \dot{\phi}_{\text{IP}}^2}{8\pi^3}, \quad (7.77)$$

where we have considered that  $\dot{\phi} > 0$  because the field is rolling towards larger values and we have assumed that the decay of the  $\chi$ -particles to radiation is instantaneous.

For each choice of  $n$ , the quintessence requirements stipulate the required value of  $\phi_F$  and hence  $\Omega_r^{\text{IP}}$ . The value of  $\Omega_r^{\text{IP}}$  is

$$\Omega_r^{\text{IP}} = \frac{\rho_\chi^{\text{IP}}}{\rho_\chi^{\text{IP}} + \rho_{\phi,a}^{\text{IP}}} = \frac{\rho_r^{\text{IP}}}{\rho_{\phi,b}^{\text{IP}}}, \quad (7.78)$$

where  $\rho_\chi^{\text{IP}} = \rho_r^{\text{IP}}$  is defined in Eq. (7.77) and the subscript ‘ $a/b$ ’ refers to after/before instant preheating. Inserting the above into Eq. (7.77), a rearrangement quickly yields:

$$g = \sqrt{\frac{8\pi^3}{\dot{\phi}_{\text{IP}}^2} \Omega_r^{\text{IP}} \rho_\phi^{\text{IP}}}, \quad (7.79)$$

where we have omitted the subscript ‘ $b$ ’ for simplicity. Note that  $\rho_{\phi,a} \simeq \rho_{\phi,b}$  when  $\Omega_r^{\text{IP}} \ll 1$ .

For each choice of  $n$ , we calculate  $\phi_F$  from Eq. (7.39) and insert this into Eq. (7.33) to obtain  $\Omega_r^{\text{IP}}$  as a function of  $n$ . As the reheating variables are also functions of  $n$ , we now have  $g$  in terms of only  $n$ . However, as noted previously,  $\phi_{\text{IP}}$  and  $\dot{\phi}_{\text{IP}}$  are themselves dependent on  $g$  and so this requires iteration. This is the procedure to obtain a value of  $g$  for a given value of  $n$ .

Constraints on the model parameters are addressed in the next section. Very high reheating efficiency is excluded because of backreaction constraints and a high reheating temperature, incompatible with gravitino over-production considerations. The spike in gravitational waves constrains too low reheating efficiencies.

## 7.9 Considerations for Instant Preheating

Before we delve into the various constraints on the efficiency of instant preheating, an immediate sanity check arises: if  $\phi_F < \phi_{\text{IP}}$  then the combination of  $n$  and  $\alpha$

$g$	Allowed $n$ values	Allowed $\kappa$ values
0.001	$119 \leq n \leq 122$	$24.3 \leq \kappa \leq 39.6$
0.01	$121 \leq n \leq 123$	$24.5 \leq \kappa \leq 40.3$
0.1	$123 \leq n \leq 124$	$24.7 \leq \kappa \leq 41.0$
1.0	$125 \leq n \leq 126$	$25.1 \leq \kappa \leq 41.7$

**Table 7.2:** Allowed  $n$  and  $\kappa$  values for specific choices of  $g$ , within the allowed  $\alpha$  range, before consideration of backreaction and gravitino constraints

is disallowed. For the complete range of allowed  $\alpha$  values,  $1.5 \leq \alpha \leq 4.2$ , we find

$$n \leq 130. \quad (7.80)$$

The fact that this approach produces an upper limit on  $n$  makes sense because a larger  $n$  value makes the potential steeper and means lower  $V$  values will be reached earlier in field space. Hence, to equate  $V(\phi_F)$  with dark energy today will require a lower value for  $\phi_F$ .

The dark energy constraints require that for a particular choice of  $n$  in the scalar field potential, the field rolls to a particular value in field space,  $\phi_F$ , to freeze at late times. The key parameter determining  $\phi_F$  is  $\Omega_{\text{IP}}$  which is controlled by the efficiency of reheating. Therefore, any restrictions on the values  $g$  can take will manifest themselves as constraints on the model parameter,  $n$ .

Constraints on  $g$  are investigated fully in Sections 7.9.1 to 7.9.4 but we initially note two extremal bounds on  $g$ . First, that of  $g < 1$  for a perturbative coupling constant, which provides a tight upper bound on  $n$ :

$$\begin{aligned} \alpha = 1.5 : \quad & n \leq 124, \\ \alpha = 4.2 : \quad & n \leq 125. \end{aligned} \quad (7.81)$$

Secondly, a constraint on a lower  $g$  value arises to ensure that radiation domination occurs before BBN, but this constraint is not a worry for we find  $T_{\text{reh}} \gg 1$  MeV in all cases.

### 7.9.1 Radiation Domination

To obtain the correct Universe history, we also need to ensure we have a period of radiation domination after instant preheating, which might provide a tighter bound on  $g$ . However, in a quintessential inflation model with a period of kination after radiation generation, this is never a problem because the density of the produced radiation scales as  $\rho_r \propto a^{-4}$  whilst the density of the kinetically dominated field scales as  $\rho_\phi \propto a^{-6}$ . Hence, all we need to do to ensure radiation domination is ensure that the scalar field remains kinetically dominated after instant preheating. Note, the transfer of energy to  $\chi$ -particles during instant preheating comes from the kinetic energy density of the inflaton only, therefore  $V(\phi_a) = V(\phi_b) \equiv V(\phi_{\text{IP}})$ . Were there not enough kinetic density left, the inflaton would become potentially dominated and would embark on a new period of inflation. Thus, we need to ensure that the kinetic energy of the inflaton is greater than the potential energy after instant preheating. This leads to

$$\rho_{\phi,a} - V(\phi_{\text{IP}}) > V(\phi_{\text{IP}}) \quad \Rightarrow \quad \rho_\chi < \rho_{\phi,b} - 2V(\phi_{\text{IP}}), \quad (7.82)$$

where we have used that  $\rho_{\phi,b} = \rho_{\phi,a} + \rho_\chi$ . Eq. (7.82) gives us an upper limit on the allowed energy density of produced  $\chi$  particles, which translates to an upper limit on the perturbative coupling  $g$ , from the equation for the energy density, Eq. (7.77). However, it turns out that this constraint is automatically satisfied for a perturbative coupling with  $g < 1$ .

Initial values for the model and inflationary parameters are shown in Tables 7.2 and 7.3 where we have used Eqs. (7.33) and (7.39), keeping  $g$  perturbative and imposing the restrictions on  $n$  from Eq. (7.81). In the following sections we consider more stringent bounds on  $g$  (and hence  $n$ ) from the backreaction of the produced particles (Section 7.9.2) and additional considerations if the model is rooted in supergravity (Sections 7.9.3 and 7.9.4).

### 7.9.2 Backreaction

We must also consider the back reaction of produced  $\chi$ -particles on  $\phi$ , which may further constrain the allowed value of  $g$ . The equation of motion for the scalar

$\alpha$	$n$	$N_*$	$n_s$	$r/10^{-3}$	$n'_s/10^{-4}$	$\kappa$	$T_{\text{reh}}$ (GeV)	$M$ (GeV)	$V_0^{1/4}$ (GeV)
1.5	118	62.7	0.968	4.42	-5.25	39.3	$3.84 \times 10^6$	$8.50 \times 10^{15}$	$1.31 \times 10^3$
1.5	124	59.1	0.966	4.97	-5.92	41.3	$2.22 \times 10^{11}$	$8.76 \times 10^{15}$	$3.01 \times 10^2$
4.2	121	63.5	0.968	11.8	-5.11	24.1	$2.35 \times 10^5$	$1.10 \times 10^{16}$	$8.04 \times 10^2$
4.2	125	59.4	0.966	13.9	-5.86	24.9	$6.07 \times 10^{10}$	$1.15 \times 10^{16}$	$3.06 \times 10^2$

**Table 7.3:** Parameter values for the allowed range of  $n$ , prior to consideration of backreaction and gravitino constraints.

field, including back reaction, is given by [87, 88, 205]

$$\ddot{\phi} + 3H\dot{\phi} + V'(\phi) = -gn_\chi \frac{\phi}{|\phi|}, \quad (7.83)$$

where

$$n_\chi = \frac{(g|\dot{\phi}|)^{3/2}}{8\pi^3} \exp\left(-\frac{\pi m_\chi^2}{\dot{m}_\chi}\right), \quad (7.84)$$

and we consider that, near the ESP,  $\varphi$  is canonically normalised ( $\varphi \simeq \phi$ ), as discussed.

The exponential is suppressed during particle production and so the right hand side of Eq. (7.83) becomes

$$\ddot{\phi} + 3H\dot{\phi} + V'(\phi) = -\frac{g^{5/2}\dot{\phi}^{3/2}}{8\pi^3}, \quad (7.85)$$

where we have also considered  $\dot{\phi} > 0$ . As back reaction increases, the magnitude of the right-hand side of this equation grows to have more and more of an effect on the dynamics [88]. This is maximised at  $\phi = \phi_{\text{IP}}$  (i.e. for maximum  $n_\chi$ ). Computing this at that moment, we find that to avoid back-reaction effects requires roughly

$$g \lesssim 10^{-3}. \quad (7.86)$$

In detail, the above upper bound on  $g$  depends on the value of  $\alpha$  as depicted in our results, see Figs. 7.10 to 7.17. Values for the model and inflationary parameters are shown in Table 7.4 where we have again used Eqs. (7.33) and (7.39), but now

$\alpha$	$n$	$N_*$	$n_s$	$r/10^{-3}$	$n'_s/10^{-4}$	$\kappa$	$T_{\text{reh}}$ (GeV)	$M$ (GeV)	$V_0^{1/4}$ (GeV)
1.5	118	62.74	0.968	4.42	-5.25	39.3	$3.84 \times 10^6$	$8.5 \times 10^{15}$	$1.31 \times 10^3$
1.5	119	62.14	0.968	4.51	-5.35	39.7	$2.39 \times 10^7$	$8.5 \times 10^{15}$	$1.03 \times 10^3$
4.2	121	63.54	0.968	11.8	-5.11	24.1	$2.35 \times 10^5$	$1.1 \times 10^{16}$	$8.04 \times 10^2$
4.2	122	62.53	0.967	12.2	-5.28	24.3	$5.07 \times 10^6$	$1.1 \times 10^{16}$	$6.31 \times 10^2$

**Table 7.4:** Final values for the parameters when considering the tightest constraints on  $g$ , from the backreaction bound.

include the tighter constraints on  $g$  from the backreaction constraints.

### 7.9.3 Overproduction of Gravitinos

As mentioned in relation to gravitational reheating, because this is a model rooted in supergravity, constraints from over-production of gravitinos have to be taken into account. The over-production of gravitinos needs to be controlled because they can either contribute to the mass of dark matter and overclose the Universe or they can decay and disrupt the production of nuclei during BBN. Gravitino production is strongly correlated with reheating temperature and avoiding their overproduction results on a bound on  $T_{\text{reh}}$ , given in Eq. (7.57).

We can derive  $T_{\text{reh}}$  for instant preheating in this model by using the relationship between the energy density of radiation and the produced thermal bath, given in Eq. (2.94), which rearranges to

$$T_{\text{reh}} = \left( \frac{30}{\pi^2 g_*} \rho_r^{\text{reh}} \right)^{1/4}. \quad (7.87)$$

Following the approach in Section 7.6 we again find

$$\rho_r^{\text{reh}} = \rho_\phi^{\text{IP}} (\Omega_r^{\text{IP}})^3, \quad (7.88)$$

and inserting this into Eq. (7.87) we find

$$T_{\text{reh}} = \left[ \frac{30}{\pi^2 g_*} \rho_\phi^{\text{IP}} (\Omega_r^{\text{IP}})^3 \right]^{1/4} = \left[ \frac{30}{\pi^2 g_*} \rho_r^{\text{IP}} (\Omega_r^{\text{IP}})^2 \right]^{1/4}, \quad (7.89)$$

where we also consider that  $\rho_r = \Omega_r \rho_\phi$ . We find  $\Omega_r^{\text{IP}}$  as follows

$$\Omega_r^{\text{IP}} = \frac{\rho_r^{\text{IP}}}{\rho_\phi^{\text{IP}}} = \frac{g^2 \dot{\phi}_{\text{IP}}^2}{8\pi^3} \frac{2}{\dot{\phi}_{\text{IP}}^2} = \frac{g^2}{4\pi^3}, \quad (7.90)$$

where we consider Eq. (7.77) and  $\rho_\phi^{\text{IP}} = \frac{1}{2} \dot{\phi}_{\text{IP}}^2$  during kination. Thus,  $\Omega_r^{\text{IP}} \sim 10^{-2} g^2$ ; since  $g < 1$ , this means  $\Omega_r^{\text{IP}}$  is very small. Given that the dependence of  $(\rho_\phi^{\text{IP}})^{1/4}$  on  $g$  is weak, Eq. (7.89) suggests  $T_{\text{reh}} \propto g^{3/2}$ . This makes sense because a large value of  $g$  means that more radiation is generated at instant preheating. Consequently, reheating happens earlier and therefore  $T_{\text{reh}}$  is large. To limit  $T_{\text{reh}}$  to small enough values we need to avoid a large  $g$ .

In our model, the bound  $T_{\text{reh}} < \mathcal{O}(10^9)$  GeV translates to an upper bound on  $g$  of roughly

$$g \lesssim 10^{-2}. \quad (7.91)$$

As in the previous subsection, in detail, the above upper bound on  $g$  depends on the value of  $\alpha$  as depicted in our results, see Figs. 7.10 to 7.17.

### 7.9.4 Overproduction of Gravitational Waves

The main motivation for studying instant preheating in the first place was the spike of gravitational waves produced in models with extended periods of kination. For our model with gravitational reheating, as we saw in Section 7.7.2,  $T_{\text{reh}}$  was too low and the spike in the gravitational wave spectrum disturbed BBN. In a similar way, we may obtain a lower bound on  $\rho_\chi^{\text{IP}}$ , and hence  $g$ , from the nucleosynthesis constraint on the energy density of produced gravitational waves during kination.

We follow the same treatment from Section 7.7.2 to find the lower bound on  $g$  and refer the reader to Eqs. (7.58) to (7.59) for the initial bound and the

definition of parameters. For instant preheating the bound is expressed as

$$\left(\frac{\rho_g}{\rho_r}\right)_{\text{reh}} = \frac{8}{9\pi} \frac{V_{\text{end}}}{m_{\text{Pl}}^4} \frac{1}{\Omega_r^{\text{IP}}} \lesssim 10^{-2}, \quad (7.92)$$

and substituting  $\Omega_r^{\text{IP}}$  in from Eq. (7.90) we get

$$g \geq 20\pi \sqrt{\frac{8}{9}} \frac{V_{\text{end}}^{1/2}}{m_{\text{Pl}}^2} \simeq 10 \left(\frac{M}{m_{\text{Pl}}}\right)^2 \sim 10^{-4}, \quad (7.93)$$

where we again use  $V_{\text{end}} = e^{-\sqrt{3\alpha}} M^4$  from Eqs. (7.8) and (7.12), and for the last equation we consider  $M \simeq 10^{16}$  GeV as suggested by Fig. 7.15.

The bounds on  $g$  from Sections 7.9.1 to 7.9.4 are summarised in Section 7.11, and Section 7.12 concludes this chapter with a discussion of the model, drawing together Section 7.3 on inflation, Section 7.5 on quintessence and the two reheating mechanisms investigated in Sections 7.6 and 7.8. However, before we conclude, there is one final consideration to address.

## 7.10 Additional Considerations

### 7.10.1 Suppressed Interactions

As introduced in Sections 2.6.2 and 2.8.2, quintessence models generally require an extremely flat potential over super-Planckian distances which can give rise to two problems: lifting of the potential via radiative corrections and sizeable violations of the Equivalence Principle via a ‘fifth force’.

However, in the context of  $\alpha$ -attractors both the above dangers are averted. Indeed, as discussed in Ref. [187, 193], when near the kinetic poles ( $\varphi/m_{\text{Pl}} \approx \pm\sqrt{6\alpha}$ , equivalently  $|\phi|/m_{\text{Pl}} \gg \sqrt{6\alpha}$ ), the inflaton interactions are exponentially suppressed and the field becomes “asymptotically free”. The same is true for the loop corrections to the potential.

We expect the inflaton to have Planck-suppressed interactions with other

fields, of the generic form

$$\delta V = \frac{1}{2} h \left( \frac{\varphi}{m_{\text{Pl}}} \right)^q \varphi^2 \sigma^2, \quad (7.94)$$

where  $\sigma$  is a scalar field coupled to the inflaton, where  $q \geq 0$  and  $h = \mathcal{O}(1)$ .

The strength of the interaction is estimated by  $\mathcal{G} = \partial_\phi^2 \partial_\sigma^2 \delta V$ . For Eq. (7.94) this becomes

$$\mathcal{G} = h(q+1)(q+2) \left( \frac{\varphi}{m_{\text{Pl}}} \right)^q \left( \frac{\partial \varphi}{\partial \phi} \right)^2. \quad (7.95)$$

From Eq. (7.2) we find

$$\frac{\partial \varphi}{\partial \phi} = \text{sech}^2 \left( \frac{\phi}{\sqrt{6\alpha} m_{\text{Pl}}} \right), \quad (7.96)$$

meaning the interaction strength is

$$\mathcal{G} = h(q+1)(q+2) \left( \frac{\varphi}{m_{\text{Pl}}} \right)^q \text{sech}^2 \left( \frac{\phi}{\sqrt{6\alpha} m_{\text{Pl}}} \right). \quad (7.97)$$

At late times, when we might worry about super-Planckian field excursions on the quintessential tail, the field is near the pole  $\varphi/m_{\text{Pl}} = \sqrt{6\alpha}$  and frozen ( $\phi \simeq \phi_F$ ), the interaction strength is therefore

$$\mathcal{G} = \frac{(q+1)(q+2) h (6\alpha)^{q/2}}{\cosh^4 \frac{\phi_F}{\sqrt{6\alpha} m_{\text{Pl}}}}. \quad (7.98)$$

Taking  $q \sim h \sim \alpha \sim 1$  and  $\phi_F \gg m_{\text{Pl}}$  we see the strength of the interaction is suppressed

$$\mathcal{G} \sim \exp \left( -\frac{4\phi_F}{\sqrt{6\alpha} m_{\text{Pl}}} \right). \quad (7.99)$$

We note here that this suppression is not due to assuming a Planck-suppressed interaction, as can be readily seen by taking  $q = 0$  in Eq. (7.98).

We can take  $\phi_F$  from Eq. (7.33) (presuming  $\phi_{\text{IP}} \ll \phi_F$  and using  $\Omega_{\text{IP}}$  from Eq. (7.90)) to obtain an estimate for  $\mathcal{G}$ :

$$\phi_F/m_{\text{Pl}} \simeq \sqrt{\frac{2}{3}} [1 - 3 \ln (g/2\pi^{3/2})]. \quad (7.100)$$

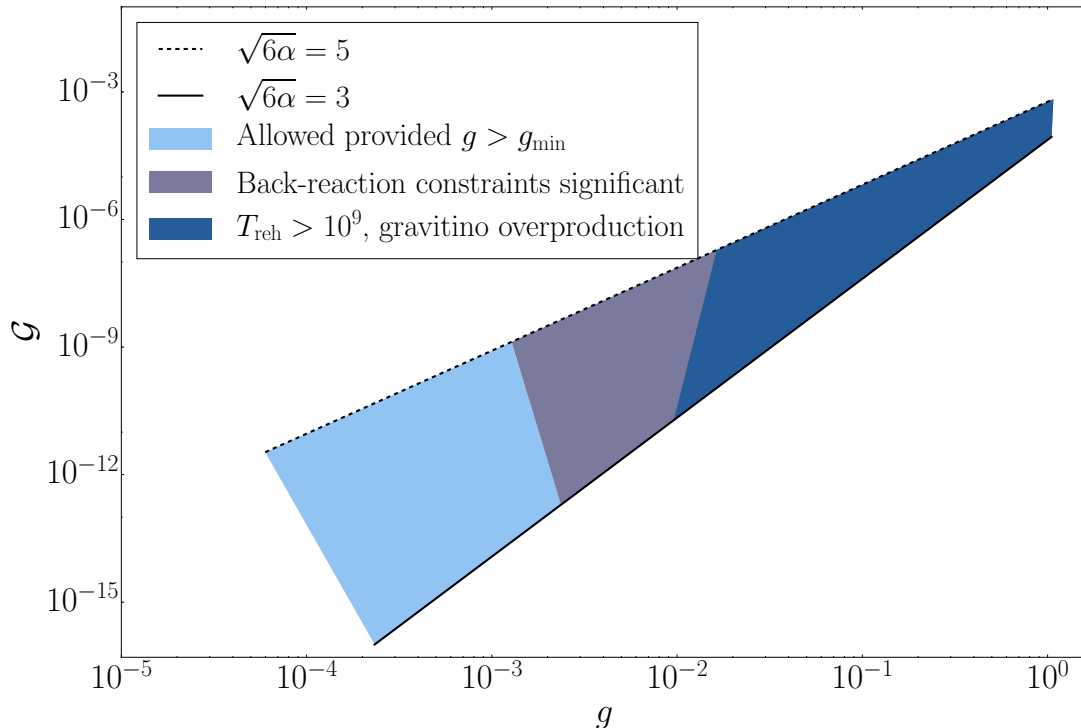


**Figure 7.9:** The interaction strength,  $\mathcal{G}$ , for the range of allowed  $g$  values and allowed  $\alpha$  values between 1.5 and 4.2. The bounds arising from backreaction and gravitino constraints are indicated.

Inserting the above into Eq. (7.99), we obtain

$$\mathcal{G} \sim e^{-4/3\sqrt{\alpha}} \left( \frac{g}{2\pi^{3/2}} \right)^{4/\sqrt{\alpha}}, \quad (7.101)$$

which is plotted in Fig. 7.9 for different values of the instant preheating coupling constant,  $g$ . Fig. 7.9 identifies the results for the allowed  $\alpha$  range between 1.5 and 4.2 and identifies the limits on  $g$  depending on whether the backreaction constraints or supergravity constraints are imposed. These are analysed in more detailed in Section 7.11 but Fig. 7.9 clearly demonstrates that the interaction strength is drastically suppressed for all scenarios considered, overcoming the 5th force problem and alleviating the problem of loop corrections lifting the quintessential tail. This argument can also be generalised to non-perturbative interactions, which are expected to be of the form  $\sim \exp(-\beta_i\varphi/m_{\text{Pl}})\mathcal{L}_i$ , where  $\mathcal{L}_i$

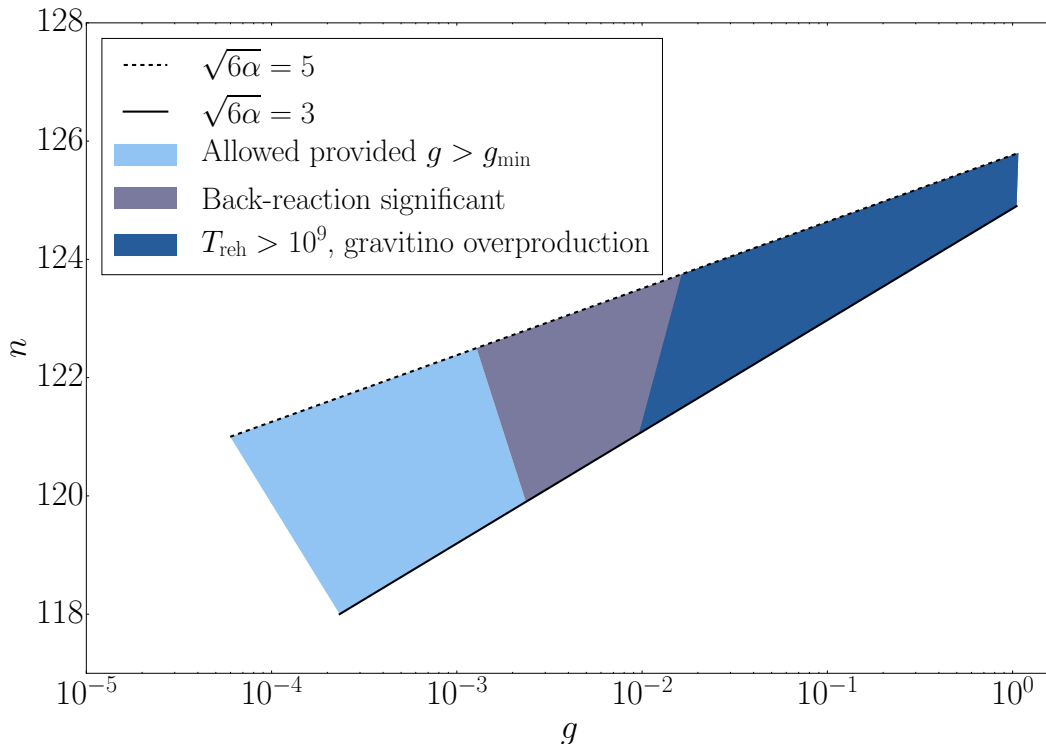


**Figure 7.10:** Final parameter spaces for  $n$ , for the range of allowed  $g$  values and allowed  $\alpha$  values between 1.5 and 4.2. The bounds arising from backreaction and gravitino constraints are indicated.

is any 4-dimensional Lorentz-invariant operator. The interaction strength always obtains a factor  $\left(\frac{\partial\varphi}{\partial\phi}\right)^2 \sim \exp\left(-\frac{4\phi_F}{\sqrt{6\alpha}m_{\text{Pl}}}\right)$  in the limit  $\varphi/m_{\text{Pl}} \rightarrow \sqrt{6\alpha}$  [187].

## 7.11 Results

The constraints on the main  $\alpha$ -attractors' parameter rise from the quintessence requirements outlined in Section 7.5 and result in

$$1.5 \leq \alpha \leq 4.2. \quad (7.102)$$

The initial analysis, concentrating on gravitational reheating constrained the model parameters to be

$$108 \leq n < 115, \quad (7.103)$$

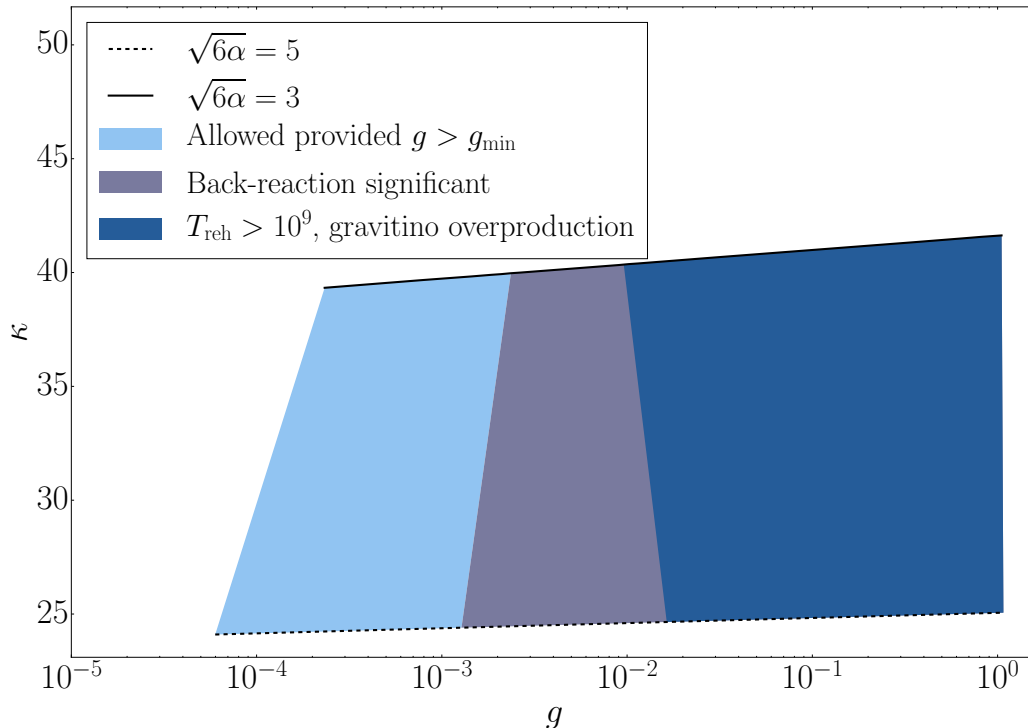


**Figure 7.11:** Final parameter spaces for  $\kappa$ , for the range of allowed  $g$  values and allowed  $\alpha$  values between 1.5 and 4.2. The bounds arising from backreaction and gravitino constraints are indicated.

$$23 \leq \kappa < 36. \quad (7.104)$$

However, the analysis in Section 7.6 subsequently showed that gravitational reheating is not a viable option for this model because of the excessive amount of gravitational waves produced.

Regarding the instant preheating analysis, two unavoidable constraints are the upper bound on  $n$  - ensuring  $g < 1$  because of perturbativity, and the lower limit on  $g$  - ensuring a period of kination does not disturb BBN through overproduction of gravitational waves, the downfall of gravitational reheating. This bound is  $g \gtrsim 10^{-4}$  and together these result in the parameter space

$$\alpha = 1.5 : \quad 118 \leq n \leq 124, \quad (7.105)$$

$$\alpha = 4.2 : \quad 121 \leq n \leq 125. \quad (7.106)$$

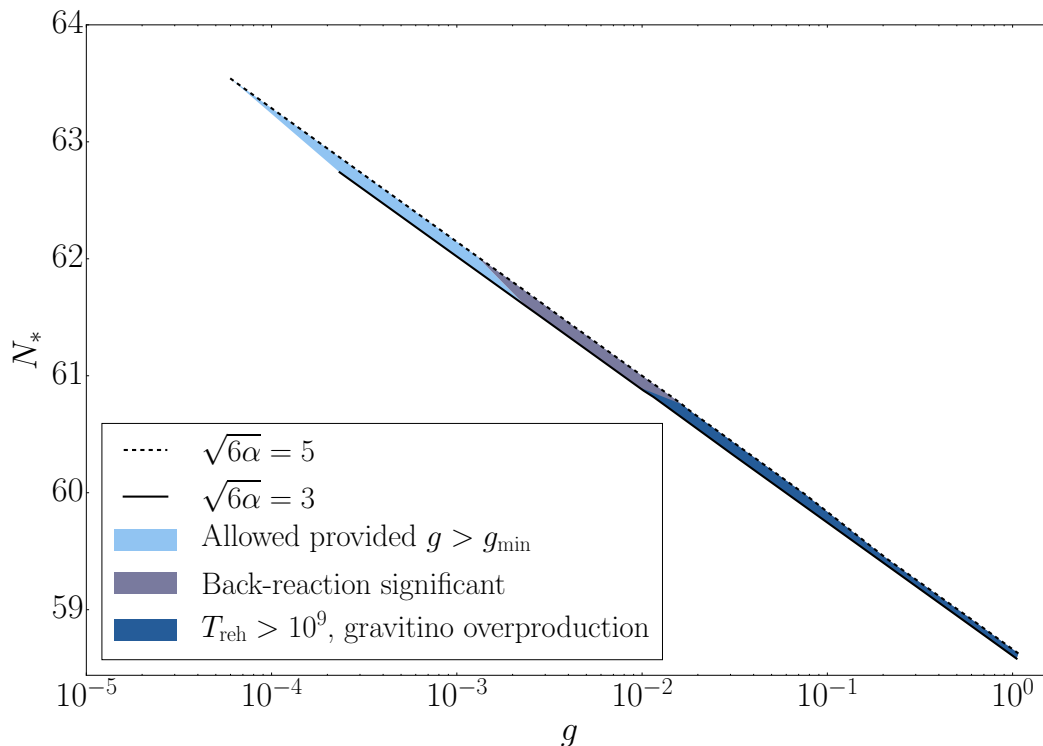


**Figure 7.12:** Final parameter spaces for  $N_*$ , for the range of allowed  $g$  values and allowed  $\alpha$  values between 1.5 and 4.2. The bounds arising from backreaction and gravitino constraints are indicated.

The upper constraint on  $g$  arising from the avoidance of backreaction in the instant preheating mechanism results in a bound of approximately  $g \lesssim 10^{-3}$ . However, this bound can be sidestepped if the decay  $\chi \rightarrow \psi\bar{\psi}$  is rapid, as is often assumed. All that is required is a large enough  $h$  value for this coupling.

The upper bound on  $g$  arising from gravitino over-production constraints is important in a model rooted in supergravity and is roughly  $g \lesssim 10^{-2}$ . This bound reduces the parameter space to

$$\alpha = 1.5 : \quad 118 \leq n \leq 122, \quad (7.107)$$

$$\alpha = 4.2 : \quad 121 \leq n \leq 124. \quad (7.108)$$

If the model is not embedded in supergravity, these constraints can also be neglected.

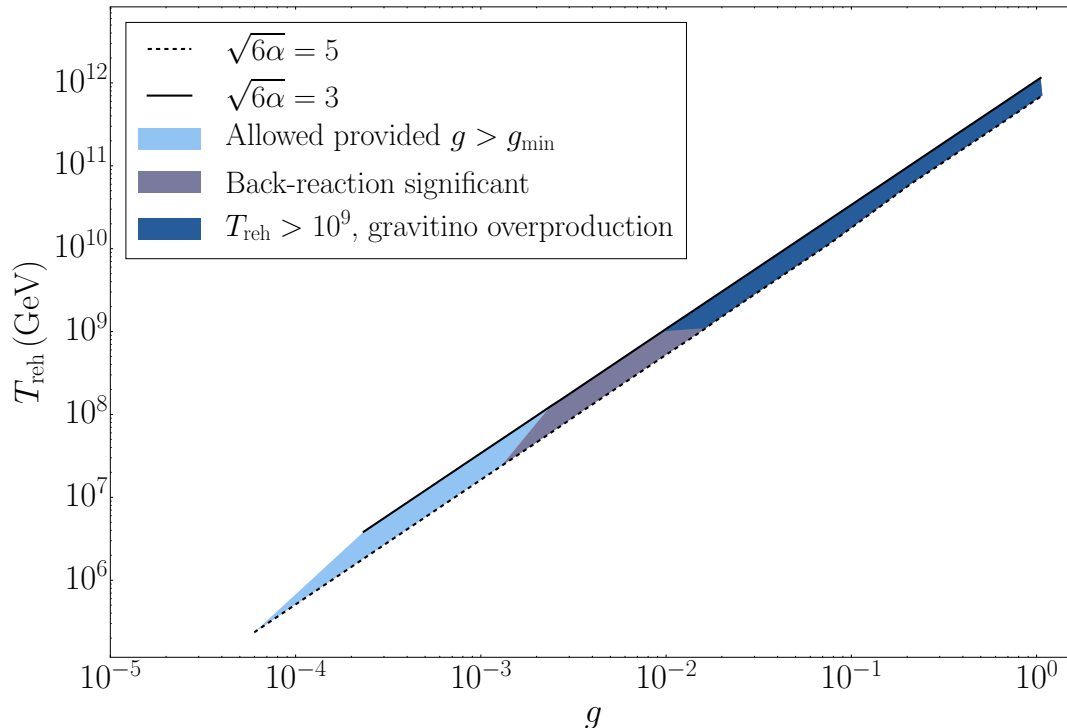


**Figure 7.13:** Final parameter spaces for  $T_{\text{reh}}$ , for the range of allowed  $g$  values and allowed  $\alpha$  values between 1.5 and 4.2. The bounds arising from backreaction and gravitino constraints are indicated.

Figs. 7.10 to 7.17 document the parameter space, distinguishing between the inclusion of the backreaction and gravitino bounds.

With a lower value of  $\Omega_r^{\text{IR}}$ , the inflaton rolls to larger distances before it freezes. To fulfil dark energy requirements, this requires a lower  $n$  value. The results found here for  $n$  demonstrate this. The two different  $\alpha$  values result in different  $n$  requirements because  $\alpha$  controls the slope of the quintessential tail (c.f. Eq. (7.9)). A smaller/larger  $\alpha$ -value means a steeper/gentler quintessential tail. Thus, for a given value of  $\phi_F$ , we require smaller/larger  $n$ -values for a smaller/larger- $\alpha$  value.

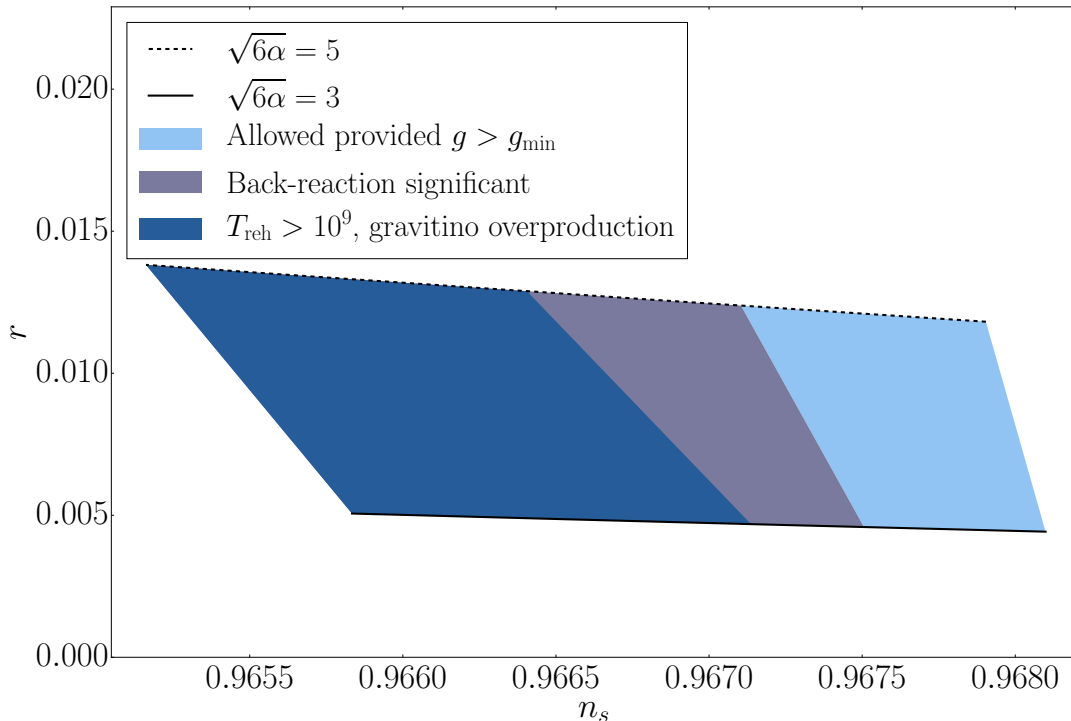


**Figure 7.14:** Final parameter spaces for the spectral index,  $n_s$  and the tensor-to-scalar ratio,  $r$ , for the range of allowed  $g$  values and allowed  $\alpha$  values between 1.5 and 4.2. The bounds arising from backreaction and gravitino constraints are indicated.

## 7.12 Discussion

This chapter presents and analyses a novel model of quintessential inflation incorporating the  $\alpha$ -attractors framework of inflationary models, which can easily be embedded in supergravity. We consider a simple exponential potential  $V(\varphi) = V_0 e^{-\kappa\varphi/m_{\text{Pl}}}$  and the standard  $\alpha$ -attractors kinetic term, which features two poles at  $\varphi = \pm\sqrt{6\alpha} m_{\text{Pl}}$ . Switching to a canonically normalised inflaton, the scalar potential gets “stretched” as the poles are transposed to infinity which generates the inflationary plateau.

The inflationary parameters are calculated and found to be effectively independent of the scalar potential parameters, as all  $\alpha$ -attractor models are. The predictions for the spectral index and tensor-to-scalar ratio fall right in the middle of the Planck contours, as expected for  $\alpha$ -attractor models. The independence of

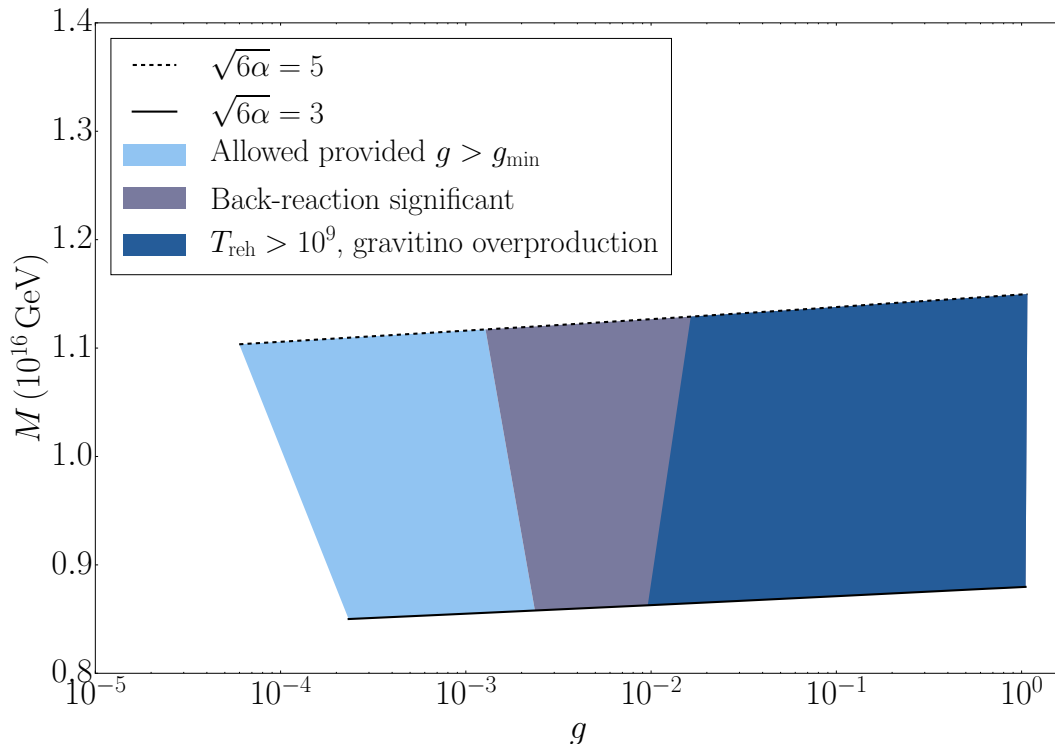


**Figure 7.15:** Final parameter spaces for the inflationary energy scale,  $M$ , for the range of allowed  $g$  values and allowed  $\alpha$  values between 1.5 and 4.2. The bounds arising from backreaction and gravitino constraints are indicated.

the inflationary observables on the model parameter,  $\kappa$ , is perfect for developing a model of QI because it allows quintessence requirements to shape the model without restriction.

After inflation, the field becomes kinetically dominated and a period of kination ensues. This necessarily ends when the Universe becomes dominated by radiation and the HBB begins. The specifics of the inflaton field in this regime are investigated and show quintessence requirements are heavily dependent on the final freezing value of the inflaton, which is mainly determined by the intricacies of reheating.

In an effort to keep the model minimal, we first consider gravitational reheating. However, we find the reheating temperature,  $T_{\text{reh}} \sim 10^6$  GeV, to be very close to the stringent constraints on the gravitational wave spike at high frequencies generated during kination. For this reason we also investigate the mechanism

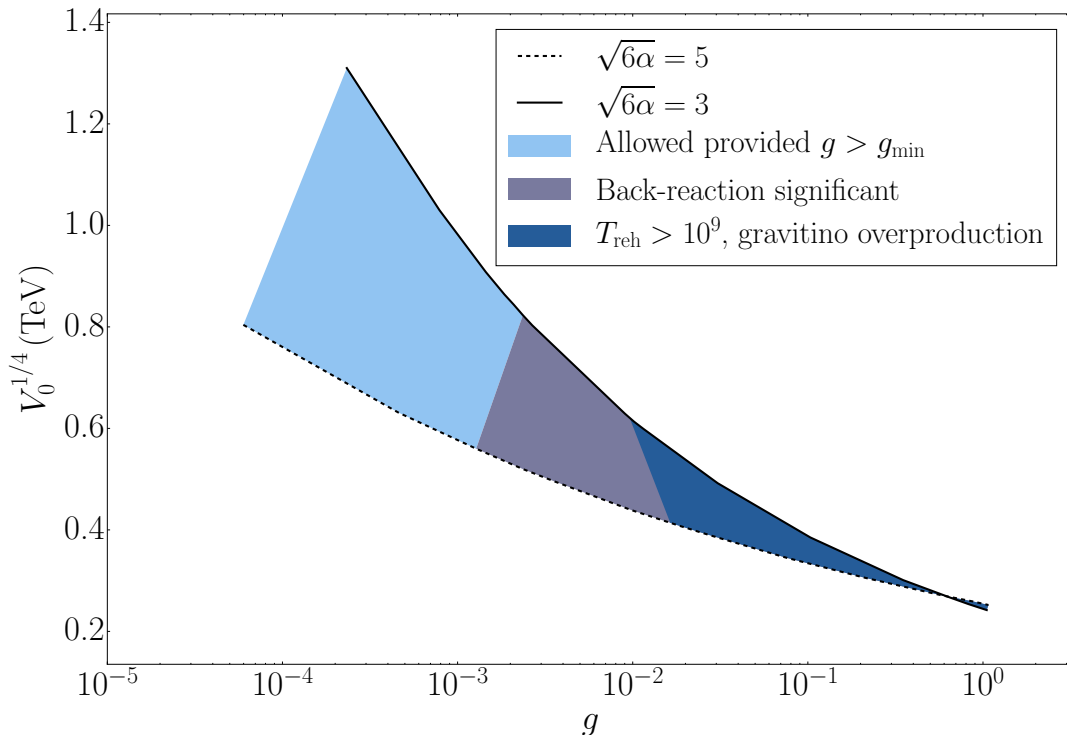


**Figure 7.16:** Final parameter spaces for  $V_0^{1/4}$  for the range of allowed  $g$  values and allowed  $\alpha$  values between 1.5 and 4.2. The bounds arising from backreaction and gravitino constraints are indicated.

of instant preheating, which can be much more efficient and considerably reduce the duration of kination. We take into account backreaction constraints, which threaten to shut down  $\chi$ -particle production and gravitino constraints on the reheating temperature, which impose limits on the coupling constant controlling instant preheating.

Observational constraints on the dark energy density and its equation of state parameter today impose constraints on the steepness and height of the late-time plateau in the model, which is the tail of the exponential function. This manifests as a constraint on both  $\alpha$  and  $\kappa$ , depending heavily on the specifics of reheating. The parameter space is investigated for the model and when all the constraints are applied we find that our model is successful for natural values of the model parameters.

In particular, for the coupling we find  $g \sim 10^{-4} - 10^{-2}$ , while we also have

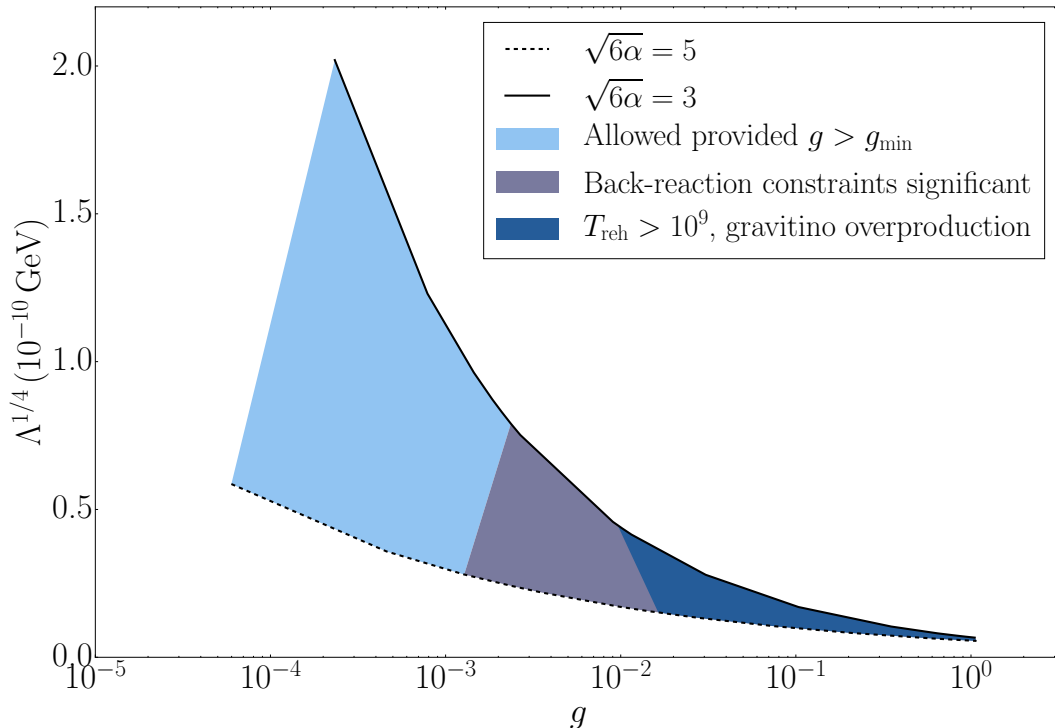


**Figure 7.17:** Final parameter spaces for  $\Lambda^{1/4}$  for the range of allowed  $g$  values and allowed  $\alpha$  values between 1.5 and 4.2. The bounds arising from backreaction and gravitino constraints are indicated.

$V_0^{1/4} \sim 1$  TeV, which is the electroweak energy scale (Fig. 7.16). The inflationary scale is  $M \simeq 10^{16}$  GeV, which is at the energy scale of grand unification (Fig. 7.15). For the slope of the exponential potential we find  $\kappa \simeq 24 - 40$  (Fig. 7.11), i.e.  $\kappa \sim 0.1 m_{\text{Pl}}/M$ , meaning that in the potential the inflaton is suppressed by the scale  $\sim 10^{17}$  GeV, which could be the string scale.

We find that the cosmological scales exit the horizon about  $N_* \simeq 62 - 63$  e-folds before the end of inflation (Fig. 7.12) and that the reheating temperature is  $T_{\text{reh}} \sim 10^5 - 10^8$  GeV (Fig. 7.13), satisfying gravitino constraints as required. For the inflationary observables we obtain the values  $n_s = 0.968$  for the spectral index and  $n'_s = -(5 - 6) \times 10^{-4}$  for its running. For the tensor-to-scalar ratio we obtain  $r \simeq 0.004 - 0.012$ , which may well be observable (Fig. 7.14). These values are within the  $1\sigma$  contour of the Planck results [204].

We are conservative in avoiding a super-Planckian non-canonical inflaton field,

$\varphi$ , even though the suppression of loop corrections and interactions of the inflaton near the poles in  $\alpha$ -attractors means that, even if the canonically normalised inflaton were super-Planckian, the flatness of the quintessential runaway potential would be preserved.

The  $\alpha$ -attractors setup may also be realised without relying on supergravity [56, 109, 180, 183], in which case gravitino constraints may not be necessary. Also, backreaction effects can be dispensed with when the  $\chi$ -particles decay rapidly into radiation, such that they don't backreact and close the resonance. If we remove these constraints, our parameter space is substantially enlarged. In particular,  $g$  can approach unity, while  $N_*$  can be as low as  $N_* \simeq 59$  and the reheating temperature can be as large as  $T_{\text{reh}} \sim 10^{11}$  GeV. Regarding the inflationary observables, the spectral index can become as low as  $n_s = 0.966$ , but  $r$  is not changed much.

The required cosmological constant is  $\Lambda^{1/4} \sim 10^{-10}$  GeV (Fig. 7.17), which is somewhat larger than the value  $\sim 10^{-3}$  eV required in  $\Lambda$ CDM, but the improvement is not much. However, we stress that our required value for  $\Lambda$  is not imposed ad-hoc to satisfy the observations, instead it is generated by the requirement that the vacuum energy asymptotes to zero (cf. Eq. (7.6)). In other words, the (unknown) mechanism which demands zero vacuum density is the one which imposes our value of  $\Lambda$ , thereby making it more natural than the  $\Lambda$  of  $\Lambda$ CDM.

Our model also considers a varying barotropic parameter of dark energy, which is distinguishable from  $\Lambda$ CDM and the precision of observational probes will hopefully allow it to be tested in the near future.

# Chapter 8

## Gauss-Bonnet Quintessential Inflation

*This chapter is based on the original research of the author, in collaboration with Konstantinos Dimopoulos, Carsten van de Bruck and Christopher Longden, submitted to Physics Review D for publication but withdrawn after the LIGO results of 2017 [155]. The research is available on the ArXiv [206].*

### 8.1 Introduction

This chapter introduces another model of Quintessential Inflation (QI), realised in a fundamentally different way to Chapter 7. We utilise a modified theory of gravity in which the scalar field in the theory non-minimally couples to the Gauss-Bonnet combination of quadratic curvature scalars,  $R^2 - 4R^{\mu\nu}R_{\mu\nu} + R^{\rho\mu\sigma\nu}R_{\rho\mu\sigma\nu}$ , detailed in the next section.

Previous work [206–208] on fields with such a coupling shows the motion of the coupled scalar field in field space is impeded when the Gauss-Bonnet coupling function becomes large. This behaviour would be very helpful in preventing a scalar field, dominated by its kinetic energy after inflation, from having a super-Planckian displacement in field space, which is necessary to avoid Fifth Force

constraints (see Section 2.8.2) and radiative corrections lifting the potential (see Section 2.6.2).

This chapter introduces Gauss-Bonnet (GB) gravity and the specific model we have chosen to investigate. We stress that this is a prototype model to assess the feasibility of Quintessential Inflation scenarios in the form of a modified gravity theory. As in all QI models, the Universe cannot reheat perturbatively after inflation and so considerations of non-perturbative reheating mechanisms need to be analysed. In this chapter we utilise instant preheating, introduced in Section 2.7.3 and studied in detail for a QI model in Chapter 7.

Gauss-Bonnet gravity is an excellent example of a cosmological model making testable predictions which can be verified by observation. Unfortunately, in this instance the observations successfully managed to rule out the Gauss-Bonnet theory as a viable description for quintessence in the late Universe. The LIGO experiment recently confirmed that gravitational waves travel at the speed of light [155] which is in contrast with the predictions of GB quintessence (along with many other modified gravity theories affecting late-time dynamics [209, 210]).

## 8.2 Gauss-Bonnet Gravity and the Model

The simplest extensions to General Relativity (GR) are  $f(R)$  theories which have actions of the form

$$S = \frac{m_{\text{Pl}}^2}{2} \int d^4x \sqrt{-g} f(R) + S_{\text{mat}}, \quad (8.1)$$

where  $S_{\text{mat}}$  is the action for matter, defined in Eq. (2.8). The Einstein-Hilbert action of GR (Eq. (2.7)) corresponds to  $f(R) = R$ , but typical  $f(R)$  theories of gravity include higher orders of the Ricci curvature scalar,  $R$ . The most recognisable is  $R + R^2$  gravity [64] which is well studied in the literature and mimics the behaviour of the  $\alpha$ -attractor family of inflationary models introduced in Chapter 7, for small  $\alpha$ , predicting observables well-aligned with the Planck observations [1]. As briefly mentioned in Section 2.6,  $f(R)$  theories of gravity are equivalent

to scalar-tensor theories, where an additional scalar field is added to the action, non-minimally coupled to gravity.

Gauss-Bonnet gravity is an extension of  $f(R)$  theories, because it contains not just higher order terms of the Ricci scalar, but also contractions of the Ricci tensor,  $R^{\mu\nu}$ , and Riemann tensor  $R^{\mu\nu\rho\sigma}$ , the definitions of which are given in Section 2.2.1. The Gauss-Bonnet (GB) combination of quadratic curvature scalars is

$$E_{GB} = R^2 - 4R^{\mu\nu}R_{\mu\nu} + R^{\mu\nu\rho\sigma}R_{\mu\nu\rho\sigma}. \quad (8.2)$$

Extensions of  $f(R)$  theories typically contain unstable extra degrees of freedom arising from higher than second order derivatives of the metric [211, 212], but this combination of the curvature scalars is special because the higher order derivatives cancel out. However, a theory of more than four dimensions is required for the GB term to have any non-trivial effect on the equations of motion when it is simply added to the action as

$$S = \frac{m_{\text{Pl}}^2}{2} \int d^4x \sqrt{-g} (R + CE_{GB}) + S_{\text{mat}}, \quad (8.3)$$

where  $C$  is a dimensionful constant, because it is a total derivative.

Alternatively, in four-dimensions the GB term can contribute to the equations of motion if we couple it to a scalar field via a coupling function,  $G(\phi)$ . The action is thus

$$S = \frac{m_{\text{Pl}}^2}{2} \int d^4x \sqrt{-g} (R - G(\phi)E_{GB}) - \int d^4x \sqrt{-g} \left( \frac{1}{2}(\partial\phi)^2 + V(\phi) \right), \quad (8.4)$$

where  $G(\phi)$  and  $V(\phi)$  are as yet unspecified functions of  $\phi$ . The GB term, as the simplest curvature scalar which does not add any additional propagating degrees of freedom to the theory, is a fairly natural object to consider when building gravity theories from the bottom up [213]. As a subset of Horndeski's theory [214–216], it is guaranteed to have second order equations of motion and no instabilities. It appears in UV theories such as string [208, 217] and braneworld-inspired [218–222] models and realisations of bouncing cosmologies have also been found in Gauss-Bonnet-containing theories [223, 224].

As a well-motivated extension of GR it is therefore unsurprising that it is well documented in the literature. However, scalar-tensor theories with such a Gauss-Bonnet coupling (and to a lesser extent, vector-tensor theories [225]) have been studied extensively with applications to inflation [206, 207, 226–233] and dark energy [234, 235] investigated separately, as well as topics such as black hole formation [236], but not in the combined form we introduce here. This makes the research in this chapter an exciting crossover combining the fields of quintessential inflation and modified gravity theories.

Considering the flat FRW metric in Cartesian co-ordinates

$$ds^2 = -dt^2 + a^2(t)(dx^2 + dy^2 + dz^2), \quad (8.5)$$

where  $a(t)$  is the scale factor, the equations of motion derived from the action, Eq. (8.3) are

$$3m_{\text{Pl}}^2 H^2 = \frac{1}{2}\dot{\phi}^2 + V(\phi) + 12m_{\text{Pl}}^2 H^3 \dot{G}, \quad (8.6)$$

$$2m_{\text{Pl}}^2 \dot{H} = -\dot{\phi}^2 + 4m_{\text{Pl}}^2 H^2 (\ddot{G} - H\dot{G}) + 8m_{\text{Pl}}^2 H \dot{H} \dot{G}, \quad (8.7)$$

$$\ddot{\phi} + 3H\dot{\phi} + V' + 12m_{\text{Pl}}^2 H^2 G'(\dot{H} + H^2) = 0. \quad (8.8)$$

We intend to investigate the ability of a GB term to impede the inflaton's motion at late times and facilitate quintessence. Therefore, we choose a prototype potential which can generate the inflationary plateau, favoured by Planck [1], as well as a quintessential tail:

$$V(\phi) = \frac{V_0}{2} \left[ 1 + \tanh \left( p \frac{\phi - \phi_c}{m_{\text{Pl}}} \right) \right], \quad (8.9)$$

where  $V_0$  is the energy density scale of inflation and  $p$  is a positive constant which controls how steep the drop from the inflationary to quintessential plateau is. We expect our results to qualitatively hold even if the precise form of the potential is changed, so long as at late times there is a plateau suitable for quintessential inflation and at early times inflation may be realised. We hence remain agnostic as to the origin of Eq. (8.9).

We need the new GB effects to be significant at late times, without disturbing inflation at early times. With this aim, we choose a fairly minimalistic coupling function of the form

$$G(\phi) = G_0 e^{-q\phi/m_{\text{Pl}}}, \quad (8.10)$$

where the pre-factor should satisfy  $G_0 m_{\text{Pl}}^2 \geq 1$  in order for GB effects to be important before the field reaches super-Planckian field values, and  $q$  is a positive constant. For the scalar field potential in Eq. (8.9), large positive  $\phi$  values correspond to the inflationary plateau and we see that for large positive  $q\phi$  values the coupling in Eq. (8.10) will be exponentially suppressed. Conversely, for negative  $q\phi$  values it will quickly grow in magnitude. As stressed already, the potential and coupling detailed here are chosen to demonstrate the effectiveness of the model, but are not requisite required forms. Also, as detailed in Section 2.8.4 and Section 7.4, after inflation the field becomes kinetically dominated and oblivious of the potential until it eventually freezes somewhere along the quintessential tail.

The value of the constant  $\phi_c$  in Eq. (8.9), under a field redefinition  $\phi \rightarrow \phi + \phi_c$ , can be absorbed into a rescaling of the constant  $G_0 \rightarrow G_0 e^{q\phi_c}$ , and so we set it to zero without loss of generality.

### 8.3 Inflation

The coupling (Eq. (8.10)) between the scalar field and the Gauss-Bonnet term is negligible during inflation ( $q\phi \gg m_{\text{Pl}}$ ) and so we investigate inflation in the usual manner, using the slow-roll formalism to determine the inflationary predictions and ignoring the GB term for now.

We find the slow-roll parameters to be

$$\epsilon \simeq \frac{m_{\text{Pl}}^2}{2} \left( \frac{V'}{V} \right)^2 = \frac{p^2}{2} \left[ 1 - \tanh \left( \frac{p\phi}{m_{\text{Pl}}} \right) \right]^2, \quad (8.11)$$

and

$$\eta \simeq \frac{V''}{V} = -2p^2 \tanh \left( \frac{p\phi}{m_{\text{Pl}}} \right) \left[ 1 - \tanh \left( \frac{p\phi}{m_{\text{Pl}}} \right) \right]. \quad (8.12)$$

Inflation ends when  $\epsilon = 1$ , which results in

$$\phi_{\text{end}} \simeq \frac{m_{\text{Pl}}}{p} \tanh^{-1} \left( 1 - \frac{\sqrt{2}}{p} \right). \quad (8.13)$$

The e-folding number (using Eq. (2.85)) is then found to be

$$N_* \simeq \frac{1}{4p^2} e^{2p\phi/m_{\text{Pl}}} + \frac{\phi}{2pm_{\text{Pl}}} - \frac{1}{2p^2} \left[ \frac{p}{\sqrt{2}} + \tanh^{-1} \left( 1 - \frac{\sqrt{2}}{p} \right) - \frac{1}{2} \right], \quad (8.14)$$

where, during inflation with  $p\phi \gg m_{\text{Pl}}$ , the exponential term is dominant, and so by inversion we find

$$\phi_* \approx \frac{m_{\text{Pl}}}{2p} \ln(4p^2 N_*). \quad (8.15)$$

We then obtain the spectral index of the scalar curvature perturbation and the tensor-to-scalar ratio:

$$n_s - 1 \simeq 2\eta - 6\epsilon \simeq -\frac{4p^2(1 + 8p^2 N_*)}{(1 + 4p^2 N_*)^2} \approx -\frac{2}{N_*}, \quad (8.16)$$

$$r \simeq 16\epsilon \simeq \frac{32p^2}{(1 + 4p^2 N_*)^2} \approx \frac{2}{p^2 N_*^2}. \quad (8.17)$$

For  $N_* = 60$ , with the final equalities in Eqs. (8.16) and (8.17) we obtain  $n_s = 0.967$  and  $r = \frac{0.0006}{p^2}$ . The scalar spectral index falls nicely within the Planck results [1] as we would expect. The tensor-to-scalar ratio is unobservably small, even for small  $p$  values, and will become increasingly smaller for larger  $p$  values, which we will see are necessary in subsequent sections.

The energy scale of inflation can be calculated from the COBE constraint, introduced in Section 2.4.5

$$\sqrt{A_s} = \frac{1}{2\sqrt{3}\pi} \frac{V^{3/2}}{m_{\text{Pl}}^3 |V'|}, \quad (8.18)$$

where  $A_s = (2.101_{-0.034}^{+0.031}) \times 10^{-9}$ , is the amplitude of the scalar curvature pertur-

bation [1]. Rearranging this gives the energy scale:

$$V_0 = \frac{12\pi^2 m_{\text{Pl}}^4 A_s}{N_*(1 + 4p^2 N_*)} \approx \frac{6.5 \times 10^{-8} m_{\text{Pl}}^4}{p^2 N_*^2}. \quad (8.19)$$

To bring the potential energy down to the dark energy scale at late times, a large suppression of many orders of magnitude is hence necessary. This implies we will need a rather large value of  $p$ .

As a first estimate at this stage, noting that for  $p\phi \ll 0$  (deeply post-inflation) the form of the potential in Eq. (8.9) is approximated by  $V_0 \exp(2p\phi/m_{\text{Pl}})$ , we can see that for a maximum field displacement of  $\mathcal{O}(m_{\text{Pl}})$ , we will need  $2p \approx \ln(V_0/\rho_{\text{DE}}) \approx \mathcal{O}(100)$  to facilitate this.

We also note here that around this expected value of  $p \simeq 100$ , Eq. (8.19) implies  $V_0 \simeq 10^{-15} m_{\text{Pl}}^4$ , or  $V_0^{1/4} \simeq 10^{14}$  GeV, close to the energy scale of Grand Unification.

## 8.4 After Inflation

The motivation of this work is the expectation that the GB coupling will impede the inflaton's motion in field space. Therefore, we expect there to be a static solution to the EoM, where  $\phi \simeq \text{constant}$ . Taking  $\dot{\phi} = \ddot{\phi} = \dot{H} = 0$  in Eqs. (8.6) and (8.8), we find

$$\phi_s/m_{\text{Pl}} \approx \frac{1}{q - 2p} \ln \left( \frac{2qV_0 G_0}{3pm_{\text{Pl}}^2} \right). \quad (8.20)$$

Numerically, we observe that this solution is approached in the post-inflationary regime as the Gauss-Bonnet term becomes important at negative field values. Specifically, we have found a solution at very late times when both the radiation and matter components of the Universe are negligible. As the field is frozen, this solution itself is an inflationary expansion with  $w < -1/3$ .

However, there is much to explore in the intervening time period, when radiation and matter are not negligible. Between the initial period of inflation and this late-time accelerating expansion there is an interval when the field is rolling quickly down the steep decline of the potential, around  $\phi = 0$ . This is a period of

ination, which we introduced in Section 2.8.4 and explored for a quintessential inflation model in Chapter 7. We know that at some point during kination the thermal bath needs to be generated in order to recover the HBB history that is confirmed by observation, which must happen before BBN. At reheating the Universe dutifully transitions into the radiation-dominated epoch and subsequently into the matter-dominated epoch before we reach the modern day where dark energy is the dominant component of the Universe.

The normal procedure in a model of QI would be to solve the Klein-Gordon (KG) equation in the kination regime, where the potential can be neglected, so that it takes the form

$$\ddot{\phi} + 3H\dot{\phi} \simeq 0, \quad (8.21)$$

to determine how far the field rolls before it freezes. The solutions to Eq. (8.21) are demonstrated in Section 2.8.4. However, in our model we have the additional GB terms in the equations of motion. The full non-linear KG equation in Eq. (8.8) is very difficult, if not impossible, to solve. We evolve the equations of motion numerically to determine constraints on the model in Section 8.7 but it is necessary to break the problem down.

We assume that immediately after reheating the Gauss-Bonnet term is still negligible and we can use the solutions to Eq. (8.21). This is desirable because if the field were to become GB-dominated, and hence freeze, immediately after reheating, its density would be too large to act as dark energy. However, we require that the GB coupling becomes significant at some, as of yet unspecified, later time, when the field has rolled further down the quintessential tail to reduce its final energy density. This means that as  $\phi$  rolls to more negative values the GB term becomes more and more important in the full KG equation, and so Eq. (8.21) is only valid for a certain amount of time before the GB term must be included too. This time can be defined as  $t_{\text{GB}}$  when

$$|\ddot{\phi}| = |12m_{\text{Pl}}^2 H^2 (\dot{H} + H^2) G'|. \quad (8.22)$$

From this point onwards we can assume the second derivative of the field is neg-

ligible and include the GB term instead so that the equation of motion becomes

$$3H\dot{\phi} + 12m_{\text{Pl}}^2 H^2 (\dot{H} + H^2) G' = 0. \quad (8.23)$$

Defining the boundary condition that the solutions to Eqs. (8.21) and (8.23) must agree at  $t_{\text{GB}}$  allows us to follow the evolution of  $\phi$  during the two regimes. Fine resolution of the evolution of  $\phi$  around  $t_{\text{GB}}$  is lost but we are able to determine the late-time behaviour.

### 8.4.1 Kinetic Regime

Solving Eq. (8.21) requires knowledge of the initial conditions. We have not yet detailed the reheating mechanism for the model but we will denote the point of reheating by  $\phi_{\text{IP}} \equiv \phi(t_{\text{IP}})$  because we intend to utilise ‘instant preheating’, detailed in Section 2.7.3. When the field is dominated by its kinetic energy, we can use Eq. (8.6) to find

$$\dot{\phi}(t_{\text{IP}}) = \dot{\phi}_{\text{IP}} = -\sqrt{6\Omega_{\text{IP}}(k/t_{\text{IP}})} m_{\text{Pl}}, \quad (8.24)$$

where  $\Omega_{\text{IP}} \equiv \Omega_{\phi}(t_{\text{IP}})$  is the density parameter of the field at the moment of instant preheating (immediately after). We assume the field is rolling towards negative values and we take  $H = k/t$ , where  $k = 1/2(2/3)$  in RD(MD) respectively, to keep the analysis general. This reduces to the general equation derived in Eq. (2.232) when  $k = 1/2$ , in the limit  $\Omega_{\text{IP}} \simeq 1$ . We will require that the produced radiation density dominates over the remaining field density, to ensure radiation domination (this is detailed in Section 8.5) which implies  $\Omega_{\text{IP}} \ll 1$ . Solving Eq. (8.21) with these conditions gives

$$\phi(t) = \phi_{\text{IP}} - m_{\text{Pl}} \sqrt{6\Omega_{\text{IP}}} \left( \frac{k}{3k-1} \right) \left[ 1 - \left( \frac{t_{\text{IP}}}{t} \right)^{3k-1} \right], \quad (8.25)$$

which is valid in the regime of kinetic domination of the inflaton’s motion, whilst  $t < t_{\text{GB}}$ .

### 8.4.2 Gauss-Bonnet Regime

As the GB-dominated equation of motion, Eq. (8.23), is first order, we only need the initial condition that at the time when the GB-dominated solution first becomes relevant,  $t_{\text{GB}}$ , the field takes the value (which will later be determined)  $\phi_{\text{GB}} = \phi(t_{\text{GB}})$ . Using this, we find the solution

$$\phi(t) = \phi_{\text{GB}} + \frac{m_{\text{Pl}}}{q} \ln \left[ 1 + 2G_0 q^2 k^2 (1-k) e^{-q\phi_{\text{GB}}/m_{\text{Pl}}} \left( \frac{1}{t^2} - \frac{1}{t_{\text{GB}}^2} \right) \right]. \quad (8.26)$$

At very late times ( $t \gg t_{\text{GB}}$ ) the field will then tend to a constant value

$$\phi(t \gg t_{\text{GB}}) = \phi_{\text{GB}} + \frac{m_{\text{Pl}}}{q} \ln \left( 1 - \frac{2k^2(1-k)G_0 q^2 e^{-q\phi_{\text{GB}}/m_{\text{Pl}}}}{t_{\text{GB}}^2} \right) \approx \phi_{\text{GB}}. \quad (8.27)$$

In the second approximate equality, we note that there is very little variation of the field in this regime as the second term is generally quite small for typical parameter values. This is expected, as the principle of our model is that a large GB coupling impedes the evolution of the field so  $\phi$  freezes almost immediately when GB becomes important.

### 8.4.3 Stitching and Boundary Condition

Having determined the evolution of the field for  $t < t_{\text{GB}}$  in Eq. (8.25), and  $t > t_{\text{GB}}$  in Eq. (8.26), we now determine the moment at which these two solutions coalesce,  $t_{\text{GB}}$ . As discussed previously, this is when  $|\ddot{\phi}| = |12m_{\text{Pl}}^2 H^2 (\dot{H} + H^2) G'|$ .

From Eq. (8.25) we find  $\ddot{\phi}$ :

$$\ddot{\phi} = \frac{3m_{\text{Pl}} \sqrt{6\Omega_{\text{IP}}} k^2}{t_{\text{IP}}^2} \left( \frac{t_{\text{IP}}}{t} \right)^{3k+1}, \quad (8.28)$$

and we evaluate the GB contribution to be

$$\left| 12m_{\text{Pl}}^2 H^2 (\dot{H} + H^2) G' \right| = 12m_{\text{Pl}} k^3 (k-1) q G_0 t^{-4} e^{\frac{-q\phi}{m_{\text{Pl}}}}. \quad (8.29)$$

Equating the two at  $t_{\text{GB}}$  we find

$$\begin{aligned} \frac{kq\sqrt{6\Omega_{\text{IP}}}t_{\text{IP}}^{3k-1}t_{\text{GB}}^{-3(k-1)}}{3k-1}\exp\left(\frac{kq\sqrt{6\Omega_{\text{IP}}}t_{\text{IP}}^{3k-1}t_{\text{GB}}^{-3k+1}}{3k-1}\right) &= \frac{4q^2k^2G_0(k-1)}{(3k-1)} \\ &\times \exp\left(\frac{-q\phi_{\text{IP}}}{m_{\text{Pl}}} + \frac{qk\sqrt{6\Omega_{\text{IP}}}}{3k-1}\right), \end{aligned} \quad (8.30)$$

where we have substituted  $\phi(t)$  from Eq. (8.25) and rearranged the terms slightly. This is to demonstrate that the equation is reminiscent of Eq. (5.30), which we solved using the Lambert W function, for which  $x = W(xe^x)$ .

To solve for  $t_{\text{GB}}$  in a similar way we need the powers of  $t_{\text{GB}}$  in the exponential and the pre-factor on the left hand side of Eq. (8.30) to be identical. To assist with this we define

$$\mu = 1 - 3k, \quad (8.31)$$

$$\nu = 3 - 3k, \quad (8.32)$$

which simplifies Eq. (8.30) to

$$\begin{aligned} \frac{-kq\sqrt{6\Omega_{\text{IP}}}t_{\text{IP}}^{-\mu}t_{\text{GB}}^{\nu}}{\mu}\exp\left(\frac{-kq\sqrt{6\Omega_{\text{IP}}}}{\mu}\left(\frac{t_{\text{GB}}}{t_{\text{IP}}}\right)^{\mu}\right) &= \frac{-4q^2k^2G_0(k-1)}{\mu} \\ &\times \exp\left(\frac{-q\phi_{\text{IP}}}{m_{\text{Pl}}} - \frac{qk\sqrt{6\Omega_{\text{IP}}}}{\mu}\right), \end{aligned} \quad (8.33)$$

and we see we are forced to raise the entire equation to the power of  $\frac{\mu}{\nu}$

$$\begin{aligned} \left(\frac{-kq\sqrt{6\Omega_{\text{IP}}}t_{\text{IP}}^{-\mu}t_{\text{GB}}^{\nu}}{\mu}\right)^{\frac{\mu}{\nu}}\exp\left(\frac{-kq\sqrt{6\Omega_{\text{IP}}}}{\nu}\left(\frac{t_{\text{GB}}}{t_{\text{IP}}}\right)^{\mu}\right) &= \left(\frac{-4q^2k^2G_0(k-1)}{\mu}\right)^{\frac{\mu}{\nu}} \\ &\times \exp\left(\frac{-q\phi_{\text{IP}}}{m_{\text{Pl}}} - \frac{qk\sqrt{6\Omega_{\text{IP}}}}{\mu}\right)^{\frac{\mu}{\nu}}, \end{aligned} \quad (8.34)$$

which leaves us with equivalent powers in  $t_{\text{GB}}$ .

To solve with the Lambert W function we require the entire pre-factor before the exponential term containing  $t_{\text{GB}}$  to match the exponential bracket, so it resembles  $xe^x$ . This requires multiplying the entire equation by a multiple of the pre-factor, leaving

$$-\frac{kq\sqrt{6\Omega_{\text{IP}}}}{\nu} \left(\frac{t_{\text{GB}}}{t_{\text{IP}}}\right)^\mu \exp\left(-\frac{kq\sqrt{6\Omega_{\text{IP}}}}{\nu} \left(\frac{t_{\text{GB}}}{t_{\text{IP}}}\right)^\mu\right) = \left(\frac{4kqG_0(k-1)}{t_{\text{IP}}^2}\right)^{\frac{\mu}{\nu}} \times \frac{kq\sqrt{6\Omega_{\text{IP}}^{2/\nu}}}{\nu} \exp\left(\frac{-q\phi_{\text{IP}}}{m_{\text{Pl}}} - \frac{qk\sqrt{6\Omega_{\text{IP}}}}{\mu}\right)^{\frac{\mu}{\nu}}, \quad (8.35)$$

and the equation is in the form we require, where  $W(y) = W(xe^x) = x$ , and in our case

$$x = \left(-\frac{kq\sqrt{6\Omega_{\text{IP}}}}{\nu} \left(\frac{t_{\text{GB}}}{t_{\text{IP}}}\right)^\mu\right). \quad (8.36)$$

Hence, our solution has the form

$$\left(-\frac{kq\sqrt{6\Omega_{\text{IP}}}}{\nu} \left(\frac{t_{\text{GB}}}{t_{\text{IP}}}\right)^\mu\right) = W\left[\left(\frac{4kqG_0(k-1)}{t_{\text{IP}}^2}\right)^{\frac{\mu}{\nu}} \frac{kq\sqrt{6\Omega_{\text{IP}}^{2/\nu}}}{\nu} \times \exp\left(\frac{-q\phi_{\text{IP}}}{m_{\text{Pl}}} - \frac{qk\sqrt{6\Omega_{\text{IP}}}}{\mu}\right)^{\frac{\mu}{\nu}}\right], \quad (8.37)$$

and we finally find

$$t_{\text{GB}} = \left(\frac{-\nu t_{\text{IP}}^\mu}{kq\sqrt{6\Omega_{\text{IP}}}} W\left[\left(\frac{4kqG_0(k-1)}{t_{\text{IP}}^2}\right)^{\frac{\mu}{\nu}} kq\sqrt{6\Omega_{\text{IP}}^{2/\nu}} \times \exp\left(\frac{-q\phi_{\text{IP}}}{m_{\text{Pl}}} - \frac{qk\sqrt{6\Omega_{\text{IP}}}}{\mu}\right)^{\frac{\mu}{\nu}}\right]\right)^{\frac{1}{\mu}}. \quad (8.38)$$

Defining two final constants

$$A = \frac{\sqrt{6\Omega_{\text{IP}}} t_{\text{IP}}^{-\mu}}{4k(1-k)qG_0} \exp\left(\frac{q\phi_{\text{IP}}}{m_{\text{Pl}}} + \frac{qk\sqrt{6\Omega_{\text{IP}}}}{\mu}\right), \quad (8.39)$$

$$B = \frac{-kq\sqrt{6\Omega_{\text{IP}}}}{\mu t_{\text{IP}}^\mu}, \quad (8.40)$$

simplifies Eq. (8.38) considerably to the form:

$$t_{\text{GB}} = \left( \frac{\nu}{B\mu} W \left[ \frac{B\mu}{\nu} \left( \frac{1}{A} \right)^{\frac{\mu}{\nu}} \right] \right)^{\frac{1}{\mu}}. \quad (8.41)$$

In the region  $-e^{-1} < x < 0$ , the Lambert W function has two branches (shown in Fig. 5.7). This implies there are two times at which the GB and second derivative contributions to the Klein-Gordon equation are equal, but of course only the earlier time of the two solutions is valid<sup>1</sup>, as Eq. (8.25) is only valid up until the GB contribution first becomes important.

Typically it is the lower ( $W_{-1}$ ) branch of the function which evaluates to the relevant value, but in cases such as those where the lower branch yields  $t_{\text{GB}} < t_{\text{IP}}$ , we instead use the principal ( $W_0$ ) branch solution. The former solution is ruled out physically because instant preheating must happen before GB-domination in order to recover a viable late-time universe.

If there is no real solution to Eq. (8.41) this physically corresponds to there being no time of equality between the kinetic and GB terms in the Klein-Gordon equation. This implies that either the GB term is already dominant at  $t_{\text{IP}}$ , or that the field remains kinetic-dominated forever. Both cases are undesirable as they do not correspond to late-time dark energy. In the former the field freezes too soon after inflation and its density is not reduced to that of dark energy. In the second case, conventional quintessential inflation is recovered, with no contribution from the GB term and the model is trivial.

The reality of Eq. (8.41) is hence an important check that we are looking at feasible models. In particular, the argument of the Lambert W function must satisfy

$$\frac{B\mu}{\nu} \left( \frac{1}{A} \right)^{\frac{\mu}{\nu}} \geq -\frac{1}{e}, \quad (8.42)$$

to have at least one real value.

Substituting the value of  $t_{\text{GB}}$  into Eq. (8.25) allows us to determine  $\phi_{\text{GB}}$ , and in turn this allows us to determine  $\phi(t)$  for  $t \gg t_{\text{GB}}$  by substituting that into

---

<sup>1</sup>Provided it obeys  $t_{\text{GB}} > t_{\text{IP}}$ .

Eq. (8.27). Doing so, we obtain

$$\phi_m = \phi(t \gg t_{\text{GB}}) \approx \phi_{\text{IP}} + \frac{m_{\text{Pl}} B}{q} (t_{\text{GB}}^\mu - t_{\text{IP}}^\mu) + \frac{m_{\text{Pl}}}{q} \ln \left( 1 + \frac{\mu B}{2} t_{\text{GB}}^\mu \right), \quad (8.43)$$

which is the value we expect the field to freeze to in a matter-dominated Universe. Now that we have the dynamics outlined we assess the period of reheating which occurs after the end of inflation, before radiation domination.

## 8.5 Reheating

As is usual in a model of QI, Gauss-Bonnet Quintessential Inflation is unsuitable for perturbative reheating [86, 206], as no oscillatory behaviour about a potential minimum exists. Around  $\phi = 0$ , when the inflaton is kinetically dominated, we instead implement instant preheating (see Section 2.7.3 and [87, 88, 205]) to recover a radiation-dominated epoch. We assume the typical coupling between the inflaton and a matter field  $\chi$ , detailed in Section 2.7.3, which leads to the production of  $\chi$  particles with total energy density (repeated from Eq. (2.212)):

$$\rho_\chi^{\text{IP}} = \frac{g^{5/2} |\dot{\phi}_{\text{IP}}|^{3/2} \phi_{\text{IP}}}{8\pi^3}, \quad (8.44)$$

which we assume to subsequently decay efficiently into radiation.

In instant preheating, particle production occurs explosively around the time when the non-adiabaticity condition,  $|\dot{m}_\chi| > m_\chi^2$ , is first satisfied, where (from Eq. (2.208))  $m_\chi \approx g|\phi|$ . We hence take this to be the time of instant preheating,  $\phi_{\text{IP}}$ , and determine when this occurs via a numerical integration of Eqs. (8.6) and (8.8) for a short time after the end of inflation.

For instant preheating to induce radiation domination, it is necessary that  $\rho_\chi$  is greater than  $\rho_\phi$  after instant preheating. Denoting the energy density of  $\phi$  before and after instant preheating occurs as  $\rho_{\phi,b}$  and  $\rho_{\phi,a}$ , respectively, we hence impose

$$\rho_\chi > \rho_{\phi,a} \quad \Rightarrow \quad \rho_\chi > \frac{1}{2} \rho_{\phi,b}, \quad (8.45)$$

where by energy conservation we require  $\rho_{\phi,a} = \rho_{\phi,b} - \rho_\chi$ .

After instant preheating, we also want the dynamics of the  $\phi$  field to be dominated by its kinetic energy density, because a potential-dominated inflaton field will quickly come to dominate again, thereby terminating the radiation-dominated epoch. As a result, we wish for the kinetic energy density of the inflaton after instant preheating to be greater than its potential. Considering that the potential remains constant<sup>1</sup> throughout instant preheating (i.e.  $V(\phi_{\text{IP}}) = V_a = V_b$ ), this means we want

$$\rho_{\phi,a} - V(\phi_{\text{IP}}) > V(\phi_{\text{IP}}) \quad \Rightarrow \quad \rho_\chi < \rho_{\phi,b} - 2V(\phi_{\text{IP}}), \quad (8.46)$$

where again we consider energy conservation. Combining the inequalities in Eqs. (8.44) and (8.46), we obtain the range of suitable  $\rho_\chi$  values

$$\frac{1}{2}\rho_{\phi,b} < \rho_\chi < \rho_{\phi,b} - 2V(\phi_{\text{IP}}). \quad (8.47)$$

This result implies that the implementation of instant preheating will only be able to succeed when it occurs at a sufficiently kinetic-dominated moment in the evolution of the inflaton. From Eq. (8.47), we find the constraint

$$\rho_{\text{kin},b} > 3V(\phi_{\text{IP}}). \quad (8.48)$$

The potential must hence be sufficiently steep that the field rolls fairly quickly after inflation. Constraints on the model parameters arising from this requirement are discussed in Section 8.7.

## 8.6 Dark Energy Today

Having confirmed that the behaviour of the field is sensible in the matter-dominated epoch and that we can suitably reheat the Universe in between, we proceed to

---

<sup>1</sup>Note that during instant preheating, it is purely kinetic energy density that is converted to radiation.

estimate the value it takes today. To recap, we have solutions for the EoM which are valid independently in the regimes  $t \ll t_{\text{GB}}$  (Eq. (8.25)),  $t \gg t_{\text{GB}}$  (Eq. (8.43)) and a late-Universe static solution when  $\Omega_m \ll 1$  (Eq. (8.20)), where  $t_{\text{GB}}$  is defined to be the time when the equality in Eq. (8.22) is obeyed, calculated in Eq. (8.41).

However, the Universe is not presently in a state of  $\Omega_{\text{DE}} \simeq 1$  or  $\Omega_m \simeq 1$ , but somewhere in between. In this picture, the past state of perfect matter domination assumed in the calculations of Section 8.4.3 is when  $\Omega_m = 1$  and  $\Omega_{\text{DE}} = 0$ . The future dark energy domination which is eventually reached by this model as matter dilutes and it tends to the static solution in Eq. (8.20) corresponds to  $\Omega_{\text{DE}} = 1$  and  $\Omega_m = 0$ , while the present day values  $\Omega_{\text{DE}} \approx 0.7$  and  $\Omega_m \approx 0.3$  indicate exactly where between these two limits we must presently lie.

We formalise this by noting that the effective equation of state of the Universe  $w = p/\rho$  and the derivative of the Hubble Parameter are related via the second Friedmann equation in Eq. (8.7) such that

$$m_{\text{Pl}}^2 \dot{H} = -\frac{1}{2}(\rho + p) = -\frac{1}{2}(1 + w)\rho = -\frac{3}{2}(1 + w)H^2 m_{\text{Pl}}^2. \quad (8.49)$$

This can be used to rewrite the Klein-Gordon equation for the Gauss-Bonnet coupled field given in Eq. (8.8) as

$$\ddot{\phi} + 3H\dot{\phi} + V' - 6H^4(1 + 3w)G'm_{\text{Pl}}^2 = 0, \quad (8.50)$$

which, under the slow-roll approximation  $\ddot{\phi} \simeq 0$ , is approximated by

$$\dot{\phi} \approx 2H^3(1 + 3w)G'm_{\text{Pl}}^2 - \frac{V'}{3H}. \quad (8.51)$$

Substituting this into the Friedman equation in the form

$$3H^2 m_{\text{Pl}}^2 \Omega_{\text{DE}} = \frac{1}{2}\dot{\phi}^2 + V + 12m_{\text{Pl}}^2 H^3 G' \dot{\phi}, \quad (8.52)$$

where  $\Omega_{\text{DE}}$  is the dark energy fraction, we obtain the approximate constraint

equation

$$V + \frac{V'^2}{18H^2} + \left( 3\Omega_{\text{DE}} + \frac{2}{3}(7 + 3w)V'G' \right) m_{\text{Pl}}^2 H^2 + 2(1 + 3w)(13 + 3w) (m_{\text{Pl}}^2 G')^2 H^6 = 0. \quad (8.53)$$

As a consistency check, upon substituting  $w = -1$ ,  $\Omega_{\text{DE}} = 1$  and  $3H^2 m_{\text{Pl}}^2 = V$ , representing perfect dark energy domination, solutions of Eq. (8.53) yield  $\phi = \phi_s$  as in Eq. (8.20), as expected, and in this limit Eq. (8.51) unsurprisingly reduces to  $\dot{\phi} = 0$ .

Rewriting Eq. (8.53) in terms of the explicit potentials of our model (assuming  $p\phi \ll 0$ ) in the form

$$V_0 e^{2p\phi_{\text{DE}}/m_{\text{Pl}}} + \frac{2p^2 V_0^2}{9H^2 m_{\text{Pl}}^2} e^{4p\phi_{\text{DE}}/m_{\text{Pl}}} + 2q^2 G_0^2 m_{\text{Pl}}^2 H^6 (1 + 3w)(13 + 3w) e^{-2q\phi_{\text{DE}}/m_{\text{Pl}}} + \frac{4}{3} qp G_0 V_0 H^2 (7 + 3w) e^{(2p-q)\phi_{\text{DE}}/m_{\text{Pl}}} - 3H^2 m_{\text{Pl}}^2 \Omega_{\text{DE}} = 0, \quad (8.54)$$

the constraint can be solved for  $\phi_{\text{DE}}$  to identify the field value necessary to achieve a specific equation of state  $w$ , dark energy fraction  $\Omega_{\text{DE}}$  and expansion rate  $H$  for a given model, specified by  $p$  and  $q$ .

Assuming that following matter-domination, the Universe contains only matter and the dark energy field, we have from observations that  $w = w_{\text{DE}} \Omega_{\text{DE}} \approx -0.7$ , and  $H_0 \approx 10^{-60} m_{\text{Pl}}$ . We use these observational values to solve Eq. (8.54) numerically and the results are presented in Section 8.7.

Interestingly, we typically find for most parameters that the  $\phi_m$  value calculated in Section 8.4.3 is larger in magnitude (more negative) than the  $\phi_{\text{DE}}$  value obtained in the above procedure. It turns out that the time at which the  $\phi_m$  solution should be reached,  $t_{\text{GB}}$  (defined in Eq. (8.41)) is very large - much greater than the age of the Universe today. We also find that earlier-time solutions of Eq. (8.54) with  $\Omega_{\text{DE}} < 0.7$  are typically found to be larger in magnitude than the  $\phi_{\text{DE}}$  value today at  $\Omega_{\text{DE}} = 0.7$ . Furthermore,  $\phi_s$ , which is achieved at later times when  $\Omega_{\text{DE}} \rightarrow 1$ , is smaller in magnitude (less negative) than  $\phi_{\text{DE}}$  today in the particular cases we have investigated in depth. These observations seem to

suggest that the field is rolling ‘backwards’ during the transition between matter and dark energy domination.

We deduce that the field does not typically freeze during matter domination, instead slowly-rolling towards, but not reaching,  $\phi_m$ . It overshoots  $\phi_{\text{DE}}$  but then turns around due to the impeding effects of the GB coupling. At present, the field is envisaged to be in a state of slowly rolling from  $\phi_{\text{DE}}$  to  $\phi_s$ .

This may not be true for all models; we do not exclude the possibility that some parameters may lead to the change in direction only occurring after  $\phi_m$ , or not at all.

## 8.7 Constraints and Results

Having established the nature of inflation, reheating and dark energy in the framework of our model, we now proceed to constrain the parameter space to realistic values. We numerically integrate the background equations of motion during inflation for a range of models (specified by their  $p$ ,  $q$ ,  $g$  and  $G_0$  values). Using these results we compute the energy density resulting from instant preheating, the behaviour of the field in matter domination, the field value today, and the far-future field value  $\phi_s$ . There are two main constraints which control the allowed combinations of the model parameters. Instant preheating should satisfy the conditions in Eq. (8.47) for a sensible choice of the perturbative coupling to matter  $g$  (i.e.  $g \leq 1$ ) and the field value today,  $\phi_{\text{DE}}$ , should be sub-Planckian ( $|\phi_{\text{DE}}| < m_{\text{Pl}}$ ) such that unknown UV physics do not strongly influence our results.

Examples of these constraints as a function of the parameter  $p$  for the case  $q = 4p$ ,  $G_0 m_{\text{Pl}}^2 = 1$  and  $g = 0.8$  are shown in Fig. 8.1. The former shows that we must have  $p > 86$  to avoid super-Planckian field values today, while the latter shows that instant preheating may not proceed according to the requirements in Eq. (8.47) unless  $p < 100$ . We tabulate the allowed parameter space of  $86 < p < 100$  for this case, alongside many other models with different  $q$ ,  $G_0$  and  $g$  values, in Table 8.1.

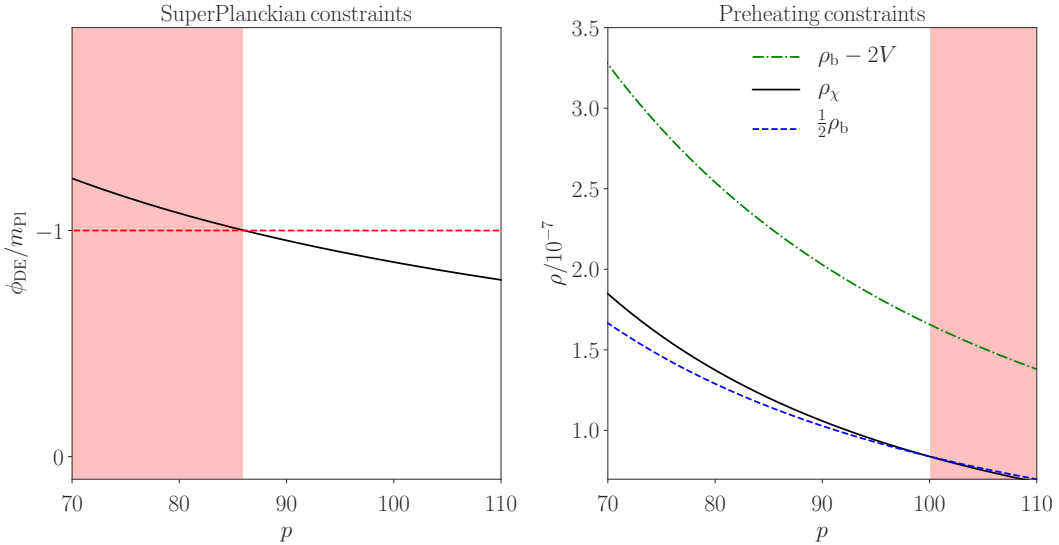


**Figure 8.1:** Constraints for a model with  $q = 4p$ ,  $G_0 m_{\text{Pl}}^2 = 1$  and  $g = 0.8$ . The left window shows the value of  $\phi_{\text{DE}}$  for a range of  $p$  values and the red shaded region represents the parameter space where  $\phi_{\text{DE}}$  is super-Planckian. The right window shows the energy densities involved in the instant preheating conditions of Eq. (8.47). The black solid line represents  $\rho_\chi$ , while the blue dashed line and green dot-dashed line respectively represent the lower and upper bounds that  $\rho_\chi$  must lie between. The shaded region on the right encloses the  $p$  values for which these inequalities are violated.

### 8.7.1 Gravitational Waves in Gauss-Bonnet

#### Gravity

As noted in the introduction of this chapter, the recent observation of a multi-messenger gravitational wave and gamma ray burst signal [155] observed that the gravitational waves and electromagnetic waves emitted by a binary neutron star merger reached detectors on Earth at exactly the same time, confirming to very high precision that the waves travel at the same speed, meaning  $c_T = 1$ .

Models with a non-trivial GB-coupling at late-times predict a deviation from  $c_T = 1$ , common to all Horndeski theories. The derivation is detailed in Ref. [210] and produces

$$c_T^2 = \frac{1 + 4\ddot{G}}{1 + 4H\dot{G}}, \quad (8.55)$$

$G_0 m_{\text{Pl}}^2$	$q/p$	$g$	$p$ limits
1	4	0.8	$86 < p < 100$
		0.9	$86 < p < 238$
		1	$86 < p < 507$
	8	0.8	$51 < p < 100$
		0.9	$51 < p < 207$
		1.0	$51 < p < 370$
100	4	0.8	$85 < p < 100$
		0.9	$85 < p < 238$
		1.0	$85 < p < 507$
	8	0.8	$51 < p < 72$
		0.9	$51 < p < 155$
		1.0	$51 < p < 258$

**Table 8.1:** Table showing limits on  $p$  in the theory for various cases of the size of  $G_0$ ,  $q$  and  $g$ , due to constraints coming from sub-Planckian field displacements and instant preheating’s efficacy. In each case, the lower bound on  $p$  occurs as, below this threshold,  $\phi_{\text{DE}}$  would have to undergo a super-Planckian displacement to serve as dark energy today. Similarly, the upper limits on  $p$  arise as, above these limits, the inequality in Eq. (8.47) is violated.

which when calculated for our model gives  $c_T \neq 1$  by a significant margin. In Ref. [210], for a specific late Universe cosmology given in [237], they constrain the coupling strength of the GB term ( $G(\phi)$  in our model) to be of the order of  $10^{-15}$ . In our model with an exponential coupling, this is always violated unless  $G_0$  is unnaturally tiny, in which case the GB term does not have the intended effect of freezing the field to support a dark energy evolution.

Whilst disappointing, it is unsurprising that we find this result, because we specifically choose such a coupling to make the effect of the GB term large at late times, to facilitate a Gauss-Bonnet mediated dark energy. These constraints require the effect of the GB term to be small at late times, in direct contrast with the motivations of the model.

Quintessential inflation models which incorporate modified theories of gravity also need to pass local gravity tests. Constraints on Gauss-Bonnet mediated dark energy theories in the literature [238–240] rely on assumptions which are not applicable in the model presented here and as the model is ruled out by the  $c_T$  constraint we do not investigate them further. Modifications such as screening

mechanisms may help to alleviate any tensions with local gravity constraints but we stress that the local gravity constraints must be considered in any modified gravity theory.

## 8.8 Discussion

This chapter studies a model of quintessential inflation where the inflaton field couples to the Gauss-Bonnet (GB) term. By design, the GB coupling is negligible at early times so inflation proceeds under standard slow-roll. Hence, we consider a scalar potential which features an inflationary plateau, as favoured by the latest CMB observations. Indeed, the scalar spectral index found,  $n_s = 0.968$ , is close to the sweet spot of Planck observations, and we find a tensor amplitude considerably below the current upper bounds.

Following on from the last chapter, this model of quintessential inflation is again non-oscillatory and so we employ the instant preheating mechanism. This successfully reproduces the HBB evolution of the Universe and afterwards, the inflaton field freezes at some value with small residual energy density to play the role of dark energy today. As we have seen previously, because of the huge difference between the energy density scale of inflation and the current energy density, the inflaton field typically rolls over super-Planckian distances in field space, if left unattended.

The research in this chapter overcomes the problems presented by super-Planckian field excursions by making sure the scalar field remains frozen today even though the quintessential tail is steep. To this end, we couple the field with the Gauss-Bonnet term, to impede the variation of the field even if the potential is steep. Thus, in our model the GB coupling becomes important at late times and makes sure the field freezes with sub-Planckian displacement, such that it becomes the dark energy today.

Quintessence is motivated only if the required tuning of the model parameters is less than the extreme fine-tuning of the cosmological constant in  $\Lambda$ CDM. In our model, we have four model parameters, which account for the requirements of both inflation and quintessence. For the GB coupling, shown in Eq. (8.10),

we assume a simple exponential dependence on the inflaton, which ensures the GB coupling becomes important only at late times. The scale of the coupling is  $G_0 \geq m_{\text{Pl}}^{-2}$ , which agrees with our effort to stay sub-Planckian. For our scalar potential, shown in Eq. (8.9), the density scale is set by the COBE constraint to be  $V_0^{1/4} \sim 10^{14}$  GeV, close to the GUT scale. In the exponent of the GB coupling and the argument of the tanh in the scalar potential, the inflaton field is suppressed by a large mass scale  $m_{\text{Pl}}/q$  and  $m_{\text{Pl}}/p$  respectively. We consider  $q \sim p$  and find that  $50 \lesssim p \lesssim 500$  (cf. Table 8.1), which means that, in both the GB coupling and the scalar potential, the inflaton field is suppressed by the scale of grand unification  $\sim 10^{16}$  GeV. Thus, we see that our model parameters avoid the extreme fine-tuning of the cosmological constant in  $\Lambda$ CDM.

We stress that the model presented in this chapter is a prototype to demonstrate the feasibility of a GB coupling impeding the motion of the inflaton in such a way as to facilitate quintessence. Unfortunately, whilst the research presented here was being considered for publication, the LIGO experiment confirmed that gravitational waves travel at the speed of light. The Gauss-Bonnet coupling predicts the opposite. Disappointingly, this rules out the mechanism presented here as a viable form of quintessential inflation. However, we hope that our approach might possibly ignite new ideas for quintessential inflation models of a similar ilk, utilising modified gravity theories that do not suffer from the same problem.

Finally, we highlight two important points prompted by the exciting observations of LIGO. Frontiers in observational astrophysics and cosmology are still being crossed and explored, making this field a thrilling arm of high energy physics. An important aspect of science is that ideas are testable and fallible, and this model of Gauss-Bonnet Quintessential Inflation made a testable prediction. Unfortunately it was found wanting, but the testability of cosmological models is an often overlooked strength.

# Chapter 9

## Conclusion

Primordial inflation elegantly solves the horizon and flatness problems of the Hot Big Bang and explains the origin of the structure in the Universe. The inflationary paradigm predicted a scale-invariant spectrum for the scalar curvature perturbations before it was subsequently detected, which cemented its place as a foundation of the modern concordance model of cosmology. Whilst the inflationary scenario deftly solves existing problems, predictions in many different model realisations can be aligned with current observational constraints and there is no model which rises above the others to be a clear forerunner as *the* model of inflation. Chapters 3 to 5 present three models of inflation which are all in excellent agreement with the Planck observations and successfully offer a possible mechanism for cosmic inflation.

The family of inflationary models in Chapter 3 approach the inflationary plateau in a power-law manner, in contrast to most models in the literature which have an exponential approach. We investigate super-Planckian field variations which leads us to embed the model in supergravity. We find the tensor-to-scalar ratio is enhanced to potentially observable scales. This, along with the power-law approach distinguishes the predictions, which could potentially be singled out by future observations.

In Chapter 4 we utilise a period of thermal inflation, after primordial inflation and reheating, to allow the e-foldings of primordial inflation since observable

---

scales left the horizon to be reduced. This brings the predictions of the model inside the constraints of the Planck satellite, reviving a model which was previously ruled out. This is motivated by the fact that hybrid inflation in minimal supergravity is a theoretically robust model because it is able to naturally evade the  $\eta$  problem which plagues inflationary models in supergravity. Whilst hybrid inflation utilises two scalar fields, the secondary ‘waterfall’ field is generally expected to be the GUT Higgs field, therefore the model is still very minimal.

Chapter 5 builds on models of inflection-point inflation in the literature, managing to alleviate the fine-tuning of A-term inflation by approximately fourteen orders of magnitude. We form a plateau in the potential via the interplay of a Coleman-Weinberg term and higher order non-renormalisable terms, which generate an inflection point. We constrain the deviation from a flat inflection point with the  $2\sigma$  observations of the spectral index of scalar curvature perturbations from the Planck satellite. The model in this chapter, whilst involving slightly more fine-tuning than power-law plateau inflation or hybrid inflation in minimal supergravity, is motivated by the absence of any exotic beyond-the-standard-model physics.

After inflation ends, the Universe reheats into the Hot Big Bang, a process during which the energy density of the inflaton field is transferred into the particles of the standard model. This can be a very intricate process and its nuances are still not fully understood. However, the duration of reheating, described by the reheating temperature, has a key implication that we do understand, it directly impacts the e-folds of inflation since observable scales left the horizon. This parameter is important because it features in most model predictions for the inflationary observables; the spectral index of scalar curvature perturbations and the tensor-to-scalar ratio, which allow us to compare and contrast models with observations.

The research in Chapter 6 differs from the rest of the thesis in that it does not specify a particular model of inflation. In fact, the results are completely independent of any inflation model, as long as inflation is followed by a period of perturbative reheating. Instead, the implications of a sub-dominant reheating bath on the formation rate of primordial black holes is investigated. We assume the reheating temperature is low and before radiation domination begins the

---

inflaton oscillates about a quadratic minimum, which is a general prediction for many reheating mechanisms, resulting in a period of effective matter domination. This is conducive to the formation of primordial black holes which has been noticed in the literature previously. However, previous analyses have taken a sharp cut-off between an effective matter dominated regime during reheating and the radiation dominated regime that follows it, resulting in a sharp suppression at the end of reheating for primordial black hole formation. However, we show in this research that the sub-dominant thermal bath slowly grows during reheating, resulting in a continuous transition between the two regimes. The restorative pressure effects of the radiation are felt earlier and therefore the primordial black hole formation rate is suppressed earlier. We demonstrate that this truncates the mass spectrum of produced primordial black holes.

The  $\Lambda$ CDM model explains observations throughout the radiation and matter dominated epochs of the Universe very well. For the mechanism generating the present day accelerated expansion of the Universe,  $\Lambda$ CDM invokes Einstein's cosmological constant, an un-diluting source of negative pressure which permeates all space-time. If this is associated with the energy density of the vacuum then  $\Lambda$ CDM runs into its first fine-tuning problem. The observed value of the cosmological constant is many orders of magnitude smaller than particle physics estimates of the vacuum energy density. To resolve this it is commonly assumed that the vacuum energy density is zero due to some unknown symmetry, leaving the cosmological constant (or dark energy in any form) free to take any value. The fact that this value only varies from zero at the 84th decimal place is fine-tuning to a staggering degree. This is the main motivation behind quintessence models of dark energy, which strive to explain the dark energy observations with a dynamical scalar field instead.

However, a quintessence field effectively shifts the fine-tuning problem from one of magnitude to one of initial conditions. The research in Chapters 7 and 8 therefore opts instead for models of quintessential *inflation*. Quintessential inflation models use a single theoretical framework to describe the primordial and late-time accelerated expansion; a single dynamical scalar field. Quintessential inflation models do not suffer from the same fine-tuning of initial conditions because they follow the inflationary attractor which naturally provides the initial

---

conditions. Both quintessential inflation models presented here take pains to avoid super-Planckian field excursions, which could threaten the flatness of the potential and give rise to long-range forces which we do not observe.

Chapter 7 extends the  $\alpha$ -attractors framework used for inflation models to include quintessence as well. The model very successfully replicates the Planck observables, as all  $\alpha$ -attractor models do. A simple exponential potential, which ensures the attractive minimality of quintessential inflation is not lost in the conception of the model, provides a late-time plateau which supports late-time accelerated expansion. After inflation, when the field is dominated by its kinetic energy density, we solve the equations of motion analytically to determine the point at which it freezes in field space, which is heavily influenced by the details of reheating. We conduct a detailed investigation into reheating, investigating two mechanisms; gravitational reheating and instant preheating.

Gravitational reheating is the most minimal approach to reheating because it requires no additional couplings for the field, but due to its inefficiency it produces a large spike in the amount of gravitational waves produced, which is a by-product of a prolonged period of kination. This may be at odds with observational constraints so we investigate instant preheating as well. Gravitational reheating is calculated analytically but instant preheating requires computational techniques to follow the evolution of the field and determine the point at which instant preheating occurs. The parameter space is constrained by the dark energy observations, most notably the equation of state parameter of the Universe and of the scalar field. The parameter space is suitably enlarged if supergravity constraints can be neglected, which we are careful to compute for both reheating mechanisms; namely the gravitino production, which depends on the reheating temperature. We also compute the backreaction constraints which arise, but these are very model dependent, depending on the subsequent decay channels and rates of the inflaton decay products.

Chapter 8 takes a very different approach to realise a model of quintessential inflation. The main stumbling block for any model of quintessential inflation is that super-Planckian field excursions are generally unavoidable if the potential is to be flat enough at late-times for accelerated expansion to proceed. In this research we utilise the Gauss-Bonnet model of modified gravity to invoke a

---

coupling at late times between the scalar field and the Gauss-Bonnet combination of quadratic curvature scalars. This acts to impede the inflaton's motion at late times via a lifted effective potential, which stops the field having a super-Planckian variation in field space.

The research in Chapter 7 provides a compelling alternative to  $\Lambda$ CDM and hopefully developments in observational probes will soon be able to distinguish once and for all between dynamical dark energy models and the cosmological constant. Unfortunately, the research in Chapter 8 was recently ruled out after the spectacular LIGO observation which proved that gravitational waves travel at the same speed as light waves. This is not predicted by models with a significant Gauss-Bonnet influence at late-times; which is a necessary requirement of the research presented in Chapter 8, so unfortunately cannot be ameliorated. However, we hope the ideas presented in Chapter 8 highlight the possibility of successfully incorporating some form of modified gravity in a quintessential inflation model to limit the evolution in field space to sub-Planckian values.

The discussion of inflation in this thesis focuses on cold inflation, whereby the inflaton field does not significantly interact with any other particle species and any other matter that may have been present before inflation is inflated away. In contrast, warm inflation supposes that the inflaton field decays substantially to another field during inflation, the decay products are not diluted away because they are constantly being replaced and hence a sub-dominant radiation bath is present during inflation. The inflaton decay introduces an extra friction term to the Klein-Gordon equation, which impedes the motion of the inflaton in field space. The extra friction term means that warm inflation allows a greater range of steep scalar field potentials to facilitate slow-roll inflation.

On-going further work by the author [241] investigates the possibility of utilising warm inflation to develop a quintessential inflation model. Starting with a potential which naturally features a suitable plateau for late-time accelerated expansion, incorporating warm inflation couplings allows for primordial inflation on the section of the potential which would traditionally be too steep to facilitate it.

As stressed in this thesis, a framework which can describe both early and late time periods of accelerated expansion without needing to invoke too many extra

---

degrees of freedom or elaborate field-theory constructions is appealing. Warm inflation has been widely investigated in the literature and it is natural to consider a radiation bath might be present during inflation [84, 242–245]. In light of the recent swampland conjectures, warm inflation is particularly pertinent because of its ability to support slow-roll without violating the conjectures [246].

Additional on-going work by the author [247] investigates the trapping mechanism which occurs when the inflaton crosses an enhanced symmetry point (ESP) [248]. The couplings between the inflaton and the decay particles generate a pseudo-linear effective potential which the inflaton becomes trapped in. This mechanism of trapping the inflaton stops its kinetically dominated motion to large field values, which is otherwise present after inflation ends. At some symmetry breaking scale, the decay field (previously held at the origin) moves to its vacuum expectation value and provides a large contribution to the inflaton’s mass, meaning it is still held at the ESP until late times. At late-times the inflaton’s energy density dominates the Universe again, providing the mechanism for the dark energy. If the decay field is the Pecci-Quinn field then the QCD phase transition will give rise to the QCD axion which is a CDM candidate. This would mean the model describes inflation, dark matter and dark energy all in one, making it a very appealing model.

The breadth of research presented in this thesis also leaves avenues of the research open for further study. The research into the formation rate of primordial black holes in Chapter 6, combined with the analysis of QI models, raises another formation rate question: how does a period of kination affect primordial black hole production? During kination the pressure is more substantial than radiation domination, so a suppression in the formation rate compared to both the radiation dominated era and an effective matter dominated era during reheating would be expected. However, the formulation of a description of the Jeans length and the entailing calculation is expected to be very complex, as the scalar field during kination does not have an obvious particle interpretation. With the swampland conjectures favouring a late-time quintessence explanation for dark energy and QI models being the most economical way to describe inflation with the same mechanism, it is imperative to understand all of the implications of these models.

---

The research presented in this thesis is the result of several fruitful collaborations and the author would like to highlight the following specific contributions from collaborators. In Chapter 6, the calculation of the mass function was undertaken by Tommi Tenkanen. The computation of the bounds on  $w$  arising from dark energy observations in Section 7.5.1 were primarily carried out by Leonora Donaldson Wood. In Chapter 8, the analytical solutions to the Klein-Gordon equation in the various evolution regimes were derived by Chris Longden. The theoretical overview in Chapters 5, 6 and 8 received significant contributions from Antonio Racioppi, Bernard Carr and Carsten van de Bruck respectively, and Konstantinos Dimopoulos provided invaluable theoretical contributions to all of the research throughout this thesis. The author again expresses her gratitude to all collaborators for the involvement in exciting projects and the warm welcome she received from the cosmology community.

---

## References

- [1] Y. Akrami et al. Planck 2018 Results. X. Constraints on Inflation. 2018.
- [2] B. J. Carr, Kazunori Kohri, Yuuiti Sendouda, and Jun'ichi Yokoyama. New Cosmological Constraints on Primordial Black Holes. *Phys. Rev.*, D81:104019, 2010.
- [3] Patrick Peter and Jean-Philippe Uzan. *Primordial Cosmology*. Oxford University Press, 2009.
- [4] N. Aghanim et al. Planck 2018 Results. VI. Cosmological Parameters. 2018.
- [5] E. Hubble. A Relation between Distance and Radial Velocity among Extra-Galactic Nebulae. *Proceedings of the National Academy of Science*, 15:168–173, March 1929.
- [6] Roger Penrose. Gravitational collapse and space-time singularities. *Phys. Rev. Lett.*, 14:57–59, Jan 1965.
- [7] Sheldon L. Glashow. Partial-symmetries of weak interactions. *Nuclear Physics*, 22(4):579 – 588, 1961.
- [8] Abdus Salam and J. C. Ward. Weak and electromagnetic interactions. *Il Nuovo Cimento (1955-1965)*, 11(4):568–577, Feb 1959.
- [9] Steven Weinberg. A model of leptons. *Phys. Rev. Lett.*, 19:1264–1266, Nov 1967.
- [10] Harald Fritzsch and Peter Minkowski. Unified interactions of leptons and hadrons. *Annals of Physics*, 93(1):193 – 266, 1975.
- [11] Jogesh C. Pati and Abdus Salam. Lepton number as the fourth "color". *Phys. Rev. D*, 10:275–289, Jul 1974.
- [12] Howard Georgi and S. L. Glashow. Unity of all elementary-particle forces. *Phys. Rev. Lett.*, 32:438–441, Feb 1974.

- 
- [13] Edward Witten. String Theory Dynamics in Various Dimensions. *Nucl. Phys.*, B443:85–126, 1995. [,333(1995)].
- [14] S. S. Gubser, Igor R. Klebanov, and Alexander M. Polyakov. Gauge Theory Correlators from Noncritical String Theory. *Phys. Lett.*, B428:105–114, 1998.
- [15] Shamit Kachru, Renata Kallosh, Andrei D. Linde, and Sandip P. Trivedi. De Sitter Vacua in String Theory. *Phys. Rev.*, D68:046005, 2003.
- [16] Hans Peter Nilles. Supersymmetry, Supergravity and Particle Physics. *Phys. Rept.*, 110:1–162, 1984.
- [17] Carlo Rovelli and Lee Smolin. Loop Space Representation of Quantum General Relativity. *Nucl. Phys.*, B331:80–152, 1990.
- [18] Carlo Rovelli and Lee Smolin. Knot theory and quantum gravity. *Phys. Rev. Lett.*, 61:1155–1158, Sep 1988.
- [19] Carlo Rovelli. Loop Quantum Gravity. *Living Rev. Rel.*, 1:1, 1998.
- [20] John Archibald Wheeler. Geons. *Phys. Rev.*, 97:511–536, Jan 1955.
- [21] Georges Aad et al. Observation of a New Particle in the Search for the Standard Model Higgs Boson with the ATLAS Detector at the LHC. *Phys. Lett.*, B716:1–29, 2012.
- [22] Serguei Chatrchyan et al. Observation of a New Boson at a Mass of 125 GeV with the CMS Experiment at the LHC. *Phys. Lett.*, B716:30–61, 2012.
- [23] P. J. E. Peebles. Recombination of the Primeval Plasma. *Astrophysical Journal*, 153:1, July 1968.
- [24] B. J. T. Jones and R. F. G. Wyse. The Ionisation of the Primeval Plasma at the Time of Recombination. *Astronomy and Astrophysics*, 149:144–150, August 1985.
- [25] Arno A. Penzias and Robert Woodrow Wilson. A Measurement of Excess Antenna Temperature at 4080-Mc/s. *Astrophys. J.*, 142:419–421, 1965.

- 
- [26] R. A. Alpher and R. Herman. Evolution of the Universe. *Nature*, 162:774–775, November 1948.
- [27] G. Gamow. The evolution of the universe. *Nature*, 162:680, 1948.
- [28] R. H. Dicke, P. J. E. Peebles, P. G. Roll, and D. T. Wilkinson. Cosmic Black-Body Radiation. *Astrophysical Journal*, 142:414–419, July 1965.
- [29] Wayne Hu and Scott Dodelson. Cosmic Microwave Background Anisotropies. *Ann. Rev. Astron. Astrophys.*, 40:171–216, 2002.
- [30] S. Perlmutter et al. Measurements of Omega and Lambda from 42 high redshift supernovae. *Astrophys. J.*, 517:565–586, 1999.
- [31] Adam G. Riess et al. Observational Evidence from Supernovae for an Accelerating Universe and a Cosmological Constant. *Astron. J.*, 116:1009–1038, 1998.
- [32] Albert Einstein. On the Electrodynamics of Moving Bodies. *Annalen Phys.*, 17:891–921, 1905. [Annalen Phys.14,194(2005)].
- [33] Albert Einstein. The Foundation of the General Theory of Relativity. *Annalen Phys.*, 49(7):769–822, 1916. [Annalen Phys.354,no.7,769(1916)].
- [34] S. Weinberg. *Gravitation and Cosmology: Principles and Applications of the General Theory of Relativity*. July 1972.
- [35] R. R. Caldwell. A Phantom Menace? *Phys. Lett.*, B545:23–29, 2002.
- [36] J. C. Mather, E. S. Cheng, R. E. Eplee, Jr., et al. A preliminary Measurement of the Cosmic Microwave Background Spectrum by the Cosmic Background Explorer (COBE) Satellite. *Astrophysical Journal, Part 2 - Letters*, 354:L37–L40, May 1990.
- [37] C. L. Bennett et al. Nine-Year Wilkinson Microwave Anisotropy Probe (WMAP) Observations: Final Maps and Results. *Astrophys. J. Suppl.*, 208:20, 2013.

- 
- [38] Ade, P. A. R. and others. Planck early results. i. the planck mission. *A&A*, 536:A1, 2011.
- [39] F. Lucchin and S. Matarrese. Power-law inflation. *Phys. Rev. D*, 32:1316–1322, Sep 1985.
- [40] Maximo Banados, Claudio Teitelboim, and Jorge Zanelli. The Black Hole in Three-dimensional Space-time. *Phys. Rev. Lett.*, 69:1849–1851, 1992.
- [41] Tirthabir Biswas and Anupam Mazumdar. Inflation with a Negative Cosmological Constant. *Phys. Rev.*, D80:023519, 2009.
- [42] Katy Clough, Eugene A. Lim, Brandon S. DiNunno, et al. Robustness of Inflation to Inhomogeneous Initial Conditions. *JCAP*, 1709(09):025, 2017.
- [43] Justin Khoury, Burt A. Ovrut, Paul J. Steinhardt, and Neil Turok. The Ekpyrotic universe: Colliding Branes and the Origin of the Hot Big Bang. *Phys. Rev.*, D64:123522, 2001.
- [44] R. Brandenberger and C. Vafa. Superstrings in the early universe. *Nuclear Physics B*, 316(2):391 – 410, 1989.
- [45] M. Novello and S. E. Perez Bergliaffa. Bouncing Cosmologies. *Phys. Rept.*, 463:127–213, 2008.
- [46] A. D. Sakharov. The Initial Stage of an Expanding Universe and the Appearance of a Nonuniform Distribution of Matter. *Soviet Journal of Experimental and Theoretical Physics*, 22:241, January 1966.
- [47] V. F. Mukhanov and G. V. Chibisov. Quantum Fluctuations and a Nonsingular Universe. *ZhETF Pisma Redaktsiiu*, 33:549–553, May 1981.
- [48] Viatcheslav F. Mukhanov and G. V. Chibisov. The Vacuum Energy and Large Scale Structure of the Universe. *Sov. Phys. JETP*, 56:258–265, 1982. [*Zh. Eksp. Teor. Fiz.*83,475(1982)].

- 
- [49] A. A. Starobinsky. Dynamics of Phase Transition in the New Inflationary Universe Scenario and Generation of Perturbations. *Physics Letters B*, 117:175–178, November 1982.
- [50] Alan H. Guth and S. Y. Pi. Fluctuations in the New Inflationary Universe. *Phys. Rev. Lett.*, 49:1110–1113, 1982.
- [51] S. W. Hawking. The Development of Irregularities in a Single Bubble Inflationary Universe. *Phys. Lett.*, 115B:295, 1982.
- [52] James M. Bardeen, Paul J. Steinhardt, and Michael S. Turner. Spontaneous Creation of Almost Scale - Free Density Perturbations in an Inflationary Universe. *Phys. Rev.*, D28:679, 1983.
- [53] James M. Bardeen. Gauge Invariant Cosmological Perturbations. *Phys. Rev.*, D22:1882–1905, 1980.
- [54] Jérôme Martin, Christophe Ringeval, Roberto Trotta, and Vincent Vennin. The Best Inflationary Models after Planck. *JCAP*, 1403:039, 2014.
- [55] P. A. R. Ade et al. Planck 2013 results. XXII. Constraints on inflation. *Astron. Astrophys.*, 571:A22, 2014.
- [56] Renata Kallosh and Andrei Linde. Universality Class in Conformal Inflation. *JCAP*, 1307:002, 2013.
- [57] John Ellis, D.V. Nanopoulos, Keith A. Olive, and K. Tamvakis. Cosmological inflation cries out for supersymmetry. *Physics Letters B*, 118(4):335 – 339, 1982.
- [58] Stephen P. Martin. A Supersymmetry Primer. pages 1–98, 1997. [Adv. Ser. Direct. High Energy Phys.18,1(1998)].
- [59] Bruno Zumino. Supersymmetry and the Vacuum. *Nucl. Phys.*, B89:535, 1975.
- [60] E. Cremmer, B. Julia, Joel Scherk, et al. Super-higgs Effect in Supergravity with General Scalar Interactions. *Phys. Lett.*, 79B:231–234, 1978.

- 
- [61] Riccardo Barbieri, S. Ferrara, Dimitri V. Nanopoulos, and K. S. Stelle. Supergravity, R Invariance and Spontaneous Supersymmetry Breaking. *Phys. Lett.*, 113B:219–222, 1982.
- [62] Edward Witten and Jonathan Bagger. Quantization of Newton’s Constant in Certain Supergravity Theories. *Phys. Lett.*, 115B:202–206, 1982.
- [63] A. A. Starobinskiĭ. Spectrum of Relic Gravitational Radiation and the Early State of the Universe. *Soviet Journal of Experimental and Theoretical Physics Letters*, 30:682, December 1979.
- [64] A.A. Starobinsky. A new type of isotropic cosmological models without singularity. *Physics Letters B*, 91(1):99 – 102, 1980.
- [65] A. H. Guth. Inflationary Universe: A Possible Solution to the Horizon and Flatness Problems. *Physical Review D*, 23:347–356, January 1981.
- [66] A. D. Linde. A New Inflationary Universe Scenario: A Possible Solution of the Horizon, Flatness, Homogeneity, Isotropy and Primordial Monopole Problems. *Physics Letters B*, 108:389–393, February 1982.
- [67] A. Albrecht and P. J. Steinhardt. Cosmology for Grand Unified Theories with Radiatively Induced Symmetry Breaking. *Physical Review Letters*, 48:1220–1223, April 1982.
- [68] Andrei D. Linde. Chaotic Inflation. *Phys. Lett.*, 129B:177–181, 1983.
- [69] Andrei D. Linde. Initial Conditions for Inflation. *Phys. Lett.*, 162B:281–286, 1985.
- [70] David H. Lyth. What Would we Learn by Detecting a Gravitational Wave Signal in the Cosmic Microwave Background Anisotropy? *Phys. Rev. Lett.*, 78:1861–1863, 1997.
- [71] Georges Obied, Hirosi Ooguri, Lev Spodyneiko, and Cumrun Vafa. De Sitter Space and the Swampland. 2018.

- 
- [72] Hiroshi Ooguri and Cumrun Vafa. On the Geometry of the String Landscape and the Swampland. *Nucl. Phys.*, B766:21–33, 2007.
- [73] Eran Palti. The Swampland: Introduction and Review. 2019.
- [74] Andrei D. Linde. Hybrid Inflation. *Phys. Rev.*, D49:748–754, 1994.
- [75] Ajit M. Srivastava. Topological defects in cosmology. *Pramana*, 53(6):1069–1076, Dec 1999.
- [76] A. Vilenkin and E. P. S. Shellard. *Cosmic Strings and Other Topological Defects*. Cambridge University Press, 2000.
- [77] Edmund J. Copeland, S. Pascoli, and A. Rajantie. Dynamics of tachyonic preheating after hybrid inflation. *Phys. Rev.*, D65:103517, 2002.
- [78] P. A. R. Ade et al. Planck 2013 results. XXV. Searches for cosmic strings and other topological defects. *Astron. Astrophys.*, 571:A25, 2014.
- [79] David H. Lyth and Ewan D. Stewart. Thermal Inflation and the Moduli Problem. *Phys. Rev.*, D53:1784–1798, 1996.
- [80] P. J. Steinhardt. Natural Inflation. In G. W. Gibbons, S. W. Hawking, and S. T. C. Siklos, editors, *Very Early Universe*, pages 251–266, 1983.
- [81] Alexander Vilenkin. Birth of inflationary universes. *Phys. Rev. D*, 27:2848–2855, Jun 1983.
- [82] Andrei D. Linde. Eternal Chaotic Inflation. *Mod. Phys. Lett.*, A1:81, 1986.
- [83] Alan H. Guth. Eternal Inflation and its Implications. *J. Phys.*, A40:6811–6826, 2007.
- [84] Arjun Berera. Warm Inflation. *Phys. Rev. Lett.*, 75:3218–3221, 1995.
- [85] Edward W. Kolb and Michael S. Turner. The Early Universe. *Front. Phys.*, 69:1–547, 1990.
- [86] Lev Kofman, Andrei D. Linde, and Alexei A. Starobinsky. Towards the Theory of Reheating after Inflation. *Phys. Rev.*, D56:3258–3295, 1997.

- 
- [87] Gary N. Felder, Lev Kofman, and Andrei D. Linde. Inflation and Preheating in NO Models. *Phys. Rev.*, D60:103505, 1999.
- [88] A. H. Campos, H. C. Reis, and R. Rosenfeld. Preheating in Quintessential Inflation. *Phys. Lett.*, B575:151–156, 2003.
- [89] L. H. Ford. Gravitational Particle Creation and Inflation. *Phys. Rev.*, D35:2955, 1987.
- [90] John R. Ellis, Andrei D. Linde, and Dimitri V. Nanopoulos. Inflation Can Save the Gravitino. *Phys. Lett.*, 118B:59–64, 1982.
- [91] Masahiro Kawasaki, Fuminobu Takahashi, and T. T. Yanagida. Gravitino Overproduction in Inflaton Decay. *Phys. Lett.*, B638:8–12, 2006.
- [92] Masahiro Kawasaki, Fuminobu Takahashi, and T. T. Yanagida. The Gravitino-overproduction Problem in Inflationary Universe. *Phys. Rev.*, D74:043519, 2006.
- [93] Edmund J. Copeland, M. Sami, and Shinji Tsujikawa. Dynamics of Dark Energy. *Int. J. Mod. Phys.*, D15:1753–1936, 2006.
- [94] G. Gamow. *My World Line; an Informal Autobiography*. Viking Press, 1970.
- [95] J. Barrow and F. Tipler. *The Cosmological Anthropic Principle*. Oxford University Press, 1988.
- [96] Leonard Susskind. The Anthropic Landscape of String Theory. pages 247–266, 2003.
- [97] W. Fischler, A. Kashani-Poor, R. McNees, and S. Paban. The Acceleration of the Universe, a Challenge for String Theory. *JHEP*, 07:003, 2001.
- [98] Simeon Hellerman, Nemanja Kaloper, and Leonard Susskind. String Theory and Quintessence. *JHEP*, 06:003, 2001.

- 
- [99] R. R. Caldwell, Rahul Dave, and Paul J. Steinhardt. Cosmological Imprint of an Energy Component with General Equation of State. *Phys. Rev. Lett.*, 80:1582–1585, 1998.
- [100] Bharat Ratra and P. J. E. Peebles. Cosmological Consequences of a Rolling Homogeneous Scalar Field. *Phys. Rev.*, D37:3406, 1988.
- [101] Edmund J. Copeland, Andrew R Liddle, and David Wands. Exponential Potentials and Cosmological Scaling Solutions. *Phys. Rev.*, D57:4686–4690, 1998.
- [102] Christopher F. Kolda and David H. Lyth. Quintessential Difficulties. *Phys. Lett.*, B458:197–201, 1999.
- [103] P. J. E. Peebles and A. Vilenkin. Quintessential Inflation. *Phys. Rev.*, D59:063505, 1999.
- [104] Konstantinos Dimopoulos. The Curvaton Hypothesis and the eta-problem of Quintessential Inflation, With and Without Branes. *Phys. Rev.*, D68:123506, 2003.
- [105] Abhineet Agarwal, R. Myrzakulov, M. Sami, and Naveen K. Singh. Quintessential Inflation in a Thawing Realization. *Phys. Lett.*, B770:200–208, 2017.
- [106] R. R. Caldwell and Eric V. Linder. The Limits of Quintessence. *Phys. Rev. Lett.*, 95:141301, 2005.
- [107] Konstantinos Dimopoulos and Charlotte Owen. Modelling Inflation with a Power-law Approach to the Inflationary Plateau. *Phys. Rev.*, D94(6):063518, 2016.
- [108] Fedor L. Bezrukov and Mikhail Shaposhnikov. The Standard Model Higgs Boson as the Inflaton. *Phys. Lett.*, B659:703–706, 2008.
- [109] Renata Kallosh, Andrei Linde, and Diederik Roest. Superconformal Inflationary  $\alpha$ -Attractors. *JHEP*, 11:198, 2013.

- 
- [110] Renata Kallosh, Andrei Linde, and Diederik Roest. Large field Inflation and Double  $\alpha$ -attractors. *JHEP*, 08:052, 2014.
- [111] F. L. Bezrukov and D. S. Gorbunov. Distinguishing between  $R^2$ -inflation and Higgs-inflation. *Phys. Lett.*, B713:365–368, 2012.
- [112] Alex Kehagias, Azadeh Moradinezhad Dizgah, and Antonio Riotto. Remarks on the Starobinsky Model of Inflation and its Descendants. *Phys. Rev.*, D89(4):043527, 2014.
- [113] Girish Kumar Chakravarty, Gaveshna Gupta, Gaetano Lambiase, and Subhendra Mohanty. Plateau Inflation in SUGRA-MSSM. *Phys. Lett.*, B760:263–266, 2016.
- [114] Girish Kumar Chakravarty, Ujjal Kumar Dey, Gaetano Lambiase, and Subhendra Mohanty. Plateau Inflation in  $R$ -parity Violating MSSM. *Phys. Lett.*, B763:501–506, 2016.
- [115] Konstantinos Dimopoulos. Shaft Inflation. *Phys. Lett.*, B735:75–78, 2014.
- [116] Konstantinos Dimopoulos. Shaft Inflation and the Planck Satellite Observations. *PoS*, PLANCK2015:037, 2015.
- [117] Michael S. Turner. Coherent scalar-field oscillations in an expanding universe. *Phys. Rev. D*, 28:1243–1247, Sep 1983.
- [118] A. de la Macorra and S. Lola. Inflation in S dual Superstring Models. *Phys. Lett.*, B373:299–305, 1996.
- [119] Andrei Linde. Single-field  $\alpha$ -attractors. *JCAP*, 1505:003, 2015.
- [120] Renata Kallosh and Andrei Linde. Planck, LHC, and  $\alpha$ -attractors. *Phys. Rev.*, D91:083528, 2015.
- [121] Konstantinos Dimopoulos and Charlotte Owen. How Thermal Inflation can Save Minimal Hybrid Inflation in Supergravity. *JCAP*, 1610(10):020, 2016.

- 
- [122] Constantinos Pallis and Qaisar Shafi. From Hybrid to Quadratic Inflation With High-Scale Supersymmetry Breaking. *Phys. Lett.*, B736:261–266, 2014.
- [123] R. Armillis, G. Lazarides, and C. Pallis. Inflation, Leptogenesis, and Yukawa Quasiunification within a Supersymmetric Left-right Model. *Phys. Rev.*, D89(6):065032, 2014.
- [124] Mansoor Ur Rehman, Qaisar Shafi, and Joshua R. Wickman. Observable Gravity Waves from Supersymmetric Hybrid Inflation II. *Phys. Rev.*, D83:067304, 2011.
- [125] George Lazarides. Inflationary Cosmology. *Lect. Notes Phys.*, 592:351–391, 2002.
- [126] Konstantinos Dimopoulos, Charlotte Owen, and Antonio Racioppi. Loop Inflection-point Inflation. *Astropart. Phys.*, 103:16–20, 2018.
- [127] Rouzbeh Allahverdi, Alexander Kusenko, and Anupam Mazumdar. A-term inflation and the smallness of the neutrino masses. *Journal of Cosmology and Astroparticle Physics*, 2007(07):018–018, jul 2007.
- [128] Juan C Bueno Sanchez, Konstantinos Dimopoulos, and David H Lyth. A-term inflation and the minimal supersymmetric standard model. *Journal of Cosmology and Astroparticle Physics*, 2007(01):015–015, jan 2007.
- [129] Rouzbeh Allahverdi, Kari Enqvist, Juan Garcia-Bellido, Asko Jokinen, and Anupam Mazumdar. MSSM Flat Direction Inflation: Slow-roll, Stability, Fine-tuning and Reheating. *JCAP*, 0706:019, 2007.
- [130] David H. Lyth. MSSM Inflation. *JCAP*, 0704:006, 2007.
- [131] Kari Enqvist, Lotta Mether, and Sami Nurmi. Supergravity Origin of the MSSM Inflation. *JCAP*, 0711:014, 2007.
- [132] Rouzbeh Allahverdi, Andrea Ferrantelli, Juan Garcia-Bellido, and Anupam Mazumdar. Non-perturbative Production of Matter and Rapid Thermalization after MSSM Inflation. *Phys. Rev.*, D83:123507, 2011.

- 
- [133] Nissan Itzhaki and Ely D Kovetz. Inflectionpoint inflation and time dependent potentials in string theory. *Journal of High Energy Physics*, 2007(10):054–054, oct 2007.
- [134] Marcin Badziak and Marek Olechowski. Volume Modulus Inflection-point Inflation and the Gravitino Mass Problem. *JCAP*, 0902:010, 2009.
- [135] Kari Enqvist, Anupam Mazumdar, and Philip Stephens. Inflection-point Inflation within Supersymmetry. *JCAP*, 1006:020, 2010.
- [136] Shaun Hotchkiss, Anupam Mazumdar, and Seshadri Nadathur. Inflection-point Inflation: WMAP Constraints and a Solution to the Fine-tuning Problem. *JCAP*, 1106:002, 2011.
- [137] Nobuchika Okada and Digesh Raut. Inflection-point Higgs Inflation. *Phys. Rev.*, D95(3):035035, 2017.
- [138] Yuta Hamada, Hikaru Kawai, Kin-ya Oda, and Seong Chan Park. Higgs Inflation is Still Alive after the Results from BICEP2. *Phys. Rev. Lett.*, 112(24):241301, 2014.
- [139] Fedor Bezrukov and Mikhail Shaposhnikov. Higgs Inflation at the Critical Point. *Phys. Lett.*, B734:249–254, 2014.
- [140] Guillermo Ballesteros and Carlos Tamarit. Radiative Plateau Inflation. *JHEP*, 02:153, 2016.
- [141] Nobuchika Okada, Satomi Okada, and Digesh Raut. Inflection-point Inflation in Hyper-charge Oriented  $U(1)_X$  Model. *Phys. Rev.*, D95(5):055030, 2017.
- [142] Kristjan Kannike, Gert Hütsi, Liberato Pizza, et al. Dynamically Induced Planck Scale and Inflation. *JHEP*, 05:065, 2015.
- [143] Massimiliano Rinaldi, Luciano Vanzo, Sergio Zerbini, and Giovanni Venturi. Inflationary Quasiscale-invariant Attractors. *Phys. Rev.*, D93:024040, 2016.

- 
- [144] Arsham Farzinnia and Seyen Kouwn. Classically Scale Invariant Inflation, Supermassive WIMPs, and Adimensional Gravity. *Phys. Rev.*, D93(6):063528, 2016.
- [145] Luca Marzola, Antonio Racioppi, Martti Raidal, Federico R. Urban, and Hardi Veermäe. Non-minimal CW Inflation, Electroweak Symmetry Breaking and the 750 GeV Anomaly. *JHEP*, 03:190, 2016.
- [146] Luca Marzola and Antonio Racioppi. Minimal but Non-minimal Inflation and Electroweak Symmetry Breaking. *JCAP*, 1610(10):010, 2016.
- [147] Michal Artymowski and Antonio Racioppi. Scalar-tensor Linear Inflation. *JCAP*, 1704(04):007, 2017.
- [148] Sidney Coleman and Erick Weinberg. Radiative corrections as the origin of spontaneous symmetry breaking. *Phys. Rev. D*, 7:1888–1910, Mar 1973.
- [149] Konstantinos Dimopoulos. Ultra Slow-roll Inflation Demystified. *Phys. Lett.*, B775:262–265, 2017.
- [150] Bernard Carr, Konstantinos Dimopoulos, Charlotte Owen, and Tommi Tenkanen. Primordial Black Hole Formation During Slow Reheating After Inflation. *Phys. Rev.*, D97(12):123535, 2018.
- [151] Stephen Hawking. Gravitationally collapsed objects of very low mass. *Mon. Not. Roy. Astron. Soc.*, 152(1):75–78, 04 1971.
- [152] S. W. Hawking. Black hole explosions? *Nature*, 248:30, 1974.
- [153] Bernard J. Carr and S. W. Hawking. Black Holes in the Early Universe. *Mon. Not. Roy. Astron. Soc.*, 168:399–415, 1974.
- [154] Bernard Carr, Martti Raidal, Tommi Tenkanen, Ville Vaskonen, and Hardi Veermäe. Primordial Black Hole Constraints for Extended Mass Functions. *Phys. Rev.*, D96(2):023514, 2017.
- [155] B. P. Abbott et al. Multi-messenger Observations of a Binary Neutron Star Merger. *Astrophys. J.*, 848(2):L12, 2017.

- 
- [156] Bernard J. Carr. Primordial Black Holes: Do They Exist and Are They Useful? In *59th Yamada Conference on Inflating Horizon of Particle Astrophysics and Cosmology Tokyo, Japan, June 20-24, 2005*, 2005.
- [157] Maxim Yu. Khlopov. Primordial Black Holes. *Res. Astron. Astrophys.*, 10:495–528, 2010.
- [158] A. G. Doroshkevich. Spatial Structure of Perturbations and Origin of Galactic Rotation in Fluctuation Theory. *Astrophysics*, 6:320–330, October 1970.
- [159] J. M. Bardeen, J. R. Bond, N. Kaiser, and A. S. Szalay. The statistics of Peaks of Gaussian Random Fields. *The Astrophysical Journal*, 304:15–61, May 1986.
- [160] Bernard J. Carr. The Primordial Black Hole Mass Spectrum. *Astrophys. J.*, 201:1–19, 1975.
- [161] M. Yu. Khlopov and A. G. Polnarev. Primordial Black Holes as a Cosmological Test of Grand Unification. *Phys. Lett.*, 97B:383–387, 1980.
- [162] A. G. Polnarev and M. Yu. Khlopov. Cosmology, Primordial Black Holes and Supermassive Particles. *Sov. Phys. Usp.*, 28:213–232, 1985. [Usp. Fiz. Nauk145,369(1985)].
- [163] Tomohiro Harada, Chul-Moon Yoo, Kazunori Kohri, Ken-ichi Nakao, and Sanjay Jhingan. Primordial Black Hole Formation in the Matter-dominated Phase of the Universe. *Astrophys. J.*, 833(1):61, 2016.
- [164] Tomohiro Harada, Chul-Moon Yoo, Kazunori Kohri, and Ken-Ichi Nakao. Spins of Primordial Black Holes Formed in the Matter-dominated Phase of the Universe. *Phys. Rev.*, D96(8):083517, 2017.
- [165] P. J. E. Peebles. Origin of the Angular Momentum of Galaxies. *Astrophysical Journal*, 155:393, February 1969.
- [166] Tomohiro Harada, Chul-Moon Yoo, and Kazunori Kohri. Threshold of Primordial Black Hole Formation. *Phys. Rev.*, D88(8):084051, 2013. [Erratum: Phys. Rev.D89,no.2,029903(2014)].

- 
- [167] Bernard Carr, Tommi Tenkanen, and Ville Vaskonen. Primordial Black Holes from Inflaton and Spectator Field Perturbations in a Matter-dominated Era. *Phys. Rev.*, D96(6):063507, 2017.
- [168] Bernard J. Carr, J. H. Gilbert, and James E. Lidsey. Black Hole Relics and Inflation: Limits on Blue Perturbation Spectra. *Phys. Rev.*, D50:4853–4867, 1994.
- [169] Juan Garcia-Bellido and Ester Ruiz Morales. Primordial Black Holes from Single Field Models of Inflation. *Phys. Dark Univ.*, 18:47–54, 2017.
- [170] Konstantinos Dimopoulos and Charlotte Owen. Quintessential Inflation with  $\alpha$ -attractors. *JCAP*, 1706(06):027, 2017.
- [171] Konstantinos Dimopoulos, Leonora Donaldson Wood, and Charlotte Owen. Instant Preheating in Quintessential Inflation with  $\alpha$ -attractors. *Phys. Rev.*, D97(6):063525, 2018.
- [172] Mehdi Eshaghi, Moslem Zarei, Nematollah Riazi, and Ahmad Kiasatpour. CMB and Reheating Constraints to  $\alpha$ -attractor Inflationary Models. *Phys. Rev.*, D93(12):123517, 2016.
- [173] Yoshiki Ueno and Kazuhiro Yamamoto. Constraints on  $\alpha$ -attractor Inflation and Reheating. *Phys. Rev.*, D93(8):083524, 2016.
- [174] John Joseph M. Carrasco, Renata Kallosh, and Andrei Linde. Cosmological Attractors and Initial Conditions for Inflation. *Phys. Rev.*, D92(6):063519, 2015.
- [175] John Joseph M. Carrasco, Renata Kallosh, and Andrei Linde.  $\alpha$ -Attractors: Planck, LHC and Dark Energy. *JHEP*, 10:147, 2015.
- [176] Diederik Roest and Marco Scalisi. Cosmological attractors from alpha-scale supergravity. *Phys. Rev.*, D92:043525, 2015.
- [177] Marco Scalisi. Cosmological  $\alpha$ -attractors and de Sitter Landscape. *JHEP*, 12:134, 2015.

- 
- [178] Michal Artymowski and Javier Rubio. Endlessly Flat Scalar Potentials and  $\alpha$ -attractors. *Phys. Lett.*, B761:111–114, 2016.
- [179] Takahiro Terada. Generalized Pole Inflation: Hilltop, Natural, and Chaotic Inflationary Attractors. *Phys. Lett.*, B760:674–680, 2016.
- [180] Sergio Ferrara, Renata Kallosh, Andrei Linde, and Massimo Porrati. Higher Order Corrections in Minimal Supergravity Models of Inflation. *JCAP*, 1311:046, 2013.
- [181] Artur Alho and Claes Uggla. Inflationary  $\alpha$ -attractor cosmology: A global dynamical systems perspective. *Phys. Rev.*, D95(8):083517, 2017.
- [182] S. D. Odintsov and V. K. Oikonomou. Inflationary  $\alpha$ -attractors from  $F(R)$  Gravity. *Phys. Rev.*, D94(12):124026, 2016.
- [183] Sergio Ferrara, Renata Kallosh, Andrei Linde, and Massimo Porrati. Minimal Supergravity Models of Inflation. *Phys. Rev.*, D88(8):085038, 2013.
- [184] K. Sravan Kumar, J. Marto, P. Vargas Moniz, and Suratna Das. Non-slow-roll Dynamics in  $\alpha$ -attractors. *JCAP*, 1604(04):005, 2016.
- [185] Alessandro Di Marco, Paolo Cabella, and Nicola Vittorio. Reconstruction of  $\alpha$ -attractor Supergravity Models of Inflation. *Phys. Rev.*, D95(2):023516, 2017.
- [186] Sergio Ferrara and Renata Kallosh. Seven-disk Manifold,  $\alpha$ -attractors, and  $B$  Modes. *Phys. Rev.*, D94(12):126015, 2016.
- [187] Renata Kallosh and Andrei Linde. Cosmological Attractors and Asymptotic Freedom of the Inflaton Field. *JCAP*, 1606(06):047, 2016.
- [188] Mario Galante, Renata Kallosh, Andrei Linde, and Diederik Roest. Unity of Cosmological Inflation Attractors. *Phys. Rev. Lett.*, 114(14):141302, 2015.
- [189] Eric V. Linder. Dark Energy from  $\alpha$ -Attractors. *Phys. Rev.*, D91(12):123012, 2015.

- 
- [190] Renata Kallosh and Andrei Linde. Superconformal Generalizations of the Starobinsky Model. *JCAP*, 1306:028, 2013.
- [191] Renata Kallosh and Andrei Linde. Multi-field Conformal Cosmological Attractors. *JCAP*, 1312:006, 2013.
- [192] Sergio Cecotti and Renata Kallosh. Cosmological Attractor Models and Higher Curvature Supergravity. *JHEP*, 05:114, 2014.
- [193] Andrei Linde. Random Potentials and Cosmological Attractors. *JCAP*, 1702(02):028, 2017.
- [194] Lars Gorlich, Shamit Kachru, Prasanta K. Tripathy, and Sandip P. Trivedi. Gaugino Condensation and Nonperturbative Superpotentials in Flux Compactifications. *JHEP*, 12:074, 2004.
- [195] Michael Haack, Daniel Krefl, Dieter Lust, Antoine Van Proeyen, and Marco Zagermann. Gaugino Condensates and D-terms from D7-branes. *JHEP*, 01:078, 2007.
- [196] Zygmunt Lalak, Graham G. Ross, and Subir Sarkar. Racetrack Inflation and Assisted Moduli Stabilisation. *Nucl. Phys.*, B766:1–20, 2007.
- [197] Sotirios Karamitsos. Beyond the Poles in Attractor Models of Inflation. 2019.
- [198] A. A. Starobinsky. The perturbation spectrum evolving from a nonsingular initially de-sitter cosmology and the microwave background anisotropy. *Soviet Astronomical letters*, 9(302), 1983.
- [199] P. A. R. Ade et al. Joint Analysis of BICEP2/*KeckArray* and *Planck* Data. *Phys. Rev. Lett.*, 114:101301, 2015.
- [200] Urbano Franca and Rogerio Rosenfeld. Fine tuning in Quintessence Models with Exponential Potentials. *JHEP*, 10:015, 2002.
- [201] James M. Cline. Quintessence, Cosmological Horizons, and Self-tuning. *JHEP*, 08:035, 2001.

- 
- [202] Christopher F. Kolda and William Lahneman. Exponential Quintessence and the End of Acceleration. 2001.
- [203] Alex Kehagias and Georgios Kofinas. Cosmology with Exponential Potentials. *Class. Quant. Grav.*, 21:3871–3886, 2004.
- [204] P. A. R. Ade et al. Planck 2015 Results. XIII. Cosmological Parameters. *Astron. Astrophys.*, 594:A13, 2016.
- [205] Gary N. Felder, Lev Kofman, and Andrei D. Linde. Instant Preheating. *Phys. Rev.*, D59:123523, 1999.
- [206] Carsten van de Bruck, Konstantinos Dimopoulos, and Chris Longden. Reheating in Gauss-Bonnet-coupled Inflation. *Phys. Rev.*, D94(2):023506, 2016.
- [207] Carsten van de Bruck and Chris Longden. Higgs Inflation with a Gauss-Bonnet term in the Jordan Frame. *Phys. Rev.*, D93(6):063519, 2016.
- [208] Shinsuke Kawai, Masa-aki Sakagami, and Jiro Soda. Instability of One Loop Superstring Cosmology. *Phys. Lett.*, B437:284–290, 1998.
- [209] Jose María Ezquiaga and Miguel Zumalacárregui. Dark Energy After GW170817: Dead Ends and the Road Ahead. *Phys. Rev. Lett.*, 119(25):251304, 2017.
- [210] Yungui Gong, Eleftherios Papantonopoulos, and Zhu Yi. Constraints on Scalar–tensor Theory of Gravity by the Recent Observational Results on Gravitational Waves. *Eur. Phys. J.*, C78(9):738, 2018.
- [211] R. P Woodard. Ostrogradsky’s theorem on Hamiltonian instability. *Scholarpedia*, 10(8):32243, 2015. revision #186559.
- [212] Fulvio Sbisà. Classical and Quantum Ghosts. *Eur. J. Phys.*, 36:015009, 2015.
- [213] John F. Donoghue. The Effective Field Theory Treatment of Quantum Gravity. *AIP Conf. Proc.*, 1483:73–94, 2012.

- 
- [214] Gregory Walter Horndeski. Second-order Scalar-tensor Field Equations in a Four-dimensional Space. *Int. J. Theor. Phys.*, 10:363–384, 1974.
- [215] Christos Charmousis, Edmund J. Copeland, Antonio Padilla, and Paul M. Saffin. Self-tuning and the Derivation of a Class of Scalar-tensor Theories. *Phys. Rev.*, D85:104040, 2012.
- [216] Edmund J. Copeland, Antonio Padilla, and Paul M. Saffin. The Cosmology of the Fab-Four. *JCAP*, 1212:026, 2012.
- [217] Shinsuke Kawai and Jiro Soda. Evolution of Fluctuations During Graceful Exit in String Cosmology. *Phys. Lett.*, B460:41–46, 1999.
- [218] Pierre Binetruy, Christos Charmousis, Stephen C Davis, and Jean-Francois Dufaux. Avoidance of Naked Singularities in Dilatonic Brane World Scenarios with a Gauss-Bonnet Term. *Phys. Lett.*, B544:183–191, 2002.
- [219] Philippe Brax and Carsten van de Bruck. Cosmology and Brane worlds: A Review. *Class. Quant. Grav.*, 20:R201–R232, 2003.
- [220] Christos Charmousis and Jean-Francois Dufaux. General Gauss-Bonnet Brane Cosmology. *Class. Quant. Grav.*, 19:4671–4682, 2002.
- [221] Cristiano Germani and Carlos F. Sopuerta. String Inspired Brane World Cosmology. *Phys. Rev. Lett.*, 88:231101, 2002.
- [222] Elias Gravanis and Steven Willison. Israel Conditions for the Gauss-Bonnet Theory and the Friedmann Equation on the Brane Universe. *Phys. Lett.*, B562:118–126, 2003.
- [223] Kazuharu Bamba, Andrey N. Makarenko, Alexandr N. Myagky, and Sergei D. Odintsov. Bouncing Cosmology in Modified Gauss-Bonnet Gravity. *Phys. Lett.*, B732:349–355, 2014.
- [224] M. Gasperini, M. Maggiore, and G. Veneziano. Towards a Nonsingular Pre-Big Bang Cosmology. *Nucl. Phys.*, B494:315–330, 1997.

- 
- [225] A. Oliveros. Slow-roll Inflation from Massive Vector Fields Non-minimally Coupled to Gravity. *Astrophys. Space Sci.*, 362(1):19, 2017.
- [226] Shinji Tsujikawa, M. Sami, and Roy Maartens. Observational Constraints on Braneworld Inflation: The Effect of a Gauss-Bonnet Term. *Phys. Rev.*, D70:063525, 2004.
- [227] Zong-Kuan Guo and Dominik J. Schwarz. Slow-roll Inflation with a Gauss-Bonnet Correction. *Phys. Rev.*, D81:123520, 2010.
- [228] Peng-Xu Jiang, Jian-Wei Hu, and Zong-Kuan Guo. Inflation Coupled to a Gauss-Bonnet Term. *Phys. Rev.*, D88:123508, 2013.
- [229] Seoktae Koh, Bum-Hoon Lee, Wonwoo Lee, and Gansukh Tumurtushaa. Observational Constraints on Slow-roll Inflation Coupled to a Gauss-Bonnet Term. *Phys. Rev.*, D90(6):063527, 2014.
- [230] Seoktae Koh, Bum-Hoon Lee, and Gansukh Tumurtushaa. Reconstruction of the Scalar Field Potential in Inflationary Models with a Gauss-Bonnet term. 2016.
- [231] Jose Mathew and S. Shankaranarayanan. Low Scale Higgs Inflation with Gauss Bonnet Coupling. *Astropart. Phys.*, 84:1–7, 2016.
- [232] Nobuchika Okada and Satomi Okada. Simple Inflationary Models in Gauss-Bonnet Brane-world Cosmology. 2014.
- [233] Igor V. Fomin and Sergey V. Chervon. A New Approach to Exact Solutions Construction in Scalar Cosmology with a Gauss-Bonnet Term. 2017.
- [234] Eric V. Linder.  $\Lambda$  is Coming: Parametrizing Freezing Fields. *Astropart. Phys.*, 91:11–14, 2017.
- [235] O. Santillan. General Aspects of Gauss-Bonnet Models without Potential in Dimension Four. 2017.
- [236] Thomas P. Sotiriou and Shuang-Yong Zhou. Black Hole Hair in Generalized Scalar-tensor Gravity. *Phys. Rev. Lett.*, 112:251102, 2014.

- 
- [237] M. Heydari-Fard, H. Razmi, and M. Yousefi. Scalar-Gauss-Bonnet Gravity and Cosmic Acceleration: Comparison with Quintessence Dark Energy. *Int. J. Mod. Phys.*, D26(02):1750008, 2016.
- [238] Thomas P. Sotiriou and Enrico Barausse. Post-Newtonian Expansion for Gauss-Bonnet Gravity. *Phys. Rev.*, D75:084007, 2007.
- [239] Luca Amendola, Christos Charmousis, and Stephen C. Davis. Constraints on Gauss-Bonnet Gravity in Dark Energy Cosmologies. *JCAP*, 0612:020, 2006.
- [240] Luca Amendola, Christos Charmousis, and Stephen C. Davis. Solar System Constraints on Gauss-Bonnet Mediated Dark Energy. *JCAP*, 0710:004, 2007.
- [241] K. Dimopoulos, L. Donaldson Wood, V. Kamali, and C. Owen. In preparation.
- [242] Mar Bastero-Gil and Arjun Berera. Warm Inflation Model Building. *Int. J. Mod. Phys.*, A24:2207–2240, 2009.
- [243] A. Berera. The Warm Inflationary Universe. *Contemp. Phys.*, 47:33–49, 2006.
- [244] Arjun Berera, Ian G. Moss, and Rudnei O. Ramos. Warm Inflation and its Microphysical Basis. *Rept. Prog. Phys.*, 72:026901, 2009.
- [245] Lisa M H Hall, Ian G Moss, and Arjun Berera. Scalar perturbation spectra from warm inflation. *Phys. Rev.*, D69:083525, 2004.
- [246] Suratna Das. A Note on Single-field Inflation and the Swampland Criteria. *Phys. Rev.*, D99(8):083510, 2019.
- [247] K. Dimopoulos, M. Karčiauskas, and C. Owen. In preparation.
- [248] Lev Kofman, Andrei D. Linde, Xiao Liu, et al. Beauty is Attractive: Moduli Trapping at Enhanced Symmetry Points. *JHEP*, 05:030, 2004.